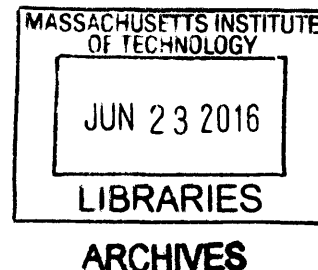**Visualizing the Attack of Bacteria by the Antimicrobial Peptide**

Human Defensin 5

by

Haritha Reddy Chileveru

M.S. and B.S. Chemistry
Indian Institute of Technology Kanpur, 2010

Submitted to the Department of Chemistry in Partial Fulfillment
of the Requirements for the Degree of

DOCTOR OF PHILOSOPHY IN BIOLOGICAL CHEMISTRY
AT THE
MASSACHUSETTS INSTITUTE OF TECHNOLOGY

June 2016

© Massachusetts Institute of Technology, 2016

Signature of
Author:

Signature redacted

Department of Chemistry
May 7th 2016

Certified
by:

Signature redacted

Elizabeth M. Nolan
Associate Professor
Thesis Advisor

Accepted
by:

Signature redacted

Robert W. Field
Haslam and Dewey Professor of Chemistry
Chairman, Departmental Committee on Graduate Studies

This doctoral thesis has been examined by a committee of the Department of Chemistry as follows:

Signature redacted

Bradley L. Pentelute
Pfizer-Laubach Career Development Assistant Professor
Committee Chairperson

Signature redacted

Elizabeth M. Nolan
Associate Professor of Chemistry
Thesis Supervisor

Signature redacted

Katharina Ribbeck
Eugene Bell Career Development Professor of Tissue Engineering
Committee Member

Visualizing the Attack of Bacteria by the Antimicrobial Peptide

Human Defensin 5

by

Haritha Reddy Chileveru

Submitted to the Department of Chemistry on May 7, 2016
in Partial Fulfillment of the Requirements for the Degree of
Doctor of Philosophy in Biological Chemistry

ABSTRACT

Bacterial infections are a major cause of concern in healthcare because of a rise in antibiotic-resistant bacteria and an increase in hospital-acquired infections. In order to combat bacterial infections, we need fundamental understanding of the host-pathogen interaction. As a part of the innate immune response, various organisms, including humans, produce antimicrobial peptides. Human defensin 5 (HD5) is a 32-aa cysteine-rich peptide produced primarily in the small intestine that exhibits broad-spectrum activity against various bacteria, fungi and viruses. In this thesis, in order to study and understand the mechanism of action of HD5, we probed the antibacterial action of HD5 and the bacterial response. We synthesized a family of HD5 analogues with functional modifications including fluorophores. With this toolkit of HD5 derivatives, we examined the effect of HD5 on various bacteria. We demonstrated that $HD5_{ox}$, the oxidized form of HD5, causes certain distinct morphological changes in Gram-negative bacteria, enters the bacterial cytoplasm and localizes near the cell poles and cell division sites. From these studies we propose that $HD5_{ox}$ overcomes the outer membrane permeability barrier and permeabilizes the inner membrane of Gram-negative bacteria, and it may interact with the cellular targets and interfere with the processes such as cell division. We extended these morphological studies of $HD5_{ox}$-treated bacteria and identified certain phenotypic responses in Gram-positive bacteria that further suggest that $HD5_{ox}$ interferes with cellular processes such as cell division.

Thesis Supervisor: Professor Elizabeth M. Nolan
Title: Associate Professor of Chemistry

Chapter Abstracts

Chapter 1. Introduction to Antibiotics and Antimicrobial Peptides

Bacterial infections have become difficult to treat in the wake of the dwindling drug pipeline for antibiotics and emerging antibiotic resistance. In nature, several organisms produce antimicrobial peptides (AMPs) to protect themselves from invading microbes. Fundamental understanding of the interaction of these AMPs and bacteria would assist in combating bacterial infections. This Chapter provides a historical overview of the discovery of antibiotics, antimicrobial peptides, and their respective bacterial targets. The major advances made in the study of the structural and functional aspects of human α-defensin 5 (HD5), the focus of this thesis, and other antimicrobial peptides are discussed. The antimicrobial and antiviral activities of the peptides along with immunomodulatory functions are described. A summary of project goals and an overall organization of the thesis are also presented.

Chapter 2. Synthesis of Human Defensin 5 and its Derivatives

Human defensin 5 (HD5) is a 32-aa peptide forming a three-stranded β-sheet structure, held together by three regiospecific disulfide linkages. There are several drawbacks to heterologous overexpression of HD5. The overexpression provides low yields and is less amenable for further functionalization of HD5. The current advancements in solid-phase peptide synthesis allow synthesis of large quantities of peptides along with a prospect to modify the peptide at desired positions using orthogonal protection strategies. In this Chapter, a robust synthesis of HD5 employing Fmoc-based solid-phase peptide synthesis protocol is presented. The synthesis was further optimized to obtain a family of fluorophore-modifed HD5 derivatives. The photophysical characterization and the antimicrobial activities of the derivatives were determined. These peptides enabled the studies on visualizing the localization of HD5 as discussed in Chapters 3-5.

Chapter 3. Visualizing the Attack of *Escherichia coli* by the Antimicrobial Peptide Human Defensin 5

In this Chapter, in order to understand how HD5 kills bacteria, the morphological consequences of HD5 treatment on the bacteria along with the localization of HD5 on bacteria are examined using the family of HD5 derivatives described in Chapter 2. The effect of $HD5_{ox}$ on *Escherichia coli*, a Gram-negative bacteria that is both commensal organism and a pathogen of the gut was investigated. Distinct morphological changes such as clumping, elongation of bacteria, and bleb formation typically at the cell poles and cell division sites, in *E. coli* were observed. When treated with $HD5_{ox}$, other Gram-negative bacteria, including human pathogens *Acinetobacter baumannii* and *Pseudomonas aeruginosa*, display similar morhological changes. Moreover, bleb formation was not observed when *E. coli* were treated with other AMPs. Employing fluorophore-modified HD5 conjugates, it was demonstrated that HD5 enters bacterial cytoplasm and localizes near the cell poles and cell division sites. These studies suggest that $HD5_{ox}$ enters bacterial cytoplasm and interacts with a potential intracellular target.

Chapter 4. Antimicrobial Activity and $HD5_{ox}$-mediated Phenotypic Effects in Gram-positive Bacteria

$HD5_{ox}$ exhibits broad-spectrum antimicrobial activity against both Gram-positive and Gram-negative bacteria. In this Chapter, we examined the phenotypic effects observed in Gram-positive strains *Staphylococcus aureus*, *Enterococcus faecalis*, and *Bacillus subtilis* treated with $HD5_{ox}$ and other AMPs. The antimicrobial activities, the effect of salt in the assay medium and morphological changes induced upon treatment with $HD5_{ox}$ were examined. These studies indicate that HD5 affects the cell septa and cytoplasmic membrane as observed by defects in the ultrastructure of all of these bacteria upon treatment with HD5, further suggesting the effect of HD5 on cell division process.

Chapter 5. Investigations of HD5$_{ox}$ Interactions with Bacterial Cellular Components

The studies in Chapters 3 and 4 indicated the HD5 interferes with certain cellular processes. In this Chapter, the effect of HD5 on select cellular components of bacteria was studied in further detail. The integrity of the lipopolysaccharide (LPS) layer of outer membrane (OM) and anionic lipids composition of membranes were varied using knockout strains of E. coli. The morphology of these strains in the presence of HD5 was examined. To examine the cell division process, the formation of FtsZ ring in the presence of HD5 was monitored. From these studies, a model is proposed where HD5 needs to overcome the OM barrier and permeabilize the inner membrane. Subsequently, HD5 can enter the bacterial cytoplasm and may interact with a potential target, possibly located at the cell division sites.

Appendix 1. Tryptophan Mutants of HD5

Tryptophan, a natural fluorophore was appended to HD5 and a set of mutants was generated by site-directed mutagenesis. These mutants were designed to contain tryptophan residues on either termini or both along with a mutant containing a short peptide-tag at N-terminus. The overexpression, folding and purification of these mutants along with structural and functional characterization were performed. From these studies, we concluded that mutants containing tryptophan residue appended at the termini of HD5 retained their ability to cause inner membrane permeabilization. However, constraints do exist on the size of the functional groups.

Appendix 2. Tools to Study HD5

Extending the family of fucntionalized HD5 analogues, a set of derivatives was generated by appending biotin (an affinity-tag) and azido-functional groups (for further modification using click-chemistry) on the N-terminus of HD5. Antibodies were also generated against both the oxidized (HD5$_{ox}$) and the linear forms of HD5 (HD5[Ser^{hexa}]). These tools will assist in future studies geared towards identifying the potential bacterial target of HD5.

To My Family,

Anji Reddy, Prameela and Sravani

Acknowledgements.

During my graduate studies, I have been through a very long and exciting journey and through this journey I had the good fortune of meeting the right people who made this journey possible. I learned and evolved over the years as both a scientist and a person, and without the support of many of the people it would not have been possible to go thorough such a journey.

First of all I would like to express gratitude to my advisor, Elizabeth M. Nolan. I remember when I first joined the Nolan Lab, I was asked to come up with a few project ideas and directions. I was excited to start this new project on human defensin 5 (HD5). Being an organic chemistry major, I had no clue about biochemistry experiments, or even how to handle a pipettemen. Liz taught me all that I know about Biochemistry. I am very thankful for her patience, even though it was a very slow learning curve for me to learn to meet the high standards of Liz. The training and guidance has enabled me to comprehend, be critical, organized, and become a better scientist. Moving forward, I will strive to achieve excellence throughout my career with this extensive training.

I would also like to acknowledge my thesis committee chair, Prof. Bradley L Pentelute. In the first couple years of my graduate studies, Brad's Lab was next door. And being the happy West Coast person he is, saying hi was sufficient to bring smiles to the person who met him. Annual meetings were exciting to discuss about science and obtain his feedback. I would also like to thank Prof. Katharina Ribbeck for serving as my thesis committee member and for her support.

I was fortunate to work in the guidance of Prof. Alan Grossmann for the past year on the *Bacillus subtilis* project. I am amazed by his ability to provide critical feedback and be a great mentor. He taught me to look at the big picture in research and reflect on what is a right direction to pursue.

I had several opportunities to teach courses at MIT and would like to acknowledge Prof Moungi G. Bawendi, Dr. John Dolhun and Prof. Alice Ting for providing me these amazing opportunities. In each of the courses, the enthusiasm of the instructors and the eagerness of

8

the students had reinforced my interest in teaching. I will carry forward and apply these learning experiences in my future.

Over the many years, I had the good company of the Nolan Lab members whom I need thank for making even the most stressful days better and manageable. I would like to thank Yoshitha, for her smiling attitude and kindness; Tengfei and her husband Yikai for being amazing friends that I could knock on their doors anytime I needed; Megan for the endless conversations on our favorites, Frozen and LOTR series; Phoom for providing beautiful SEM images; Justin for his big wide smile and bear hugs; Josh, Tim and Andy for many discussions on science and for general advice in life; Jill for providing great feedback on my project; the European club: Fabien, Julie and Simone for teaching me to enjoy science and have fun outside lab; and Toshiki, Lisa, Jules, Rose, Fangting, Claire, I-Ling Chiang, Andrea, Shion, Hope and I cannot leave out Anmol for making lab a good place to work.

I also fondly remember my first year of graduate studies, going through classes and cumes with my classmates Megan, Kanchana, Amy, Harris and Austin. During these years I made some great friends at MIT. In my first year I met my roommates Akane Sano and Amy Gao, two of the most amazing, kind and fun people I got to know at MIT. I shared my happiest moments along with my most difficult times with them. After all these years, they still appreciate my different sense of humor. I also need to specifically thank Stephanie Lam for many coffee discussions on research, life and God, even making me feel at home every Thanksgiving. I had a great support from my friend Diviya Sinha whom I have known since my undergraduates studies. I spent countless hours on skype with my friends back in India Sahil, Rishanth, Sharada and Nisha, who were there for me despite different time zones.

I need to thank the most important people in my life, my family Mom, Dad and my Sister. Their unconditional love and support is what propelled me in all of my endeavors. All these years, they had to make many sacrifices and yet they stood by me. Without them, this thesis and any of the successful milestones in my life would not have been possible. I dedicate this thesis to them.

Table of Contents

List of Tables

List of Schemes

List of Figures

Chapter 3.

Abbreviations

aa	Amino acid
ABU	γ-Aminobutyric acid
ADEP	Acyldepsipeptide
AMA	Antimicrobial activity
AMP	Antimicrobial peptides
ATCC	American Type Culture Collection
ATCUN	amino terminal Cu and Ni binding motif
BD	Big defensins
BHD5	Biotin-ABU-HD5
BHI	Brain-heart infusion media
Boc	*tert*-Butyloxycarbonyl
Bn	Benzyl
B. subtils	*Bacillus subtilis*
C-HD5	Coumarin 343 (**1**)-labeled Hd5
C. albicans	*Candida albicans*
C. crescentus	*Caulobacter crescentus*
CD	Circular dichroism
CFU	Colony forming unit
CL	Cardiolipin
CNBr	Cyanogen bromide
Crp-4	Cryptdin-4 (a murine α-defensin)
DIPEA	*N,N*-Diisopropylethylamine
DMAP	4-Dimethyaminopyridine
DMF	*N,N*-Dimethylformamide
DMSO	Dimethylsulfoxide
E. coli	*Escherichia coli*
ECA	Enterobacterial common antigen
EDT	1,2-Ethanedithiol
E. faecalis	*Enterococcus faecalis*
eq	Equivalents
ESI	Electrospray Ionization
ESKAPE	*Enterococcus faecium, Staphylococcus aureus, Klebsiella pneumoniae, Acinetobacter baumannii* and *Enterobacter spp.*
EtOH	Ethanol
FL-HD5	5(6)-Carboxyfluorescein (**2**)-labeled HD5
FL-HD5-TE	5(6)-Carboxyfluorescein (**2**)-labeled HD5-TE
FM4-64	(*N*-(3-Triethylammoniumpropyl)-4-(6-(4-diethylamino)phenyl)hexatrienyl) pyridiniumdibromide

FM1-43	(*N*-(3-Triethylammoniumpropyl)-4-(4-(dibutylamino) styryl)pyridiniumdibromide)
Fmoc	Fluorenylmethyloxycarbonyl
GduHCl	Guanidine hydrochloride
GSH	Reduced glutathione
GSSG	Oxidized glutathione
HOAt	1-Hydroxy-7-azabenzotriazole
HATU	*O*-(7-Azabenzotriazol-1-yl)-*N,N, N',N'* -tetramethyluronium hexafluorophosphate
HBTU	*O*-(Benzotriazol-1-yl)-*N,N,N',N'*-tetramethyluronium hexafluorophosphate
HBD	Human β-defensin
HD5	Human α-defensin 5
HD6	Human α-defensin 6
HD5$_{red}$	Reduced form of human α-defensin 5
HD5$_{ox}$	Oxidized form of human α-defensin 5
HD5-TE	Linear form of human α-defensin 5 (2-iodoacetamide-capped)
HD5-CD	Human α-defensin 5 covalent dimer
HEPES	2[4-(2-Hydroxyethyl)-1-piperazinyl]ethanesulfonic acid
HNP	Human neutrophil peptide
Hst	Histatin
HOAt	1-Hydroxy-7-azabenzotriazole
HPLC	High-performance liquid chromatography
HMDS	Hexamethyldisilazane
IM	Inner membrane
K. pneumoniae	*Klebsiella pneumoniae*
LAP	Lingual antimicrobial peptide
LB	Luria Broth
LC-MS	Liquid chromatography-mass spectrometry
LPS	Lipopolysaccharide
LTA	Lipoteichoic acids
NaPB	Sodium phosphate buffer
NEC	Necrotizing enterocolitis
N$_3$-HD5	Azido-functionalized HD5
Ni-NTA	Nickel-nitrilotriacetic acid
NMR	Nuclear magnetic resonance
MeCN	Acetonitrile
MIC	Minimal inhibition concentration
NAO	10-*N*-nonyl acridine orange
OD	Optical density
ONP	*o*-Nitrophenol

ONPG	*o*-Nitrophenyl-*β*- galactopyranoside
OM	Outer membrane
OMV	Outer membrane vesicles
P. aeruginosa	*Pseudomonas aeruginosa*
PBP	Penicillin binding protein
PCR	Polymerase chain reaction
PG	Peptidoglycan
PI	Propidium iodide
PMN	Polymorphonuclear neutrophils
PMSF	Phenylmethylsulfonyl fluoride
PyAOP	(7-azabenzotriazol-1-yloxy)tripyrrolidinophosphonium hexafluorophosphate
R-HD5	Rhodamine (**3**)-labeled HD5
R-HD5-TE	Rhodamine (**3**)-labeled HD5-TE
R-HD5[R9K]	Rhodamine (**3**)-labeled HD5[R9K]
R-HD5[R13K]	Rhodamine (**3**)-labeled HD5[R13K]
RhodB	Rhodamine B 4-(3-carboxypropionyl)piperazine amide (**3**)
R101	Rhodamine 101
ROI	Region of interest
rt	Room temperature
RT-PCR	Reverse transcription polymerase chain reaction
S. aureus	*Staphylococcus aureus*
SDS	Sodium dodecyl sulfate
SEM	Scanning electron microscopy
sPLA$_2$	Secretory Phospholipase A$_2$
SV	Sedimentation velocity
tBu	*tert*-Butyl
TAP	Tracheal antimicrobial peptide
TCEP	Tris(2-carboxyethyl)phosphine hydrochloride
TEM	Transmission electron microscopy
TIS	Triisopropylsilane
TFA	Trifluoroacetic acid
TMP	2,3,5-Trimethylpyridine
Tris	Tris(hydroxymethyl)aminomethane
TSB	Trypticase soy broth
UTI	Urinary tract infection
w/o	without
WTA	Wall teichoic acids

Chapter 1

Introduction to Antibiotics and Antimicrobial Peptides

1A. Bacterial Infections

Bacterial infections are one of the leading causes of mortality worldwide. For instance, tuberculosis (9.6 million infected, 1.5 million deaths, in 2014)[1] and pneumonia are two infectious diseases that are a major cause of concern for both developed and developing nations due to the development of multidrug resistance. The statistics are even grimmer for children below 5 years of age, as 15% of total mortality (955,000 deaths, in 2014) is caused by pneumonia alone.[1] Apart from mortality, the direct medical costs of healthcare-associated infections (HAI) are estimated in billions of dollars per year.[2] The discovery of antibiotics is one of the greatest achievement of the pharmaceutical industry.[3] However, as the drug pipeline for antibiotics is dwindling, along with the rapid development of resistance to existing antibiotics,[4] the pressure is enormous to develop novel antimicrobials for the treatment of microbial infections, including those caused by drug-resistant pathogens.

In this fight against pathogens, many are looking at the huge repertoire of natural host-defense peptides as inspirations for drug discovery. Extensive investigations towards elucidating the mechanisms of the native peptides and the bacterial responses are essential for understanding how the host combats the microbial infections. In this Chapter, historical account of various antibiotics and antimicrobial peptides, along with major advances made in the study of their structural and functional aspects are discussed.

1B. Bacterial Cellular Components as Targets for Antibiotic Development

Bacteria have a cell wall, cytoplasm, nucleoid, and cell membrane. Bacteria are broadly classified as either Gram-positive or Gram-negative based on a test developed by Christian Gram in 1884.[5] The staining pattern is a result of the structural components of bacteria. In Gram-positive bacteria, only one cellular membrane envelops the bacterial cytoplasm and is coated with very thick (10 to 20 layers) peptidoglycan (PG) (Figure 1.1A).[6,7] In contrast, Gram-negative bacteria have an inner membrane (IM) surrounding the cytoplasm, a thin (1 to 3 layers) peptidoglycan located in the periplasm, and enclosed by an outer membrane (OM)

(Figure 1.1B).[6,7]

The membrane compositions further differentiate Gram-positive and Gram-negative bacteria. The Gram-negative OM is a bilayer. The outer leaflet is composed of lipopolysaccharide (LPS), which is the source of the overall negative charge of the OM, and the inner leaflet is composed of phospholipids.[8] The glycolipid LPS molecules are held together by Mg^{2+} ions. The outer membrane also contains lipoproteins and β-barrel proteins (porins). The OM is attached to the peptidoglycan layer by an abundant lipoprotein named Lpp.[9] The periplasm contains the peptidoglycan layer, proteins such as chaperones, transport proteins for sugars and amino acids, biosynthetic machinery, RNAse and other enzymes.[10] The Gram-negative IM is a bilayer of phospholipids such as phosphatidyl ethanolamine, phosphatidyl glycerol and to lesser extent phosphatidyl serine and cardiolipin.[11] The IM contains membrane-associated proteins (e.g. proteins involved in oxidative phosphorylation and electron transport).[12]
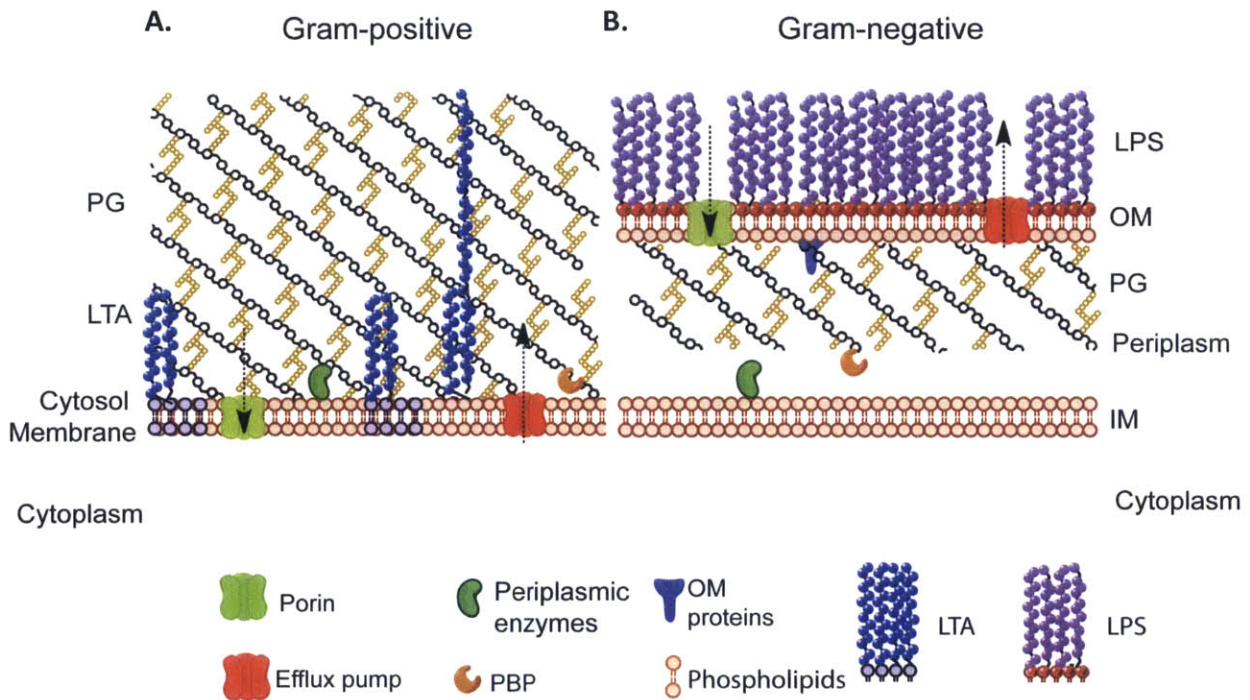
Figure 1.1. Cellular composition of A) Gram-positive and B) Gram-negative bacteria.

The Gram-positive cell envelope lacks an OM, and heavily relies on the thick peptidoglycan layer to support the turgor pressure.[6] The peptidoglycan layer is laced with anionic glycolipid polymers called wall teichoic acids (WTA) and lipoteichoic acids (LTA).[13] Because of the absence of the periplasmic compartment, the surface of Gram-positive bacteria also contains proteins analogous to the periplasmic proteins of Gram-negative membranes.[14] Many of these proteins are either directly attached to the membrane or to the peptidoglycan layer.[14]

1C.   Antibiotics

Antibiotics are classified as either bacteriocidal or bacteriostatic. Bacteriocidal antibiotics kill bacteria whereas bacteriostatic antibiotics inhibit the growth of bacteria. Several antibiotics have been developed against the cell wall synthesis machinery, as no such counterpart exists in eukaryotic cells.[15–17] In addition to targeting the synthesis of the peptidoglycan layer, many antibiotics target machinery in the cytoplasm, including components of replication, transcription, translation, cell division and metabolism (Scheme 1.1).[18] In addition to these effects, antibiotics may trigger oxidative stress and thereby cause more damage to the bacterial cell.[19] The antibiotics discussed below are grouped based on the bacterial targets.

i.   **History and Timeline of Antibiotic Development.** Salvasaran, an arsenic-based drug with an unknown mechanism of action discovered by Paul Ehrlich and his group, was the first successful drug administered to treat syphilis.[20] Paul Ehrlich envisioned the term "magic-bullets" to describe drugs that target specific pathogen without harming the host.[21] During his search for magic bullets, he developed extensive screening methods. This work paved the way for new drug discoveries.

During the early discovery period, the first antibiotics used for treating bacterial infections were the sulfa drugs, which target folate biosynthesis in bacteria. Prontosil was the

first sulfanilamide-based antibiotic, developed by Gerhard Domagk in 1935, and many pharmaceutical companies later developed modified analogues.[22] Excessive use of sulfa drugs led to the development of antibiotic resistance; therefore, the drugs are currently used only for treating urinary tract infections (UTIs).[22]

Scheme 1.1. Antibiotics Targeting Various Cellular processes in Bacteria. The targets are highlighted in red.
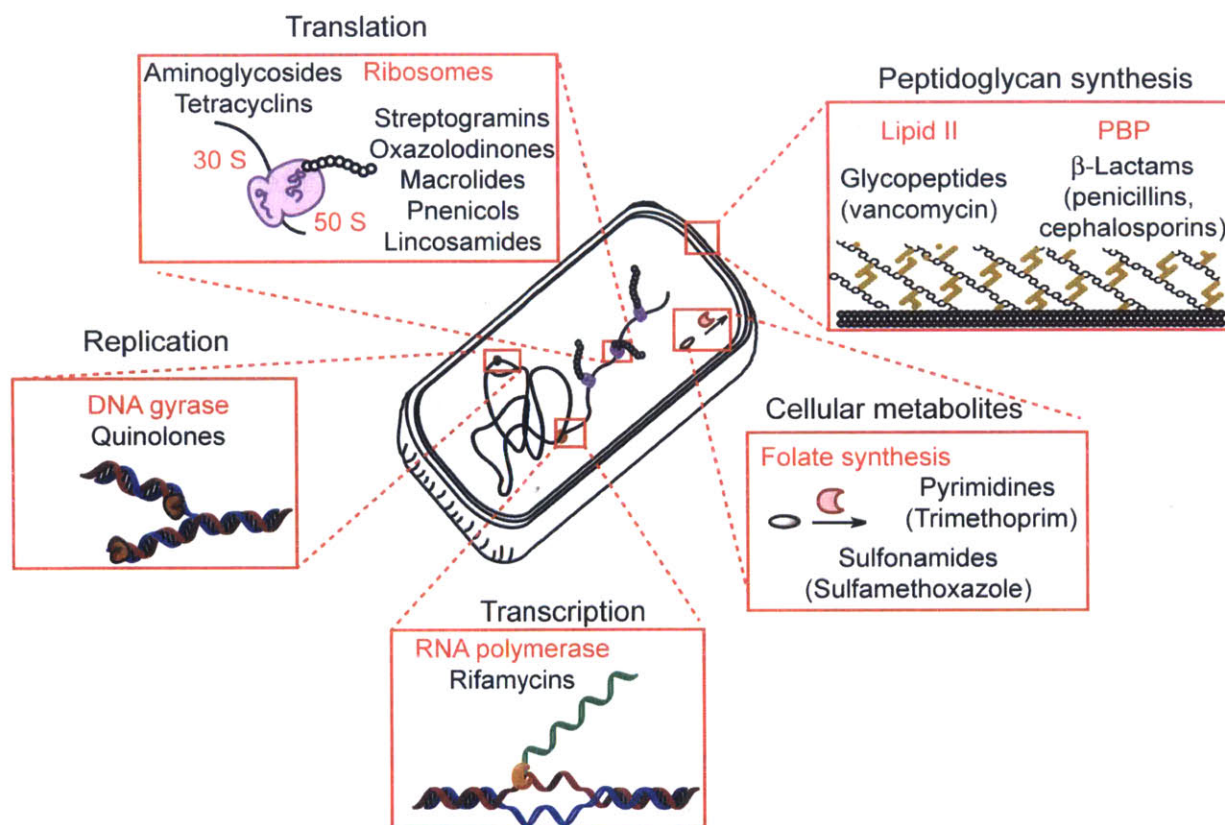
ii. **Antibiotics Targeting Cell Wall Biosynthesis.** In 1928, Alexander Fleming discovered Penicillin from the mold *Penicillium notatum*. Penicillin, is a β-lactam antibiotic that targets the synthesis of the bacterial cell wall. The development and optimization of large-scale culturing, extraction and purification methods by Howard Florey and Ernst Chain made this drug available in bulk quantities in the market by 1944.[22] The discovery of penicillin and related β-lactam antibiotics marked the peak of the "Golden era" of antibiotic discovery.

The synthesis of the peptidoglycan layer involves the incorporation of *N*-acetylglucosamine-β-1,4-*N*-acetylmuramyl-pentapeptide-pyrophosphoryl-undecaprenol (lipid II) units into the existing glycan chains through a transglycosylation step.[18] These layers of glycan chains are further strengthened by the crosslinking of the peptide side chains through a transpeptidase step, forming a meshwork that provides support for bacteria against osmotic stress. Penicillin and other β-lactams such as cephalosporins target the transpeptidase domains of the penicillin binding proteins (PBPs) and thereby inhibit PG synthesis. Furthermore, vancomycin and related glycopeptides bind to the D-Ala-D-Ala dipeptide unit of lipid II and prevent the transpeptidase domain from accessing its substrate. Other antibiotics such as fosfomycin, ramoplanin, and bacitracin also target PG biosynthesis by interfering with various other steps and enzymes involved in PG synthesis.[3,18]

There has been a steady rise of resistance to penicillin and later generations of the β-lactam antibiotics. Bacteria have acquired resistance to the β-lactams by evolving and acquiring β-lactamases, enzymes that degrade these antibiotics. Moreover, resistance to the vancomycin family of antibiotics occurs when bacteria modify the dipeptide unit of the lipid II. In the case of Gram-negative bacteria, these drugs also need to overcome the OM permeability barrier and efflux pumps that actively remove the drugs from bacteria.[18]

iii.   **Antibiotics Targeting the DNA/RNA Synthesis.** Many small molecule antibiotics block DNA or RNA synthesis. Quinolones, such as ciprofloxacin, target DNA gyrase, a type II topoisomerase involved in the uncoiling of DNA.[23] Rifamycins target DNA-dependent RNA polymerase and inhibit transcription.[24] Sulfamethoxazole and trimethoprim interfere with folate metabolism and thereby DNA synthesis.[25] The main mechanisms by which bacteria have developed resistance for such drugs are by increasing drug efflux and modifying the enzyme targets.

iv. **Antibiotics Targeting Protein Synthesis.** Many classes of antibiotics target protein synthesis by inhibiting ribosomes.[26] These antibiotics can be further grouped as drugs targeting the 50S subunit and those that bind to the 30S subunit of the bacterial ribosome. Macrolides, streptogamins, lincosamides, and oxazolidones target the 50S subunit. Aminoglycosides and tetracyclines target the 30S subunit. The main resistance mechanisms for translation inhibitors include (i) modification of the drug itself by phosphorylation, acetylation, glycosylation, nucleotidylation, etc.; (ii) modification of the ribosome and (iii) increased drug efflux.[18]

v. **Other Classes of Antibiotics.** A series of acyldepsipeptide (ADEP) antibiotics were recently isolated and found to activate the bacterial chambered protease ClpP, leading to uncontrolled proteolysis and cell death.[27] ADEPs are not yet used clinically, whereas the rest of the antibiotics that were discussed in this Chapter are already available in market.

Although a vast repertoire of antibiotics is currently available, very few new classes of antibiotics have been discovered (Scheme 1.2). Bacteria have developed resistance to almost all of the available drugs or will quickly develop resistance in the near future. With the dwindling pipeline of drugs reaching clinical trials, it is of outmost importance that new classes

Scheme 1.2. Timeline for the Discovery of Antibiotics
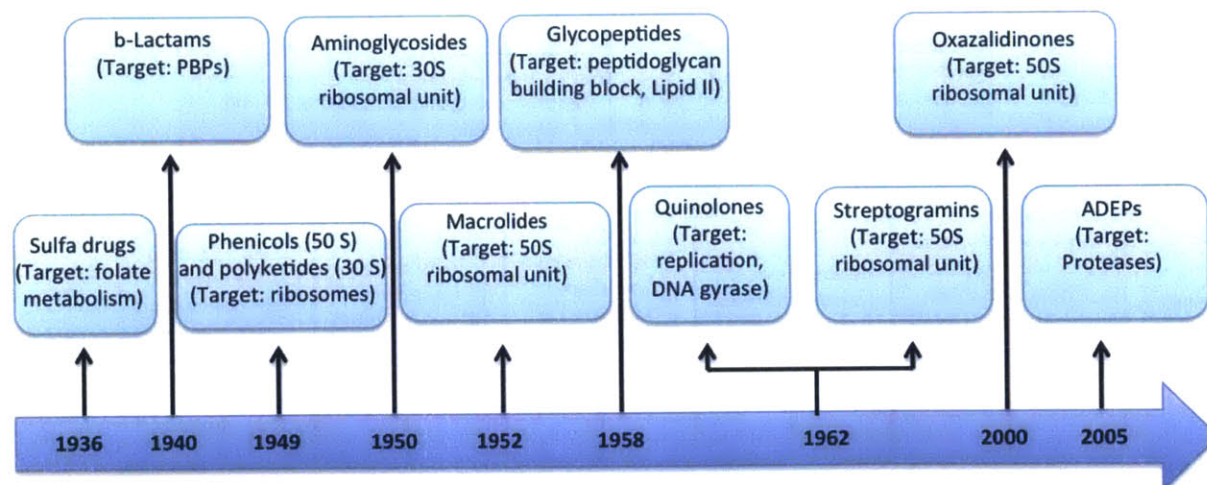
Timeline is not drawn to scale

of antibiotics be developed to fight against the emerging multidrug resistant pathogens.

In this regard, one area of current research is directed towards investigating the antimicrobial peptides (AMPs) that are a part of the natural armor of the host. In many organisms, antimicrobial peptides, and more broadly "host-defense peptides", maintain microbial homeostasis and protect the host from pathogenic attacks. Fundamental understanding of the structure and function of these peptides may provide new insights for antibacterial development.

1D.   Antimicrobial Peptides

Before the discovery of penicillin, Alexander Fleming had discovered a human antimicrobial protein called lysozyme (130 amino acids).[28] Since then, antimicrobial peptides and proteins have been discovered in lower through higher eukaryotes (Scheme 1.3). Some peptides that were first described as antimicrobial peptides, are now termed "host-defense peptides" because they have known or putative roles as signaling molecules and immune response regulators.[29] Moreover, many facets of these host-defense peptides and their functions in their host remain uncovered, indicating that the antimicrobial properties of these

Scheme 1.3. Timeline for the Discovery of Human AMPs
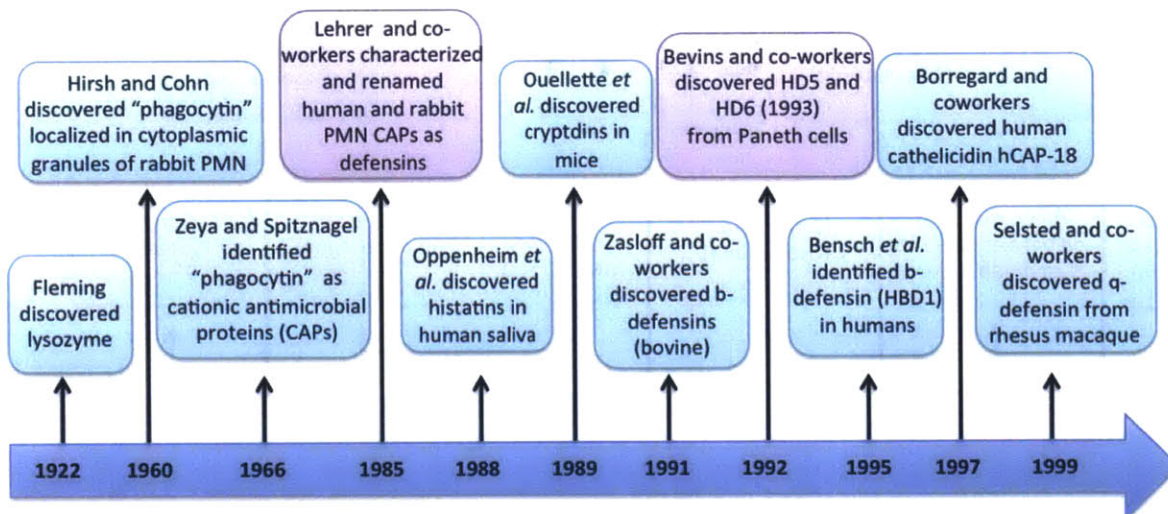
Timeline is not drawn to scale

peptides are only a tip of the iceberg.

Listed below are a few examples from the ever-growing inventory of the host-defense peptides, and are highlighted for the major contributions towards advancing of the structure and mechanism of action studies in the AMP field. Human defensin 5 (HD5), the focus of this thesis is discussed in further detail in this chapter.

1E. Defensins

Ehrlich received Nobel Prize for Physiology or Medicine 1908 along with Ilya Mechnikov for the discovery of phagocytosis. The study of phagocytosis and the mechanism of bacterial killing led to the discovery of antimicrobial peptides called defensins, the focus of this thesis. When probing phagocytosis and the bacterial killing in the phagosomes, acid extracts of rabbit polymorphonuclear neutrophils (PMNs) were found to exhibit antimicrobial properties. The antimicrobial component was named phagocytin, and was localized in the cytoplasmic granules of PMNs.[30,31] Later, Zeya and Spitznagel discovered that phagocytin was comprised of a group of cationic antimicrobial proteins (CAPs).[32] Lehrer and coworkers subsequently characterized the CAPs and determined the primary sequences; this work led to renaming CAPs as defensins.[33–36]

Defensins are a class of cysteine and β-sheet rich host-defense peptides produced by various eukaryotes that include fungi,[37] fish,[38] plants,[39] insects,[40] arthropods,[41] birds,[42] and mammals, including humans.[43] Defensins are ribosomally encoded peptides of <50 amino acids in length with two to four regiospecific disulfide linkages. Vertebrate defensins, insect defensins, and certain fungal defensins contain three disulfide bonds whereas plant defensins have four disulfide linkages.[40,44]

The vertebrate defenisns are further classified into α-, β- and θ-defensins based on their regiospecific disulfide linkages. The six cysteines found in α- and β-defensins are linked as $Cys^I–Cys^{VI}/Cys^{II}–Cys^{IV}/Cys^{III}–Cys^V$ (α-defensins) or $Cys^I–Cys^V/Cys^{II}–Cys^{IV}/Cys^{III}–Cys^{VI}$ (β-defensins) that maintain a three-stranded β-sheet fold. The peptide backbone of the θ-defensins is formed

by cyclization of two β-sheet peptide fragments linked head to tail. The six cysteines are linked as three disulfide linkages displaying the cyclic cysteine ladder motif.[45] Mammalian defensins are considered to have evolved from the big defensin (BD) family of peptides.[46,47] Big defensins consist of 79–94 amino acids that form two distinct structural and functional domains. The C-terminal region adopts the typical β-defensin fold with identical disulfide linkage patterns, suggesting that β-defensins emerged from an ancestral big defensin.

The α-defensins are only found in mammals and marsupials, whereas the β-defensins are found even in other organisms including avian and amphibian species. Defensin strategies vary form organism to organism. For example, humans express α-defensins in their polymorphonuclear neutrophils (PMN) and in the small intestine. In contrast, mice do not have any α-defensins in their PMN;[48] however, they express various α-defensins in their gut (cryptdins).[49] Another example is that cows do not produce α-defensins, while their PMNs contain both cathelicidins and β-defensins.[50] Currently, θ-defensins are only identified in non-human primates.[51] Although humans possess the genes encoding θ-defensins, the peptides are not expressed due to a premature stop codon.[51] The first α-defensins identified were from human neutrophils[35] and rabbit granulocytes.[36] The first β-defensins identified were from bovine trachea,[52] and the θ-defensin was first identified in rhesus macaque leukocytes.[53] In an effort to develop defensin-based therapeutics, synthetic peptides based on retrocylin, a θ-defensin were generated and were found to inhibit Herpes simplex viruses, HSV-1 and HSV-2.[54]

i.   Human Defensins

Defensins are expressed as prepropeptides containing a signal peptide, a propiece and the mature peptide.[46,47] Two α-defensins are primarily identified as the enteric defensins, HD5 and HD6. Four myeloid α-defensins are identified as human neutrophil peptides (HNP 1-4). The four human β-defensins (HBD1-4) are primarily identified as epithelial defensins. However, recent studies indicate that several defensins can be expressed in other organs and sites.[55] For

instance, the expression of HD5 is also found in uro-genital tract and female reproductive system.[56,57]

In humans, six α-defensins and four β-defensins have been well characterized, although many more (about 40) β-defensins genes have been identified.[58] All of the human defensin genes are encoded on the chromosome 8p23.[58] Of the six α-defensins, DEFA1 (encoding human HNP1, HNP2) and DEFA3 (encoding HNP3, HNP2) have multi-copy genes, whereas DEFA4, DEFA5 and DEFA6 (encoding HNP4, human defensin 5 (HD5) and human defensin 6 (HD6), respectively) are single-copy genes.[59] Apart from DEFB1 (encoding HBD1), other β-defensins are also encoded as multi-copy genes (DEFB103A encoding HBD3, DEFB4 encoding HBD2, and DEFB104A encoding HBD4) due to copy number polymorphisms.[59] Although correlations of the copy numbers and the expression of these peptides with certain diseases are made, the consensus and complete understanding is not yet reached.[60]

ii. α-Defensins

Enteric Defensins. In humans, specialized secretory epithelial cells called Paneth cells[61] are present in the crypts of Lieberkühn. The Paneth cells are adjacent to the small intestinal stem cells and express many antimicrobial factors.[62] Paneth cells express two enteric α-defensins named HD5[63] and HD6.[64] It is to be noted that whereas humans express only two enteric α-defensins, at least six cryptdin peptides (murine Paneth cell α-defensins) are identified in mice.[65] In humans, HD5 and HD6 are expressed as prepropetides (Figure 1.2); the signal peptide for secretory pathway is cleaved and the propeptide is stored in the secretory granules of Paneth cells.[61,66] The granules also contain high amounts of labile zinc of unknown function,[67,68] along with other antimicrobial peptides such as lysozyme and secretory phospholipase A_2 (sPLA$_2$).[69] The contents of these granules are released into the lumen upon microbial attack. The current model indicates that Paneth cell trypsin cleaves the propeptides and releases the mature forms of these defensins in the intestinal lumen to ward off invading pathogens.[62,70] The misregulation in the expression of enteric defensins is correlated with

certain diseases such as Crohn's disease (CD) and inflammatory dowel disease (IBD).[71] Therefore, a clear understanding of the mechanism of antimicrobial action of defensins is fundamental for delineating the roles of defensins in human health as well as microbial pathogenesis.

A.

Cleavage

| Signal | Propiece | Mature peptide |

B.

HNP1	A CYCRI PACIA GERRY GTCIY QGRLW AFCC
HNP2	CYCRI PACIA GERRY GTCIY QGRLW AFCC
HNP3	D CYCRI PACIA GERRY GTCIY QGRLW AFCC
HNP4	V CSCRL VFCRR TELRV GNCLI GGVSF TYCCTRVD
HD5	AT CYCRT GRCAT RESLS GVCEI SGRLY RLCCR
HD6	AFT CHCRR _SCYS TEYSY GTCTV MGINH RFCCL
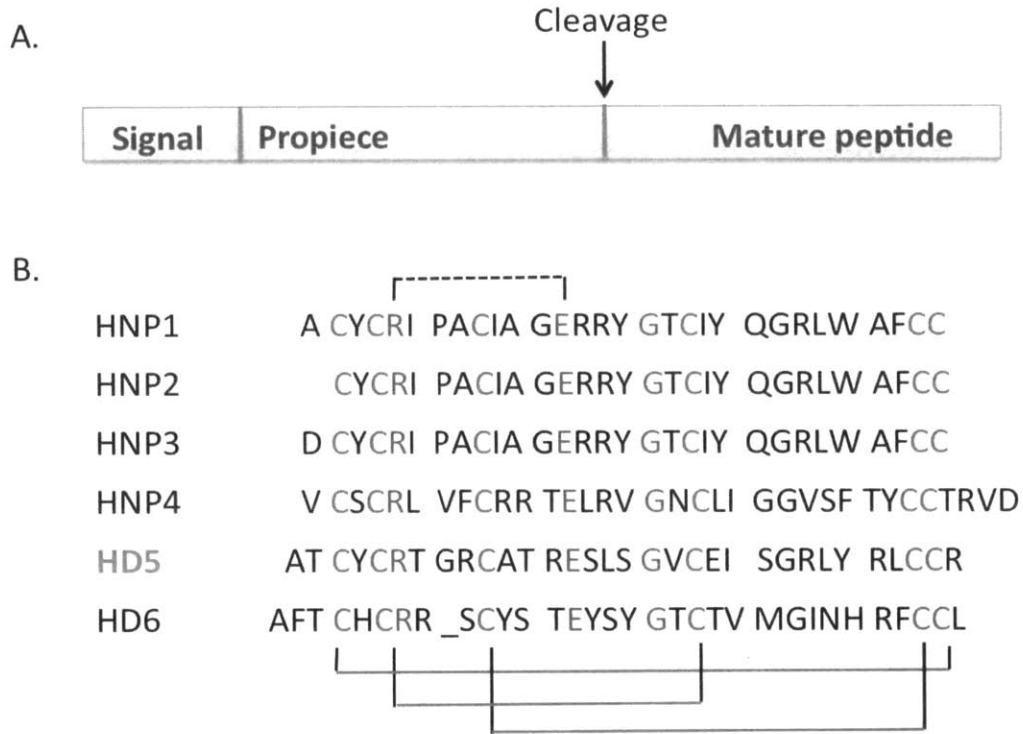
Figure 1.2. α-Defensins are expressed as prepropeptide and share certain conserved features in their mature peptides. **A)** Schematic of the prepropeptide form of α-defensins. **B)** Amino acid sequences of the mature α-defensins peptides where the following conserved features are highlighted: cysteine residues and the regiospecific disulfide linkages are in red; residues Glu - Arg forming the salt bridge are in blue; and Glycine in GXC motif forming β-bulge are in green. HD5, the focus of this thesis, is in orange.

1F. Human α-Defensin 5 (HD5)

i.   Expression and Significance of HD5 in Disease. HD5, the focus of this thesis, was first identified in the human small intestine.[63] However, the expression of HD5 is detected in other tissues and organs, such as the urogenital tracts and female genital tract.[56,57] In the intestine, HD5 is constitutively expressed and is the most abundant Paneth cell antimicrobial peptide.[69,72]

The quantification of mRNA transcripts indicates that HD5 is about four- to six-fold higher than HD6, and even higher than other antimicrobial peptides in the granules.[73] The expression of defensin genes in the small intestine of the fetus is observed by 14 weeks and the localization of HD5 to the small intestine coincides with the appearance of Paneth cells.[74] The number of Paneth cells and the expression of defensins are low in preterm neonates compared to full-term newborns and adults.[74] This comparison suggests that the immune system of the fetus is less developed, and hence more predisposed to the necrotizing enterocolitis (NEC), a condition predominantly observed only in preterms.[75] Also, the expression of the enteric defensins, and especially HD5, is reduced in patients suffering from ileal Crohn's disease, compared to the control individuals.[69]

HD5 and HD6 are expressed in the duodenum, jejunum, and ileum with highest expression observed in the ileum, but not in the colon.[73] Compared to the colon, which houses high loads of commensal bacteria, the small intestine is considered to be relatively sterile.[76] Various host factors such as the enteric defensins contribute in preventing the attack by pathogens and maintaining microbial homeostasis.[77,78] HD5 exhibits broad-spectrum antimicrobial activity against various bacteria and fungi *in vitro* and also has antiviral activity.[79–82] Transgenic mice expressing HD5 are more resistant to *Salmonella* challenge than wild-type mice.[83] Studies of the resident intestinal microbiota suggest that HD5 contributes to controlling its composition.[83,84] This seminal work provided convincing evidence for the importance of HD5 in the maintenance of small intestinal barrier against the pathogenic bacteria and contributing to microbial homeostasis.

In the female reproductive tract, Quayle *et al.* identified the expression of HD5 mRNA transcripts in epithelia along with the peptide in both the apical epithelium and cervical fluid.[57] In contrast to expression of HD5 in Paneth cells where constitutive expression is observed, HD5 is expressed and secreted in a distinct pattern during each menstral cycle, possibly via hormonal regulation.[57] In this study, HD5 expression is also upregulated during inflammation in the female reproductive tract.[57] A possible role in prevention of microbial invasion during the

ovulation was proposed.[57] Recently, HD5 expression was also identified in the kidneys and urinary tract.[56]

The Paneth cell granules contain high concentrations of labile zinc. Moreover, granule depletion and Paneth cell abnormalities, degeneration, and apoptosis are some phenotypes observed in conditions of zinc deficiency.[85] Despite the observations, the role of zinc co-packaging with the defensins in the granules is not understood. Studies in the Nolan Lab demonstrated that the reduced form of HD5 (HD5$_{red}$) binds zinc and a complex of two zinc ions per HD5 molecule can be formed.[86] The redox mid-point potential of HD5 was determined to be -257 mV and the thioredoxin system is able to reduce HD5.[86] The physiological redox potential in the gut is in the range to promote the reduction of HD5. Therefore, it is possible that HD5 can be reduced and can bind to zinc forming an HD5:Zn^{2+} complex *in vivo*.

It is interesting to note that the expression (mRNA) of HD5 and HD6 is also observed in the pancreas, another labile zinc-storage organ.[73] Even in the reproductive tract where zinc is secreted, expression and secretion of HD5 is observed.[57] Moreover, at other sites where zinc storage or release is not significantly detected, including liver, bone marrow, esophagus, and stomach, no detectable peptide is observed.[74] Although these observations might be mere correlational inferences, further investigation is needed in the role of zinc and HD5, along with the HD5 colocalization.

ii.   Structure and Folding of HD5. HD5 is expressed as a 94-residue prepropeptide that includes a 19-aa signal peptide at the N-terminus. Following the cleavage of the signal peptide, the propeptide comprising residues 20-94 is stored in the Paneth cell granules. [63,72] In the Intestinal lumen, various partially cleaved fragments of the propeptide were identified suggesting that the propeptide form of HD5 is released into the intestinal lumen. Trypsin is identified as the protease that cleaves the proform to release the mature 32-residue peptide with an overall charge of +4 at neutral pH (Figure 1.3).[70] Among various α-defensins from different organisms, the 6-cysteines, the residues Glu[14] - Arg[6] (using HD5 numbering) forming a

salt bridge, and Gly[18] are conserved (Figure 1.2, 1.3). An elegant study by W. Lu and coworkers suggested that the presence of the propeptide in the granules reduces the cytoxicity of defensins by masking the activity of the mature peptide. Along these lines, the AMA activity of HD5 is reduced *in vitro* in the presence of the propiece.[87] This study also indicated that the canonical α-defensin salt bridge between Arg[6] and Glu[14] is required for the proper folding of the HD5 in the absence of the prodomain.[87] The salt bridge also provides proteolytic stability of HD5 against trypsin digestion. However, the salt bridge is not required for the antimicrobial activity of HD5. When Glu[14] is mutated to Gln, the antimicrobial activity of the HD5[E14Q] mutant increases, possibly resulting from an increase in the overall charge of the peptide.[87]

A.

B.
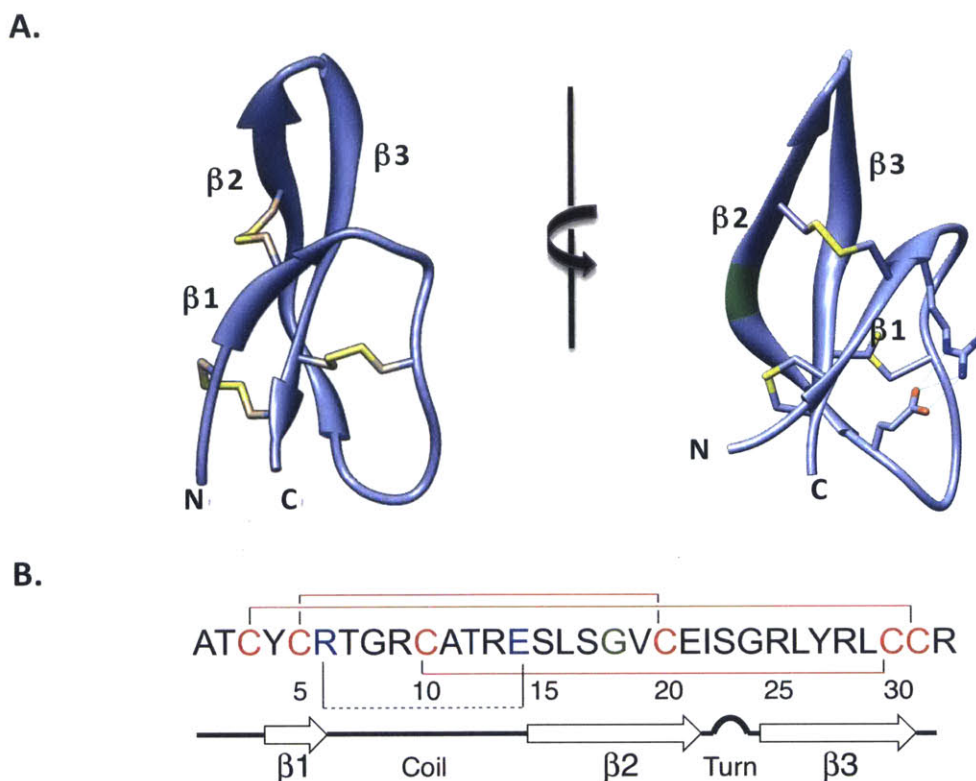
Figure 1.3. Structure of the HD5$_{ox}$ monomer determined by solution NMR (PDB 2LXZ)[90] and amino acid sequence. The β-sheets (β1, β2 and β3), Gly[18] (green), salt bridge formed by Glu[14]-Arg[6] (blue), and the regiospecific disulfide bond linkages (red) are indicated in **A)** the structure and **B)** the sequence of HD5$_{ox}$.

The conserved glycine is a component of a GXC motif that provides the classic β-bulge on the β2-strand. In the absence of Gly, the presence of a D-amino acid is required for providing the allowed torsional angles.[88] HD5 folds into the conserved three-stranded β-sheet structure of the α-defensins (Figure 1.3).[89,90] In the Nolan Lab, a family of disulfide mutants was generated where cysteines in each of the disulfide linkages replaced with serine residues.[91] By employing this extensive family of mutants, the disulfide linkages were shown to be important for the stability of HD5 against various proteolytic enzymes.[91] The three disulfide linkages of HD5 (and of defensins in general) provide both stability to the β-sheet structure and resistance against protease degradation.[91–93] Mutating one or more disulfide linkages resulted in complete loss of antimicrobial activity against *Staphylococcus aureus*. However, the antimicrobial activity of the disulfide mutants of HD5 was less affected compared to the native peptide against *Escherichia coli*. The significance of disulfide linkages for the strain-specific antimicrobial activity of HD5 was also supported by the studies done by W. Lu and coworkers employing Cys→Abu (α-aminobutyric acid) mutants of HD5.[94] In another study, they observed a similar antimicrobial activity of L-and D-enantiomers of HD5 against *E. coli*, whereas lower antimicrobial activity of D-HD5 was observed against *S. aureus* than L-HD5. Taken together, these results suggest that proper folding of HD5 is required for the antimicrobial activity of HD5 against *S. aureus* whereas overall structure is less important for activity against *E. coli*. It needs to be determined if separate modes of action against Gram-positive vs. against Gram-negative strains exist for HD5.

HD5 displays amphipathic behavior, with all the cationic residues aligned on one face of the monomer and the other face being predominantly hydrophobic in nature.[95] The quaternary structure and the oligomerization of HD5 were probed using various techniques including crystallography, NMR spectroscopy, analytical ultracentrifugation and surface-plasmon resonance.[89,90,96] A non-covalent dimeric unit (Figure 1.4), as observed from the crystal structure (PDB 1ZMP)[89] indicates that the HD5 monomers interact via hydrophobic side (β2) to form an extended six-stranded β-barrel like structure.[89,90] NMR studies of HD5 further supported formation of dimers (at pH 4.0).[90] Formation of dimers and potential higher-order
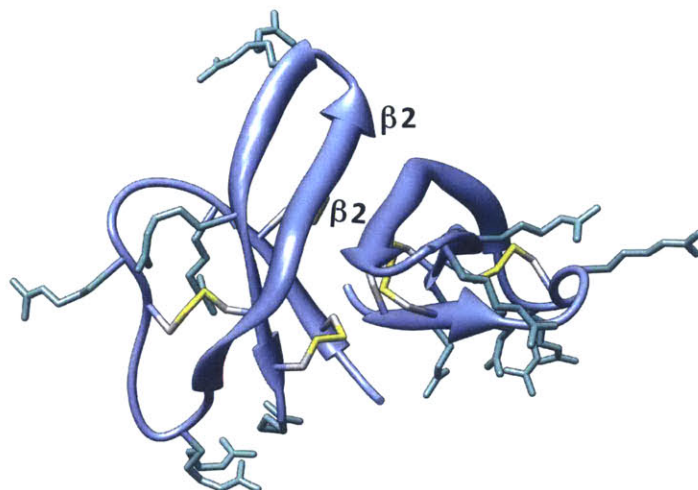
Figure 1.4. Structure of HD5$_{ox}$ indicating the non-covalent dimer in the crystal structure (PDB 1ZMP).[89] The hydrophobic residues are oriented at the dimer interface (β2- β2) and arginine residues (green) are oriented in the other direction rendering HD5$_{ox}$ amphipathic.

oligomers of HD5 was studied by surface-plasmon resonance.[95] HD5 exists as tetramers in solution at neutral pH, as observed by the analytical ultracentrifugation studies from the Nolan Lab.[90] Furthermore, under appropriate oxidizing conditions, HD5-CD, a non-canonical C$_2$-symmetric β-barrel-like covalent dimer of HD5, was discovered in the Nolan Lab.[82] HD5-CD displays broad-spectrum antimicrobial activity against various bacteria along with antifungal activities. In both HD5-CD and HD5$_{ox}$, the arginine residues are surface exposed and form a coat of charged residues.[82] How the structure influences the killing activity of HD5-CD and HD5 needs to be studied in further detail.

iii. **Functional and Antimicrobial Properties of HD5.** HD5 is active against various Gram-negative and Gram-positive strains.[79,80,82,97] Recently, HD5 was shown to be active against the hypervirulent strains of *Clostridium difficile* that are resistant to other AMPs such as polymyxin and nisin.[98] HD5 also displays antiviral[99,100] and antifungal properties.[82,89] HD5 exhibits immunomodulatory behavior; HD5 and other defensins act as chemoattractants for macrophages, lymphocytes, and mast cells.[101]

Mechanism of action studies of many defensins, have been focused on cationic nature of the peptide and its interaction with the negatively charged bacterial membranes. Historically, biophysical studies on the disruption of artificial membrane vesicles by antimicrobial peptides have supported mechanisms involving pore formation and membrane perturbations.[102] The bacterial inner membrane permeabilization of various defensins was studied using *E. coli* ML-35, a lactose-permease deficient strain with cytoplasmic β-galactosidase activity. When *E. coli* ML35 strain was treated with cryptdin-4, mouse Paneth cell α-defensin, IM permeabilization of the bacteria was observed.[103] In this direction, studies in the Nolan Lab have shown that HD5 also causes bacterial IM permeabilization.[91]

HD5 displays lectin-like behavior and bind to glycosylated proteins.[96] The inhibition of bacterial toxins such as anthax lethal factor by HD5 and other human defensins were examined.[104] Recently, a comprehensive study on various bacterial exotoxin inactivation by defensins was reported.[105] The study focused on HNP1, but also considered HD5. In this investigation, it was determined that HD5 bind to the toxins, cause local unfolding of these toxins and precipitation, along with exposing them to proteolysis. In these studies, the amphiphilic nature of defensins is shown to be important in their interactions with the toxins. Further studies on the importance of the hydrophobic pocket of HD5 and the dimerization/oligomerization of HD5 on the antibacterial activity have been reported.[90,95,96] Recently, many defensins have shown to be exerting antimicrobial action affecting multiple cellular targets and pathways in the bacteria.[92,106–109] In this regard, further studies are needed to elucidate the exact mechanism of action of HD5.

Currently, in regard to antifungal properties, minimum inhibitory concentration (MIC) values of HD5 against *Candida albicans*, as a model organism are reported.[80,82] Further extensive studies for determining the antifungal activities of HD5 and mechanism of action are greatly needed. Activity of HD5 against other organisms such as viruses is also studied. HD5 is active against non-enveloped viruses and prevents the viral uncoating.[100] HD5 displays lectin-like behavior and binds to the viral glycoproteins such as gp120 and gD1.[96] Furthermore, HD5

and HNP1 bind to gp120 and CD4 and cause inhibition of HIV-1.[110] The role of specific arginine residues, hydrophobicity at the dimer interface, and the oligomerization of HD5 for the antiviral activity were probed using various mutants.[100] In general, the oligomerization of HD5 and the orientation of its arginine residues at the surface interacting with the virus capsid were shown to be important for the antiviral activity.[100] Recently, it was found that *Neisseria gonorrhoeae* modulates expression of HD5 during HIV infection,[111] which results in increase in the HIV infection. Previously, the expression of HD5 in the female reproductive tract was found to be inducible.[57] Considering the complexity of defensins, and more broadly the interaction between the host and pathogens, further investigation is needed to determine the mechanism by which HD5 modulates HIV infection.

1G.   Human α-Defensin 6 (HD6)

i.   Expression and Significance of HD6 in Disease. HD6 is expressed primarily in the Paneth cells of the small intestine as a prepropeptide and stored in the granules of Paneth cells as the propetide.[64] Proposed model by the Bevins Lab in collaboration with the Nolan Lab suggests that the Paneth cell trypsin as the enzyme involved in cleavage of the propeptide to release the mature HD6 in the intestinal lumen.[66] As observed for HD5, the expression of HD6 is reduced in certain diseased conditions such as ileal Crohn's disease.[69]

ii.   Structural and Functional Properties of HD6. HD6 is a 32-aa residue peptide with an overall charge +2 at neutral pH (Figure 1.5).[79] However, for a long period, HD6 was an enigma because it exhibited no *in vitro* antimicrobial activity.[79] When the crystal structure of HD6 was initially solved, the intermolecular interactions were found to be different from other α-defensins.[89] The hydrophobic residues of each monomer were identified in pocket region located at the interface of the four-monomer units in the crystal structure.[89] However, it was only recently that the formation of higher-order oligomers resulting in "nanonets" was identified.[112] These nanonets entrapped bacteria and prevented their invasion into host cells. In
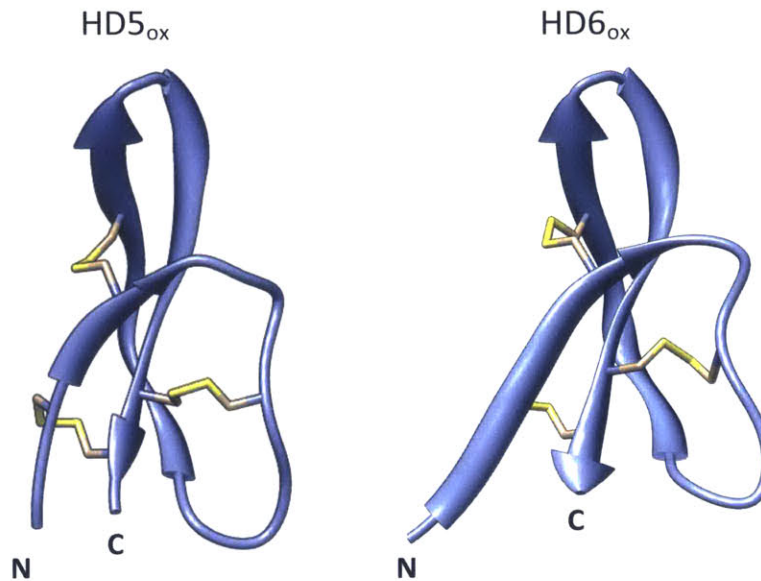
Figure 1.5. Structure of $HD5_{ox}$ (solution NMR structure, PDB 2LXZ)[90] and $HD6_{ox}$ (crystal structure, PDB 1ZMQ)[89] monomer units indicating similar tertiary structures.

this study, the nanonet hypothesis was supported by elegant studies using a transgenic mice model that expressed HD6 in the Paneth cells.[112] When mice were subjected to oral *Salmonella* challenge, the transgenic mice survived better than the wild-type mice even though no reduction was observed in the intestinal bacterial loads. It was found that the bacteria were unable to invade the transgenic mice, and hence the bacterial loads in the lymph nodes were reduced. Subsequently, the Phe residues (2 and 29) on the HD6 sequence were identified as key residues for nanonet formation.[113] It appears that the enteric defensins elected two different mechanisms of host protection, one (HD5) involves direct killing whereas the other (HD6) involves prevention of invasion. Recently, the reduced form of HD6 is found to exhibit antimicrobial activity against *Bifidobacterium adolescentis*.[114] Further investigation is needed to determine the physiologically relevant forms of HD6.

1H.   Human Neutrophil Peptides (HNPs)

i.   Expression of HNPs. Rabbit neutrophil peptides were the first α-defensins to be identified and characterized.[33] Human neutrophil peptides (HNP1-3) were isolated from the

human neutrophils in 1985.[34,35] HNP1-3 constitute about 30-50% of the proteins in azurophil granules and 5-7% of total neutrophil protein content.[115] HNP4 was identified in 1989 through genomic data and later its expression was confirmed.[116] In humans, HNPs are also expressed in monocytes[117] and natural killer T cells.[118] The peptide are synthesized as prepropeptides in the promyelocytes and during the maturation of bone marrow cells, the propiece is cleaved.[119] Thus, the mature HNPs are stored in the azurophil granules.[119,120] In the neutrophils alone, ~250 mg of HNPs in total are produced per day. When the neutrophils engulf pathogenic bacteria, the antimicrobial contents of the granules are released into the phagocytic vacuoles, making the local concentrations of the HNPs ~10 mg/mL.[47] The peptides display broad-spectrum antimicrobial activities against Gram-positive and Gram-negative bacteria, antifungal activity, and activity against enveloped viruses.[34]

ii.   **Structure and Folding of HNPs.** HNP1 (30-aa) and HNP3 (30-aa) differ from HNP2 (29-aa) by single amino acid at the N-terminus (Figure 1.2).[35] In contrast, HNP4 is 34-amino acid peptide with a different sequence.[121] The structural elements such as the invariant Gly resulting in the β-bulge,[122] and the Arg-Glu salt bridge described above for HD5 are conserved in all of the α-defensins.[88] The first crystal structure of α-defensin reported was of HNP3, that revealed the distinct three-stranded β-sheet structure of the α-defensins.[123] This seminal work also indicated self-association and dimerization of defensins, later commonly observed for many defensins. Another detailed study on structure of HNP1 using solid-state NMR studies suggested a possible conformation of the membrane-inserted dimer-pore structure.[124]

iii.   **Functional and Antimicrobial Properties of HNPs.** The broad-spectrum antimicrobial activities of HNPs against various Gram-positive and Gram-negative bacteria, fungi, and viruses were attributed to the cationic nature of these peptides.[125] The interaction of HNP1-3 with bacterial outer and inner-membranes was tested using lactose permease deficient *E. coli* ML-35 and *E. coli* ML-35p strains.[125] The *E. coli* ML-35 strain express cytoplasmic β-galactosidase while

E. coli ML-35p express both cytoplasmic β-galactosidase and a periplasmic lactase. Employing these strains, membrane permeabilization of HNPs was determined. In this work, Lehrer and coworkers showed that the cytoplasmic membrane permeabilization is required for the bacterial cell death. HNP1 displayed lectin-like behavior similar to HD5.[96,104] When studied further, H. G. Sahl and colleagues found that HNP1 binds weakly to lipid II, a precursor for the synthesis of peptidoglycan layer with a K_d of 2.19 x 10^{-6} M.[106] HNP1–3 are chemotactic for T lymphocytes or dendritic cells *in vitro*.[79]

1I. Human β-Defensins (HBDs)

i. **Expression and Significance of HBDs in Disease.** Zasloff and coworkers first isolated β-defensins, bovine tracheal antimicrobial peptide (TAP),[52] and bovine lingual antimicrobial peptide (LAP).[126] LPS activates and upregulates the induction of TAP.[127] The expression of β-defensins was identified not only in epithelial tissues, but also in PMN of cow (bovine β-defensin),[128] and chicken (gallinacins).[129]

In humans, the first β-defensin HBD1 was identified from the hemofiltrate.[130] HBD1 is present in nanomolar concentrations in the human plasma. Human epithelial tissues produce β-defensins in concentrations ranging from 10-100 μg/mL,[131] either constitutively (HBD-1)[131] or in response to infection (HBD2-4).[132] HBD2 and HBD3 were isolated from skin of patients suffering from psoriasis.[132,133] The β-defensins are not packaged in granules. Instead, the lipid permeability barrier of the skin contains these defensins, stored as mature peptides in the lamellar bodies of the skin.[134] The peptide concentrations vary in certain disease conditions. Increased amounts of HBD2 and HBD3 are expressed on the skin of patients suffering from psoriasis, while decreased expression is observed in a case of atopic dermatitis.[55] In the intestinal epithelium, the expression of HBDs is reduced in irritable bowel disease and Crohn's disease.[135] Antimicrobial activity of HBD1 is salt sensitive; in cystic fibrosis, HBD1 is inactivated due to high salt concentration in the airway surface liquid.[136] However, antimicrobial activity of HBD3 was found to be salt insensitive.[93,133]

ii.   Structure and Folding of HBDs. The β-defensins are struturally distinct from the α-defensins; HBDs contain an N-terminal α-helical motif followed by the three-stranded β-sheet structure (Figure 1.6).[137] The HBDs also form dimers and oligomers by aligning the β-2 strands of each monomer and forming extended β-sheet structures. Moreover, the formation of octamers of HBD2 was observed from the crystal structure.[138] In the β-defensins, the Glycine in (GXC)- motif on β2 involved in the formation of the β-bulge is conserved.[128] However, residues forming salt bridge in α-defensins are not conserved in β-defensins.[128]

iii.   Functional and Antimicrobial Properties of HBDs. HBDs display broad-spectrum antimicrobial activities against both Gram-positive and Gram-negative strains of bacteria along with antifungal and antiviral activities. Although the oxidized form HBD1 displays the least potent antimicrobial activity among HBD1-3 and is sensitive to salt concentrations, HBD1 is constitutively expressed on various epithelial tissues including skin and airway epithelia.[131,132,136] It was only recently that the reduced form of HBD1 was shown to exhibit potent antimicrobial activity.[139] Moreover, antimicrobial activity HBD2 is more selective against Gram-negative bacteria and *Candida albicans*. HBD3 is less sensitive to salt concentration in the assay buffer, and is active against both Gram-positive and Gram-negative bacteria.[133] *S. aureus* treated with HBD3 displayed distinct morphological changes, suggesting perforation of the cell wall and thereby lysis.[108] HBD3-treated cells accumulated UDP-MurNAc-pp, a precursor of lipid II in cell wall biosynthesis. Treatment of *Enterococcus faecalis* with HBD2 resulted in the focal disruption of virulence factors.[140] HBD2 also caused the toxin unfolding as observed with HNP1 and HD5.[105]

iv. **Immunomodulatory and Other Functions of HBDs.** HBDs play an important role in the sperm function including maturation and motility.[141] β-defensins activate adaptive immune responses by recruiting dendritic cells and T cells to sites of infection.[142] HBDs produced by keratinocytes contribute to in wound healing.[143]

Scheme 1.4. Timeline for Major Contributions in Defensin Field

Timeline is not drawn to scale
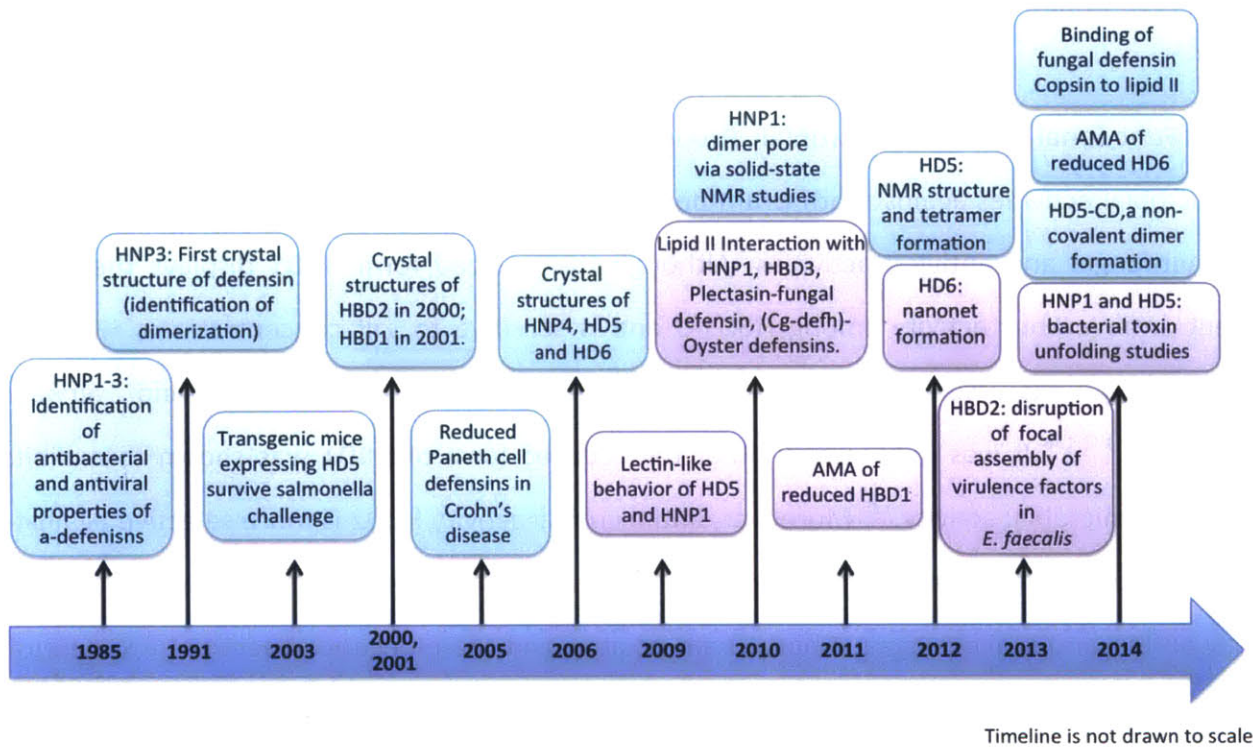
1J. Insect, Fungal, and Plant Defensins Displaying the CSαβ-motif

Invertebrate defensins display different tertiary structure to mammalian defensins. A structure consisting of an α-helical domain linked via disulfide linkages to a two-stranded antiparallel β-sheet, resulting in the cysteine-stabilized α-helix β-sheet (CSαβ) motif is a common feature in certain insect, plant, and fungal defensins. Though these peptides vary in the total number of cysteine residues and disulfide linkages, the CSαβ structural motif appears to be conserved.[39,40] It is interesting to note that the mammalian β-defensins display αββ-type

motif with a N-terminal α-helix and a three-stranded β-sheet motif that is similar in overall 3-D structural fold with the CSαβ motif.[39] The invertebrate, plant and fungal defensins that share such a CSαβ motif also seem to have 1) higher affinity to lipid II molecules, and 2) strain-selective activity, with more potent antibacterial activity against Gram-positive strains or antifungal properties.[39,92,109,144] Correspondingly, the vertebrate defensins do not have such a CSαβ motif and exhibit broad-spectrum antimicrobial activities.[44,107]

| α-defensin | β-defensin | θ-defensin | insect defensin CSαβ- fold |
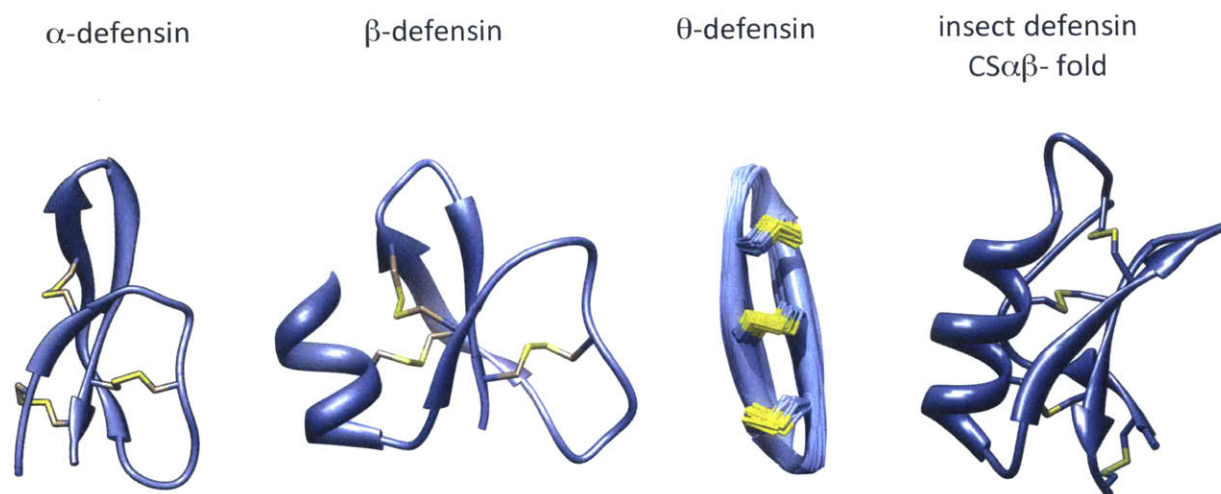
Figure 1.6. Structural features of vertebrate and invertebrate defensins. Representative structure of α-defensin (HD5, PDB 2LXZ)[90], β-defensin (HBD1, PDB 1IJV)[137], θ-defensin (RTD1, PDB 2LFY),[45] and insect defensin displaying CSαβ- fold (drosomycin, PDB 1MYN)[183].

1K.   Cathelicidins

Cathelicidins are structurally diverse group of peptides, all containing a conserved cathelin (acronym for cathepsin L inhibitor) domain at the N-terminus of the precursor peptide domain, which is cleaved to provide the mature cathelicidins.[145] These peptides are identified only in mammals so far, including humans, monkeys, horses, cattle, mice, pigs, rabbits, sheep, and goats.[146] The peptides are active against various bacteria, fungi, enveloped viruses, and parasites.[147] In cattle, sheep and pigs, more than ten cathelicidin genes are identified; whereas, in humans and mice only a single cathelicidin peptide is identified.[148] The primary site of

expression of cathelicidin in many animals is identified as the myeloid cells, and the peptides are stored as a propeptide in the large granules of neutrophils.[149]

The cathelicidins can be sub-classified based on structural properties (i.e., peptides with α-helical structures, extended helical, loop and β-sheet peptides with disulfide bridges). Human (LL37), rabbit (CAMP), mice (CRAMP) and monkey (RL-37) cathelicidins exhibit α-helical structure.[146] Several cathelicidins are rich in certain amino acid residues. For example, indolicidins are tryptophan-rich peptides expressed in cow and peptides rich in Pro-Arg (PR-motifs) such as PR-39 and bactenecins in cattle are certain examples of cathelicidins rich in specific amino acids.[149] Protegrins are two-disulfide linkages containing β-hairpin-type peptides of 16-18 residue length expressed in pigs.

Organisms (α-helical peptides)		Organism	Cow	Sheep	Pig
		α-helical peptides	BMAP-27, BMAP-28, BMAP-35	SMAP-29, SMAP-34,	PMAP-23, PMAP-36, PMAP-37
Human (hCAP-18)					
Rhesus macaque (RL-37)		β-hairpin-type peptides	dodecapeptide	s-dodecapeptide	Protegrins 1-5
Rabbit (CAP-18)		Pro-Arg rich peptides	Bac 5, Bac7	sBac7.5, sBac5	PR-39
Mouse (CRAMP)					
Rat (rCRAMP)		Tryptophan-rich peptide	Indolicidin		
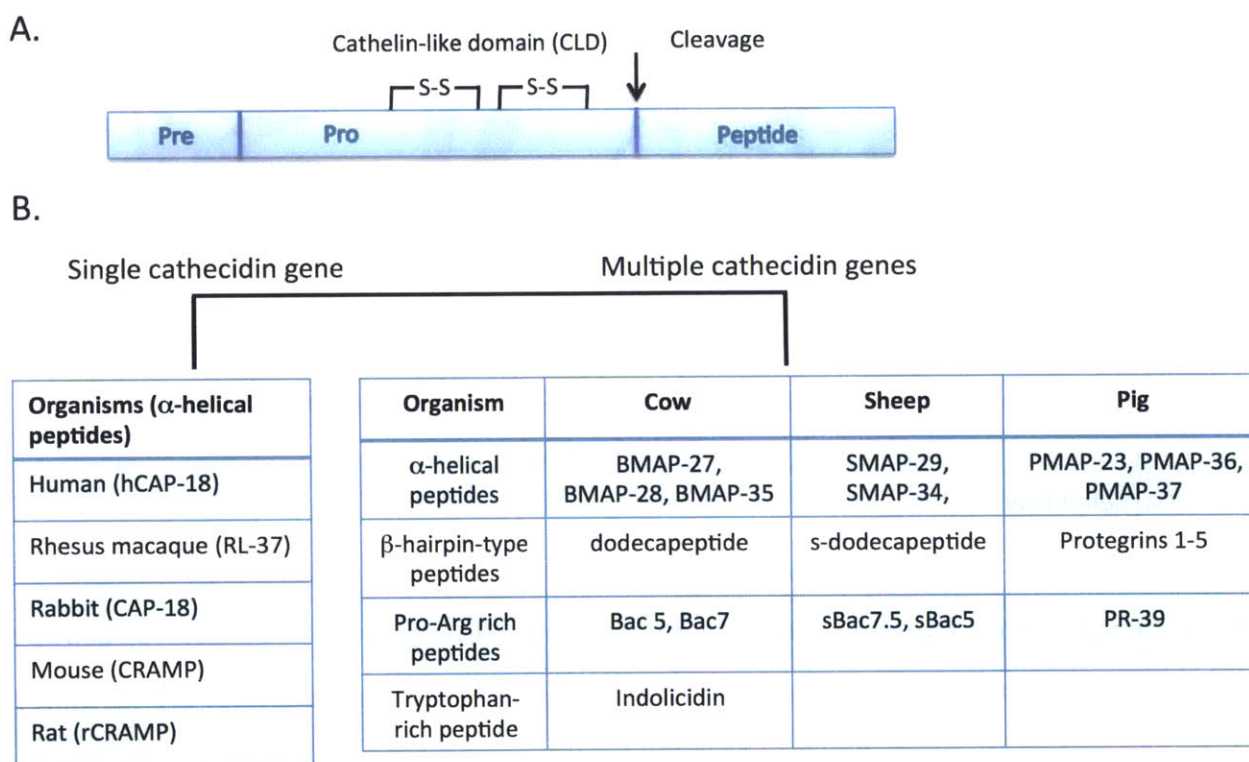
Figure 1.7. A) Schematic representation of prepropeptides of the cathelicidin family. **B)** Cathelicidin peptides from various organisms containing single and multiple cathelicidin genes, and displaying different structural characteristics are indicated.

Human Cathelicidin (LL-37).

In humans, the propeptide hCAP-18 (Figure 1.7) is processed to a 37 residue peptide fragment LL-37.[150] LL-37, expressed in neutrophils, is also identified at many epithelial sites including the airway epithelial cells along with the myeloid-derived cells.[151–153] In the neutrophils, hCAP-18 is stored in the peroxidase-negative specific granules.[150] Subsequently, after release from the granules, hCAP18 is cleaved by the enzyme proteinase 3, to release a 37-residue mature active peptide LL-37.[150] The peptide LL-37 itself displays broad-spectrum antimicrobial activity and exhibits synergy with other antimicrobial proteins such as lysozyme and lactoferrin.[152] Moreover, LL-37 binds to LPS and neutralizes the endotoxin shock.[153,154] The peptide also modulates the adaptive immune system and plays an important role in wound healing.[155] Mechanism of action studies with LL-37 suggest that the peptide kills bacteria via a carpet-model of bacterial membrane destabilization.[156,157]

1L.   Histatins

i.   **Expression and Significance of Histatins in Disease**. Histatins are a family of histidine-rich peptides (<40 residue length) secreted by human salivary glands.[158] Of the histatins, Hst1 and Hst3 are encoded by different genes, and the rest of the histatins are cleavage products of these two peptides.[159] Histatins display some antibacterial activity and potent antifungal activity at physiological concentrations (MIC ~ 15-30 µM).[160–162] Hst5, a cleavage product of Hst3, is the most active histatin against *Candida albicans*, an opportunistic pathogen that causes lesions in the mouth of immuno-compromised patients.[163]

ii.   **Structural and Functional Properties of Hst5**. Biophysical studies on the structure of Hst5 revealed that the peptide can adopt a non-amphipathic α-helical conformation and also bind to Zn^{2+} via a C-terminal (HisAspXXHis) motif.[164] Zinc binding increases the antibacterial activity of Hst5 against *Enterococcus faecalis*.[165] The N-terminal DSH sequence of Hst5 peptide is also an ATCUN motif (amino 'A' terminal 'T' copper 'C' and nickel 'N' binding motif).[166] By

retaining both metal-binding motifs, an analog of Hst5 that binds to DNA was constructed and has nuclease activity.[167]

iii.   Mechanism of Action of Hst5 Against *Candida albicans*. Studies have addressed the antifungal activity of Hst5. Hst5 did not cause membrane damage in *Candida albicans*.[160] A model that suggests the efflux and loss of ATP followed by increase in permeability to small molecules was proposed to explain the activity of Hst5 against *C. albicans*.[160] Another model suggested that Hst5 interferes with mitochondrial respiration chain and subsequently cause the formation of reactive oxygen species (ROS), leading to cell death.[168]

1M.   Antimicrobial Peptides from Invertebrates and Amphibians

Several peptides from invertebrates and amphibians have contributed to the fundamental understanding in the antimicrobial peptide field. Below are a few examples that provided major contributions toward mechanism of action and biophysical studies, paving the way for later AMP studies. The following linear antimicrobial peptides have the propensity to fold into α-helical structures. These peptides are often amphiphilic and interact with the negatively charged membranes of the microbial membranes.

i.   Melittin. Melittin is a 26-aa peptide toxin isolated from bee venom. It was the first peptide from insects reported to exhibit antimicrobial activity.[169] The N-terminus is hydrophobic, the C-terminal lobe is hydrophilic, and the C-terminus is amidated.[170] The peptide forms tetramers, and assumes a bent α-helical structure in solution.[170] Melittin integrates spontaneously in membranes, forming pores and causing lysis in both eukaryotic and microbial membranes.[169]

ii.   Cecropins: The cecropins (~40 aa) were isolated from giant silk worm *Hyalophora cecropia*.[171] Hans Boman and colleagues characterized these peptides and illustrated the role of

these AMPs in the protection of the silk worms which lack an adaptive immune system, against invading microbes.[172] The cecropins are produced as prepropeptides, which are processed to release the mature peptides.[173] 2D NMR studies of cecropin A revealed two helical domains.[174] The cecropins form bent α-helical structures and contain a proline hinge region.[175] The cecropins exhibit C-terminal amidation, a basic N-terminal lobe, and a hydrophobic C-terminal lobe. This hinge region separates the N- and C-terminal lobes. The cecropins exhibit broad-spectrum antimicrobial activity.[172] However, they do not exhibit toxicity to the host and differ from melittin in their hemolytic activities.[175]

iii.   **Magainins**. The first AMPs isolated from amphibians are bombinins,[176] and many of the peptides in this class are linear helical peptides. However, major advances in the field of antimicrobial peptides were made after the discovery of magainins, peptides isolated from the skin secretions of *Xenopus laevis* by Zasloff and coworkers.[177] The magainins, also produced as prepropeptides, are processed to release one copy of magainin 1 and two copies of magainin 2.[177] Similar to cecropins, magainins exhibit broad-spectrum antimicrobial activity and are not hemolytic.[178] The magainins are unstructured in solution and adopt α-helical structures when they come in contact with negatively charged membranes.[179] The L- and D-forms magainins displayed similar antimicrobial activity, suggesting that the peptide acted via formation of oligomeric pores, and without interacting with any specific cellular receptors during its antimicrobial action.[180] Transgenic plants expressing antimicrobial peptides, such as cecropin and magainin analogues, survived better against attacks from phytopathogens.[181] The magainins were also active against human melanoma cells in a study of local therapy in mice, further emphasizing the therapeutic potential of these peptides.[182]

1N.   Summary and Overview of the Thesis Chapters

The motivation for this work is to gain more insights into, and to understand the fundamental details of the antimicrobial activity of HD5. A major challenge in studying HD5 had

been to obtain large quantities of pure peptide. Recombinant methods for overexpression of HD5 can be time-consuming, and are less amenable to modifying HD5 with desired functional groups such as fluorophores and affinity tags. **In Chapter 2**, the development of robust synthetic protocols for obtaining HD5 and modified HD5 using Fmoc-based solid-phase peptide synthesis are discussed. Using these synthetic protocols, functional moieties such as fluorophores were appended to HD5 at various positions. The fluorophore-modified peptides were folded to the desired oxidized forms and their photophysical characterization was performed. The antimicrobial activities of the generated family of HD5 derivatives were also evaluated. This work provided the peptide toolkit necessary for the studies, which are described in **Chapters 3 and 4**.

In Chapter 3, the attack of HD5 on Gram-negative bacteria was studied using *E. coli, a* commensal and an opportunistic pathogen in the gut, as a model organism. The attack of *E. coli* and localization of HD5 was visualized using various microscopy-based techniques. HD5 treatment caused distinct morphological changes such as bleb formation, clumping, and elongation in *E. coli* and other Gram-negative bacteria. The effect of growth phase, the presence of salt and cations in the antimicrobial assay buffer, and the significance of disulfide linkages on the antimicrobial activity of HD5 were probed. Employing fluorophore-labeled HD5 derivatives, we determined that HD5 enters bacterial cytoplasm and localizes near the cell poles and cell septa. This study suggests that a target-mediated antimicrobial mechanism may be at play.

In Chapter 4, the attack of HD5 on Gram-positive bacteria was studied using *S. aureus, E. faecalis*, and *B. subtilis*. These three strains correspond to pathogenic, opportunistic pathogen, and non-pathogenic bacteria, respectively. The antimicrobial activity of HD5 against these organisms was determined and the effect of salt in the AMA media was probed. The morphological changes induced upon treatment of bacteria with HD5 were visualized using various microscopy techniques. In this study, we demonstrate that the morphology of $HD5_{ox}$

treated Gram-positive bacteria is distinct from the morphology of lysis-mediated cell death caused by other antimicrobial peptides such as LL-37 and melittin.

In the course of identifying putative target or affected cellular process, HD5 interaction with certain cellular components of *E. coli* was investigated and these studies are discussed in **Chapter 5.** The effect of outer-membrane composition was studied using various strains from the Keio Collection and mutants with leaky outer membranes. Additionally, the effect of various anionic lipids on the localization of HD5 during antimicrobial action was explored. Preliminary studies were performed to examine the assembly of bacterial cell division machinery upon treatment with HD5. From these studies, it can be inferred that during the attack of HD5 on Gram-negative bacteria, HD5 crosses the outer membrane, permeabilizes the inner membrane and kills the bacteria via. a non-lytic mechanism of action.

In Appendix 1, the overexpression, purification and characterization of a family of tryptophan mutants of HD5 are discussed. The details of development of another set of tools and handles such as biotin- and azide- modification on HD5 are discussed in the **Appendix 2**.

10.   References

(1) World Health Organization. (2015) World Health Statistics 2015.

(2) Zimlichman, E., Henderson, D., Tamir, O., Franz, C., Song, P., Yamin, C. K., Keohane, C., Denham, C. R., and Bates, D. W. (2013) Health care–associated Infections. *JAMA Intern. Med. 173*, 2039–2046.

(3) Walsh, C. (2003) Antibiotics: Actions, Origins, Resistance. ASM Press, Washington, DC.

(4) Davies, J., and Davies, D. (2010) Origins and evolution of antibiotic resistance. *Microbiol. Mol. Biol. Rev. 74*, 417–433.

(5) Gram, H. C. (1884) Über die isolierte Färbung der Schizomyceten in Schnitt- und Trockenpräparaten. *Fortschr. Med. 2*, 185–189.

(6) Silhavy, T. J., Kahne, D., and Walker, S. (2010) The bacterial cell envelope. *Cold Spring Harb. Perspect. Biol. 2*, a000414.

(7) Scheffers, D.-J., and Pinho, M. G. (2005) Bacterial cell wall synthesis: new insights from localization studies. *Microbiol. Mol. Biol. Rev. 69*, 585–607.

(8) Raetz, C. R. H., and Whitfield, C. (2002) Lipopolysaccharide endotoxins. *Annu. Rev. Biochem.*

71, 635–700.

(9) Dramsi, S., Magnet, S., Davison, S., and Arthur, M. (2008) Covalent attachment of proteins to peptidoglycan. *FEMS Microbiol. Rev. 32*, 307–320.

(10) Wülfing, C., and Plückthun, A. (1994) Protein folding in the periplasm of *Escherichia coli. Mol. Microbiol. 12*, 685–692.

(11) Raetz, C. R. H., and Dowhan, W. (1990) Biosynthesis and function of phospholipids in *Escherichia coli. J. Biol. Chem. 265*, 1235–1238.

(12) Dalbey, R. E., Wang, P., and Kuhn, A. (2011) Assembly of bacterial inner membrane proteins. *Annu. Rev. Biochem. 80*, 161–187.

(13) Weidenmaier, C., and Peschel, A. (2008) Teichoic acids and related cell-wall glycopolymers in Gram-positive physiology and host interactions. *Nat. Rev. Microbiol. 6*, 276–287.

(14) Scott, J. R., and Barnett, T. C. (2006) Surface proteins of Gram-positive bacteria and how they get there. *Annu. Rev. Microbiol. 60*, 397–423.

(15) Walsh, C. (2003) Where will new antibiotics come from? *Nat. Rev. Microbiol. 1*, 65–70.

(16) Fischbach, M. A., and Walsh, C. T. (2009) Antibiotics for emerging pathogens. *Science 325*, 1089–1093.

(17) Walsh, C. (2000) Molecular mechanisms that confer antibacterial drug resistance. *Nature 406*, 775–781.

(18) Wong, K. K., and Pompliano, D. L. (1998) Peptidoglycan biosynthesis: unexploited antibacterial targets within a familiar pathway, in *Resolving the antibioitc paradox: progress in understanding drug resistance and development of new antibiotics* (Rosen, B. P., and Mobashery, S., Eds.), pp 197–217. Springer US, Boston, MA.

(19) Dwyer, D. J., Belenky, P. A., Yang, J. H., MacDonald, I. C., Martell, J. D., Takahashi, N., Chan, C. T. Y., Lobritz, M. A., Braff, D., Schwarz, E. G., Ye, J. D., Pati, M., Vercruysse, M., Ralifo, P. S., Allison, K. R., Khalil, A. S., Ting, A. Y., Walker, G. C., and Collins, J. J. (2014) Antibiotics induce redox-related physiological alterations as part of their lethality. *Proc. Natl. Acad. Sci. U. S. A. 111*, E2100–E2109.

(20) Bosch, F., and Rosich, L. (2008) The contributions of Paul Ehrlich to pharmacology: a tribute on the occasion of the centenary of his Nobel Prize. *Pharmacology 82*, 171–179.

(21) Winau, F., Westphal, O., and Winau, R. (2004) Paul Ehrlich - In search of the magic bullet. *Microbes Infect. 6*, 786–789.

(22) Rubin, R. P. (2007) A brief history of great discoveries in pharmacology: in celebration of the centennial anniversary of the founding of the American Society of Pharmacology and Experimental Therapeutics. *Pharmacol. Rev. 59*, 289–359.

(23) Wolfson, J. S., and Hooper, D. C. (1989) Fluoroquinolone antimicrobial agents. *Clin. Microbiol. Rev. 2*, 378–424.

(24) Wehrli, W., and Staehelin, M. (1971) Actions of the rifamycins. *Bacteriol. Rev. 35*, 290–309.

(25) Masters, P. A., O'Bryan, T. A., Zurlo, J., Miller, D. Q., and Joshi, N. (2003) Trimethoprim-sulfamethoxazole revisited. *Arch. Intern. Med. 163*, 402–410.

(26) Goldberg, I. H. (1965) Mode of action of antibiotics. II. Drugs affecting nucleic acid and protein synthesis. *Am. J. Med. 39*, 722–752.

(27) Brötz-Oesterhelt, H., Beyer, D., Kroll, H.-P., Endermann, R., Ladel, C., Schroeder, W., Hinzen, B., Raddatz, S., Paulsen, H., Henninger, K., Bandow, J. E., Sahl, H.-G., and Labischinski, H. (2005) Dysregulation of bacterial proteolytic machinery by a new class of antibiotics. *Nat. Med. 11*, 1082–1087.

(28) Fleming, A. (1922) On a remarkable bacteriolytic element found in tissues and secretions. *Proc. R. Soc. London.Series B, 93*, 306–317.

(29) Hancock, R. E. W., and Sahl, H.-G. (2006) Antimicrobial and host-defense peptides as new anti-infective therapeutic strategies. *Nat. Biotechnol. 24*, 1551–1557.

(30) Hirsch, J. G., and Cohn, Z. A. (1960) Degranulation of polymorphonuclear leucocytes following phagocytosis of microorganisms. *J. Exp. Med. 112*, 1005–1014.

(31) Hirsch, J. G. (1956) Phagocytin: A bacterial substance from polymorphonuclear leucocytes. *J. Exp. Med. 103*, 589–611.

(32) Zeya, H. I., and Spitznagel, J. K. (1966) Antimicrobial specificity of leukocyte lysosomal cationic proteins. *Science. 154*, 1049–1051.

(33) Lehrer, R. I., Selsted, M. E., Szklarek, D., and Fleischmann, J. (1983) Antibacterial activity of microbicidal cationic proteins 1 and 2, natural peptide antibiotics of rabbit lung macrophages. *Infect. Immun. 42*, 10–14.

(34) Ganz, T., Selsted, M. E., Szklarek, D., Harwig, S. S. L., Daher, K., Bainton, D. F., and Lehrer, R. I. (1985) Defensins. Natural peptide antibiotics of human neutrophils. *J. Clin. Invest. 76*, 1427–1435.

(35) Selsted, M. E., Harwig, S. S. L., Ganz, T., Schilling, J. W., and Lehrer, R. I. (1985) Primary structures of three human neutrophil defensins. *J. Clin. Invest. 76*, 1436–1439.

(36) Selsted, M. E., Szklarek, D., and Lehrer, R. I. (1984) Purification and antibacterial activity of antimicrobial peptides of rabbit granulocytes. *Infect. Immun. 45*, 150–154.

(37) Wu, J., Gao, B., and Zhu, S. (2014) The Fungal Defensin Family Enlarged. *Pharmaceuticals 7*, 866–880.

(38) Zou, J., Mercier, C., Koussounadis, A., and Secombes, C. (2007) Discovery of multiple beta-defensin like homologues in teleost fish. *Mol. Immunol. 44*, 638–647.

(39) Thomma, B. P. H. J., Cammue, B. P. A., and Thevissen, K. (2002) Plant defensins. *Planta 216*, 193–202.

(40) Hoffmann, J. A. (1995) Innate immunity of insects. *Curr. Opin. Immunol. 7*, 4–10.

(41) Destoumieux, D., Bulet, P., Loew, D., Dorsselaer, A. Van, Rodriguez, J., and Bachère, E. (1997) Penaeidins , a new family of antimicrobial peptides isolated from the shrimp Penaeus vannamei (Decapoda). *J. Biol. Chem. 272*, 28398–28406.

(42) Zhang, G., and Sunkara, L. T. (2014) Avian antimicrobial host defense peptides: from biology to therapeutic applications. *Pharmaceuticals 7*, 220–247.

(43) Lehrer, R. I., and Ganz, T. (1999) Antimicrobial peptides in mammalian and insect host defence. *Curr. Opin. Immunol. 11*, 23–27.

(44) Wilmes, M., and Sahl, H.-G. (2014) Defensin-based anti-infective strategies. *Int. J. Med. Microbiol. 304*, 93–99.

(45) Conibear, A. C., Rosengren, K. J., Harvey, P. J., and Craik, D. J. (2012) Structural characterization of the cyclic cystine ladder motif of θ-defensins. *Biochemistry 51*, 9718–9726.

(46) Iwanaga, S., Kawabata, S., and Muta, T. (1998) New types of clotting factors and defense molecules found in horseshoe crab hemolymph: their structures and functions. *J. Biochem. 123*, 1–15.

(47) Lehrer, R. I., and Lu, W. (2012) α-Defensins in human innate immunity. *Immunol. Rev. 245*, 84–112.

(48) Eisenhauer, P. B., and Lehrer, R. I. (1992) Mouse neutrophils lack defensins. *Infect. Immun. 60*, 3446–3447.

(49) Ouellette, A. J., Hsieh, M. M., Nosek, M. T., Cano-Gauci, D. F., Huttner, K. M., Buick, R. N., and Selsted, M. E. (1994) Mouse Paneth cell defensins: primary structures and antibacterial activities of numerous cryptdin isoforms. *Infect. Immun. 62*, 5040–5047.

(50) Fjell, C. D., Jenssen, H., Fries, P., Aich, P., Griebel, P., Hilpert, K., Hancock, R. E. W., and Cherkasov, A. (2008) Identification of novel host defense peptides and the absence of alpha-defensins in the bovine genome. *Proteins 73*, 420–30.

(51) Nguyen, T. X., Cole, A. M., and Lehrer, R. I. (2003) Evolution of primate θ-defensins: A serpentine path to a sweet tooth. *Peptides 24*, 1647–1654.

(52) Diamond, G., Zasloff, M., Eck, H., Brasseur, M., Maloy, W. L., and Bevins, C. L. (1991) Tracheal antimicrobial peptide, a cysteine-rich peptide from mammalian tracheal mucosa: peptide isolation and cloning of a cDNA. *Proc. Natl. Acad. Sci. U. S. A. 88*, 3952–3956.

(53) Tang, Y. Q., Yuan, J., Osapay, G., Osapay, K., Tran, D., Miller, C. J., Ouellette, A. J., and Selsted, M. E. (1999) A cyclic antimicrobial peptide produced in primate leukocytes by the ligation of two truncated alpha-defensins. *Science 286*, 498–502.

(54) Yasin, B., Wang, W., Pang, M., Cheshenko, N., Hong, T., Waring, A. J., Herold, B. C., Wagar, E. A., and Lehrer, R. I. (2004) Theta defensins protect cells from infection by herpes simplex virus by inhibiting viral adhesion and entry. *J. Virol. 78*, 5147–5156.

(55) Selsted, M. E., and Ouellette, A. J. (2005) Mammalian defensins in the antimicrobial immune response. *Nat. Immunol. 6*, 551–557.

(56) Spencer, J. D., Hains, D. S., Porter, E., Bevins, C. L., DiRosario, J., Becknell, B., Wang, H., and Schwaderer, A. L. (2012) Human alpha defensin 5 expression in the human kidney and urinary tract. *PLoS One 7*, e31712.

(57) Quayle, A. J., Porter, E. M., Nussbaum, A. A., Wang, Y. M., Brabec, C., Yip, K.-P., and Mok, S. C. (1998) Gene expression, immunolocalization, and secretion of human defensin-5 in human female reproductive tract. *Am. J. Pathol. 152*, 1247–1258.

(58) Linzmeier, R., Ho, C. H., Hoang, B. V., and Ganz, T. (1999) A 450-kb contig of defensin genes on human chromosome 8p23. *Gene 233*, 205–211.

(59) Linzmeier, R. M., and Ganz, T. (2005) Human defensin gene copy number polymorphisms: Comprehensive analysis of independent variation in alpha-and beta-defensin regions at 8p22-p23. *Genomics 86*, 423–430.

(60) Hollox, E. J. (2008) Copy number variation of beta-defensins and relevance to disease. *Cytogenet. Genome Res. 123*, 148–155.

(61) Clevers, H. C., and Bevins, C. L. (2013) Paneth cells: maestros of the small intestinal crypts. *Annu. Rev. Physiol. 75*, 289–311.

(62) Sato, T., van Es, J. H., Snippert, H. J., Stange, D. E., Vries, R. G., van den Born, M., Barker, N., Shroyer, N. F., van de Wetering, M., and Clevers, H. (2011) Paneth cells constitute the niche for Lgr5 stem cells in intestinal crypts. *Nature 469*, 415–418.

(63) Jones, D. E., and Bevins, C. L. (1992) Paneth cells of the human small intestine express an antimicrobial peptide gene. *J. Biol. Chem. 267*, 23216–23225.

(64) Jones, D. E., and Bevins, C. L. (1993) Defensin-6 mRNA in human Paneth cells: implications for antimicrobial peptides in host defense of the human bowel. *FEBS Lett. 315*, 187–192.

(65) Ouellette, A. J., and Selsted, M. E. (1996) Paneth cell defensins: endogenous peptide components of intestinal host defense. *FASEB J. 10*, 1280–1289.

(66) Chairatana, P., Chu, H., Castillo, P. A., Shen, B., Bevins, C. L., and Nolan, E. M. (2016) Proteolysis triggers self-assembly and unmasks innate immune function of a human α-defensin peptide. *Chem. Sci. 00*, 1–15.

(67) Giblin, L. J., Chang, C. J., Bentley, A. F., Frederickson, C., Lippard, S. J., and Frederickson, C. J. (2006) Zinc-secreting Paneth cells studied by ZP fluorescence. *J. Histochem. Cytochem. 54*, 311–316.

(68) Dinsdale, D. (1984) Ultrastructural localization of zinc and calcium within the granules of rat Paneth cells. *J. Histochem. Cytochem. 32*, 139–145.

(69) Wehkamp, J., Salzman, N. H., Porter, E., Nuding, S., Weichenthal, M., Petras, R. E., Shen, B., Schaeffeler, E., Schwab, M., Linzmeier, R., Feathers, R. W., Chu, H., Lima, H., Fellermann, K., Ganz, T., Stange, E. F., and Bevins, C. L. (2005) Reduced Paneth cell alpha-defensins in

ileal Crohn's disease. *Proc. Natl. Acad. Sci. U. S. A. 102*, 18129–18134.

(70) Ghosh, D., Porter, E., Shen, B., Lee, S. K., Wilk, D., Drazba, J., Yadav, S. P., Crabb, J. W., Ganz, T., and Bevins, C. L. (2002) Paneth cell trypsin is the processing enzyme for human defensin-5. *Nat. Immunol. 3*, 583–590.

(71) Wehkamp, J., Wang, G., Kübler, I., Nuding, S., Gregorieff, A., Schnabel, A., Kays, R. J., Fellermann, K., Burk, O., Schwab, M., Clevers, H., Bevins, C. L., and Stange, E. F. (2007) The Paneth cell alpha-defensin deficiency of ileal Crohn's disease is linked to Wnt/Tcf-4. *J. Immunol. 179*, 3109–3118.

(72) Porter, E. M., Liu, L., Oren, A., Anton, P. A., and Ganz, T. (1997) Localization of human intestinal defensin 5 in Paneth cell granules. *Infect. Immun. 65*, 2389–2395.

(73) Wehkamp, J., Chu, H., Shen, B., Feathers, R. W., Kays, R. J., Lee, S. K., and Bevins, C. L. (2006) Paneth cell antimicrobial peptides: Topographical distribution and quantification in human gastrointestinal tissues. *FEBS Lett. 580*, 5344–5350.

(74) Mallow, E. B., Harris, A., Salzman, N., Russell, J. P., DeBerardinis, R. J., Ruchelli, E., and Bevins, C. L. (1996) Human enteric defensins. Gene structure and developmental expression. *J. Biol. Chem. 271*, 4038–4045.

(75) Salzman, N. H., Polin, R. A., Harris, M. C., Ruchelli, E., Hebra, A., Zirin-Butler, S., Jawad, A., Martin Porter, E., and Bevins, C. L. (1998) Enteric defensin expression in necrotizing enterocolitis. *Pediatr. Res. 44*, 20–26.

(76) Hooper, L. V, and Gordon, J. I. (2001) Commensal host-bacterial relationships in the gut. *Science 292*, 1115–1118.

(77) Hooper, L. V, Littman, D. R., and Macpherson, A. J. (2012) Interactions between the microbiota and the immune system. *Science 336*, 1268–1273.

(78) Vaishnava, S., Behrendt, C. L., Ismail, A. S., Eckmann, L., and Hooper, L. V. (2008) Paneth cells directly sense gut commensals and maintain homeostasis at the intestinal host-microbial interface. *Proc. Natl. Acad. Sci. U. S. A. 105*, 20858–20863.

(79) Ericksen, B., Wu, Z., Lu, W., and Lehrer, R. I. (2005) Antibacterial activity and specificity of the six human alpha-defensins. *Antimicrob. Agents Chemother. 49*, 269–275.

(80) Porter, E. M., van Dam, E., Valore, E. V, and Ganz, T. (1997) Broad-spectrum antimicrobial activity of human intestinal defensin 5. *Infect. Immun. 65*, 2396–2401.

(81) Nuding, S., Zabel, L. T., Enders, C., Porter, E., Fellermann, K., Wehkamp, J., Mueller, H. A. G., and Stange, E. F. (2009) Antibacterial activity of human defensins on anaerobic intestinal bacterial species: a major role of HBD-3. *Microbes Infect. 11*, 384–393.

(82) Wommack, A. J., Ziarek, J. J., Tomaras, J., Chileveru, H. R., Zhang, Y., Wagner, G., and Nolan, E. M. (2014) Discovery and characterization of a disulfide-locked C_2-symmetric defensin peptide. *J. Am. Chem. Soc. 136*, 13494–13497.

(83) Salzman, N. H., Ghosh, D., Huttner, K. M., Paterson, Y., and Bevins, C. L. (2003) Protection

against enteric salmonellosis in transgenic mice expressing a human intestinal defensin. *Nature 422*, 522–526.

(84) Salzman, N. H., Hung, K., Haribhai, D., Chu, H., Karlsson-Sjöberg, J., Amir, E., Teggatz, P., Barman, M., Hayward, M., Eastwood, D., Stoel, M., Zhou, Y., Sodergren, E., Weinstock, G. M., Bevins, C. L., Williams, C. B., and Bos, N. A. (2010) Enteric defensins are essential regulators of intestinal microbial ecology. *Nat. Immunol. 11*, 76–83.

(85) Kelly, P., Feakins, R., Domizio, P., Murphy, J., Bevins, C., Wilson, J., McPhail, G., Poulsom, R., and Dhaliwal, W. (2004) Paneth cell granule depletion in the human small intestine under infective and nutritional stress. *Clin. Exp. Immunol. 135*, 303–309.

(86) Zhang, Y., Cougnon, F. B. L., Wanniarachchi, Y. A., Hayden, J. A., and Nolan, E. M. (2013) Reduction of human defensin 5 affords a high-affinity zinc-chelating peptide. *ACS Chem. Biol. 8*, 1907–1911.

(87) Rajabi, M., de Leeuw, E., Pazgier, M., Li, J., Lubkowski, J., and Lu, W. (2008) The conserved salt bridge in human alpha-defensin 5 is required for its precursor processing and proteolytic stability. *J. Biol. Chem. 283*, 21509–21518.

(88) Wu, Z., Li, X., de Leeuw, E., Ericksen, B., and Lu, W. (2005) Why Is the Arg5-Glu13 Salt Bridge Conserved in Mammalian -Defensins? *J. Biol. Chem. 280*, 43039–43047.

(89) Szyk, A., Wu, Z., Tucker, K., Yang, D., Lu, W., and Lubkowski, J. (2006) Crystal structures of human alpha-defensins HNP4, HD5, and HD6. *Protein Sci. 15*, 2749–2760.

(90) Wommack, A. J., Robson, S. A., Wanniarachchi, Y. A., Wan, A., Turner, C. J., Wagner, G., and Nolan, E. M. (2012) NMR solution structure and condition-dependent oligomerization of the antimicrobial peptide human defensin 5. *Biochemistry 51*, 9624–9637.

(91) Wanniarachchi, Y. A., Kaczmarek, P., Wan, A., and Nolan, E. M. (2011) Human defensin 5 disulfide array mutants: disulfide bond deletion attenuates antibacterial activity against *Staphylococcus aureus. Biochemistry 50*, 8005–8017.

(92) Essig, A., Hofmann, D., Münch, D., Gayathri, S., Künzler, M., Kallio, P. T., Sahl, H.-G., Wider, G., Schneider, T., and Aebi, M. (2014) Copsin, a novel peptide-based fungal antibiotic interfering with the peptidoglycan synthesis. *J. Biol. Chem. 289*, 34953–34964.

(93) Dhople, V., Krukemeyer, A., and Ramamoorthy, A. (2006) The human beta-defensin-3, an antibacterial peptide with multiple biological functions. *Biochim. Biophys. Acta 1758*, 1499–1512.

(94) de Leeuw, E., Burks, S. R., Li, X., Kao, J. P. Y., and Lu, W. (2007) Structure-dependent functional properties of human defensin 5. *FEBS Lett. 581*, 515–520.

(95) Rajabi, M., Ericksen, B., Wu, X., de Leeuw, E., Zhao, L., Pazgier, M., and Lu, W. (2012) Functional determinants of human enteric α-defensin HD5: crucial role for hydrophobicity at dimer interface. *J. Biol. Chem. 287*, 21615–21627.

(96) Lehrer, R. I., Jung, G., Ruchala, P., Andre, S., Gabius, H. J., and Lu, W. (2009) Multivalent binding of carbohydrates by the human alpha-defensin, HD5. *J. Immunol. 183*, 480–490.

(97) Nuding, S., Gersemann, M., Hosaka, Y., Konietzny, S., Schaefer, C., Beisner, J., Schroeder, B. O., Ostaff, M. J., Saigenji, K., Ott, G., Schaller, M., Stange, E. F., and Wehkamp, J. (2013) Gastric antimicrobial peptides fail to eradicate Helicobacter pylori infection due to selective induction and resistance. *PLoS One 8*, e73867.

(98) Furci, L., Baldan, R., Bianchini, V., Trovato, A., Ossi, C., Cichero, P., and Cirillo, D. M. (2015) New role for human α-defensin 5 in the fight against hypervirulent *Clostridium difficile* strains. *Infect. Immun. 83*, 986–995.

(99) Smith, J. G., Silvestry, M., Lindert, S., Lu, W., Nemerow, G. R., and Stewart, P. L. (2010) Insight into the mechanisms of adenovirus capsid disassembly from studies of defensin neutralization. *PLoS Pathog. 6*, e1000959.

(100) Gounder, A. P., Wiens, M. E., Wilson, S. S., Lu, W., and Smith, J. G. (2012) Critical determinants of human α-defensin 5 activity against non-enveloped viruses. *J. Biol. Chem. 287*, 24554–24562.

(101) Grigat, J., Soruri, A., Forssmann, U., Riggert, J., and Zwirner, J. (2007) Chemoattraction of macrophages, T lymphocytes, and mast cells is evolutionarily conserved within the human alpha-defensin family. *J. Immunol. 179*, 3958–3965.

(102) Brogden, K. A. (2005) Antimicrobial peptides: pore formers or metabolic inhibitors in bacteria? *Nat. Rev. Microbiol. 3*, 238–250.

(103) Hadjicharalambous, C., Sheynis, T., Jelinek, R., Shanahan, M. T., Ouellette, A. J., and Gizeli, E. (2008) Mechanisms of alpha-defensin bactericidal action: comparative membrane disruption by Cryptdin-4 and its disulfide-null analogue. *Biochemistry 47*, 12626–12634.

(104) Wei, G., de Leeuw, E., Pazgier, M., Yuan, W., Zou, G., Wang, J., Ericksen, B., Lu, W.-Y., Lehrer, R. I., and Lu, W. (2009) Through the looking glass, mechanistic insights from enantiomeric human defensins. *J. Biol. Chem. 284*, 29180–29192.

(105) Kudryashova, E., Quintyn, R., Seveau, S., Lu, W., Wysocki, V. H., and Kudryashov, D. S. (2014) Human defensins facilitate local unfolding of thermodynamically unstable regions of bacterial protein toxins. *Immunity 41*, 709–721.

(106) de Leeuw, E., Li, C., Zeng, P., Li, C., Diepeveen-de Buin, M., Lu, W.-Y., Breukink, E., and Lu, W. (2010) Functional interaction of human neutrophil peptide-1 with the cell wall precursor lipid II. *FEBS Lett. 584*, 1543–1548.

(107) Wilmes, M., Cammue, B. P. A., Sahl, H.-G., and Thevissen, K. (2011) Antibiotic activities of host defense peptides: more to it than lipid bilayer perturbation. *Nat. Prod. Rep. 28*, 1350–1358.

(108) Sass, V., Schneider, T., Wilmes, M., Körner, C., Tossi, A., Novikova, N., Shamova, O., and Sahl, H.-G. (2010) Human beta-defensin 3 inhibits cell wall biosynthesis in *Staphylococci*. *Infect. Immun. 78*, 2793–2800.

(109) Schneider, T., Kruse, T., Wimmer, R., Wiedemann, I., Sass, V., Pag, U., Jansen, A., Nielsen, A. K., Mygind, P. H., Raventós, D. S., Neve, S., Ravn, B., Bonvin, A. M. J. J., De Maria, L.,

Andersen, A. S., Gammelgaard, L. K., Sahl, H.-G., and Kristensen, H.-H. (2010) Plectasin, a fungal defensin, targets the bacterial cell wall precursor Lipid II. *Science 328*, 1168–1172.

(110) Furci, L., Tolazzi, M., Sironi, F., Vassena, L., and Lusso, P. (2012) Inhibition of HIV-1 Infection by Human α-Defensin-5, a Natural Antimicrobial Peptide Expressed in the Genital and Intestinal Mucosae. *PLoS One 7*, e45208.

(111) Klotman, M. E., Rapista, A., Teleshova, N., Micsenyi, A., Jarvis, G. A., Lu, W., Porter, E., and Chang, T. L. (2008) Neisseria gonorrhoeae-Induced Human Defensins 5 and 6 Increase HIV Infectivity: Role in Enhanced Transmission. *J. Immunol. 180*, 6176–6185.

(112) Chu, H., Pazgier, M., Jung, G., Nuccio, S.-P., Castillo, P. A., de Jong, M. F., Winter, M. G., Winter, S. E., Wehkamp, J., Shen, B., Salzman, N. H., Underwood, M. A., Tsolis, R. M., Young, G. M., Lu, W., Lehrer, R. I., Bäumler, A. J., and Bevins, C. L. (2012) Human α-defensin 6 promotes mucosal innate immunity through self-assembled peptide nanonets. *Science 337*, 477–481.

(113) Chairatana, P., and Nolan, E. M. (2014) Molecular basis for self-assembly of a human host-defense peptide that entraps bacterial pathogens. *J. Am. Chem. Soc. 136*, 13267–13276.

(114) Schroeder, B. O., Ehmann, D., Precht, J. C., Castillo, P. A., Küchler, R., Berger, J., Schaller, M., Stange, E. F., and Wehkamp, J. (2014) Paneth cell α-defensin 6 (HD-6) is an antimicrobial peptide. *Mucosal Immunol. 8*, 661–671.

(115) Rice, W. G., Ganz, T., Kinkade, J. M., Selsted, M. E., Lehrer, R. I., and Parmley, R. T. (1987) Defensin-rich dense granules of human neutrophils. *Blood 70*, 757–765.

(116) Harwig, S. S. L., Park, A. S. K., and Lehrer, R. I. (1992) Characterization of defensin precursors in mature human neutrophils. *Blood 79*, 1532–1537.

(117) Mackewicz, C. E., Yuan, J., Tran, P., Diaz, L., Mack, E., Selsted, M. E., and Levy, J. A. (2003) alpha-Defensins can have anti-HIV activity but are not CD8 cell anti-HIV factors. *AIDS 17*, F23–32.

(118) Chalifour, A., Jeannin, P., Gauchat, J.-F., Blaecke, A., Malissard, M., N'Guyen, T., Thieblemont, N., and Delneste, Y. (2004) Direct bacterial protein PAMP recognition by human NK cells involves TLRs and triggers alpha-defensin production. *Blood 104*, 1778–1783.

(119) Cowland, J. B., and Borregaard, N. (1999) The individual regulation of granule protein mRNA levels during neutrophil maturation explains the heterogeneity of neutrophil granules. *J. Leukoc. Biol. 66*, 989–995.

(120) Liu, L., and Ganz, T. (1995) The pro region of human neutrophil defensin contains a motif that is essential for normal subcellular sorting. *Blood 85*, 1095–1103.

(121) Wu, Z., Ericksen, B., Tucker, K., Lubkowski, J., and Lu, W. (2004) Synthesis and characterization of human alpha-defensins 4-6. *J. Pept. Res. 64*, 118–125.

(122) Xie, C., Prahl, A., Ericksen, B., Wu, Z., Zeng, P., Li, X., Lu, W.-Y., Lubkowski, J., and Lu, W. (2005) Reconstruction of the conserved beta-bulge in mammalian defensins using D-

amino acids. *J. Biol. Chem. 280*, 32921–32929.

(123) Hill, C. P., Yee, J., Selsted, M. E., and Eisenberg, D. (1991) Crystal structure of defensin HNP-3, an amphiphilic dimer: mechanisms of membrane permeabilization. *Science 251*, 1481–1485.

(124) Zhang, Y., Lu, W., and Hong, M. (2010) The membrane-bound structure and topology of a human α-defensin Indicate a dimer pore mechanism for membrane disruption. *Biochemistry 49*, 9770–9782.

(125) Lehrer, R. I., Barton, A., Daher, K. A., Harwig, S. S. L., Ganz, T., and Selsted, M. E. (1989) Interaction of human defensins with *Escherichia coli*. Mechanism of bactericidal activity. *J. Clin. Invest. 84*, 553–561.

(126) Schonwetter, B. S., Stolzenberg, E. D., and Zasloff, M. A. (1995) Epithelial antibiotics induced at sites of inflammation. *Science 267*, 1645–1648.

(127) Diamond, G., Russell, J. P., and Bevins, C. L. (1996) Inducible expression of an antibiotic peptide gene in lipopolysaccharide-challenged tracheal epithelial cells. *Proc. Natl. Acad. Sci. U. S. A. 93*, 5156–5160.

(128) Selsted, M. E., Tang, Y. Q., Morris, W. L., McGuire, P. A., Novotny, M. J., Smith, W., Henschen, a. H., and Cullor, J. S. (1993) Purification, primary structures, and antibacterial activities of beta-defensins, a new family of antimicrobial peptides from bovine neutrophils. *J. Biol. Chem. 268*, 6641–6648.

(129) Harwig, S. S. L., Swiderek, K. M., Kokryakov, V. N., Tan, L., Lee, T. D., Panyutich, E. A., Aleshina, G. M., Shamova, O. V, and Lehrer, R. I. (1994) Gallinacins: cysteine-rich antimicrobial peptides of chicken leukocytes. *FEBS Lett. 342*, 281–285.

(130) Bensch, K. W., Raida, M., Mägert, H.-J., Schulz-Knappe, P., and Forssmann, W.-G. (1995) hBD-1: a novel β-defensin from human plasma. *FEBS Lett. 368*, 331–335.

(131) Valore, E. V, Park, C. H., Quayle, A. J., Wiles, K. R., McCray, P. B., and Ganz, T. (1998) Human beta-defensin-1: an antimicrobial peptide of urogenital tissues. *J. Clin. Invest. 101*, 1633–1642.

(132) Harder, J., Bartels, J., Christophers, E., and Schröder, J. M. (1997) A peptide antibiotic from human skin. *Nature 387*, 861.

(133) Harder, J., Bartels, J., Christophers, E., and Schroder, J.-M. (2001) Isolation and Characterization of Human -Defensin-3, a Novel Human Inducible Peptide Antibiotic. *J. Biol. Chem. 276*, 5707–5713.

(134) Oren, A., Ganz, T., Liu, L., and Meerloo, T. (2003) In human epidermis, beta-defensin 2 is packaged in lamellar bodies. *Exp Mol Pathol 74*, 180–182.

(135) Gersemann, M., Wehkamp, J., and Stange, E. F. (2012) Innate immune dysfunction in inflammatory bowel disease. *J. Intern. Med. 271*, 421–428.

(136) Goldman, M. J., Anderson, G. M., Stolzenberg, E. D., Kari, U. P., Zasloff, M., and Wilson, J.

M. (1997) Human beta-defensin-1 is a salt-sensitive antibiotic in lung that is inactivated in cystic fibrosis. *Cell 88*, 553–560.

(137) Hoover, D. M., Chertov, O., and Lubkowski, J. (2001) The structure of human beta-defensin-1: new insights into structural properties of beta-defensins. *J. Biol. Chem. 276*, 39021–39026.

(138) Hoover, D. M., Rajashankar, K. R., Blumenthal, R., Puri, A., Oppenheim, J. J., Chertov, O., and Lubkowski, J. (2000) The structure of human beta -defensin-2 shows evidence of higher order oligomerization. *J. Biol. Chem. 275*, 32911–32918.

(139) Schroeder, B. O., Wu, Z., Nuding, S., Groscurth, S., Marcinowski, M., Beisner, J., Buchner, J., Schaller, M., Stange, E. F., and Wehkamp, J. (2011) Reduction of disulphide bonds unmasks potent antimicrobial activity of human β-defensin 1. *Nature 469*, 419–423.

(140) Kandaswamy, K., Liew, T. H., Wang, C. Y., Huston-Warren, E., Meyer-Hoffert, U., Hultenby, K., Schröder, J. M., Caparon, M. G., Normark, S., Henriques-Normark, B., Hultgren, S. J., and Kline, K. A. (2013) Focal targeting by human β-defensin 2 disrupts localized virulence factor assembly sites in *Enterococcus faecalis*. *Proc. Natl. Acad. Sci. U. S. A. 110*, 20230–20235.

(141) Dorin, J. R., and Barratt, C. L. R. (2014) Importance of β-defensins in sperm function. *Mol. Hum. Reprod. 20*, 821–826.

(142) Yang, D., Chertov, O., Bykovskaia, S. N., Chen, Q., Buffo, M. J., Shogan, J., Anderson, M., Schröder, J. M., Wang, J. M., Howard, O. M. Z., and Oppenheim, J. J. (1999) Beta-defensins: linking innate and adaptive immunity through dendritic and T cell CCR6. *Science 286*, 525–528.

(143) Sørensen, O. E., Cowland, J. B., Theilgaard-Mönch, K., Liu, L., Ganz, T., and Borregaard, N. (2003) Wound healing and expression of antimicrobial peptides/polypeptides in human keratinocytes, a consequence of common growth factors. *J. Immunol. 170*, 5583–5589.

(144) Schmitt, P., Wilmes, M., Pugnière, M., Aumelas, A., Bachère, E., Sahl, H.-G., Schneider, T., and Destoumieux-Garzón, D. (2010) Insight into invertebrate defensin mechanism of action: oyster defensins inhibit peptidoglycan biosynthesis by binding to lipid II. *J. Biol. Chem. 285*, 29208–29216.

(145) Zanetti, M., Gennaro, R., and Romeo, D. (1995) Cathelicidins: A novel protein family with a common proregion and a variable C-terminal antimicrobial domain. *FEBS Lett. 374*, 1–5.

(146) Gennaro, R., and Zanetti, M. (2000) Structural features and biological activities of the cathelicidin-derived antimicrobial peptides. *Biopolymers 55*, 31–49.

(147) Zanetti, M. (2004) Cathelicidins, multifunctional peptides of the innate immunity. *J. Leukoc. Biol. 75*, 39–48.

(148) Lehrer, R. I., and Ganz, T. (2002) Cathelicidins: a family of endogenous antimicrobial peptides. *Curr. Opin. Hematol. 9*, 18–22.

(149) Zaiou, M., and Gallo, R. L. (2002) Cathelicidins, essential gene-encoded mammalian

antibiotics. *J. Mol. Med. 80*, 549–561.

(150) Sørensen, O. E., Follin, P., Johnsen, A. H., Calafat, J., Sandra Tjabringa, G., Hiemstra, P. S., and Borregaard, N. (2001) Human cathelicidin, hCAP-18, is processed to the antimicrobial peptide LL-37 by extracellular cleavage with proteinase 3. *Blood 97*, 3951–3959.

(151) Sørensen, O., Arnljots, K., Cowland, J. B., Bainton, D. F., and Borregaard, N. (1997) The human antibacterial cathelicidin, hCAP-18, is synthesized in myelocytes and metamyelocytes and localized to specific granules in neutrophils. *Blood 90*, 2796–2803.

(152) Bals, R., Wang, X., Zasloff, M., and Wilson, J. M. (1998) The peptide antibiotic LL-37/hCAP-18 is expressed in epithelia of the human lung where it has broad antimicrobial activity at the airway surface. *Proc. Natl. Acad. Sci. U. S. A. 95*, 9541–9546.

(153) Turner, J., Cho, Y., Dinh, N.-N., Lehrer, R. I., and Waring, A. J. (1998) Activities of LL-37 , a Cathelin-Associated Antimicrobial Peptide of Human Neutrophils Activities of LL-37 , a Cathelin-Associated Antimicrobial Peptide of Human Neutrophils *42*, 2206–2214.

(154) Larrick, J. W., Hirata, M., Balint, R. F., Lee, J., Zhong, J., and Wright, S. C. (1995) Human CAP18: A novel antimicrobial lipopolysaccharide-binding protein. *Infect. Immun. 63*, 1291–1297.

(155) Shaykhiev, R., BeiBwenger, C., Kändler, K., Senske, J., Püchner, A., Damm, T., Behr, J., and Bals, R. (2005) Human endogenous antibiotic LL-37 stimulates airway epithelial cell proliferation and wound closure. *Am. J. Physiol. Lung Cell. Mol. Physiol. 289*, L842–L848.

(156) Barns, K. J., and Weisshaar, J. C. (2013) Real-time attack of LL-37 on single *Bacillus subtilis* cells. *Biochim. Biophys. Acta 1828*, 1511–1520.

(157) Sochacki, K. A., Barns, K. J., Bucki, R., and Weisshaar, J. C. (2011) Real-time attack on single Escherichia coli cells by the human antimicrobial peptide LL-37. *Proc. Natl. Acad. Sci. U. S. A. 108*, E77–E81.

(158) Oppenheim, F. G., Xu, T., McMillian, F. M., Levitz, S. M., Diamond, R. D., Offner, G. D., and Troxler, R. F. (1988) Histatins, a novel family of histidine-rich proteins in human parotid secretion. Isolation, characterization, primary structure, and fungistatic effects on *Candida albicans. J. Biol. Chem. 263*, 7472–7477.

(159) Sabatini, L. M., and Azen, E. A. (1989) Histatins, a family of salivary histidine-rich proteins, are encoded by at least two loci (HIS1 and HIS2). *Biochem. Biophys. Res. Commun. 160*, 495–502.

(160) den Hertog, A. L., van Marle, J., van Veen, H. A., Van't Hof, W., Bolscher, J. G. M., Veerman, E. C. I., and Nieuw Amerongen, A. V. (2005) Candidacidal effects of two antimicrobial peptides: histatin 5 causes small membrane defects, but LL-37 causes massive disruption of the cell membrane. *Biochem. J. 388*, 689–695.

(161) Raj, P. A., Edgerton, M., and Levine, M. J. (1990) Salivary histatin 5: Dependence of sequence, chain length, and helical conformation for candidacidal activity. *J. Biol. Chem.*

265, 3898–3905.

(162) Xu, T., Levitz, S. M., Diamond, R. D., and Oppenheim, F. G. (1991) Anticandidal activity of major human salivary histatins. *Infect. Immun. 59*, 2549–2554.

(163) Helmerhorst, E. J., Reijnders, I. M., van't Hof, W., Simoons-Smit, I., Veerman, E. C. I., and Nieuw Amerongen, A. V. (1999) Amphotericin B- and fluconazole-resistant Candida spp., Aspergillus fumigatus, and other newly emerging pathogenic fungi are susceptible to basic antifungal peptides. *Antimicrob. Agents Chemother. 43*, 702–704.

(164) Melino, S., Rufini, S., Sette, M., Morero, R., Grottesi, A., Paci, M., and Petruzzelli, R. (1999) Zn(2+) ions selectively induce antimicrobial salivary peptide histatin-5 to fuse negatively charged vesicles. Identification and characterization of a zinc-binding motif present in the functional domain. *Biochemistry 38*, 9626–9633.

(165) Rydengård, V., Nordahl, E. A., and Schmidtchen, A. (2006) Zinc potentiates the antibacterial effects of histidine-rich peptides against *Enterococcus faecalis. FEBS J. 273*, 2399–2406.

(166) Harford, C., and Sarkar, B. (1997) Amino terminal Cu(II)-and Ni(II)-binding (ATCUN) motif of proteins and peptides: metal binding, DNA cleavage, and other properties. *Acc. Chem. Res. 30*, 123–130.

(167) Melino, S., Gallo, M., Trotta, E., Mondello, F., Paci, M., and Petruzzelli, R. (2006) Metal-binding and nuclease activity of an antimicrobial peptide analogue of the salivary histatin 5. *Biochemistry 45*, 15373–15383.

(168) Helmerhorst, E. J., Breeuwer, P., Van 't Hof, W., Walgreen-Weterings, E., Oomen, L. C. J. M., Veerman, E. C. I., Amerongen, A. V. N., and Abee, T. (1999) The cellular target of histatin 5 on *Candida albicans* is the energized mitochondrion. *J. Biol. Chem. 274*, 7286–7291.

(169) Habermann, E. (1972) Bee and wasp venoms. *Science 177*, 314–322.

(170) Terwilliger, T. C., and Eisenberg, D. (1982) The structure of melittin. II. Interpretation of the structure. *J. Biol. Chem. 257*, 6016–6022.

(171) Hultmark, D., Steiner, H., Rasmuson, T., and Boman, H. G. (1980) Insect immunity. Purification and properties of three inducible bactericidal proteins from hemolymph of immunized pupae of Hyalophora cecropia. *Eur. J. Biochem. 106*, 7–16.

(172) Steiner, H., Hultmark, D., Engström, Å., Bennich, H., and Boman, H. G. (1981) Sequence and specificity of two antibacterial proteins involved in insect immunity. *Nature 292*, 246–248.

(173) van Hofsten, P., Faye, I., Kockum, K., Lee, J. Y., Xanthopoulos, K. G., Boman, I. A., Boman, H. G., Engström, A., Andreu, D., and Merrifield, R. B. (1985) Molecular cloning, cDNA sequencing, and chemical synthesis of cecropin B from Hyalophora cecropia. *Proc. Natl. Acad. Sci. U. S. A. 82*, 2240–2243.

(174) Holak, T. A., Engström, A., Kraulis, P. J., Lindeberg, G., Bennich, H., Jones, T. A.,

Gronenborn, A. M., and Clore, G. M. (1988) The solution conformation of the antibacterial peptide cecropin A: a nuclear magnetic resonance and dynamical simulated annealing study. *Biochemistry 27*, 7620–7629.

(175) Schlamadinger, D. E., Wang, Y., McCammon, J. A., and Kim, J. E. (2012) Spectroscopic and computational study of melittin, cecropin A, and the hybrid peptide CM15. *J. Phys. Chem. B 116*, 10600–10608.

(176) Simmaco, M., Kreil, G., and Barra, D. (2009) Bombinins, antimicrobial peptides from Bombina species. *Biochim. Biophys. Acta - Biomembr. 1788*, 1551–1555.

(177) Zasloff, M. (1987) Magainins, a class of antimicrobial peptides from Xenopus skin: isolation, characterization of two active forms, and partial cDNA sequence of a precursor. *Proc. Natl. Acad. Sci. U. S. A. 84*, 5449–5453.

(178) Soravia, E., Martini, G., and Zasloff, M. (1988) Antimicrobial properties of peptides from Xenopus granular gland secretions. *FEBS Lett. 228*, 337–340.

(179) Marion, D., Zasloff, M., and Bax, a. (1988) A two-dimensional NMR study of the antimicrobial peptide magainin 2. *FEBS Lett. 227*, 21–26.

(180) Bessalle, R., Kapitkovsky, a., Gorea, a., Shalit, I., and Fridkin, M. (1990) All-D-magainin: Chirality, antimicrobial activity and proteolytic resistance. *FEBS Lett. 274*, 151–155.

(181) Vilcinskas, A., and Gross, J. (2005) Drugs from bugs: the use of insects as a valuable source of transgenes with potential in modern plant protection strategies. *J. Pest Sci. (2004). 78*, 187–191.

(182) Soballe, P. W., Maloy, W. L., Myrga, M. L., Jacob, L. S., and Herlyn, M. (1995) Experimental local therapy of human melanoma with lytic magainin peptides. *Int. J. Cancer 60*, 280–284.

(183) Landon, C., Sodano, P., Hetru, C., Hoffmann, J., and Ptak, M. (1997) Solution structure of drosomycin, the first inducible antifungal protein from insects. *Protein Sci. 6*, 1878–1884.

Chapter 2.

Synthesis of HD5 and its derivatives

2A. Introduction

Human α-defensin 5 (HD5) exhibits broad-spectrum antimicrobial activity against various Gram-positive and Gram-negative bacteria,[1] as well as antiviral[2] and antifungal activities.[3] HD5 provides a first line of defense against the invading pathogens in the gut lumen.[1,2,4] Recent reports also identified HD5 in the urogenital tract and female reproductive tract, indicating a possible role in innate immunity at these locations.[5,6] Several possible mechanisms of action including pore formation, cell membrane destabilization, and target-mediated cell death have been proposed for defensins.[7] However, how HD5 kills microbes is not yet clearly understood. The aims of this project are to 1) study the structural and functional properties of HD5 that influence the antimicrobial action of HD5; 2) visualize the site of action of HD5 during bacterial killing and 3) investigate the bacterial response HD5. In order to study these fundamental aspects of HD5, we developed robust methods employing Fmoc-solid-phase peptide synthesis to obtain $HD5_{ox}$ in high purity with the correct disulfide linkages. To visualize the localization of HD5, we designed a family of HD5 analogues and optimized the synthesis of fluorophore-labeled HD5 and other modified analogues. We describe these studies in this Chapter.

Until recently, obtaining considerable quantities of HD5 has been a daunting process. Both bacterial and yeast recombinant systems can be employed for the overexpression of cysteine-rich defensins.[8-12] With heterologous overexpression in bacteria, and standard affinity tags, defensins mainly form inclusion bodies and therefore need to be purified from the insoluble fraction. Moreover, oxidation *in vitro* using one of a variety of oxidative folding conditions is required to isolate the native regioisomer.[13-15] In initial work, we developed expression systems for overexpressing HD5 and human α-defensin 6 (HD6) in *E. coli*.[10,16] The yield of the peptide obtained from such recombinant systems is often low, ~ 10 mg for 12 liters of bacterial culture. A recent recombinant overexpression of HD5 in yeast is reported to afford better yields,[12] although the protocol in our hands has been difficult to reproduce.[17] The

drawbacks of overexpression systems, along with the current advancements in the solid-phase peptide synthesis protocols, prompted us to pursue the synthesis of HD5.

i.   **Solid-phase Peptide Synthesis**

The general solid-phase peptide synthesis protocol requires covalent attachment of the growing peptide chain to an insoluble anchoring resin. First, the C-terminal amino acid is attached to the resin, following which the coupling of the amino acids proceed in the C → N terminus direction. The N-alpha of the amino acid is temporarily protected and the C-terminus is activated using coupling reagents. This activated amino acid is coupled to the free amino terminus of the previous residue on the resin. The amino acid side chains are further protected to prevent side reactions, and side chains with orthogonal protecting groups can be used to append desired functionalities to the peptides that can be selectively modified later. The excess reagents added drive the reaction towards products and the unreacted reagents can be removed from the reaction by simple filtration. The selective deprotection of the N-terminus exposes the free amine for the next cycle of amino acid coupling. Following complete peptide assembly on the resin, the final cleavage of the peptide from the resin support and a

Scheme 2.1. General Scheme for Fmoc-based Solid-phase Peptide Synthesis

73
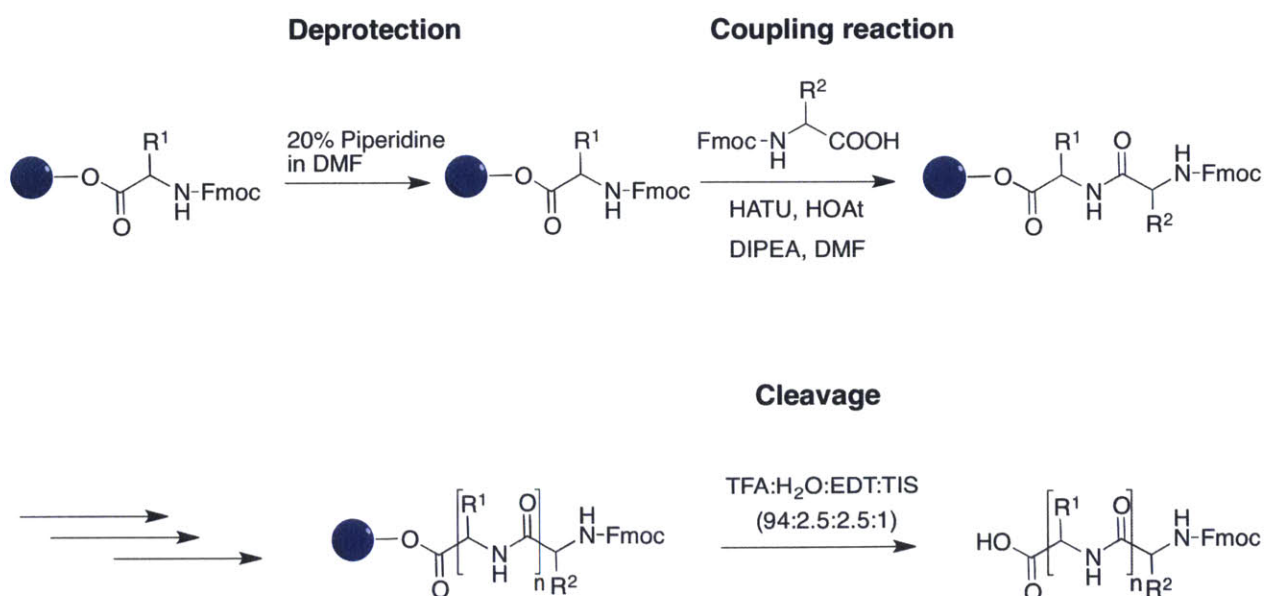
subsequent purification of the crude peptide mixture afford the desired peptide.

Scheme 2.2. Fmoc-deprotection, Amino Acid Activation and Coupling Reactions.
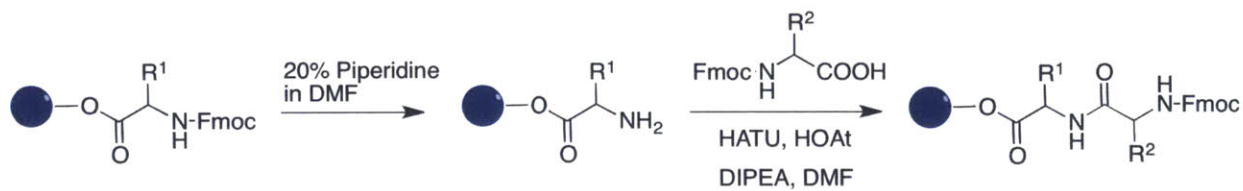
Fmoc Deprotection
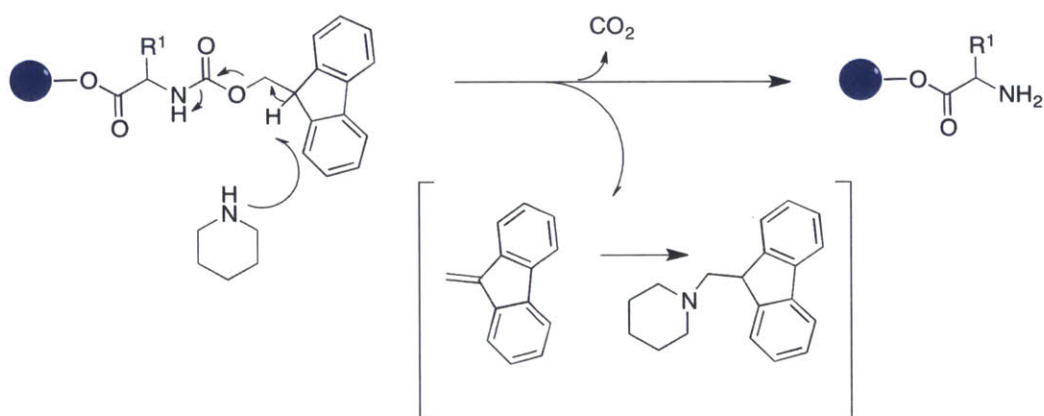
Amino Acid Activation and Coupling Reaction
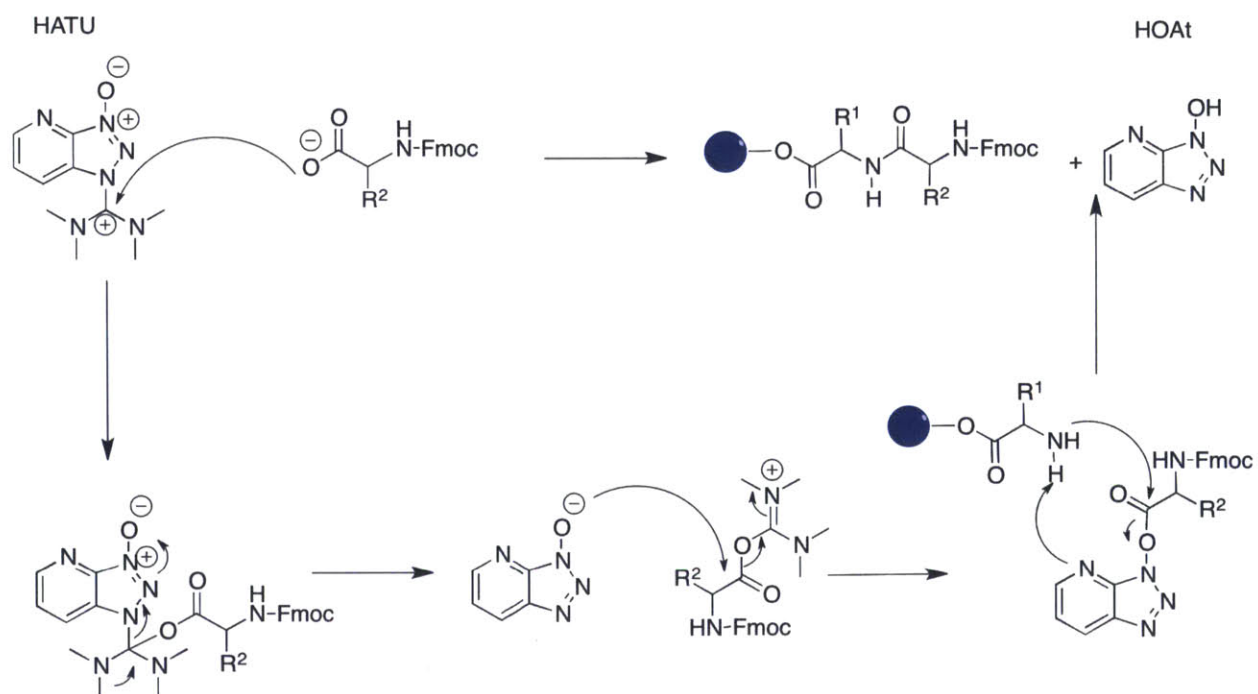
Boc and Fmoc protection are the two main N-alpha protecting groups and Bzl and tBu protection are the two respective side chain protecting groups, used for peptide synthesis. Although Boc-based synthesis provides better yields, the cleavage of peptide from the resin by standard methods requires use of corrosive acids such as HF, notorious for its toxicity, difficulty in handling and requirement for special setup. For this reason, Fmoc-based solid-phase peptide synthesis protocols that require milder reagents (TFA) are routinely used (Scheme 2.1 and 2.2).

ii.   **Synthesis of HD5**

HD5 was first synthesized using Boc-chemistry by Lu and coworkers (10% overall yield).[14] For developing a robust protocol for the routine synthesis of HD5 in our Lab, we decided to employ Fmoc-based solid-phase synthesis. HD5 is 32-aa peptide folded to a 3-stranded β-sheet structure and held rigidly by three regiospecific disulfide linkages (Figure 2.1A). From a synthetic perspective, peptides rich in β-sheets have the tendency to aggregate during synthesis on the resin, and prevent coupling of later amino acids and consequently reduce the overall yield.[18,19] One solution to overcome this aggregation is by introducing "pseudoproline dipeptides" at regular intervals in the peptide sequence (Figure 2.1B).[19]
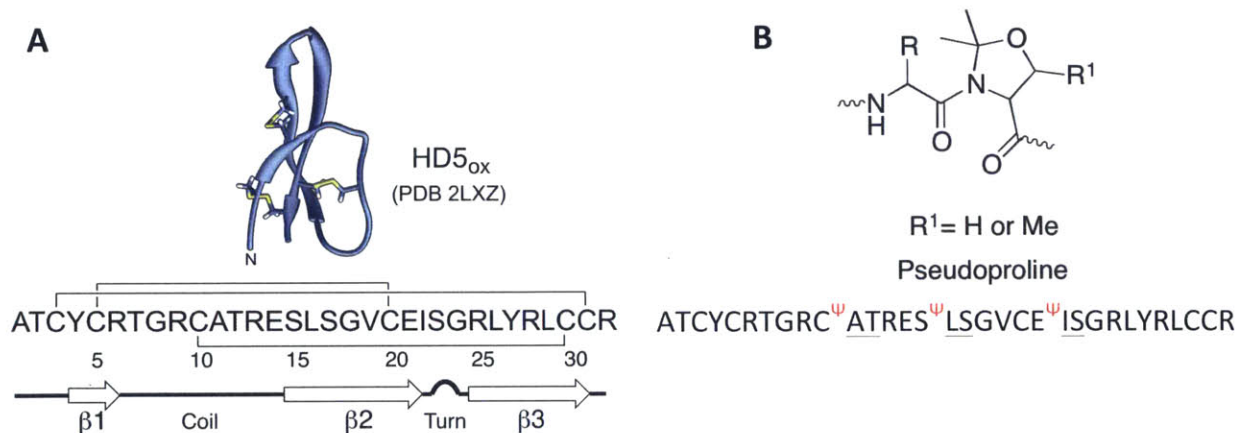
Figure 2.1. A) Structure of the $HD5_{ox}$ monomer determined by solution NMR (PDB 2LXZ)[32] and amino acid sequence. The regiospecific disulfide bond linkages and secondary structure are indicated. **B)** Structure of pseudoproline dipeptides introduced at regular intervals of HD5 sequence.

Pseudoproline dipeptides, introduce a bent structure in the peptide backbone because of the temporary backbone cyclization rendering their structure similar to prolines.

2B. Experimental Section

i. Chemicals, Solvents, and Buffers. Tetrakis(triphenylphosphine)palladium(0) [Pd(PPh$_3$)$_4$], piperidine, phenylsilane, trifluoroacetic acid were obtained from Alfa Aesar; piperazine, 5(6)-carboxyfluorescein, rhodamine B base, rhodamine 101 (R101), EDT, TIS, and triethylamine from Sigma Aldrich; coumarin 343 from Acros Organics; fluorescein from Fluka Chemicals. All Fmoc-protected amino acids used for solid-phase peptide synthesis (Fmoc-Cys(Trt)-OH, Fmoc-Ser(OtBu)-OH, Fmoc-Thr(OtBu)-OH, Fmoc-Arg(Pbf)-OH, Fmoc-Tyr(OtBu)-OH, Fmoc-Glu(tBu)-OH, Fmoc-Ala-OH, Fmoc-Val-OH, Fmoc-Gly-OH, Fmoc-Leu-OH) and pseudoproline dipeptides[20] (Fmoc-Ala-Thr($\Psi^{Me,Me}$pro)-OH, Fmoc-Ile-Ser($\Psi^{Me,Me}$pro)-OH, Fmoc-Leu-Ser($\Psi^{Me,Me}$pro)-OH) were obtained from AAPPTec, LLC. Fmoc-Arg(pbf)-Novasyn@TGA resin was purchased from EMD Chemicals. All peptide-coupling reagents were obtained from AK Scientific, Inc. HPLC-grade acetonitrile (MeCN) and HPLC-grade trifluoroacetic acid (TFA) were purchased from either EMD Chemicals or Alfa Aesar. ULTROL-grade HEPES was purchased from Calbiochem; guanidine hydrochloride from AMRESCO, Inc; and sodium phosphate was obtained from BDH Chemicals.

Peptides. HD5 was either (i) overexpressed from *E. coli* BL21(DE3) cells containing a plasmid encoding His$_6$-Met-HD5, and HD5$_{ox}$ was purified following His$_6$-tag cleavage and oxidative folding as described previously,[10] or (ii) synthesized by Fmoc solid-phase synthesis as described below. HD5-CD was prepared by Dr. Andrew Wommack from HD5$_{red}$ or HD5$_{ox}$ as described elsewhere.[3] All peptides were stored as either lyophilized powder or stock solution at -20 °C. Cryptdin-4, obtained from heterologous expression in *E. coli* as described elsewhere,[21] was provided by I-Ling Chiang.

The peptide solutions and buffers for antimicrobial activity assays were sterile-filtered (0.2-µm filter) prior to the assays. Peptide stock solutions were prepared in Milli-Q water, aliquoted, and stored at -20 °C until use. Peptide concentrations were routinely determined

using calculated extinction coefficients (Table 2.2) and a BioTek Synergy HT plate-reader outfitted with a BioTek Take 3 Micro-Volume Plate. Quantitative amino acid analysis (Dana-Farber Cancer Institute, Boston MA) was employed to determine the concentration of fluorophore-HD5 stock solutions. For each peptide stock solution, the analysis was performed three times and the resulting average employed as the working concentration.

ii.   General Methods

HPLC. Preparative-scale HPLC was performed on an Agilent PrepStar 218 instrument outfitted with an Agilent ProStar 325 dual-wavelength UV-Vis detector, and a Luna 100 Å C-18 column (10-μm pore, 21.2 x 250 mm, Phenomenex) at a flow rate of 10 mL/min. An Agilent 1200 series instrument equipped with an autosampler set at 4 °C and column compartment set at 20 °C was employed for analytical and semi-preparative HPLC. Analytical HPLC was performed using a Clipeus C-18 column (5-μm pore, 4.6 x 250 mm, Higgins Analytical, Inc.) operated at a flow rate of 1 mL/min. For semi-preparative HPLC, a Zorbax C-18 column (5-μm pore, 9.4 x 250 mm, Agilent Technologies, Inc.) at a flow rate of 5 mL/min was employed. For each HPLC system, solvent A was Milli-Q water containing 0.1% TFA that was passed through a 0.2-μm filter before use and solvent B was HPLC-grade MeCN containing 0.1% TFA.

ESI-MS. ESI-MS was performed on a LC/MS system comprised of an Agilent 1260 LC outfitted with a Poroshell 120 EC, C-18 column (2.7-μm pore, 3.0 x 50 mm, Agilent Technologies, Inc.) and connected to an Agilent 6230 TOF system housing an Agilent Jetstream ESI source. LC/MS-grade water and MeCN containing 0.1% formic acid (Fluka Chemicals) were used as solvent A and solvent B, respectively. The samples were run at a flow rate of 0.4 mL/min using a gradient of 0-95% of solvent B over 5 min.

iii.   Solid-phase Synthesis and Purification of HD5 and its Derivatives

Fmoc Solid-phase Peptide Synthesis of HD5$_{red}$. The manual solid-phase synthesis of HD5 was initiated by employing a previously described procedure used for the synthesis of Cys→Ser

HD5 variants.[10] However, the synthesis was unsuccessful and as a result needed further optimization. The synthesis was modified to improve efficiency and yield as detailed below. A custom-made 25-mL glass reaction vessel outfitted with a medium porosity frit and a "T"-bore for N_2 gas bubbling was purchased from Chemglass Life Sciences and employed for all manual syntheses. Fmoc-deprotection was performed with 20% piperidine in DMF solution (3 x 5 min). All amino acids were coupled to the resin using Fmoc-amino acid (10 eq) activated with HATU (10 eq), HOAt (10 eq), and DIPEA (20 eq) except for Fmoc-Cys(Trt)-OH (4 eq) and pseudoproline dipeptides ($^{\Psi}$AT, $^{\Psi}$ES and $^{\Psi}$LS) (4 eq). Each coupling reaction was agitated for 10-15 min at room temperature with N_2 bubbling. For coupling cysteine, Fmoc-Cys(Trt)-OH (4 eq) was dissolved in a CH_2Cl_2/DMF (1:1) mixture containing HATU (4 eq), HOAt (4 eq) and TMP (4 eq) as a mild base instead of DIPEA to minimize racemization.[22] Each amino acid was coupled at least twice. Residues identified as difficult to couple during trial syntheses were the Arg and pseudoprolines residues as well as Ser_{15}, Glu_{21}, Cys_{30} and Cys_{31}. After each coupling step, thorough washing of the resin with CH_2Cl_2 was performed (3 x 3 min). The capping of unreacted N-termini by 1-acetylimidazole, which was performed in the initial syntheses,[10] was omitted. After coupling the last amino acid, the N-terminal Fmoc-group was removed and the resin was thoroughly washed with CH_2Cl_2 (3 x 3 min). After drying the resin *in vacuo*, 20 mL of cold cleavage mixture containing TFA: EDT: H_2O: TIS (94: 2.5: 2.5: 1) was added and reaction was agitated with N_2 bubbling for 3 h, and the cleavage mixture was drained and the filtrate collected. To the resin, another 15 mL of fresh cleavage mixture was added and reaction was agitated for 30 min. The filtrates were combined and concentrated under N_2 to a final volume of 5 mL. The crude peptide was precipitated from the cleavage mixture using 30 mL of pre-cooled diethyl ether (−20 °C). The resulting mixture was centrifuged (3500 rpm x 4 °C for 20 min) and the supernatant was removed. The pellet was then dissolved in 1:1 mixture of 0.1 M acetic acid and acetonitrile mixture until fully dissolved, and the resulting solution was flash frozen in liquid nitrogen and lyophilized to obtain the crude peptide. The synthesis on a 0.0345-mmol scale, following cleavage and global deprotection, afforded 80 mg of crude peptide (64% yield). The

crude peptide was reduced with TCEP and purified following general procedures below to obtain 19 mg (15% overall yield) of HD5$_{red}$. Representative HPLC traces are provided in Figure 2.2.

General Method for the Purification of Reduced Form of HD5 and its Analogues. The crude peptide was dissolved in 75 mM HEPES, 6 M GduHCl, pH 8.2 to afford a 10 mg/mL solution and incubated with 10 mM TCEP for 15 min at which time the reaction was quenched by addition of 6% v/v TFA in Milli-Q water to afford 2% v/v TFA. The quenched reaction was centrifuged (3500 rpm x 5 min) and the supernatant was filtered (0.4-μm filter). The filtrate was purified by preparative RP-HPLC and the desired reduced peptide (e.g., HD5$_{red}$) was isolated using a gradient of 10-60% solvent B over 30 min (10 mL/min). Table 2.2 lists the HPLC retention times and *m/z* values for each peptide.

General Method for Oxidative Folding of Reduced Peptides. The purified reduced peptide (e.g., HD5$_{red}$) was dissolved in an oxidative folding solution containing 12 mM GSH, 1.2 mM GSSG and 6 M GduHCl to afford a 2-mg/mL solution. To this mixture, 250 mM Na$_2$HCO$_3$ was added to afford a peptide concentration of 0.5 mg/mL (pH ~ 8.2). The reaction mixture was placed on a nutating table for 4-5 h at room temperature. The extent of oxidation was examined using analytical RP-HPLC with a gradient of 10-60% solvent B over 30 min (1 mL/min). The desired folded peptide (e.g., HD5$_{ox}$) was purified by preparative RP-HPLC using a gradient of 10-60% solvent B over 30 min (10 mL/min). Table 2.2 lists the HPLC retention times and *m/z* values for each peptide.

Fmoc Solid-Phase Syntheses of HD5 with N-terminal Fluorophores. The synthesis of HD5 was performed on a 0.25 mmol scale of the Fmoc-Arg(pbf)-Novasyn@TGA resin using standard Fmoc solid-phase peptide synthesis procedures as described above. Portions of the Fmoc-HD5-resin were employed for on-resin coupling of fluorophores directly to the HD5 N-terminus as described below. The overall yields are calculated from resin loading (theoretical yield), and the corresponding folding yields are reported for the oxidative folding reaction alone.

Synthesis of Fluorescein-HD5 (FL-HD5). 5(6)-Carboxyfluorescein (FL) was obtained as a 1:1 mixture of isomers and used without further purification. A 0.08-mmol portion of Fmoc-HD5-resin was subjected twice to Fmoc deprotection using 10 mL of 20% piperidine in DMF. A mixture of FL (10 eq), HATU (10 eq) and HOAt (10 eq), was dissolved in 10 mL of DMF, and activated with DIPEA (20 eq) prior to coupling. This mixture was stirred at room temperature until it clarified and the solution color changed from yellow-orange to red, and was then added to the resin. Because the coupling conditions could also result in formation of carboxyfluorescein oligomers,[23] a wash with 20% piperidine in DMF was performed.[24] Cleavage of the peptide from the resin using a TFA: EDT: H_2O: TIS (94: 2.5: 2.5: 1) mixture afforded crude FL-HD5 (150 mg, 46% yield). The crude mixture was treated with 10 mM TCEP and purified following the general method for reduced peptides, which afforded FL-HD5$_{red}$ (32 mg, 10% yield). A 12-mg portion of FL-HD5$_{red}$ was oxidized using the general oxidative folding method. FL-HD5$_{ox}$ was obtained following purification (7 mg, 58% folding yield, 6% overall yield).

Synthesis of Rhodamine-HD5 (R-HD5). Rhodamine B 4-(3-carboxypropionyl)piperazine amide (rhodamine B derivative (**3**)) was synthesized from rhodamine B base following an established procedure,[25] and coupled to HD5 using a 0.06-mmol portion of Fmoc-HD5 on the resin. Following Fmoc-deprotection of the peptide, the coupling reaction was carried out twice with a mixture containing the rhodamine B derivative (**3**) (10 eq), HATU (10 eq) and HOAt (10 eq) in 10 mL of DMF and activated with DIPEA (20 eq) as described above. The crude peptide (98 mg, 39% yield) obtained after cleavage was purified by the general method to afford R-HD5$_{red}$ (16 mg, 9% yield). Oxidative folding of R-HD5$_{red}$ (9.5 mg) using the standard method afforded R-HD5$_{ox}$ (8.3 mg, 87% folding yield, 7% overall).

Synthesis of Coumarin-HD5 (C-HD5). The synthesis of coumarin 343-modified HD5 (C-HD5) was performed on a 0.05-mmol portion of Fmoc-HD5 on the resin. Following Fmoc-deprotection, the coupling reaction was performed with coumarin 343 (5 eq) dissolved in 15 mL of DMF containing HATU (5 eq), HOAt (5 eq) and DIPEA (10 eq). Coumarin 343 exhibited poor solubility in DMF and hence the coupling reaction was performed three times. The crude

peptide (104 mg, 54% overall yield) obtained following cleavage was treated with 10 mM TCEP and purified following the general protocol for reduced peptides, which provided C-HD5$_{red}$ (11 mg, C-HD5$_{red}$). During preliminary oxidative folding experiments using the general method, an orange, insoluble fiber-like solid formed on the walls of the centrifuge tubes containing the folding reaction. Formation of this solid was prevented by incubating the folding mixture at 37 °C with gentle shaking, which maintained a clear solution. Using this approach, C-HD5$_{red}$ (11 mg) was folded to yield C-HD5$_{ox}$ (2.5 mg, 22% folding yield, 2% overall yield).

Synthesis of HD5-TE and Fluorophore-HD5-TE by Carboxymethylation. HD5-TE and fluorophore-HD5-TE were prepared by modification of a reported procedure.[26] HD5$_{red}$ or fluorophore-HD5$_{red}$ (0.5 mg/mL) were dissolved in 470 μL of 0.6 M Tris-HCl buffer, 6 M GduHCl, pH 8.6 containing a 30-μL aliquot of freshly prepared 75 mM TCEP. To this mixture, 50 μL of a 500 mM stock solution of 2-iodoacetamide was added and the resulting mixture was incubated for 1-2 h in the dark at rt. The reaction was monitored using analytical RP-HPLC and, following completion, centrifuged (13000 rpm x 5 min). The crude product was purified by semi-preparative RP-HPLC (10-60% B over 30 min at 5 mL/min) to obtain the desired cysteine-capped products. Table 2.2 lists the HPLC retention times and *m/z* values for the carboxymethylated peptides.

General Method for Syntheses of HD5[R9K] and HD5[R13K]. The syntheses were performed using the standard Fmoc solid-phase peptide synthesis procedures reported for HD5 with several modifications.[3,10] The syntheses of HD5[R9K] and HD5[R13K] were each performed on a 0.1-mmol scale of Fmoc-Arg(pbf)-Novasyn@TGA resin. At amino acid position 9 (for HD5[R9K]) or 13 (for HD5[R13K]), Fmoc-Lys(Alloc)-OH was coupled thrice using Fmoc-Lys(Alloc)-OH (10 eq) dissolved in DMF (15 mL) containing HATU (10 eq), HOAt (10 eq) and DIPEA (20 eq). After coupling of the N-terminal Ala residue, each resin-bound peptide was subjected to Alloc deprotection under mild conditions by treatment with PhSiH$_3$ (25 eq) and catalytic [Pd(PPh$_3$)$_4$] (0.10 eq) in 10 mL of CH$_2$Cl$_2$ at rt for 1 h. The deprotection reaction was repeated three times.

The resins were dried and used for the preparation of HD5[R9K], HD5[R13K], R-HD5[R9K], and R-HD5[R13K] as described below.

Synthesis of HD5[R9K]. Fmoc-deprotection followed by cleavage of 0.025-mmol portion of Fmoc-HD5[R9K]-resin afforded crude HD5[R9K] (45 mg, 50% yield). Purification of the crude peptide by the general method afforded HD5[R9K]$_{red}$ (6 mg, 7% overall yield), which was oxidized using the standard method. Purification of the oxidative folding mixture afforded HD5[R9K]$_{ox}$ (2 mg, 2% overall yield).

Synthesis of HD5[R13K]. Fmoc-deprotection followed by cleavage reaction of 0.025-mmol portion of Fmoc-HD5[R13K]-resin afforded crude HD5[R13K]$_{red}$ (52 mg, 56% yield). Purification of the crude peptide by the general method afforded HD5[R13K]$_{red}$ (11 mg, 12% overall yield), which was oxidized using the standard method. Purification of the oxidative folding mixture afforded HD5[R13K]$_{ox}$ (3 mg, 3% overall yield).

Synthesis of R-HD5[R9K]. After Alloc deprotection of Lys9, a 0.05-mmol portion of Fmoc-HD5[R9K]-resin was thoroughly washed with CH_2Cl_2 before coupling of rhodamine B derivative (**3**), to the free ε-amino group of Lys9. The coupling reaction was repeated three times with the functionalized rhodamine (**3**) (122 mg, 4 eq, 0.2 mmol) dissolved in 10 mL of DMF containing HATU (4 eq), HOAt (4 eq) and DIPEA (8 eq). Then, the resin was thoroughly washed with CH_2Cl_2, the Fmoc was removed, and the cleavage reaction was performed to obtain crude R-HD5[R9K] (90 mg, 43% crude yield). The crude peptide was reduced by the general method and purified to afford R-HD5[R9K]$_{red}$ (7 mg, 4% overall yield). The reduced peptide was folded using the standard method to yield R-HD5[R9K]$_{ox}$ (1.5 mg, 1% overall yield).

Synthesis of R-HD5[R13K]. As described for R-HD5[R9K] using a 0.05-mmol portion of Fmoc-HD5[R13K] resin. Reduction and purification of R-HD5[R13K] (96 mg, 46% crude yield) by the general method afforded R-HD5[R13K]$_{red}$ (9 mg, 4% overall yield). The reduced peptide was folded by the standard procedure to yield HD5[R13K]$_{ox}$ (2 mg, 2% overall yield).

Synthesis of HD5[Ser^{hexa}]. HD5[Ser^{hexa}] was performed using a semi-automated approach with a custom-made stainless steel fritted reaction vessel on a 0.038 mmol scale.[27]

Standard solid-phase methodology for Fmoc chemistry was employed and preloaded Fmoc-Arg(Pbf)-NovaSyn TGA resin was utilized (0.19 mmol/g loading). Fmoc-protected amino acids (1 mmol) were coupled at 60 °C after dissolution in 2.5 mL DMF containing 0.38 mM HBTU. Following addition of DIPEA (450 μL for standard residues and 200 μL for Cys), the activated amino acid was administered to the warmed reactor at a flow rate of 6 mL/min, and then the resin was washed with DMF (60 sec at 20 mL/min). The Fmoc was removed with 20% piperidine in DMF (25 sec at 20 mL/min), and the resin was washed with DMF (70 sec at 20 mL/min).

After coupling the N-terminal Fmoc-Ala-OH, Fmoc deprotection with 20% piperidine in DMF was performed, and the resin was washed with DMF and transferred to a 50-mL centrifuge tube. The resin was dried and global deprotection was performed using 20 mL of solution containing TFA: EDT: H_2O: TIS (94: 2.5: 2.5: 1) mixture for 10 min at 60 °C. The mixture was concentrated to a volume of ca. 5 mL by using a gentle stream of N_2. Ice-cold Et_2O was added to the resulting concentrate, which resulted in precipitation of the crude peptide, and the mixture was centrifuged (2000 rpm x 15 min, 4 °C). The organic supernatant was decanted, and the pelleted precipitate was re-dissolved in 5 mL of 5% TFA in H_2O/MeCN (3:2). Preparative RP-HPLC purification (10-60% B over 30 min, 10 mL/min) afforded HD5[Ser^{hexa}] (20.2 mg, 15% overall yield, Figure 2.4).

iv.   Photophysical Characterization of Fluorophore-HD5 Conjugates.

General Conditions. All spectroscopic characterization of fluorophore-derivatized peptides was performed at pH 7.4 (75 mM HEPES, 100 mM NaCl). The buffer was prepared using Chelex-treated Milli-Q water (5 g/L stirred overnight, and passed through 0.4-μm filter). The buffer was filtered (0.4-μm filter) prior to being stored in 50-mL polypropylene centrifuge tubes.

Optical Absorption Spectroscopy. Optical absorption spectra were acquired on a Beckman UV-Vis spectrophotometer thermostated at 25 °C (1-cm path-length quartz cuvettes, Starna).

Fluorescence Spectroscopy. Fluorescence spectra were acquired using a PTI Quanta Master 40 spectrofluorimeter thermostated at 25 °C by a circulating water bath (1 cm x 1 cm quartz cuvettes, Starna). Emission spectra were collected with the following instrument settings: 2 nm slit widths, 60 nm/min scan speed, 1-s integration time. The spectra were integrated using the manufacturer's FelixG software.

Quantum Yield Determination. The relative quantum yields for fluorescence of the fluorophore-HD5 conjugates were determined by comparison of the integrated area of the emission spectrum of the samples with that of a standard. Rhodamine 101 in methanol (Φ = 0.99),[28,29] fluorescein in 0.1 N NaOH (Φ = 0.95)[30] and coumarin 343 in ethanol (Φ = 0.64)[31] were used as standards for rhodamine B-, carboxyfluorecein-, and coumarin 343-derivatives of HD5, respectively. The stock solutions of the fluorophores were prepared in DMSO, aliquoted, and stored at -20 °C. The concentrations of the stock solutions were verified using the reported extinction coefficients.[28–31] The aliquots of the standards were subjected to only one freeze-thaw cycle. To determine the relative quantum yields, the concentrations of the respective references were adjusted such that the A_{max} of the reference matched the A_{max} of the sample (absorbance value between 0.04 to 0.06). Then, the emission spectrum of each solution was recorded using a wavelength at which the absorption traces of both standard and sample overlap as the excitation wavelength. The quantum efficiencies of fluorophore-conjugates were calculated using the equation 1

$$\phi_x = \phi_{std}\left(\frac{I_x}{I_{std}}\right)\left(\frac{\eta_x^2}{\eta_{std}^2}\right)\left(\frac{Abs_{std}}{Abs_x}\right) \tag{1}$$

where Φ_x and Φ_{std} are the relative quantum yield of the sample and reference, respectively; I_x I_{std} are the integrated emission of the sample and reference, respectively; η_x and η_{std} are the refractive indices of the sample and reference solvents, respectively; Abs_x and Abs_{std} are the absorbance of the standard and reference at the wavelength of excitation. On the basis of the experimental protocol, the Abs_{std}/Abs_x ratio is 1.

v. **Antimicrobial Activity Assays.** Antimicrobial activity (AMA) assays were performed using a micro-drop colony forming units (CFU) method described previously.[3] The bacteria were grown overnight in TSB (without dextrose) medium. The overnight cultures were diluted 1:100 and grown in TSB (without dextrose) to an OD_{600} = 0.6 for *Escherichia coli* and OD_{600} = 0.5 for *Staphylococcus aureus*. The bacterial cultures were centrifuged (3500 rpm x 6 min, 4 °C) and resuspended in AMA buffer (10 mM sodium phosphate buffer, pH 7.4, supplemented with 1% v/v TSB (without dextrose)). The process was repeated once to remove any residual medium. The OD_{600} was measured again and adjusted to 0.6 and 0.5 (2.5×10^8 CFU/mL) for *E. coli* and *S. aureus* respectively, and the cultures were further diluted 250-fold to a cell count of 1×10^6 CFU/mL. AMA assays were performed in 96-well plates. Each well contained 10 μL of stock peptide solution (10x concentration in Milli-Q water) and 90 μL of bacterial culture (1×10^6 CFU/mL). For the control wells containing no peptide, 10 μL of Milli-Q water was combined with 90 μL of the bacterial culture. The assay plates were incubated for 1 h (130 rpm, 37 °C). For assays with fluorophore-labeled peptides, the plates were incubated in the dark (covered with aluminum foil). After incubation, a 20-μL aliquot from each well was diluted with 180 μL of AMA buffer in a new 96-well plate to obtain a 10^{-1} dilution. This 10^{-1} dilution was serially diluted in AMA buffer to obtain 10^{-2}, 10^{-3}, and 10^{-4} dilutions. From each dilution, a 5-μL aliquot was spotted on TSB (without dextrose) agar plates. The agar plates were air dried at room temperature for 30 min, subsequently incubated at 37 °C for 16 h, and the resulting colonies were counted.

2C.   Results and Discussion

i.   **Pseudoprolines Improve the Synthesis of HD5.** Fmoc-based solid-phase synthesis of HD5 was performed manually using Fmoc-Arg(pbf)-Novasyn@TGA resin (0.19 mmol/g) and standard Fmoc amino acids. In the absence of pseudoprolines ($^\Psi$AT, $^\Psi$ES and $^\Psi$LS), HD5 was not identified in the crude mixture (data not shown). Therefore, following the solid-phase peptide synthesis procedure reported previously for disulfide mutants generated in the Nolan Lab by

Dr. Piotr Kaczmarek, pseudoproline residues were introduced in the peptide sequence at regular intervals (HD5: ATCYCRTGRC $^\Psi$ ATRES $^\Psi$ LSGVCE $^\Psi$ ISGRLYRLCCR). This modification afforded full-length HD5, but the synthesis needed further optimization as many undesired side products were identified (Figure 2.2A). Therefore, the synthesis was repeated in order to optimize the yields.

The optimized synthesis of HD5 was performed on a 0.25 mmol of arginine-preloaded resin. The pseudoprolines were employed in order to minimize the aggregation of the peptide on the resin. A few changes from the initial synthesis procedure were made for a rapid synthesis. i) The overall duration of deprotection (3 x 7 min), coupling (2 x 10-15 min) and wash steps (3 x 3 min) were significantly reduced from previous synthesis. ii) The synthesis was performed such that resin shrinkage, storage and swelling steps are avoided in the middle of the synthesis. iii) The capping of unreacted N-termini by 1-acetylimidazole was omitted. Fmoc-Cys(trt)-OH, Fmoc-Arg(pbf)-OH and the difficult amino acids as identified from initial optimization, such as Fmoc-Glu(OtBu)-OH at position 21, were coupled three times each and the rest of the amino acids were double-coupled. The pseudoprolines were coupled multiple times until the maximum loading was achieved (as confirmed by resin cleavage on 10 mg-scale and LC-MS). After the completion of synthesis, a 0.005-mmol portion of resin was cleaved for analysis by HPLC to confirm the presence of product. The reaction yield improved significantly with the desired HD5 peak as major peak. The crude peptide (8.3 mg; 46% yield) was reduced in the presence of excess TCEP and purified to achieve 1 mg (6%) of the desired peptide (1: HD5$_{red}$). The side products of the reaction indicated in Figure 2.2B were identified as truncation peptides (2: ISGRLYRLCR, 3: LSGVCEISGRLYRLCR) that also had a cysteine deletion at the C-terminus (Table 2.1). The resin containing Fmoc-HD5 was stored and employed for further N-terminal modifications.

A

B
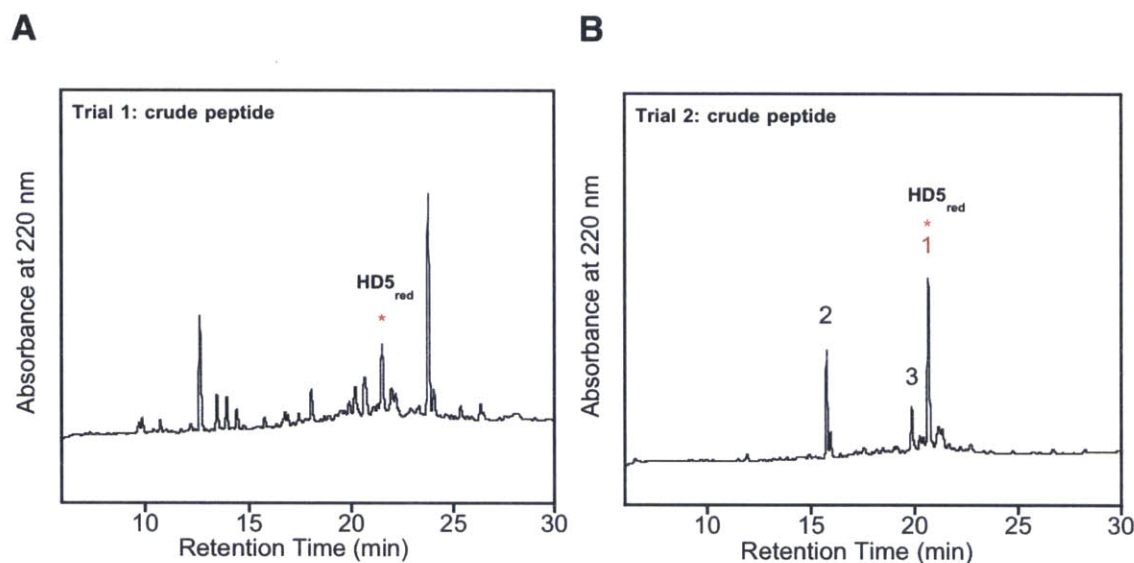
Figure 2.2. Optimization of manual Fmoc-based solid-phase peptide synthesis of HD5. Analytical HPLC traces of **A**) first synthesis of HD5 and **B**) optimized manual solid-phase peptide synthesis of HD5. Star (*) indicates the peak corresponding to the desired HD5$_{red}$.

Table 2.1. ESI-MS of Major Peaks Observed in HPLC Trace of Crude HD5 from Figure 2.2B.

Peak	Retention Time (min) ^{a}	Observed mass m/z [M+H]$^+$	Possible fragments	Calculated mass m/z [M+H]$^+$
1	15.6	1237.68	ISGRLYRLCR	1237.51
2	19.5	1825.02	LSGVCEISGRLYRLCR	1824.95
3	20.8	3585.67	HD5$_{red}$	3585.70

^{a} Retention time corresponds to the analytical run with a gradient of 10-60% B for 30 min at 1 mL/min [A: water (0.1% TFA), B: acetonitrile (0.1% TFA)].

ii.   **Design and Synthesis of Fluorophore-modified HD5 Derivatives**

In order to study the cellular localization of HD5 using fluorescence microscopy, we sought to generate a family of fluorophore-modified HD5 derivatives. The fluorophores should possess good photophysical properties, be easily synthesized or obtained commercially, and should not affect the structural and functional properties of HD5. The fluorophores coumarin 343 (**1**), 5(6)-carboxyfluorescein (**2**) and a rhodamine B derivative (**3**) were selected for HD5 modification. These fluorophores can be obtained in gram quantities and possess photophysical

properties compatible with the microscopy experiments. Of note, the folding and antimicrobial activity assays of the tryptophan mutants (Appendix 1) suggested that modifications at the termini of HD5 are tolerated.

Considering the ease of modifying the N-terminus vs. the C-terminus in Fmoc-based solid-phase peptide synthesis, free amine at the N-terminus of HD5 was selected for appending the fluorophores having carboxyl functional group using peptide-coupling reagents (Scheme 2.3). The fluorophores were appended to peptide on the resin. The modified peptides were simultaneously subjected to global deprotection and cleavage using the TFA cleavage mixture. The reduced form of the peptides was purified from the crude peptide mixture, and the desired peptides were obtained by oxidative folding. The folding reactions each afforded a single major

Scheme 2.3. Design of a Family of N-terminal Fluorophore-modified HD5 Conjugates.

X = Coumarin 343 (**1**)
C-HD5$_{ox}$

X = 5(6)-Carboxyfluorescein (**2**)
FL-HD5$_{ox}$, FL-HD5-TE

X = Rhodamine B derivative (**3**)
R-HD5$_{ox}$, R-HD5-TE
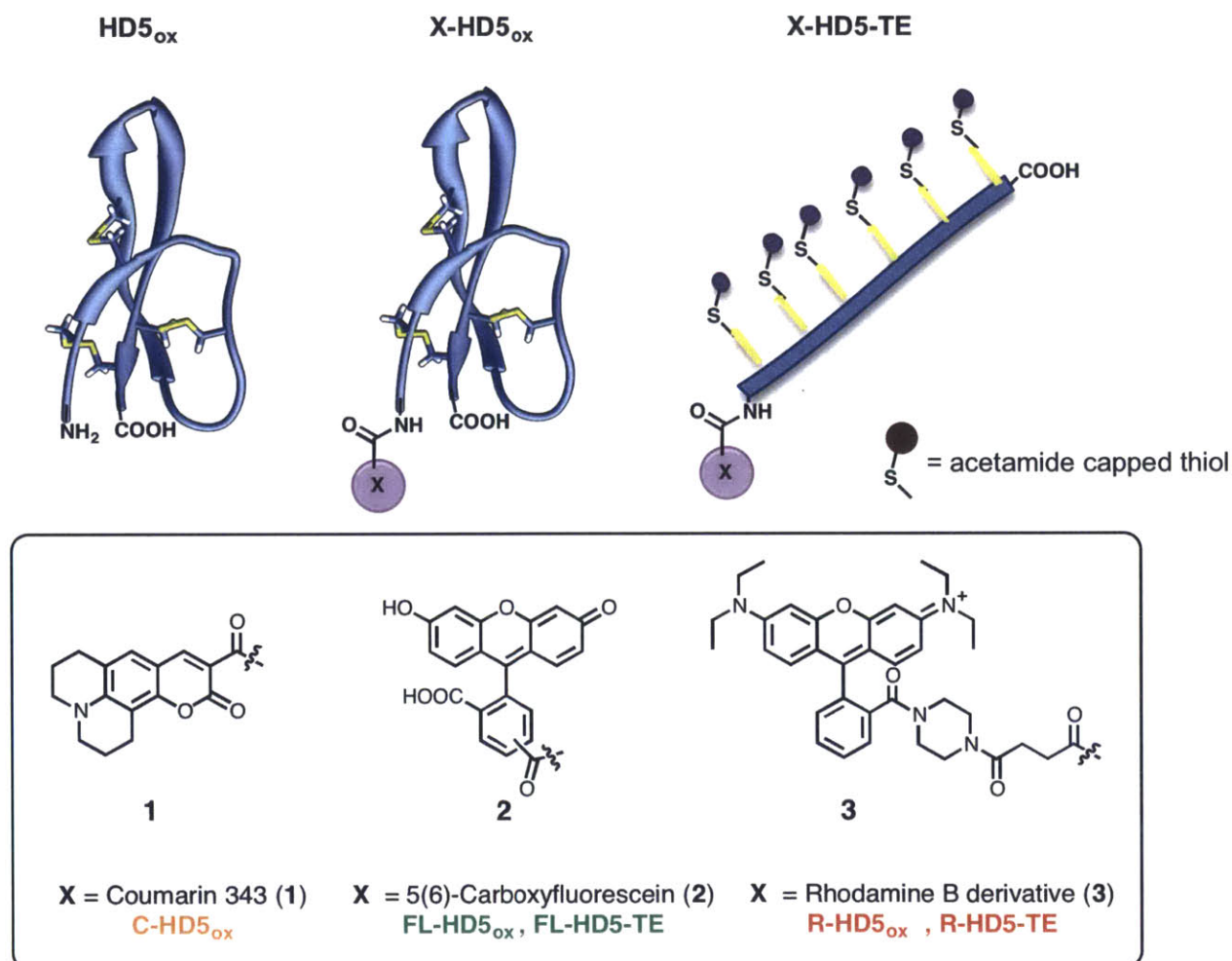
peak, similar to unmodified peptide HD5$_{red}$ that folds to the desired regioisomer HD5$_{ox}$ (Figure 2.3). The regiospecific disulfide linkages in HD5 (Figure 1) are important not only for structural integrity but also for the antimicrobial activity of HD5.[10,32,33] Therefore, in order to probe the effect of loss of disulfides and tertiary structure, we also synthesized linear peptides (e.g., HD5-TE), with cysteine residues capped with 2-iodoacetamide (Scheme 2.3, Figure 2.4)[26] and HD5[Ser^{hexa}].
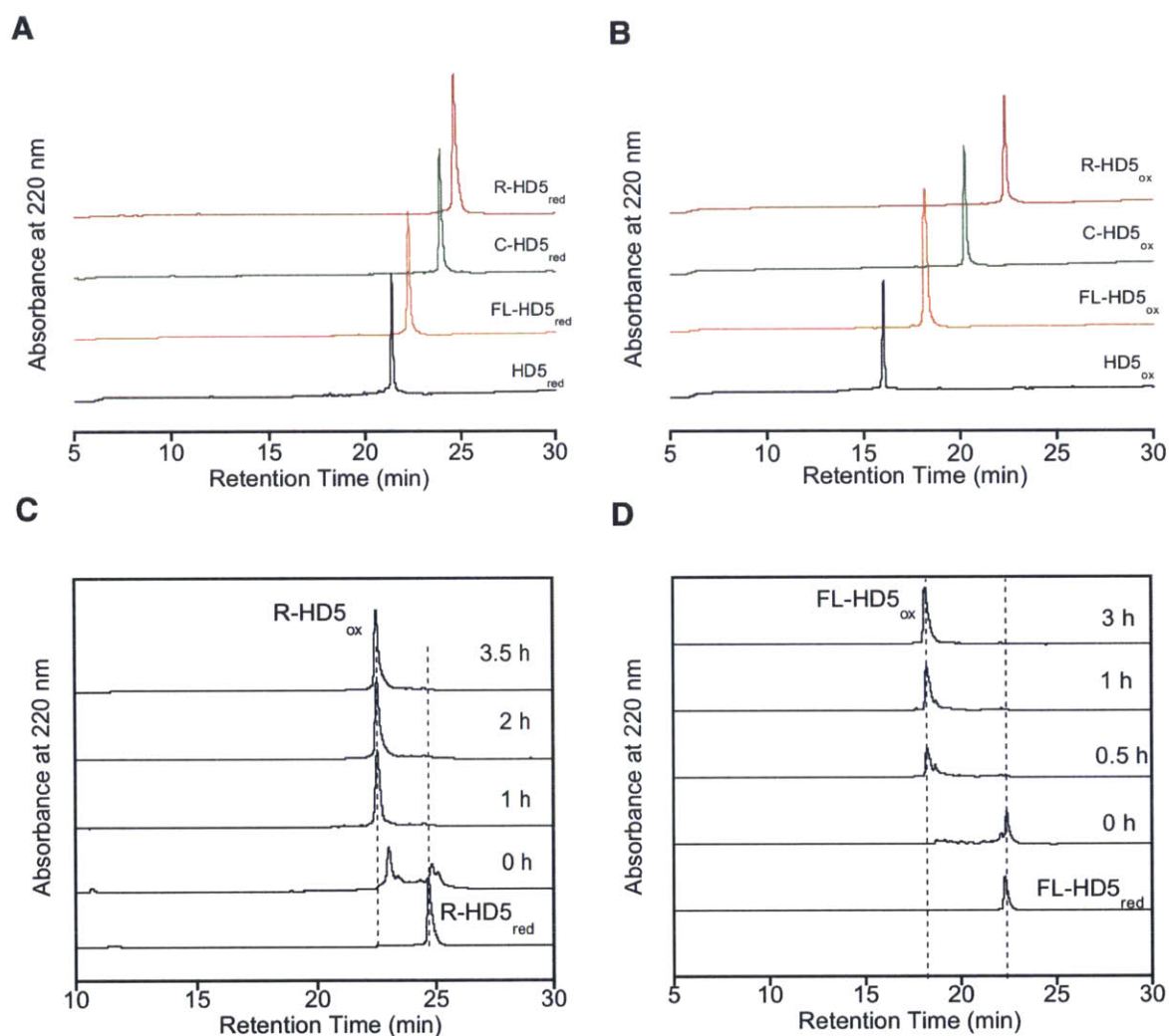
Figure 2.3. Purification and refolding of fluorophore-modified HD5 analogues. Analytical HPLC traces of **A)** reduced forms of fluorophore-labeled HD5; **B)** oxidized forms of fluorophore-labeled HD5; oxidative folding reaction of **C)** R-HD5 and **D)** Fl-HD5. Dashed lines (---) in **C** and **D** traces indicate the retention times of respective reduced and final oxidized forms of peptides.
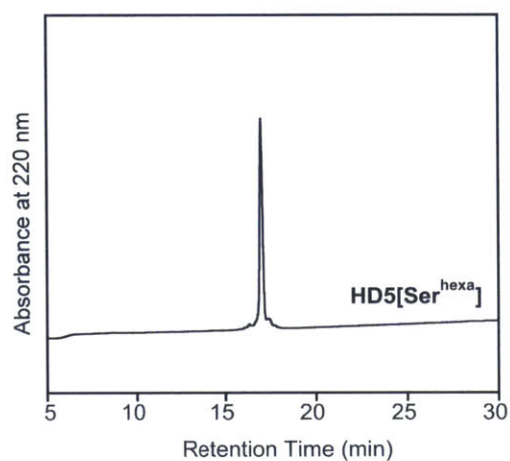
Figure 2.4. Analytical HPLC trace of purified HD5[Ser^{hexa}]. The sample was subjected to a gradient of 10- 60% of solvent B over 30 min at a flow rate of 1 mL/min.

Scheme 2.4. Design of Arg→Lys HD5 Variants and their Fluorophore-conjugates.
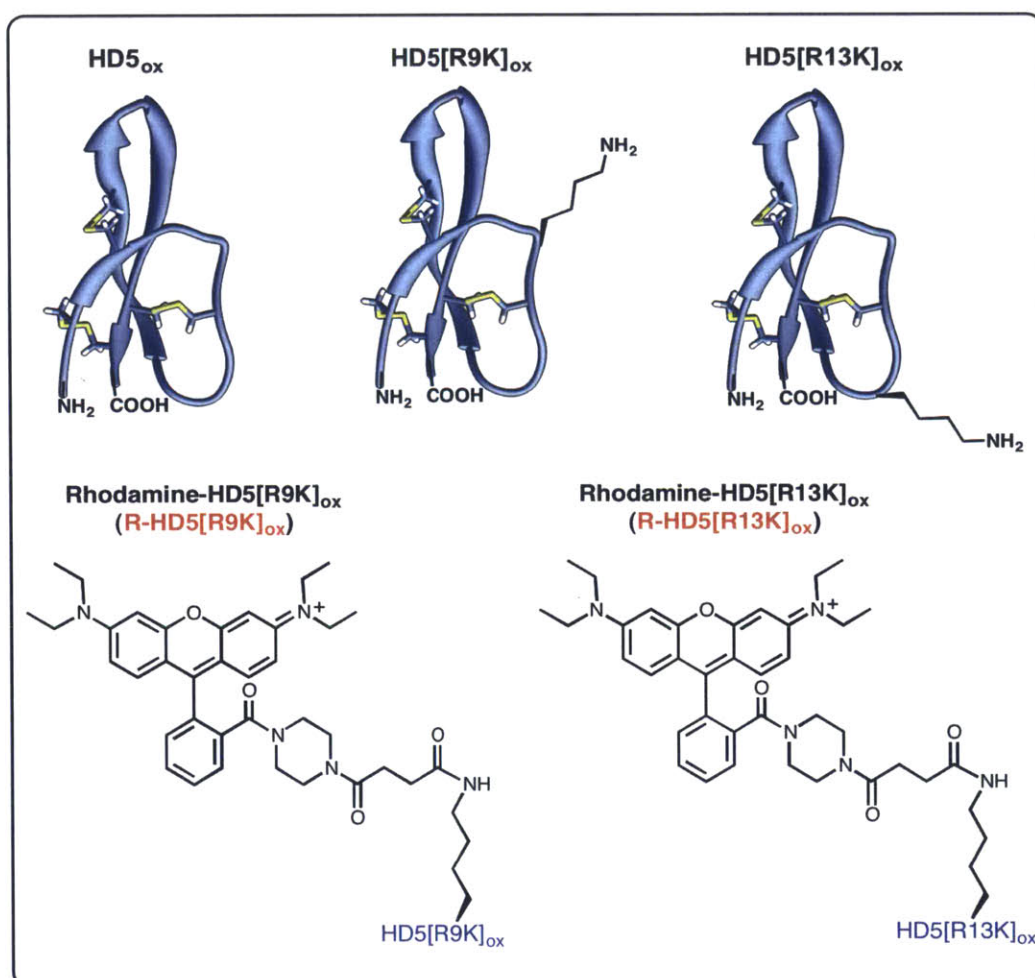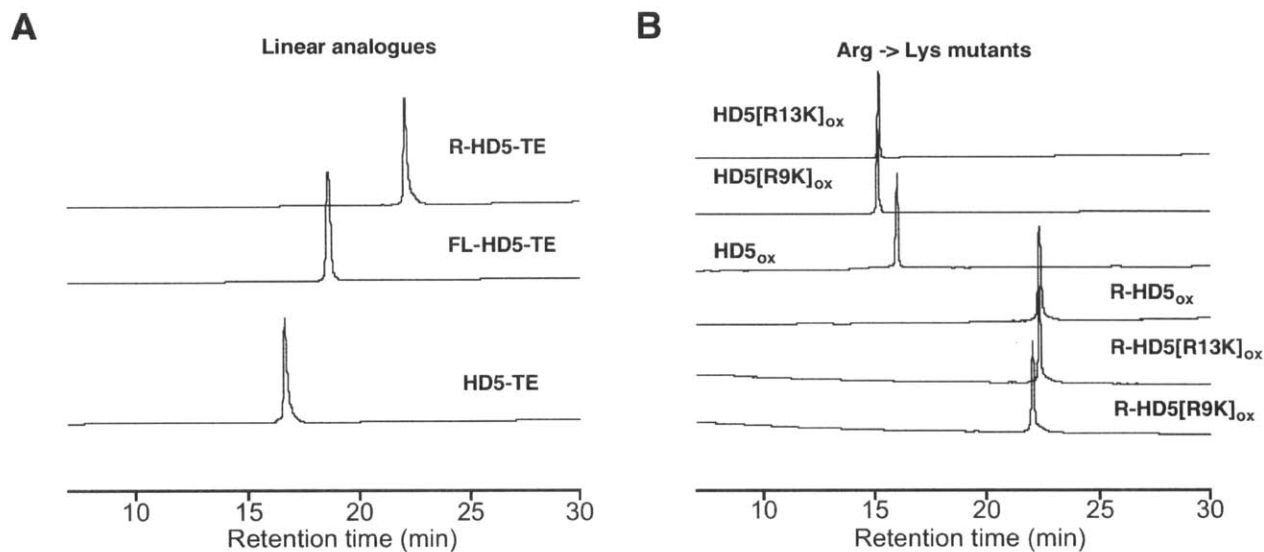
Figure 2.5. The HPLC traces of the purified linear analogues and Arg→Lys mutants of HD5. Analytical HPLC traces for the purified **A)** linear fluorophore-peptides and **B)** Arg→Lys mutants.

In order to investigate the influence of position of fluorophore attachment on the antimicrobial activity of HD5 and the labeling pattern, a new family of HD5 analogues was synthesized (Scheme 2.4). Motivated to append fluorophores at other positions, we selected Arg→Lys mutations to site-specifically modify with rhodamine B derivative. The previous work by Lu *et al.*[2,34] and Froy *et al.*[35] with Arg→Ala mutants and Arg→Lys double mutants suggested that R9, R13 or R32 might retain some activity when mutated to lysine compared to other arginine residues in the sequence. Further, positions R9 and R13 were selected as their side-chains were directed away from the dimer interface of native $HD5_{ox}$ as observed from the NMR analysis and crystal structure (PDB: 2LXZ, 1ZMP). Hence, the syntheses of HD5[R9K] and HD5[R13K] were undertaken. To couple the fluorophore on the resin similar to synthesis of N-terminal modifications, we sought to incorporate an orthogonal protection of lysine using an Alloc-group during assembly of HD5 on resin. Alloc deprotection and coupling of fluorophore to the Fmoc-HD5[R9K] and Fmoc-HD5[R13K] afforded fluorophore-labeled peptides. Subsequent

to Fmoc-deprotection, the peptides were cleaved off the resin following global deprotection and purified on HPLC (Figure 2.5).

Table 2.2. HPLC and Mass Spectrometry of HD5 and its Derivatives Employed in this Work.

Peptide	Retention Time (min) [a]	Calculated Mass [M+H]$^+$ m/z [b]	Observed Mass [M+H]$^+$ m/z	Overall/folding Yield (%) [c]
HD5$_{red}$	20.4	3585.67	3585.76	6 %
HD5$_{ox}$	15.3	3579.62	3579.62	4% / 70%
HD5-TE	16.6	3928.92	3928.91	72%
C-HD5$_{red}$	23.9	3854.76	3854.77	6%
C-HD5$_{ox}$	20.2	3848.72	3848.72	2% / 28%
FL-HD5$_{red}$	22.2	3944.72	3944.72	10%
FL-HD5$_{ox}$	18.2	3938.67	3938.67	6% / 58%
FL-HD5-TE	18.6	4287.60	4287.60	97%
R-HD5$_{red}$	24.7	4179.99	4179.98	9%
R-HD5$_{ox}$	22.3	4173.93	4173.94	7% / 87%
RHD5-TE	22.1	4523.10	4523.10	100%
R-HD5[R9K]$_{red}$	24.2	4151.99	4152.14	4%
R-HD5[R9K]$_{ox}$	21.9	4145.93	4145.94	1% / 25%
R-HD5[R13K]$_{red}$	24.3	4151.99	4152.12	4%
R-HD5[R13K]$_{ox}$	22.1	4145.93	4145.94	2% / 50%
HD5[R9K]$_{red}$	19.9	3558.62	3558.63	13%
HD5[R9K]$_{ox}$	15.1	3552.62	3552.63	4% / 30%
HD5[R13K]$_{red}$	19.9	3558.64	3558.64	12%
HD5[R13K]$_{ox}$	15.2	3552.62	3552.63	3% / 25%

[a] Retention times obtained from analytical RP-HPLC using a gradient 10-60% B over 30 min, 1 mL/min.
[b] Calculated by using PROTEIN CALCULATOR v3.3 (http://www.scripps.edu/~cdputnam/protcalc.html).
[c] The overall yield is calculated by using the resin loading (mmol/g) as the theoretical yield. The folding yield is for the oxidative folding reaction alone. When only one value is listed, it is the overall yield.
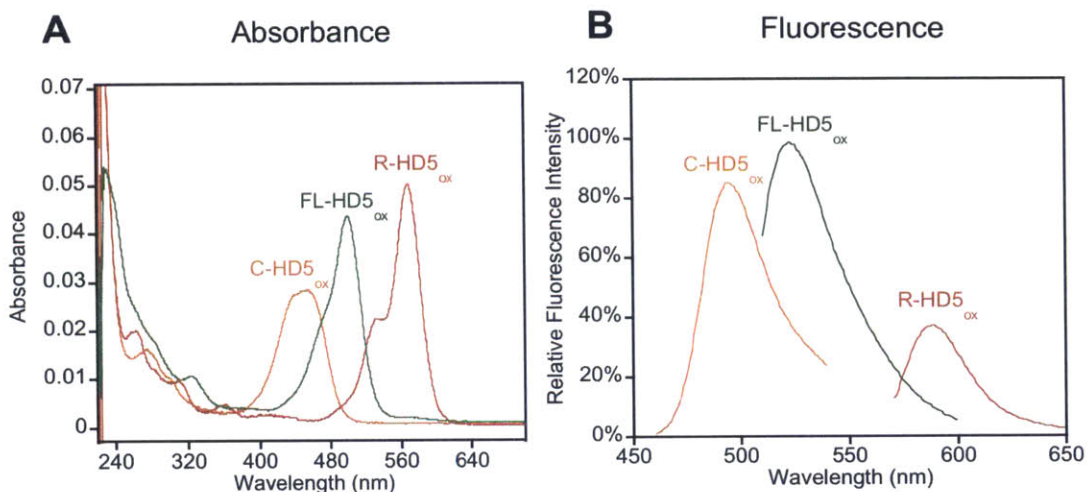
Figure 2.6. Fluorophore-HD5 derivatives span wide range of absorption and emission spectra. **A)** Absorbance and **B)** fluorescence spectra of fluorophore-modified HD5 conjugates (1 µM) measured in 75 mM HEPES, 100 mM NaCl and pH 7.4. Samples were excited at the absorption maxima of the respective peptides. Emission spectra are normalized to the intensity of FL-HD5$_{ox}$ for depiction. Emission spectra were obtained at 25 °C with a slit width of 1.4 nm.

iii. Photophysical Characterization of Fluorophore-HD5 Derivatives.

The photophysical properties of modified peptides should be compatible with physiological buffer conditions for the purposes of microscopy experiments. An ideal fluorophore should be bright and photostable in the physiological conditions for the duration of the experiment. The photophysical properties of desired fluorophore should be minimally perturbed upon appending the fluorophore to peptide. Therefore, a comprehensive photophysical characterization of family of fluorophore-modified peptides was performed.

Extinction Coefficient Determination. The concentrations of fluorophore-labeled peptides obtained from quantitative amino acid analysis were utilized for extinction coefficient determination. The samples were submitted for amino acid analysis at the Dana Farber Cancer Institute. The concentrations of iodoacetamide-capped peptides were determined from the mass of peptide dissolved in the Milli-Q. In order to study the effect of appending fluorophore to HD5, each parent fluorophore, fluorophore-modified HD5 and some standard fluorophores were studied. All measurements of modified peptides were acquired under simulated

physiological condition (75 mM HEPES, 100 mM NaCl, pH 7.4). The extinction coefficients of the peptides were determined and compared to the extinction coefficients of the standards (Table 2.3). The photophysical properties of modified peptides were compared in other solvents to the standards (Table 2.3). The extinction coefficients of the modified peptides were lower than the parent fluorophores. Absorption maxima of the modified peptides were slightly red-shifted compared to the parent fluorophores (Table 2.3). The extinction coefficients of the rhodamine B-modified Arg→Lys mutants were lower than N-terminal rhodamine B derivative.

Quantum Yield Determination. The emission spectra of modified peptides were acquired in buffer (75 mM HEPES, 100 mM NaCl, pH 7.4). Quantum yields of the modified peptides were determined with respective standards along with the parent compounds. The quantum yields of C-HD5$_{ox}$ were determined with coumarin 343 (Φ = 0.64, in ethanol)[31] as standard. Quantum yields of FL-HD5$_{ox}$ and FL-HD5-TE were determined with fluorescein (Φ = 0.95, in 0.1 N NaOH)[30] and finally R-HD5$_{ox}$, R-HD5-TE, R-HD5[R9K]$_{ox}$ and R-HD5[R13K]$_{ox}$ were measured with rhodamine 101 (Φ = 1.0, in methanol)[28] as respective standards. In order to study the effect of coupling of fluorophore to peptide, the parent fluorophores, coumarin 343 (**1**), 5(6)-carboxyfluorescein (**2**) and rhodamine B piperazine conjugate (**3**) were also studied.

The fluorescence emission of the peptide conjugates is lower in buffer compared to the solvents used for their respective standards, indicating a solvent effect (Table 2.3). The emission spectra of respective standards were also acquired in buffer to verify if the reduced emission in buffer is a result of fluorophore modification. Coumarin 343 (**1**) had displayed lower emission in buffer compared to the ethanol, and rhodamine 101 also exhibited lower emission in buffer compared to methanol (Table 2.3). It was observed that there was no significant difference in the emission of fluorescein in buffer (pH = 7.4) compared to the emission in 0.1 N NaOH.

The quantum yields of the peptides (Table 2.3) were subsequently determined. The observed quantum yields of rhodamine B derivative (**3**) indicate that the emission is quenched in aqueous solvents (Φ = 0.28, buffer) compared to the organic solvent (Φ = 0.43, methanol).

Thus, the lower quantum yield observed for R-HD5$_{ox}$ (Φ = 0.22) in buffer is not entirely due to peptide coupling but also due to the solvent effect. A similar solvent effect was observed for C-HD5$_{ox}$ (Φ = 0.32, buffer).

FL-HD5$_{ox}$ has lower quantum yield (Φ = 0.28, buffer) than the unmodified fluorophore even though carboxyfluorescein had negligible effect of solvent (Φ = 0.74, buffer) indicating that the peptide coupling had effected FL-HD5 fluorescence, and resulted in some degree of quenching. R-HD5[R13K]$_{ox}$ displayed lower quantum yield (Φ = 0.12, buffer) compared to R-HD5[R9K]$_{ox}$ (Φ = 0.20, buffer) and R-HD5$_{ox}$ (Φ = 0.22, buffer).

Table 2.3. Photophysical Characterization of Fluorophore-modified HD5-derivatives.

Compound	λ_{ex} (nm)	Extinction coefficient ε ($M^{-1}cm^{-1}$)	λ_{em} (nm)	Quantum yield Φ	Brightness (Φ x ε) ($M^{-1}cm^{-1}$)
R-HD5$_{ox}$	568	54500	585	0.22 ± (0.01) (n = 3)[a]	11400
R-HD5-TE	567	63600	589	0.31 ± (0.02) (n = 4)	19590
R-HD5[R9K]$_{ox}$	566	28400	584	0.20 ± (0.02) (n = 6)	5680
R-HD5[R13K]$_{ox}$	567	19500	587	0.12 ± (0.02) (n = 6)	2350
Rhodamine B derivative (3)	565	67600	587	0.28 ± (0.01) (n = 2)	18900
Rhodamine 101 (MeOH)[b]	567	120000	588	0.99 (n = 1)	118800
FL-HD5$_{ox}$	500	44800	522	0.28 ± (0.04) (n = 6)	12500
FL-HD5-TE	497	29100	522	0.64 ± (0.01) (n = 3)	18600
5(6)-Carboxyfluorescein (2)	492	73700	515	0.74 (n = 1)	54600
Fluorescein (0.1 N NaOH)[b]	490	76900	512	0.95 (n = 1)	73050
C-HD5$_{ox}$	456	21500	494	0.32 ± (0.02) (n = 7)	6900
Coumarin 343 (1)	429	36200	487	0.58 ± (0.005) (n = 3)	21200
Coumarin 343 (EtOH)[b]	443	44000	486	0.64 (n = 1)	28200

[a] n = total number of trials for quantum yield determination. The error is the standard deviation of the mean for n independent measurements. [b] The values are obtained from reported literature.[24,28,29,31]

In general, the photophysical properties indicated that 1) the emission of the fluorophores was lower in the buffer (75 mM HEPES, 100 mM NaCl, pH 7.4) compared to the solvents used for quantum yield measurements of respective standards, and 2) the quantum yields of modified peptides were lower than both the standards and their parent fluorophores. Nevertheless, the synthesized fluorophore-modified peptides (Table 2.3) were bright and suitable for microscopy-based experiments. These observations further emphasize the importance of the characterization of photophysical properties of fluorophore-appended to peptides, before employing them for elaborate microscopy experiments.

iv.   Antimicrobial Activity Assays of HD5 and its Derivatives

In order to assess the effect of modifying HD5 with a fluorophore on function, the antimicrobial activity of the fluorophore conjugates was evaluated using a colony forming units (CFU/mL) counting assay. The antimicrobial activities of modified peptides along with native HD5 were determined against *E. coli* ATCC 25922 and *S. aureus* ATCC 25923.

The antimicrobial activity assay against *E. coli* (1×10^6 CFU/mL) (Figure 2.6) indicated that $HD5_{ox}$ (4 µM) displayed most potent activity and this synthetic $HD5_{ox}$ had similar activity as $HD5_{ox}$ obtained from recombinant overexpression.[3,10] The fluorophore-conjugated derivatives displayed attenuated activity as R-$HD5_{ox}$ (16 µM) > C-$HD5_{ox}$ (28 µM) >> FL-$HD5_{ox}$ (>128 µM). The assay against *S. aureus* (Figure 2.7) also revealed a similar trend with $HD5_{ox}$ (2 µM) displaying most potent activity, and the modified peptides exhibited an attenuated activity as R-$HD5_{ox}$ (8 µM) > C-$HD5_{ox}$ (>28 µM) >> FL-$HD5_{ox}$ (>128 µM). The antimicrobial activity assays indicated that 1) fluorophore-conjugation attenuates the antimicrobial activity of HD5 and 2) the activity of conjugated peptides follows a trend in loss of activity with increasing negative charge on the fluorophore (R-$HD5_{ox}$ > C-$HD5_{ox}$ >> FL-$HD5_{ox}$). The variation observed in the antimicrobial activities of fluorophore-modified peptides could be a result of either appended parent fluorophore itself or any structural changes of HD5 due to fluorophore modification (e.g. change in the oligomeric state of HD5).

Finally, in order to verify the significance of site of fluorophore modification on the antimicrobial activity and localization of HD5$_{ox}$, another family of HD5 analogues with rhodamine B modification on internal side chains as opposed to N-terminus was examined. The
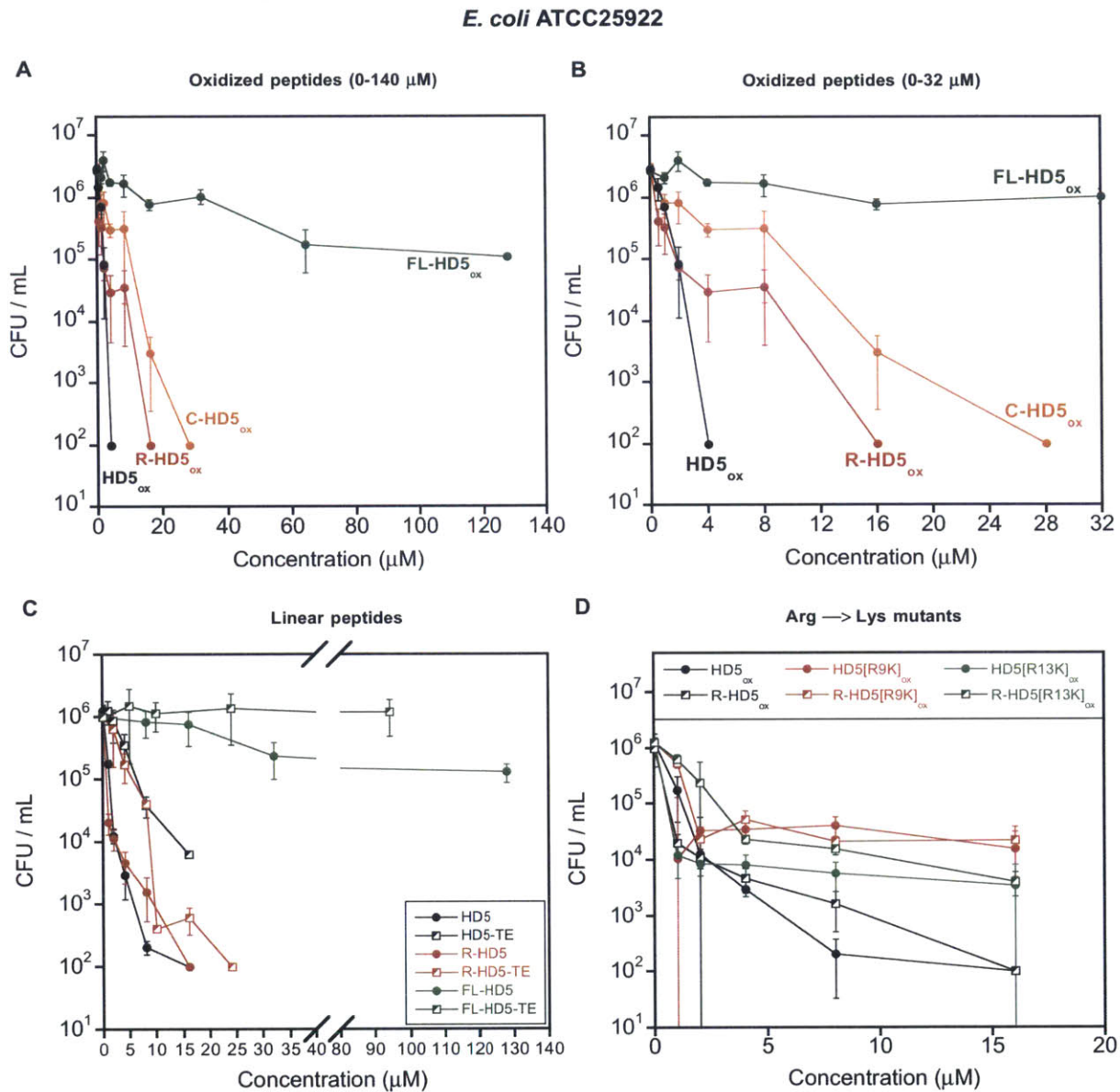
Figure 2.7. Antimicrobial activity of the peptides against *E. coli* ATCC 25922. The antimicrobial activity of **A)** oxidized forms of N-terminal fluorophore derivatives; **B)** an expansion of the low concentration range of panel A; **C)** Linear derivatives and **D)** Arg→Lys mutants of HD5. The bacteria (1 x 10^6 CFU/mL, mid-log) were treated with peptides for 1 h at 37 °C, 150 rpm (10 mM sodium phosphate buffer, 1% v/v TSB without dextrose, pH 7.4) (mean ± SD, n = 3).

Arg→Lys mutants were tested for antimicrobial action both with a rhodamine appended and unmodified forms. It was observed that the activity of these unmodified HD5[R9K]$_{ox}$ (MIC = >16 µM) and HD5[R13K]$_{ox}$ (MIC = 16 µM) were more active than their fluorophore modified
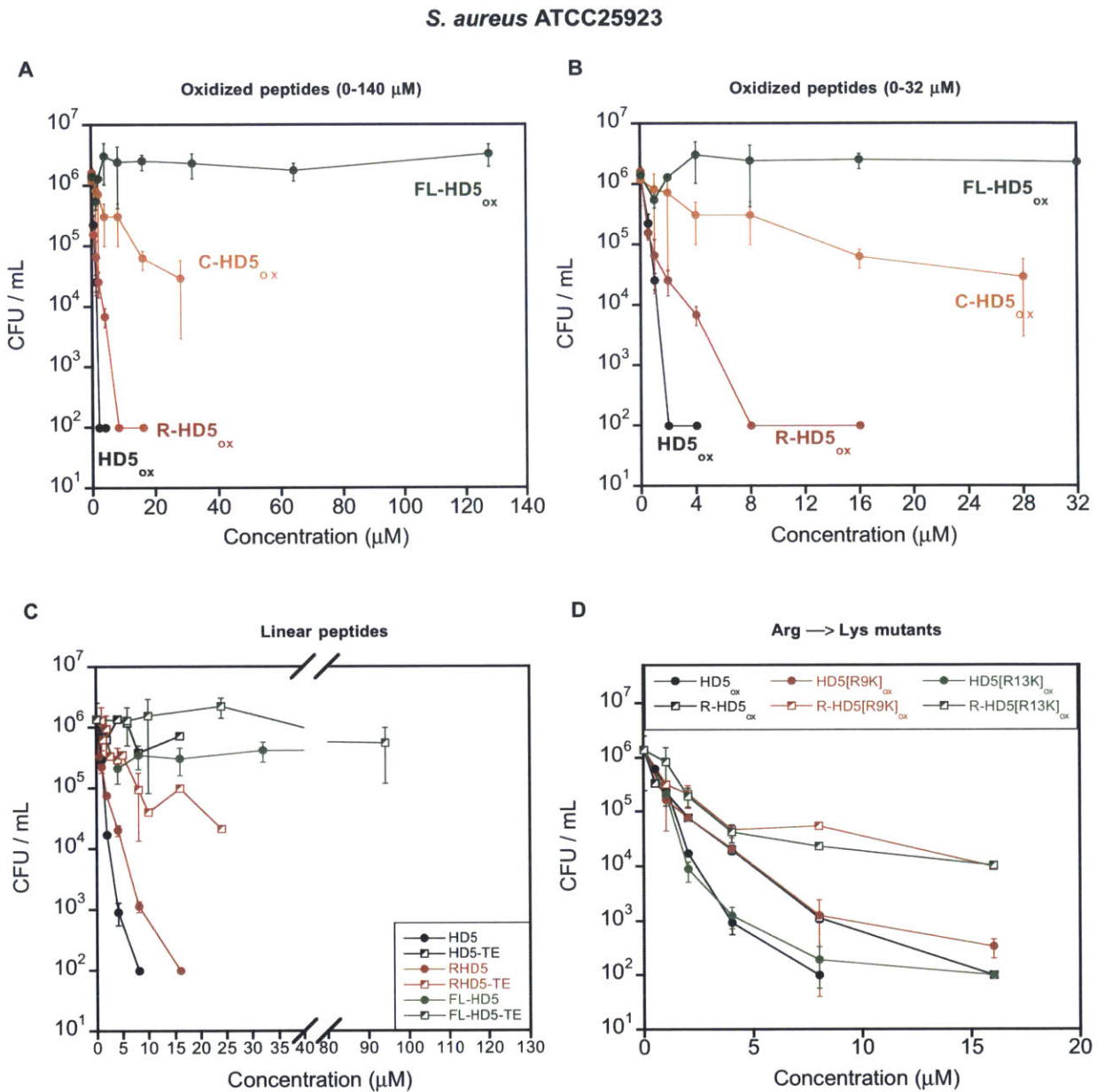
S. aureus ATCC25923

Figure 2.8. Antimicrobial activity of the peptides against *S. aureus* ATCC 25923. The antimicrobial activity of **A**) oxidized forms of N-terminal fluorophore derivatives; **B**) an expansion of the low concentration range of panel A; **C**) Linear derivatives and **D**) Arg→Lys mutants of HD5. The bacteria (1 x 10^6 CFU/mL, mid-log) were treated with peptides for 1 h at 37 °C, 150 rpm (10 mM sodium phosphate buffer, 1% v/v TSB without dextrose, pH 7.4) (mean ± SD, n = 3).

analogues against *S. aureus*. The Arg→Lys mutants were less active against *E. coli*, and both the fluorophore-labeled and unmodified peptides exhibited similar antimicrobial activity.

The linear peptides, as expected based on the published work,[10] were less active against both *E. coli* and *S. aureus* than their oxidized counterparts (Figures 2.7 and 2.8). When activity of HD5-TE (16 µM) and R-HD5-TE (25 µM) against *E. coli* (> two log- and > four log-fold of CFU/mL reduction, respectively) was compared to activity against *S. aureus* (< log- and < two log-fold CFU/mL reduction), the loss of activity was more pronounced against *S. aureus*. This result is in accordance with prior work, where as a general trend, it was observed that the activity of HD5 and its variants against Gram-negative bacteria were less dependent on the overall tertiary structure compared to Gram-positive bacteria.[10,36,37]

2D.   Summary

We established robust protocols for the synthesis and purification of HD5 and other analogues, including fluorophore-modified HD5 derivatives. The fluorophore-modified HD5 conjugates harboring rhodamine and coumarin display desirable photophysical properties and antibacterial activity against *E. coli* and *S. aureus*. These peptides enabled the studies of HD5 localization presented in Chapter 3.

2E.   Acknowledgements

2F.   References

(1) Ericksen, B., Wu, Z., Lu, W., and Lehrer, R. I. (2005) Antibacterial activity and specificity of the six human alpha-defensins. *Antimicrob. Agents Chemother. 49*, 269–275.

(2) Gounder, A. P., Wiens, M. E., Wilson, S. S., Lu, W., and Smith, J. G. (2012) Critical determinants of human α-defensin 5 activity against non-enveloped viruses. *J. Biol. Chem. 287*, 24554–24562.

(3) Wommack, A. J., Ziarek, J. J., Tomaras, J., Chileveru, H. R., Zhang, Y., Wagner, G., and Nolan, E. M. (2014) Discovery and characterization of a disulfide-locked C_2-symmetric defensin peptide. *J. Am. Chem. Soc. 136*, 13494–13497.

(4) Wehkamp, J., Salzman, N. H., Porter, E., Nuding, S., Weichenthal, M., Petras, R. E., Shen, B., Schaeffeler, E., Schwab, M., Linzmeier, R., Feathers, R. W., Chu, H., Lima, H., Fellermann, K., Ganz, T., Stange, E. F., and Bevins, C. L. (2005) Reduced Paneth cell alpha-defensins in ileal Crohn's disease. *Proc. Natl. Acad. Sci. U. S. A. 102*, 18129–18134.

(5) Spencer, J. D., Hains, D. S., Porter, E., Bevins, C. L., DiRosario, J., Becknell, B., Wang, H., and Schwaderer, A. L. (2012) Human alpha defensin 5 expression in the human kidney and urinary tract. *PLoS One 7*, e31712.

(6) Quayle, A. J., Porter, E. M., Nussbaum, A. A., Wang, Y. M., Brabec, C., Yip, K.-P., and Mok, S. C. (1998) Gene expression, immunolocalization, and secretion of human defensin-5 in human female reproductive tract. *Am. J. Pathol. 152*, 1247–1258.

(7) Brogden, K. A. (2005) Antimicrobial peptides: pore formers or metabolic inhibitors in bacteria? *Nat. Rev. Microbiol. 3*, 238–250.

(8) Figueredo, S., Mastroianni, J. R., Tai, K. P., and Ouellette, A. J. (2010) Expression and purification of recombinant alpha-defensins and alpha-defensin precursors in *Escherichia coli.*, in *Antimicrobial Peptides Methods and Protocols* (Giuliani, A., and Andrea C. Rinaldi, Eds.), pp 47–60. Springer New York.

(9) Marquès, L., Oomen, R. J. F. J., Aumelas, A., Le Jean, M., and Berthomieu, P. (2009) Production of an Arabidopsis halleri foliar defensin in *Escherichia coli. J. Appl. Microbiol. 106*, 1640–1648.

(10) Wanniarachchi, Y. A., Kaczmarek, P., Wan, A., and Nolan, E. M. (2011) Human defensin 5 disulfide array mutants: disulfide bond deletion attenuates antibacterial activity against *Staphylococcus aureus. Biochemistry 50*, 8005–8017.

(11) Pazgier, M., and Lubkowski, J. (2006) Expression and purification of recombinant human alpha-defensins in *Escherichia coli. Protein Expr. Purif. 49*, 1–8.

(12) Wang, A., Wang, S., Shen, M., Chen, F., Zou, Z., Ran, X., Cheng, T., Su, Y., and Wang, J. (2009) High level expression and purification of bioactive human alpha-defensin 5 mature peptide in *Pichia pastoris. Appl. Microbiol. Biotechnol. 84*, 877–884.

(13) Kubo, S., Tanimura, K., Nishio, H., Chino, N., Teshima, T., Kimura, T., and Nishiuchi, Y.

(2008) Optimization of the oxidative folding reaction and disulfide structure determination of human alpha-defensin 1, 2, 3 and 5. *Int. J. Pept. Res. Ther. 14*, 341–349.

(14) Wu, Z., Ericksen, B., Tucker, K., Lubkowski, J., and Lu, W. (2004) Synthesis and characterization of human alpha-defensins 4-6. *J. Pept. Res. 64*, 118–125.

(15) Wu, Z., Hoover, D. M., Yang, D., Boulègue, C., Santamaria, F., Oppenheim, J. J., Lubkowski, J., and Lu, W. (2003) Engineering disulfide bridges to dissect antimicrobial and chemotactic activities of human beta-defensin 3. *Proc. Natl. Acad. Sci. U. S. A. 100*, 8880–8885.

(16) Chairatana, P., and Nolan, E. M. (2014) Molecular basis for self-assembly of a human host-defense peptide that entraps bacterial pathogens. *J. Am. Chem. Soc. 136*, 13267–13276.

(17) Moser, S., and Nolan, E. M. Overexpression of HD5 in yeast, unpublished work.

(18) Bedford, J., Hyde, C., Johnson, T., Jun, W., Owen, D., Quibell, M., and Sheppard, R. C. (1992) Amino acid structure and "difficult sequences" in solid phase peptide synthesis. *Int. J. Pept. Protein Res. 40*, 300–307.

(19) Goncalves, V., Gautier, B., Huguenot, F., Leproux, P., Garbay, C., Vidal, M., and Inguimbert, N. (2009) Total chemical synthesis of the D2 domain of human VEGF receptor 1. *J.Pept.Sci. 15*, 417–422.

(20) Wöhr, T., Wahl, F., Nefzi, A., Rohwedder, B., Sato, T., Sun, X., and Mutter, M. (1996) Pseudo-prolines as a solubilizing, structure-disrupting protection technique in peptide synthesis. *J. Am. Chem. Soc. 118*, 9218–9227.

(21) Chileveru, H. R., Lim, S. A., Chairatana, P., Wommack, A. J., Chiang, I.-L., and Nolan, E. M. (2015) Visualizing attack of *Escherichia coli* by the antimicrobial peptide human defensin 5. *Biochemistry 54*, 1767–1777.

(22) Han, Y., Albericio, F., and Barany, G. (1997) Occurrence and minimization of cysteine racemization during stepwise solid-phase peptide synthesis. *J. Org. Chem. 62*, 4307–4312.

(23) Weber, P. J., Bader, J. E., Folkers, G., and Beck-Sickinger, A. G. (1998) A fast and inexpensive method for N-terminal fluorescein-labeling of peptides. *Bioorg. Med. Chem. Lett. 8*, 597–600.

(24) Fischer, R., Mader, O., Jung, G., and Brock, R. (2003) Extending the applicability of carboxyfluorescein in solid-phase synthesis. *Bioconjug. Chem. 14*, 653–660.

(25) Nguyen, T., and Francis, M. B. (2003) Practical synthetic route to functionalized rhodamine dyes. *Org. Lett. 5*, 3245–3248.

(26) Zhang, Y., Cougnon, F. B. L., Wanniarachchi, Y. A., Hayden, J. A., and Nolan, E. M. (2013) Reduction of human defensin 5 affords a high-affinity zinc-chelating peptide. *ACS Chem. Biol. 8*, 1907–1911.

(27) Simon, M. D., Heider, P. L., Adamo, A., Vinogradov, A. A., Mong, S. K., Li, X., Berger, T., Policarpo, R. L., Zhang, C., Zou, Y., Liao, X., Spokoyny, A. M., Jensen, K. F., and Pentelute, B. L. (2014) Rapid flow-based peptide synthesis. *Chembiochem 15*, 713–720.

(28) Karstens, T., and Kobs, K. (1980) Rhodamine B and rhodamine 101 as reference substances for fluorescence quantum yield measurements. *J. Phys. Chem. 84*, 1871–1872.

(29) Drexhage, K. H. (1973) Structure and properties of laser dyes, in *Dye Lasers* (Schäfer FP, Ed.), pp 144–193. Springer-Verlag Berlin Heidelberg.

(30) Sjöback, R., Nygren, J., and Kubista, M. (1995) Absorption and fluorescence properties of fluorescein. *Spectrochim. Acta Part A Mol. Biomol. Spectrosc. 51*, L7–L21.

(31) Reynolds, G. A., and Drexhage, K. H. (1975) New coumarin dyes with rigidized structure for flashlamp-pumped dye lasers. *Opt. Commun. 13*, 222–225.

(32) Wommack, A. J., Robson, S. A., Wanniarachchi, Y. A., Wan, A., Turner, C. J., Wagner, G., and Nolan, E. M. (2012) NMR solution structure and condition-dependent oligomerization of the antimicrobial peptide human defensin 5. *Biochemistry 51*, 9624–9637.

(33) Szyk, A., Wu, Z., Tucker, K., Yang, D., Lu, W., and Lubkowski, J. (2006) Crystal structures of human alpha-defensins HNP4, HD5, and HD6. *Protein Sci. 15*, 2749–2760.

(34) de Leeuw, E., Rajabi, M., Zou, G., Pazgier, M., and Lu, W. (2009) Selective arginines are important for the antibacterial activity and host cell interaction of human alpha-defensin 5. *FEBS Lett. 583*, 2507–2512.

(35) Chapnik, N., Levit, A., Niv, M. Y., and Froy, O. (2012) Expression and structure/function relationships of human defensin 5. *Appl. Biochem. Biotechnol. 166*, 1703–1710.

(36) de Leeuw, E., Burks, S. R., Li, X., Kao, J. P. Y., and Lu, W. (2007) Structure-dependent functional properties of human defensin 5. *FEBS Lett. 581*, 515–520.

(37) Wei, G., de Leeuw, E., Pazgier, M., Yuan, W., Zou, G., Wang, J., Ericksen, B., Lu, W.-Y., Lehrer, R. I., and Lu, W. (2009) Through the looking glass, mechanistic insights from enantiomeric human defensins. *J. Biol. Chem. 284*, 29180–29192.

Chapter 3

Visualizing the of Attack of *Escherichia coli* by the Antimicrobial Peptide Human Defensin 5

3A.   Introduction

Human defensins are established contributors to immunity, and many exhibit broad-spectrum *in vitro* antimicrobial activity; however, details pertaining to the physiological function of each peptide are often unclear.[1-3] Human defensin 5 (HD5) is the most abundant Paneth cell antimicrobial peptide,[4] and it exhibits broad-spectrum antimicrobial activity *in vitro*.[5-8] In this Chapter, we focus on a fundamental and outstanding question: how does HD5 kill bacteria?

How defensins kill bacteria as well as how *in vitro* antibacterial activity relates to the physiological milieu are questions of current interest and debate.[2] The oxidized α-defensins display remarkable similarity in their tertiary structure, and most characterized to date are cationic and amphipathic.[9] Moreover, defensins from various organisms have the capacity to disrupt bacterial cell membranes.[10-12] On the basis of early investigations, including seminal structural studies of HNP3,[13] a working model whereby defensins kill bacteria by non-specific membrane destabilization was presented.[10,13] Over the years, this type of model was generalized for many defensins and other antimicrobial peptides.[2] Nevertheless, defensins exhibit remarkable diversity in primary sequence, and recent studies support alternative mechanisms of action for some family members. Fungal plectasin,[14] oyster defensin,[15] and fungal copsin[16] bind lipid II and block cell wall biosynthesis. The human defensins human neutrophil peptide 1 (HNP1, α-defensin)[17] and human β-defensin 3 (HBD3)[18] are also reported to bind lipid II to varying degrees.[19] Studies of HBD3 attributed the *in* vitro antibacterial activity against *Staphylococcus aureus* to lipid II binding and subsequent cell wall lysis.[18] Recently, Human β-defensin 2 (HBD2) was found to localize at septal foci of *Enterococcus faecalis* and disrupt virulence factor assembly.[20] Although human α-defensin 6 (HD6) lacks antimicrobial activity *in vitro*, it is proposed to serve a host-defense function by self-assembling into a web-like structure termed "nanonet" that captures bacteria in the intestinal lumen.[21,22] A recent study identified that the reduced form of HD6 exhibits antimicrobial activity.[23] Taken together, these investigations highlight tremendous variation in defensin mechanism of action despite

similar tertiary structures, and demonstrate that membrane permeabilization is only one of the many factors that contribute to the *in vitro* antimicrobial activities demonstrated by this vast peptide family.

Paneth cells,[24] located in the crypts of Lieberkühn, contain granules that store two α-defensins, HD5 and HD6, as well as other antimicrobial peptides, proteases, and a labile zinc pool of unknown function.[25,26] The enteric α-defensin HD5 (Figure 3.1), the focus of this thesis, is an abundant constituent of small intestinal Paneth cell granules;[24,27–29] it has been estimated that up to 450 µg/cm^2 is stored in the ileal mucosa, with concentrations of 50 - 250 µg/mL,[30] in the range of minimum inhibitory concentration (MIC) for HD5 *in vitro*. Moreover, transgenic mice expressing HD5 are more resistant to *Salmonella* challenge than wild-type mice,[31] and studies of the resident intestinal microbiota suggest that HD5 contributes to controlling its composition.[31,32] In humans suffering from ileal Crohn's disease, an inflammatory disorder of the small bowel, a deficiency in Paneth cell defensins is observed.[4] Despite these compelling observations, the antimicrobial mechanism of action of HD5 is not well understood.

HD5 is a 32-residue peptide with an overall charge of +4 at neutral pH (Figure 3.1). Over the past decade, structure-activity relationship studies of HD5$_{ox}$ evaluated the importance of
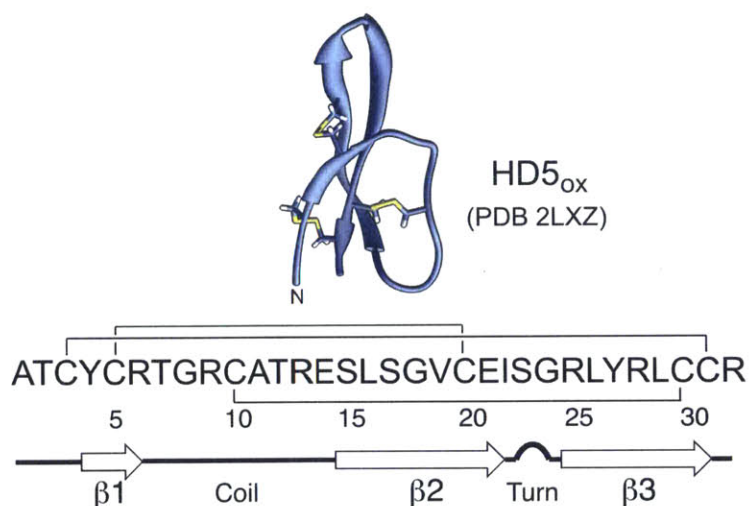
Figure 3.1. Structure of the HD5$_{ox}$ monomer determined by solution NMR (PDB 2LXZ)[56] and amino acid sequence. The regiospecific disulfide bond linkages and secondary structure are indicated.

quaternary structure,[8,33] disulfide linkages[34,35] cationic residues,[36] the canonical α-defensin salt bridge between [Arg^6] and [Glu^{14}],[37] and chirality[38] for its *in vitro* bactericidal activity. Results from several recent studies probing interactions between $HD5_{ox}$ and *E. coli* support a model whereby (i) the Gram-negative outer membrane serves as a permeability barrier for $HD5_{ox}$[39,40] and (ii) the inner membrane becomes damaged as a result of $HD5_{ox}$ exposure.[34]

In the studies described in this Chapter, we utilize microscopy to investigate the attack of $HD5_{ox}$ on Gram-negative bacteria. We detail a systematic study to investigate the effect of HD5 on various bacteria and examine their response to various HD5 analogues. We observe that *E. coli* treated with native $HD5_{ox}$ exhibit distinct morphologies that include clumping, cell elongation, and formation of one or more cellular blebs typically at the cell poles or division site. We demonstrate that similar morphological changes occur for other Gram-negative bacteria, including the opportunistic human pathogens *Acinetobacter baumannii* and *Pseudomonas aeruginosa*, following $HD5_{ox}$ exposure. Employing a family of fluorophore-HD5 conjugates described in the Chapter 2, we report that rhodamine- and coumarin-modified $HD5_{ox}$ enter the *E. coli* cytoplasm. Moreover, the localization of these fluorophore-HD5 conjugates preferentially at cell poles and cell division sites in *E. coli*, suggests a possible intracellular target at these sites.

3B.   Experimental Methods and Materials

i.   Chemicals, Solvents, and Buffers. Propidium iodide, FM4-64, and FM1-43 were obtained from Molecular Probes. Sodium phosphate was obtained from BDH Chemicals. TSB without dextrose was obtained from Becton Dickinson (BD). HD5 was either (i) overexpressed from *E. coli* BL21(DE3) cells as described previously,[34] or (ii) synthesized by Fmoc solid-phase synthesis as reported in Chapter 2.[8,34] HD5-CD from $HD5_{red}$ or $HD5_{ox}$, $HD5[E21S]_{ox}$, cryptdin-4 and HD5-TE were prepared as described elsewhere.[8,41] LL-37 and rhodamine-modified LL-37 were purchased from Bachem Americas, Inc. Melittin and colistin sulfate were obtained from

Enzo Life Sciences Inc. All peptides were stored at -20 °C. The peptide stock solutions and buffers for antimicrobial activity assays are prepared as described in Chapter 2.

ii.   Antimicrobial Activity Assays. Antimicrobial activity (AMA) assays were performed in 96-well plates using a micro-drop colony forming units (CFU) method described previously in Chapter 2.[8] The bacteria were grown overnight in TSB (without dextrose) medium with antibiotics when necessary and the cultures were diluted further (Table 3.1) to a cell count of 1 x 10^8 CFU/mL or 10^6 CFU/mL.

Table 3.1. Strains and Growth Conditions Employed in this Work.

Strain	Source	AMA dilution factor[a]	Growth medium
E. coli 25922	ATCC	1:200	TSB w/o dextrose
E. coli CFT073	ATCC	1:200	TSB w/o dextrose
A. baumannii 17961	ATCC	1:200	TSB w/o dextrose
K. pneumoniae 13883	ATCC	1:100	TSB w/o dextrose
P. aeruginosa PAO1	Prof. Katharina Ribbeck, MIT	1:100	TSB w/o dextrose
E. coli K-12	Keio collection[42]	1:200	TSB w/o dextrose
E. coli peri-GFP	MG1655/ pDKR2 (dsbA$_{ss}$-sfgfp)[43] transformed in E. coli K-12	1:200	TSB w/o dextrose, 50 µg/mL kanamycin
E. coli cyto-GFP	pBBR1(MCS5)-P$_{lac}$-gfp[44] transformed in E. coli 25922	1:200	TSB w/o dextrose, 10 µg/mL gentamycin

[a] The AMA dilution factor indicates the dilution of each mid-log phase culture employed in the antimicrobial activity assays to achieve 1 x 10^6 CFU/mL.

iii.   Scanning Electron Microscopy. For the preparation of samples for scanning electron microscopy (SEM), AMA assays were performed as described above except that each sample well contained a higher starting bacterial count (1 x 10^8 CFU/mL), and a total five wells of 100 µL each were set up per condition. After incubation at 37 °C for 1 h, the contents of the five wells for each condition were combined and centrifuged (8000 rpm x 5 min, 4 °C). The resulting

bacterial cell pellet was resuspended and fixed in modified Karnovsky's fixative (2.0% paraformaldehyde and 2.5% glutaraldehyde in 0.067 M sodium phosphate buffer, pH 7.3) overnight at room temperature. The sample was then centrifuged (8000 rpm x 5 min, 4 °C) and the pellet was resuspended gently in 0.5 mL of 133 mM sodium phosphate buffer, pH 7.3. A glass coverslip (12 mm, round) was bathed in 0.5 mL of 0.1% aqueous poly-L-lysine hydrobromide (Polysciences) for at least 1 h. The excess poly-L-lysine was removed by blotting with filter paper and the coverslip was bathed in the bacterial sample for at least 1 h. The coverslip was then washed with 0.5 mL of 0.133 M fresh sodium phosphate buffer, pH 7.3. The sample on the coverslip was then dehydrated in multiple steps using 0.5 mL of ascending concentrations of EtOH, (30%, 50%, 70%), three rounds of 95% and two steps of 100% (200 proof) EtOH for 10 min at each step. The sample was further dried in 0.5 mL of 2:1 (EtOH: HMDS), 1:1 (EtOH: HMDS), 1:2 (EtOH: HMDS) mixtures and 3 rounds of 100% HMDS for 15 min at each step. The last HMDS was removed and the sample was allowed to dry in a dust-free environment. Then, the sample was mounted on specimen support stubs using double-stick carbon tape. The sample was sputter coated with 5 nm of gold. The stubs were stored in a dust-free and dry environment. The images were acquired either at 10-kV or 15-kV accelerating voltage using JEOL 6010LA scanning electron microscope at the Institute for Soldier Nanotechnologies, MIT (Cambridge, MA).

iv. **Transmission Electron Microscopy.** *E. coli* ATCC 25922 (1×10^8 CFU/mL) were treated with either Milli-Q water (no peptide control) or 40 μM $HD5_{ox}$ (10 wells x 100 μL) following the standard AMA assay described above. The samples for each condition were pooled and were centrifuged (13000 rpm x 10 min, 4 °C), and the pellet was resuspended in 0.1 M sodium cacodylate buffer, pH 7.4 (containing 2% gluteraldehyde, 3% paraformaldehyde, 5% sucrose). The samples were further processed at the W.M. Keck Biological Imaging Facility of the Whitehead Institute (Cambridge, MA). The samples were rinsed in 0.1 M cacodylate buffer (containing 7.5% sucrose), treated with Palade's osmium (1% osmium tetroxide) for 1 h, and

rinsed in deionized water before staining with Kellenberger's uranyl acetate. The pellet was dehydrated in a series of ascending ethanol solutions from 50 to 100%, and embedded in epoxy resin. The resin was cured at 60 °C for 24 h. Thin sections were cut mounted on formvar coated grids and stained with uranyl acetate and lead citrate. The TEM images were collected on FEI Technai Spirit Transmission Electron Microscope.

v.   General Methods and Image Analysis for Phase-contrast and Fluorescence Microscopy

Phase-contrast Microscopy. For morphology studies, standard AMA assays were performed in 96-well plates (100 μL sample volume per well) using 1 x 10^8 CFU/mL of bacteria. Following each 1-h incubation, a 5-μL sample from each condition was placed on 1% agarose pads and each sample was topped with a coverslip. To prepare the agarose pads, 1% w/w agarose was mixed with AMA buffer and heated, and 100 μL of the heated liquid agarose was poured onto a glass microscope slide and allowed to cool and solidify before use. Imaging was performed in the W.M. Keck Biological Imaging Facility of the Whitehead Institute (Cambridge, MA). For light microscopy studies of samples treated with HD5$_{ox}$, HD5-TE, HD5-CD, HD5[E21S]$_{ox}$, and other AMPs, a Zeiss Axioplan2 upright microscope was employed.

Assay Conditions for Fluorescence Microscopy Experiments. Bacteria (180 μL of a 1 x 10^8 CFU/mL culture suspended in 10 mM sodium phosphate buffer, 1% TSB without dextrose, pH 7.4) were placed on a poly-D-lysine coated MatTek plate, and 20 μL of a 10x peptide stock solution was added. The AMA assay was performed following the standard method except that the plates were incubated in the dark for 1 h (130 rpm, 37 °C). For microscopy experiments, stock solutions of parent fluorophores, propidium iodide, and FM dyes were prepared in DMSO, aliquoted, and frozen at -20°C. For experiments using parent fluorophores or other dyes (e.g. propidium iodide), the DMSO stock solution of each dye was diluted with AMA buffer (10 mM sodium phosphate buffer, 1% TSB without dextrose, pH 7.4) to afford a 10x working concentration and a 20-μL aliquot was added to the plate. For all experiments, the final DMSO concentration was <5% v/v. The bacteria on the MatTex plate were thoroughly yet gently

washed with AMA buffer (3 x 3 mL), which removed detached bacteria and excess fluorophore. Then, 3 mL of AMA buffer was added and the plate was covered and sealed with parafilm. When membrane-labeling FM dyes were employed, the bacteria (10^8 CFU/mL) were incubated with the indicated dye (2 μg/mL) for 15 min at room temperature, subsequently washed with AMA buffer (3 x 3 mL) and imaged. For time-lapse experiments, the bacteria (1 x 10^8 CFU/mL in AMA buffer) were incubated at 37 °C on MatTek plates for 15 min and excess unbound bacteria were removed by gentle wash steps with AMA buffer (3 x 3 mL). The bacteria were covered with 1 mL of AMA buffer and the plate was subsequently positioned on the microscope stage, maintained at 37 °C using an incubation chamber. To the immobilized cells, 2 mL of $HD5_{ox}$ (30 μM stock resulting in a final 20 μM $HD5_{ox}$) in AMA buffer was added to the plate and image acquisition was initiated immediately.

Fluorescence Microscopy. For the time-lapse studies, images were collected on a Nikon-TE 2000 U wide-field inverted microscope fitted with an incubation enclosure. The images were obtained with a Hamamatsu ORCA CCD camera. Texas Red (ex: 532-587 nm, em: 608-683 nm, red channel) and GFP (ex: 457-487 nm, em: 502-538, green channel) filters were used. Confocal microscopy was performed with an Andor Spinning Disk Confocal microscope. The confocal microscopy data were collected using Andor IQ acquisition software and Andor iXion+ EMCCD cameras. Excitation lasers set at 488 and 561 nm were used for the green and red channels, respectively. All images were collected, irrespective of microscope, using 100x oil-immersion objective lenses.

Image Analysis. Image analysis was performed with the ImageJ software. Fluorescence background subtraction was performed using rolling ball method with a radius of 150 pixels. The cell outline was manually identified and used to define the region of interest (ROI). From the identified ROI, ImageJ was used to measure cell length. When cells exhibiting particular morphologies were counted, cells of length ≥ 5 μm were categorized as elongated. Cells with blebs were manually identified and counted.

Image Processing and Analysis for GFP Intensity Distribution Studies: The intensities of the fluorescence images to be analyzed were set to a minimum of 0 and a maximum of 3500. The images were then converted to 8-bit tiff files and the ROIs were analyzed using ImageJ.

Time-lapse Experiments: The time-lapse data were collected and the cells were aligned using registration Linear Stack Alignment with the SIFT plugin.

Intensity Profiles and Surface Plots: The fluorescence intensity profiles along the cell length and at the cell poles of bacteria treated with fluorophore-HD5 conjugates were plotted using 8-bit tiff files of cropped single cells. Using the line tool and plot profile tool, the intensity profiles were plotted to indicate the localization of labeled peptide with respect to the cell membrane. The 3D surface plots were obtained using imageJ.

3C.   Results and Discussion

i.   HD5 Causes Distinct Morphological Changes in *Escherichia coli.* For morphology studies, we selected to image Gram-negative *E. coli.* This microbe is a commensal microbe of the human gut as well as a pathogen of the gut and urogenital tract, and a number of studies have probed the antibacterial activity of $HD5_{ox}$ against this strain.[5,34,37] In AMA assays, the concentration of $HD5_{ox}$ required to kill *E. coli* (e.g., lethal dose 99.99% or 4-fold log reduction in CFU/mL) depends on the number of colony forming units. Our standard AMA assay for evaluating $HD5_{ox}$ activity employs mid-log phase bacteria at $\approx 1 \times 10^6$ CFU/mL cultured in an AMA buffer (10 mM sodium phosphate buffer pH 7.4, 1% v/v TSB without dextrose). Under these conditions, the concentration of $HD5_{ox}$ required to kill 99.99% of *E. coli* is ≈ 4 μM depending on the precise starting CFU/mL. Treatment of mid-log-phase *E. coli* ATCC 25922 (1 x 10^6 CFU/mL) with $HD5_{ox}$ (2 and 4 μM) under standard AMA assay conditions resulted in marked changes to the bacterial morphology observable by phase-contrast microscopy that included the formation of large bulges, hereafter called blebs (Figure 3.2).
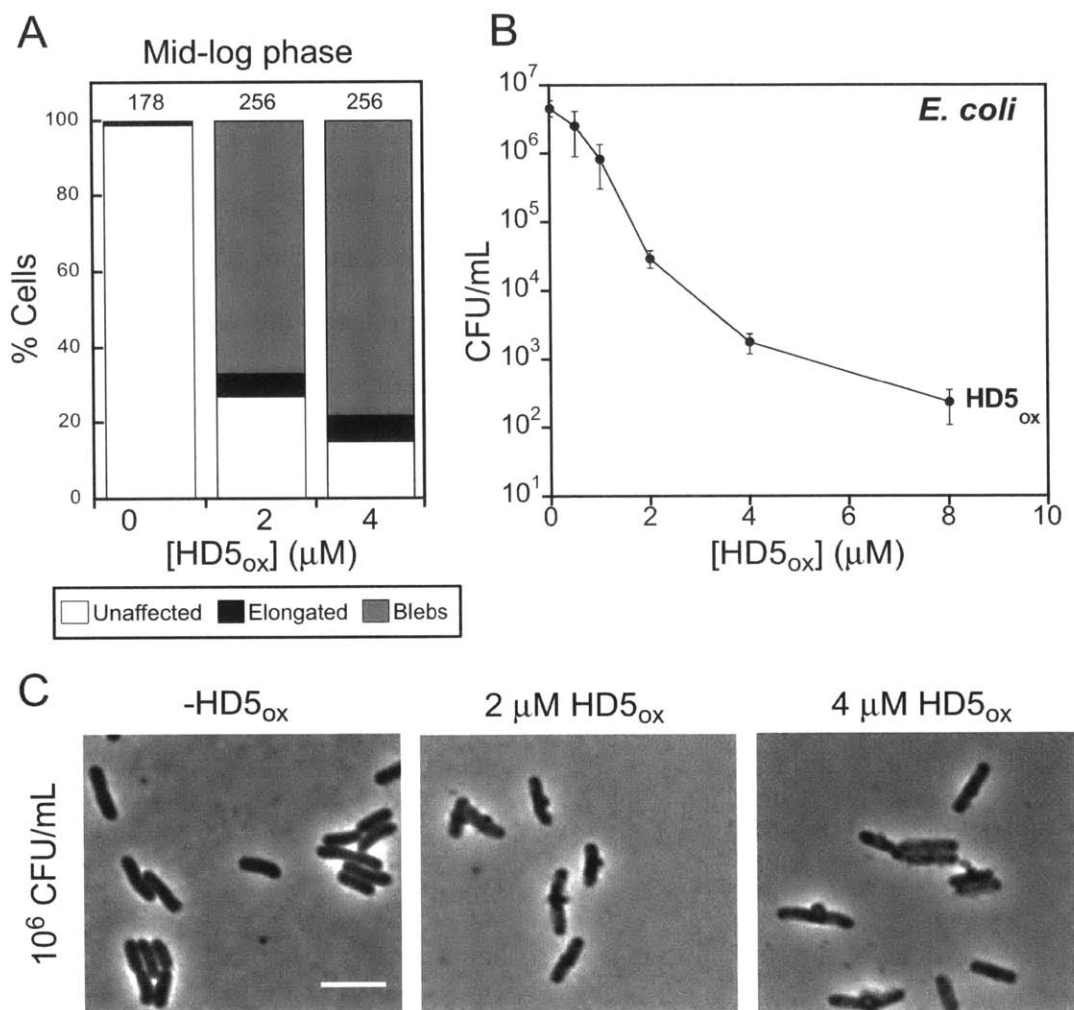
Figure 3.2. HD5$_{ox}$ affects the morphology of *E. coli* under standard AMA assay conditions. *E. coli* ATCC 25922 (1 x 10^6 CFU/mL, mid-log phase) were treated with 0 - 4 μM HD5$_{ox}$ at 37 °C (10 mM sodium phosphate buffer, pH 7.4, 1% v/v TSB w/o dextrose) for 1 h. **A)** Quantification of number of cells displaying morphological changes upon HD5$_{ox}$ treatment. **B)** Antimicrobial activity of HD5$_{ox}$ (n = 3, standard deviation). **C)** Morphology of HD5$_{ox}$ treated *E. coli*. Scale bar = 5 μm.
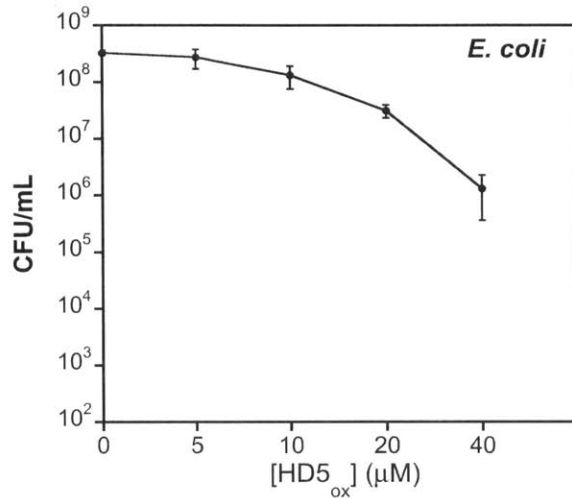
Figure 3.3. Antimicrobial activity of $HD5_{ox}$ against *E. coli* (10^8 CFU/mL). The assay was performed with *E. coli* ATCC 25922 (1×10^8 CFU/mL, mid-log phase) treated with 0 - 40 μM $HD5_{ox}$ at 37 °C (10 mM sodium phosphate buffer, pH 7.4, 1% v/v TSB w/o dextrose) for 1 h (n = 3, standard deviation).
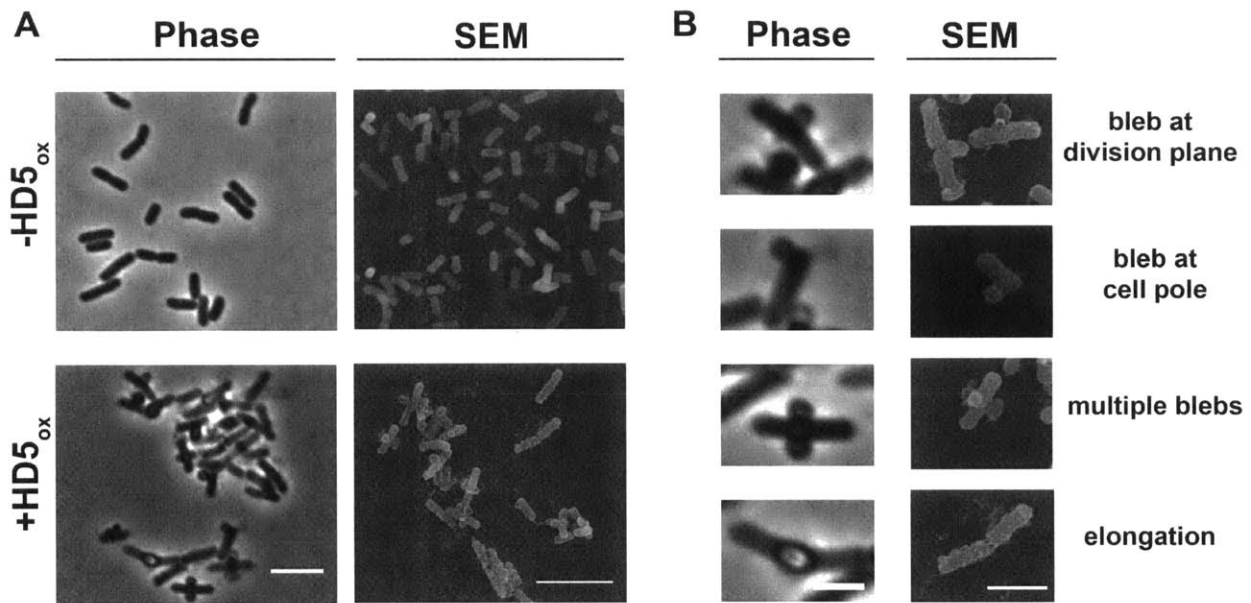
Figure 3.4. $HD5_{ox}$ causes distinct morphological changes in *E. coli* that include bleb formation, cellular elongation, and clumping. **A)** Phase-contrast and the SEM images of *E. coli* ATCC 25922 (1×10^8 CFU/mL) in the absence ($-HD5_{ox}$) or presence ($+HD5_{ox}$) of 20 μM $HD5_{ox}$, scale bar= 5 μm. **B)** Phase-contrast and the SEM images of single cells illustrate the various morphologies caused by $HD5_{ox}$, scale bar = 2 μm.

113

To facilitate visualizing more cells per experiment, we modified the standard AMA conditions and employed a greater number of cells (1×10^8 CFU/mL) and higher concentrations of $HD5_{ox}$ (0-80 μM). Under these conditions, $HD5_{ox}$ displays AMA, and $\approx$2-fold log reduction in CFU/mL is observed following treatment of the *E. coli* with 40 μM $HD5_{ox}$ (Figure 3.3). Moreover, the *E. coli* displayed distinct morphological changes as observed in the preliminary experiment (Figure 3.2 and 3.4). On the basis of this similarity, we employed the modified conditions with greater cell density and higher $HD5_{ox}$ concentration for further imaging experiments. The morphologies observed under these conditions included cellular elongation and the formation of blebs (Figure 3.4). Clumping of *E. coli* was also observed. Bacterial cells with lengths of 5 μm or greater were categorized as elongated, and cells with lengths in the 10-15 μm range were periodically observed following $HD5_{ox}$ treatment. The blebs were typically localized at the cell division sites and cell poles; however, some bacteria displayed blebs along the cell body, and some bacteria exhibited multiple blebs per cell. The blebs remained intact during the centrifugation and wash steps required for scanning electron microscopy (SEM) sample preparation. Indeed, the blebs as well as what appeared to be outer membrane vesicles (Figure 3.5) and cellular debris (*vide infra*) were markedly apparent in SEM images (Figure 3.4). Neither blebs nor elongation were observed for untreated cells, and the number of cells exhibiting these morphological changes increased with increasing $HD5_{ox}$ (0-80 μM) (Figure 3.6). Following exposure to 20 μM $HD5_{ox}$, $\approx$17% of cells exhibited blebs and 2% were elongated (n = 212 cells). These values increased to $\approx$30% and $\geq$4% at $\geq$40 μM $HD5_{ox}$, respectively (n = 203 cells). We performed time-course experiments where *E. coli* were exposed to 20 μM $HD5_{ox}$ on the microscope stage and imaged over time ($\approx$2 h). Many of the treated cells displayed blebs, and the blebbing cells did not lyse over the course of this experiment (Figure 3.7). Propidium iodide (PI) uptake was therefore employed to evaluate the viability of $HD5_{ox}$-treated cells, and the cells exhibiting blebs were labeled with PI, which indicated that bleb formation correlated with cell death (Figure 3.8). The morphological changes observed for *E. coli* ATCC 25922 were comparable to those we recently reported for *E. coli* K-12.[40]
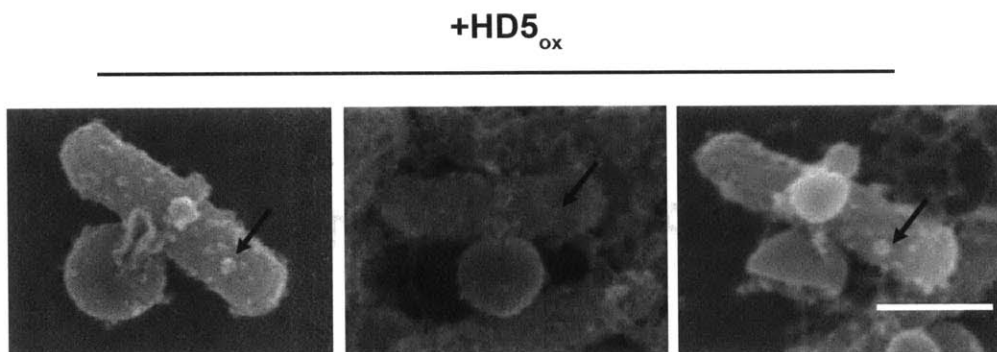
+HD5$_{ox}$

Figure 3.5. *E. coli* treated with HD5$_{ox}$ display membrane vesicles as well as large blebs. The arrow in each SEM image points to the observed membrane vesicles. *E. coli* ATCC 25922 (1 x 10^8 CFU/mL, mid-log phase) were treated with 40 μM HD5$_{ox}$ at 37 °C (10 mM sodium phosphate buffer, pH 7.4, 1% v/v TSB without dextrose) for 1 h prior to fixation. Scale bar = 1 μm.
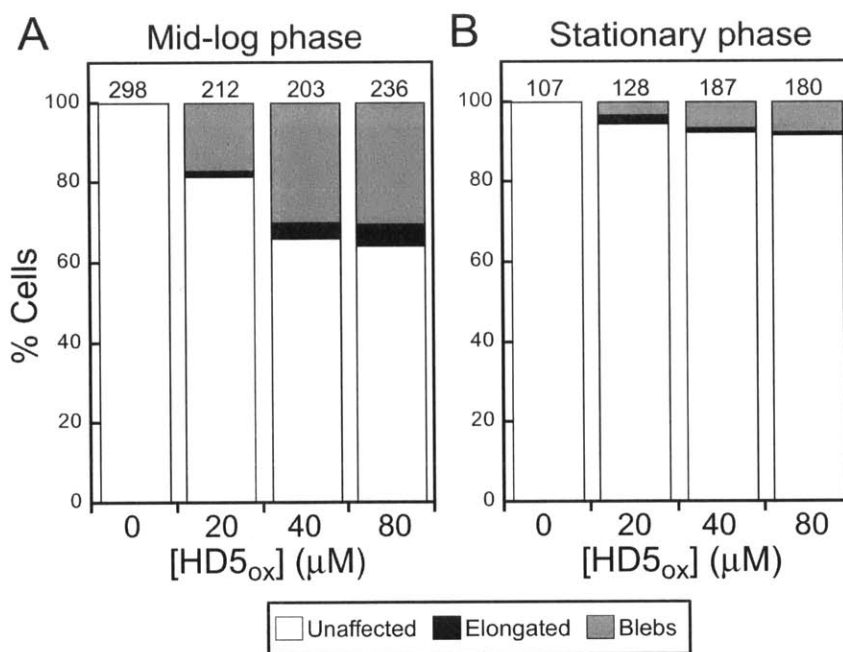
Figure 3.6. Quantification of the morphological changes induced by HD5$_{ox}$ treatment on *E. coli* ATCC 25922. The cells (1 x 10^8 CFU/mL) were treated with varying concentrations of HD5$_{ox}$ for 1 h at 37 °C (10 mM sodium phosphate buffer, pH 7.4, 1% (v/v) TSB). **A)** Quantification of unaffected as well as elongated and bleb morphologies for mid-log phase and **B)** stationary-phase *E. coli*. The number above each bar indicates the number of cells counted.

115
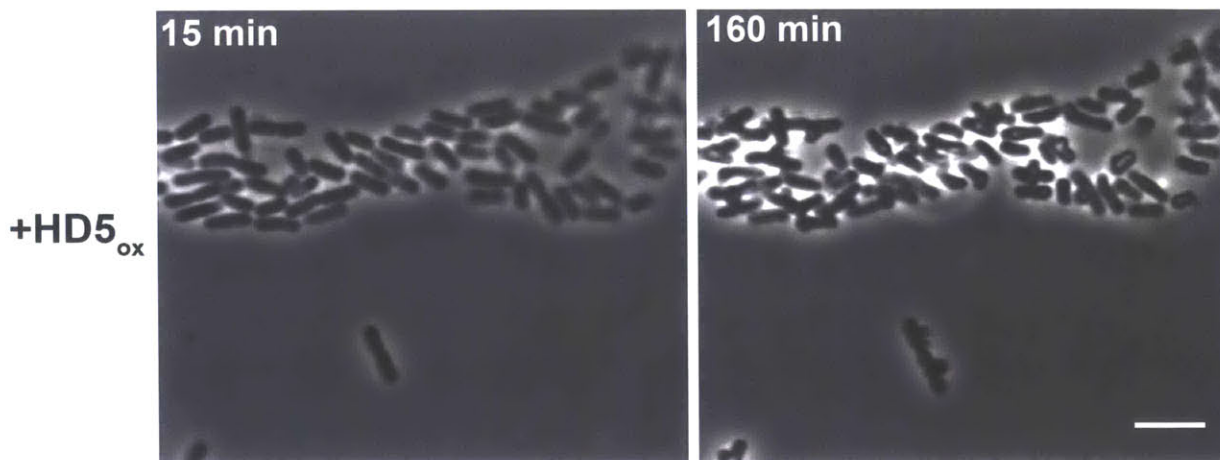
Figure 3.7. Time-lapse imaging of *E. coli* ATCC 25922 (1×10^7 CFU/mL, mid-log phase) treated with 20 µM HD5$_{ox}$ at 37 °C (10 mM sodium phosphate buffer, pH 7.4, 1% v/v TSB without dextrose). The phase-contrast image panels indicate the sample incubated for 15 min (left) and 160 min (right) after addition of HD5$_{ox}$. Scale bar = 5 µm.
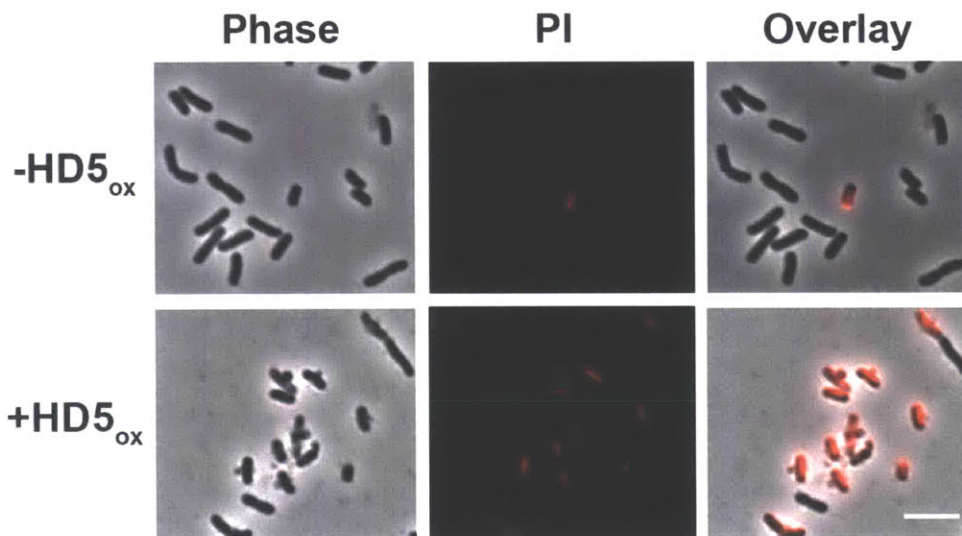
Figure 3.8. *E. coli* treated with HD5$_{ox}$ that display morphological changes (e.g., blebs) are not viable as indicated by propidium iodide (PI) uptake. *E. coli* ATCC 25922 (1×10^8 CFU/mL, mid-log phase) exposed to 20 µM HD5$_{ox}$ (+HD5$_{ox}$) or control (-HD5$_{ox}$) for 1 h at 37 °C, 130 rpm (10 mM sodium phosphate buffer, 1% v/v TSB without dextrose, pH 7.4), were stained with 5 µg/mL PI for 15 min prior to imaging. Scale bar = 5 µm. Excitation wavelength: 561 nm.
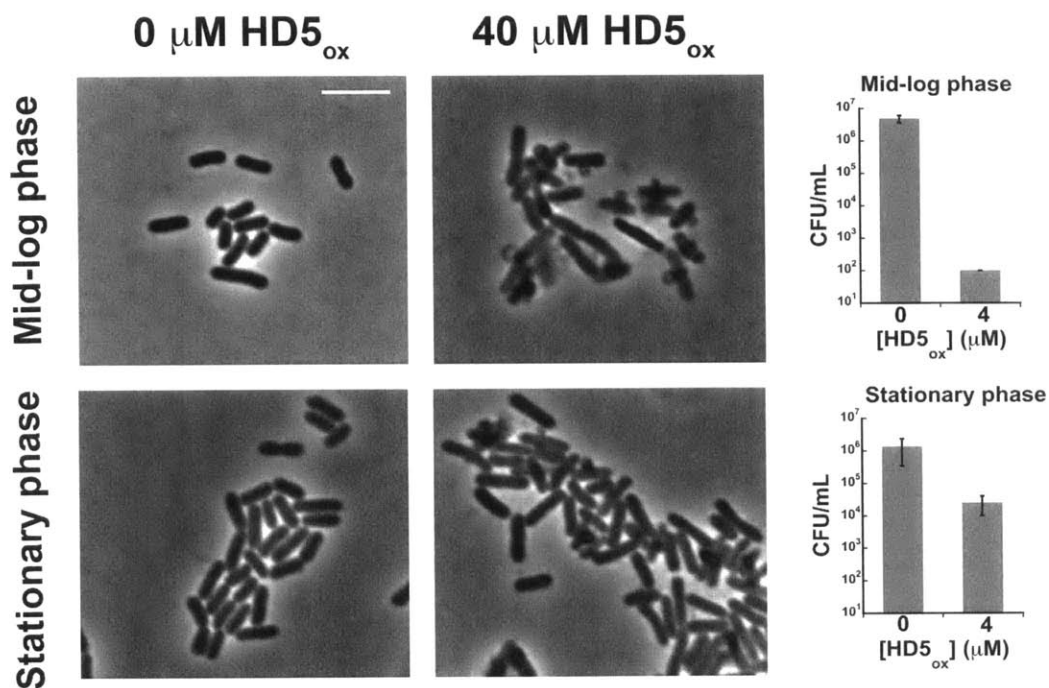
Figure 3.9. $HD5_{ox}$ is less active against stationary phase than mid-log phase *E. coli* ATCC 25922. Cultures were grown to either mid-log phase or stationary phase, and the *E. coli* (1 x 10^8 CFU/mL) were treated with 40 μM $HD5_{ox}$ for 1 h at 37 °C, 130 rpm (10 mM sodium phosphate buffer, 1% v/v TSB without dextrose, pH 7.4). Scale bar = 5 μm. The panels on the right of phase contrast images indicate the surviving colonies in the AMA assay performed with *E. coli* ATCC 25922 (1 x 10^6 CFU/mL) in either mid-log phase or stationary phase.

The susceptibility of *E. coli* to $HD5_{ox}$ depends on the growth phase, and stationary phase cultures exhibit resistance to $HD5_{ox}$ relative to mid-log phase cultures as observed for other defensins.[6,10] In this work, treatment of mid-log phase *E. coli* with 4 μM $HD5_{ox}$ resulted in a ≈4-fold log-reduction in CFU/mL whereas only ≈2-fold log-reduction was observed for stationary phase *E. coli* (Figure 3.9). In agreement with this trend, fewer morphological changes were observed for stationary phase cells treated with $HD5_{ox}$ (Figures 3.6 and 3.9). Taken together, the microscopy and antimicrobial activity assays with $HD5_{ox}$ and *E. coli* provided a correlation between bacterial susceptibility and altered cellular morphology.
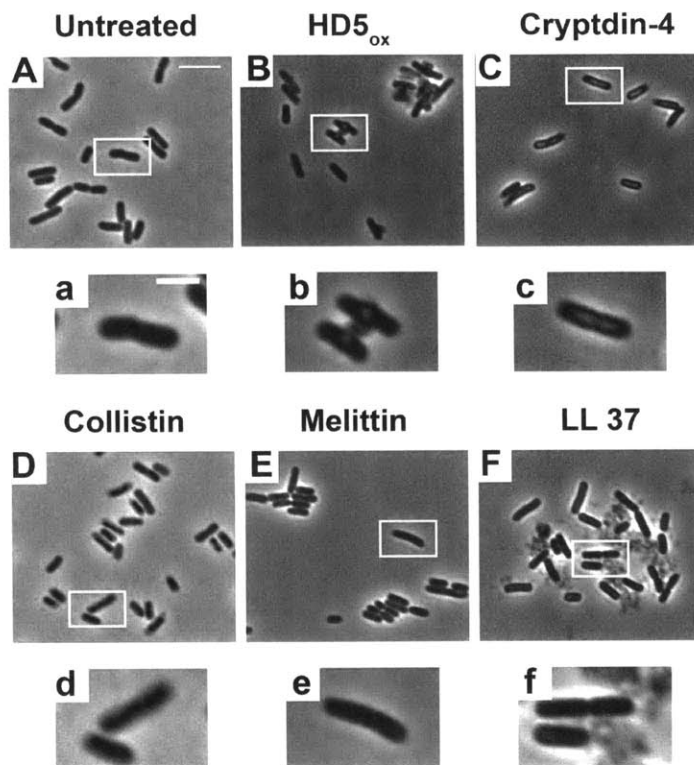
Figure 3.10. The consequences of various antimicrobial peptides on *E. coli* morphology. *E. coli* ATCC 29522 (1 x 10^8 CFU/mL, mid-log phase) were exposed to each peptide (20 μM) for 1 h at 37 °C (10 mM sodium phosphate buffer, pH 7.4, 1% (v/v) TSB) prior to imaging. Top panels, (**A-F**) scale bar = 5 μm; bottom panels, (**a-f**) scale bar= 2 μm.

ii. **Treatment of *E. coli* with Other AMPs Does Not Result in the Bleb Morphology.** We questioned whether other antimicrobial peptides confer the same morphological changes observed for $HD5_{ox}$ under the experimental conditions used in this work. Prior biophysical studies proposed the ability of the murine Paneth cell defensin cryptdin-4 to induce negative curvature on bacterial membranes, resulting in structures called blebs or pores.[45] The *E. coli* treated with cryptdin-4 (20 μM) did not form large blebs as observed for $HD5_{ox}$ (Figure 3.10). Likewise, *E. coli* did not exhibit blebs following exposure to the pore-forming antimicrobial peptide melittin[46] (20 μM), the LPS-associated membrane-destabilizing peptide colistin[47] (20 μM), or the pore-forming antimicrobial peptide human LL-37[48] (20 μM) (Figure 3.10). The bacteria treated with LL-37 were somewhat elongated relative to the untreated control cells. Small membrane protrusions (< 100 nm wide) and surface roughness observed for bacteria

treated with AMPs such as magainin 2[49] and Bac8c[50] have been described as blebs. To the best of our knowledge, larger blebs ($\approx$1-μm wide), formed preferentially at poles and cell division sites as observed for HD5$_{ox}$, have not been reported for a human host-defense peptide. Certain outer membrane protrusions of defensin-treated bacteria are reported in literature as blebs.[19,51] The most similar bleb morphologies we identified in the literature are the bulges that result from β-lactam treatment.[52] Moreover, a knockout mutant of elyC,[53] an inner-membrane protein involved in peptidoglycan synthesis from the Keio Collection, and some Tol-Pal mutants of *Caulobacter crescentus*,[54] are reported to display large blebs. On the basis of this modest AMP screen, we concluded that HD5$_{ox}$ affects *E. coli* differently than the other AMPs considered in this work, including the murine α-defensin cryptdin-4. Although morphology comparisons alone do not provide detailed insight into antibiotic mechanisms, our imaging results suggest that the mechanism of action of HD5$_{ox}$ against *E. coli* cannot be explained fully by membrane permeabilization.

iii. HD5$_{ox}$ Causes Similar Morphological Changes in Other Gram-negative Organisms.

HD5$_{ox}$ exhibits broad-spectrum antibacterial activity[5,6,8] and whether its mechanism of action is general or strain-specific remains unclear. Several structure/activity relationship studies indicated that HD5$_{ox}$ operates by different mechanisms for Gram-negative and –positive organisms, but these studies were limited to comparisons between *E. coli* and *Staphylococcus aureus*.[34,35,38] To delineate whether HD5$_{ox}$ perturbs the morphologies of other Gram-negative strains, four human pathogens, *Acinetobacter baumannii* 17978, *Klebsiella pneumoniae* 13883, *Pseudomonas aeruginosa* PAO1, and *E. coli* CFT073, were evaluated along with the laboratory strain *E. coli* K-12 (Figure 3.11). As for non-pathogenic *E. coli* ATCC 25922 and K-12, bleb formation, elongation, and clumping were observed for the pathogenic strains. We previously reported that *A. baumannii* exhibits relatively high sensitivity to HD5$_{ox}$.[8] In accordance with this observation, *A. baumannii* displayed blebs at 10 μM HD5$_{ox}$ (Figure 3.12). *P. aeruginosa* is less susceptible to HD5$_{ox}$ killing,[8] and blebs were only observed with 40 μM of HD5$_{ox}$ (Figure 3.12).
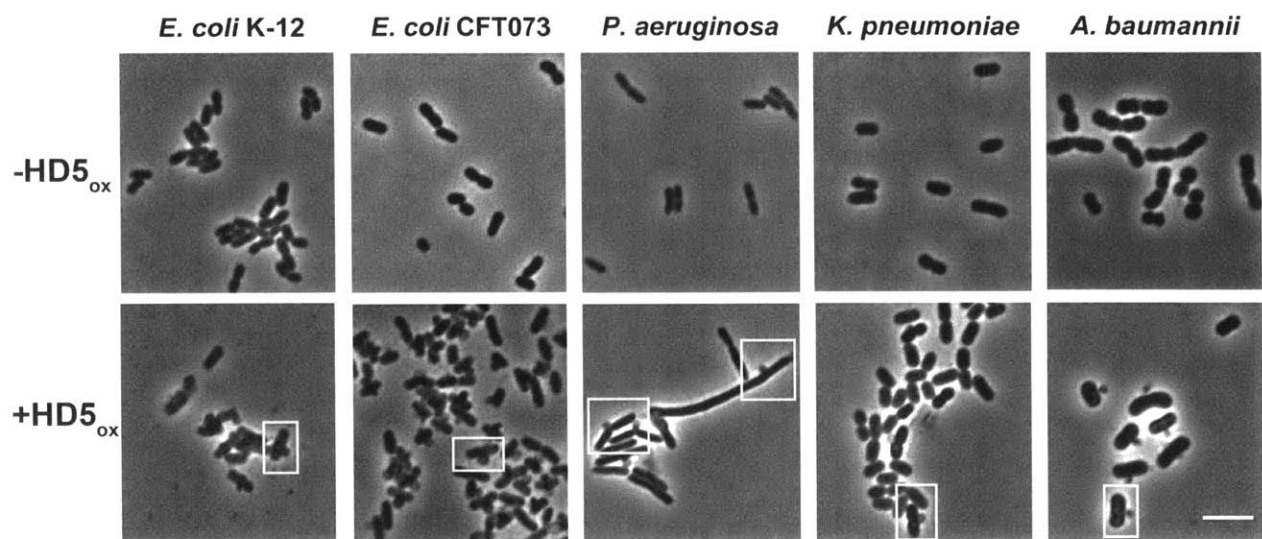
Figure 3.11. The effect of $HD5_{ox}$ exposure on the morphology of Gram-negative bacteria. Each microbe (1 x 10^8 CFU/mL, mid-log phase) was exposed to $HD5_{ox}$ (20 μM except for *P. aeruginosa* where 40 μM was used) for 1 h at 37 °C (10 mM sodium phosphate buffer, pH 7.4, 1% v/v TSB) prior to imaging. Scale bar= 5 μm. Additional images are provided in Figure 3.12.
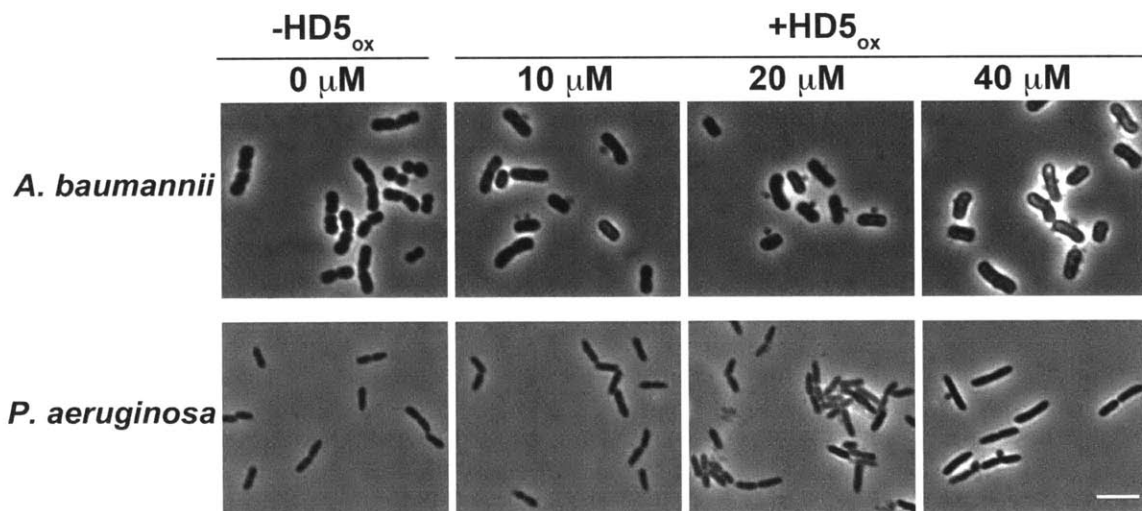
Figure 3.12 *Pseudomonas aeruginosa* PAO1 is less sensitive to $HD5_{ox}$ and blebs are only observed at relatively high concentrations (40 μM) of $HD5_{ox}$. *Acinetobacter baumannii* 17978 displays blebs even at relatively low (10 μM) concentrations of $HD5_{ox}$. *P. aeruginosa* and *A. baumannii* (1 x 10^8 CFU/mL, mid-log) were treated with $HD5_{ox}$ for 1 h at 37 °C, 130 rpm (10 mM sodium phosphate buffer, 1% v/v TSB without dextrose, pH 7.4). Scale bar = 5 μm.
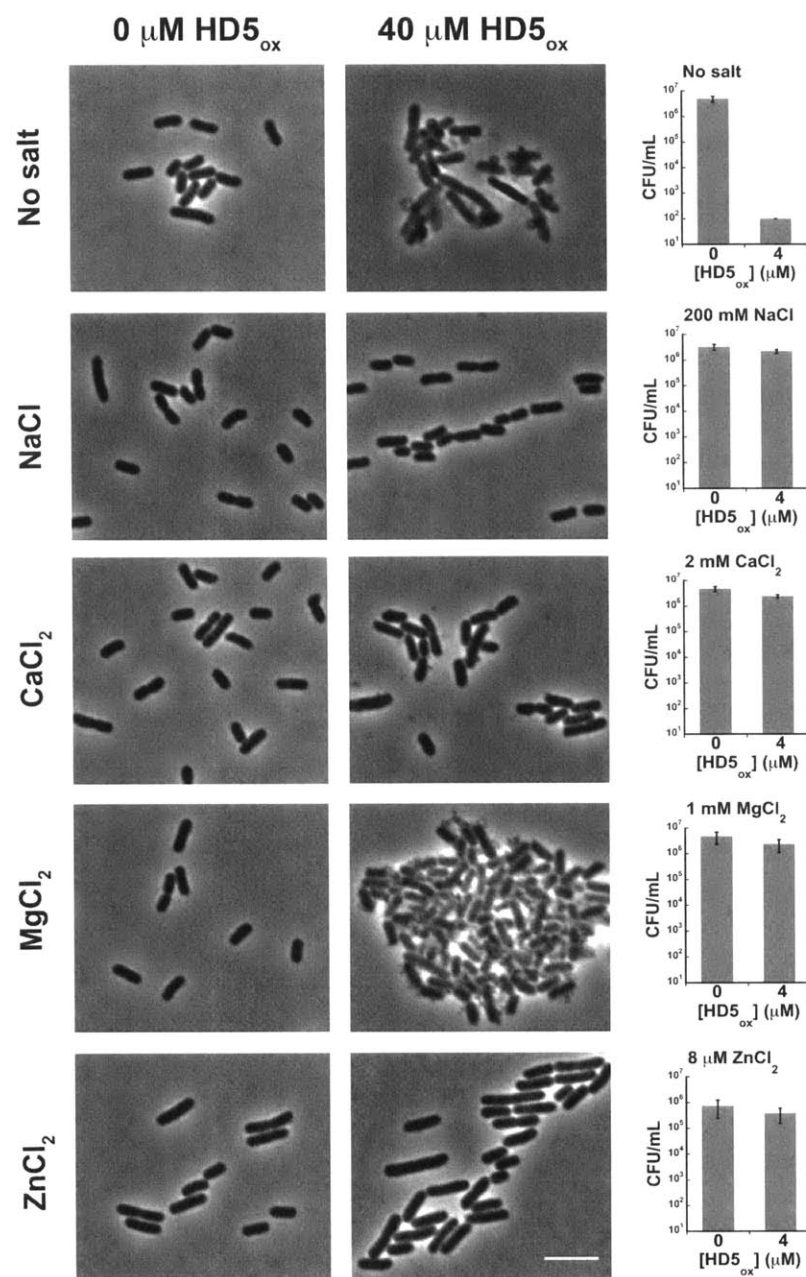
Figure 3.13. The presence of metal salts in the assay buffer attenuates morphological change as well as antibacterial activity. *E. coli* ATCC 25922 (1×10^8 CFU/mL, mid-log phase) were treated with 40 μM HD5$_{ox}$ for 1 h at 37 °C, 130 rpm (10 mM sodium phosphate buffer, 1% v/v TSB without dextrose, pH 7.4) in the presence of NaCl (200 mM), CaCl$_2$ (2 mM), MgCl$_2$ (1 mM), or ZnCl$_2$ (80 μM). Scale bar = 5 μm. The panels on the right present the results of antimicrobial activity assays (1×10^6 CFU/mL *E. coli*) performed in the presence of NaCl, CaCl$_2$, MgCl$_2$, or ZnCl$_2$.

iv.   Salt and Divalent Metal Ions Attenuate HD5-induced Morphological Changes. The *in vitro* antimicrobial activity of many defensins is attenuated by the presence of salt and divalent cations.[55] This phenomenon is commonly attributed to a disruption of electrostatic interactions between the cationic defensin and anionic bacterial cell membrane.[2] Like many defensins, the antibacterial activity of $HD5_{ox}$ is attenuated by milli-molar concentrations of sodium chloride.[6] We observed that NaCl prevents bleb formation and other morphological changes associated with $HD5_{ox}$ activity. Indeed, *E. coli* co-treated with $HD5_{ox}$ (40 μM) and NaCl (200 mM) displayed a smooth morphology similar to that of the untreated control (Figure 3.13). The divalent cations Ca(II), Mg(II) and Zn(II) also blocked $HD5_{ox}$ activity (Figure 3.13). This effect was most potent for Zn(II) where a 2:1 Zn(II):$HD5_{ox}$ molar ratio resulted in a loss of antibacterial activity and $HD5_{ox}$-associated morphologies. This observation is of broad interest because the Paneth cell granules, which harbor HD5, also contain a labile zinc pool of unknown function.[25]

v.   Disulfide Bonds Are Necessary for the Bleb Morphology. The canonical α-defensin disulfide array provides a three-stranded β-sheet fold to each $HD5_{ox}$ monomer. This compact structure orients the positively charged residues on one face of the peptide and the hydrophobic residues on the opposite, rendering $HD5_{ox}$ amphipathic.[56] To investigate the structural requirements for $HD5_{ox}$ activity, we evaluated the consequences of treating *E. coli* with three HD5 derivatives, HD5-TE, HD5-CD, and $HD5[E21S]_{ox}$, selected to probe the disulfide array as well as quaternary structure. HD5-TE is a linear disulfide-null analogue where the six cysteines are carboxymethylated with 2-iodoacetamide.[57] Defensins have the propensity to self-associate, and in prior work we reported that $HD5_{ox}$ forms tetramers at neutral pH.[56] HD5-CD is a C_2-symmetric covalent dimer of $HD5_{ox}$ with a cationic surface that results from intermolecular disulfide exchange between the Cys^5–Cys^{20} disulfide bonds (canonical Cys^{II}–Cys^{IV}) of two HD5 monomers.[8] We also prepared and characterized $HD5[E21S]_{ox}$, a new $HD5_{ox}$ mutant that forms a non-covalent dimer, but not a tetramer, at neutral pH.[41]
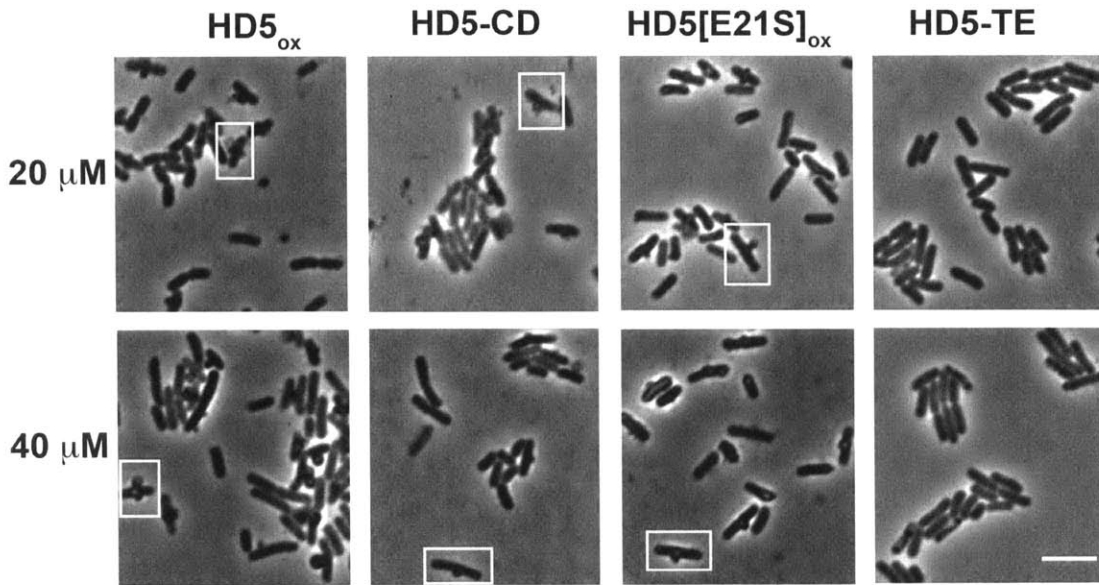
Figure 3.14. *E. coli* morphologies in the presence of HD5 derivatives reveal that the disulfide bonds are necessary for bleb formation. *E. coli* ATCC 25922 (1 x 10^8 CFU/mL, mid-log phase) was exposed to each peptide for 1 h at 37 °C (10 mM sodium phosphate buffer, pH 7.4, 1% v/v TSB) prior to imaging. Scale bar = 5 μm.
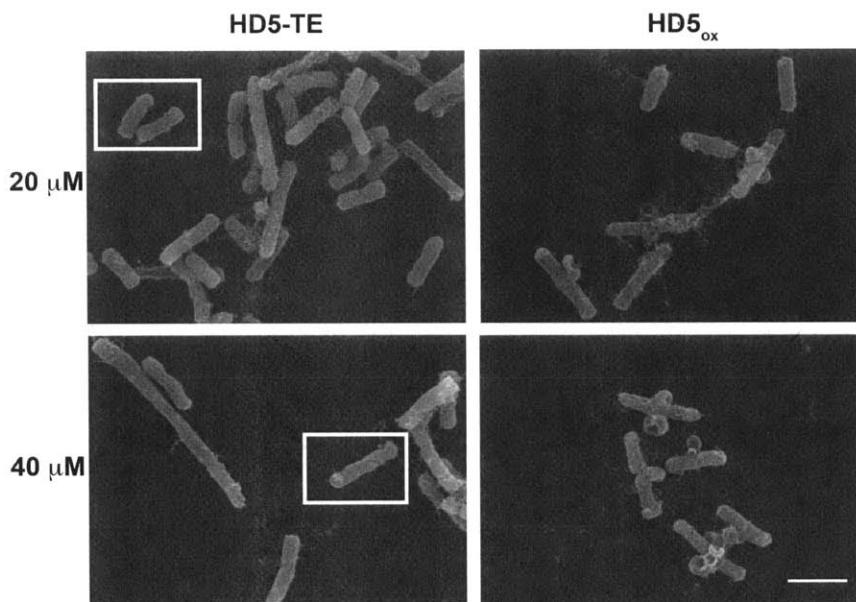
Figure 3.15. No blebs are observed following treatment of *E. coli* ATCC 25922 with HD5-TE. The cells treated with HD5-TE become elongated and more corrugated (highlighted in boxes). *E. coli* ATCC 25922 (1 x 10^8 CFU/mL, mid-log phase) were treated with 20 μM and 40 μM of HD5-TE or HD5$_{ox}$ for 1 h at 37 °C, 130 rpm (10 mM sodium phosphate buffer, 1% v/v TSB without dextrose, pH 7.4) prior to fixing and subsequent SEM imaging. Scale bar = 2 μm.

E. coli treated with HD5-CD or HD5[E21S]$_{ox}$ were indistinguishable from those treated with HD5$_{ox}$ (Figure 3.14), in agreement with antimicrobial activity assays where both HD5[E21S]$_{ox}$ and HD5-CD killed *E. coli*.[41] In contrast, the antimicrobial activity of linear and unstructured HD5-TE against *E. coli* was attenuated (2-fold log reduction of CFU/mL at 16 μM) relative to HD5$_{ox}$. HD5-TE did not cause bleb formation (Figure 3.14); however, SEM revealed that the cells treated with HD5-TE were corrugated and frequently elongated (Figure 3.15). These results highlight the importance of cysteine residues housed in disulfide linkages in the overall antimicrobial activity of HD5 and the induced morphological changes.

vi.   Blebs Accumulate the Cytoplasmic Contents. The blebs observed in this work are reminiscent of the cellular morphologies that result from treatment of *E. coli* with β-lactams, and *E. coli* strains expressing GFP have proven to be useful in imaging studies of β-lactam action.[52,58] Guided by this work, we investigated the contents as well as time-dependent formation of the blebs by employing an *E. coli* strain that expresses cytoplasmic GFP (*E. coli* cyto-GFP). Mid-log phase *E. coli* cyto-GFP formed blebs following exposure to HD5$_{ox}$. The blebs
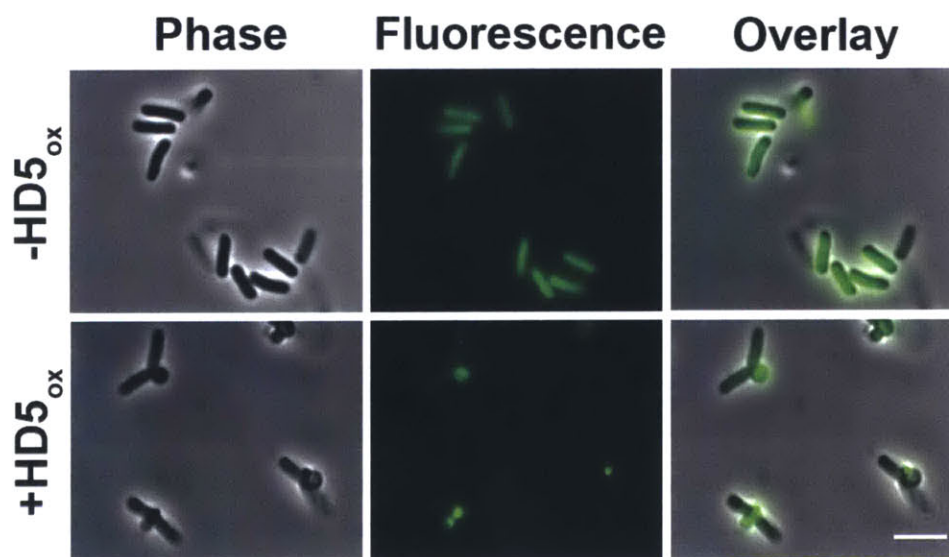
Figure 3.16. Treatment of *E. coli* cyto-GFP with HD5$_{ox}$ reveals that the cytoplasmic contents leak into the blebs. *E. coli* cyto-GFP (1 × 10^{7}CFU/mL, mid log phase) were exposed to 4 μM HD5$_{ox}$ for 1 h at 37 °C [10 mM sodium phosphate buffer (pH 7.4) and 1% (v/v) TSB] prior to imaging. Scale bar = 5 μm.

displayed GFP emission, and the GFP emission from the cell body was markedly reduced, suggesting that cytoplasmic contents localized to the blebs (Figure 3.16). Some additional phenotypes were observed for dividing cells. In several instances where a dividing cell exhibited a bleb at the cell division site, the GFP localization differed between the daughter cells (Figure 3.17).
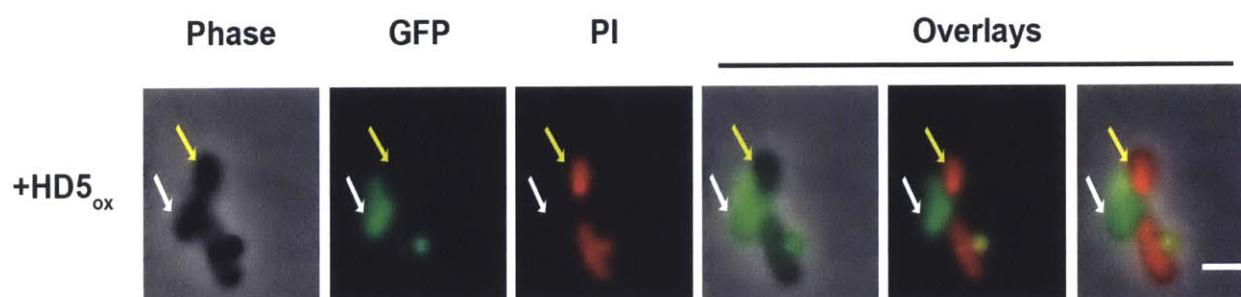
Figure 3.17. GFP distribution and propidium iodide (PI) labeling of select daughter cells (indicated by yellow and white arrows). *E. coli* cyto-GFP (1 x 10^8 CFU/mL, mid-log phase) treated with 20 μM of $HD5_{ox}$ for 1 h at 37 °C, 130 rpm (10 mM sodium phosphate buffer, 1% v/v TSB without dextrose, pH 7.4) were subsequently incubated with 5 μg/mL of PI for 15 min prior to imaging (Excitation wavelengths: 561 nm, PI; 488 nm, GFP). Scale bar = 2 μm

Moreover, for cells with blebs at the cell division site, the GFP intensity in the region between the two daughter cells was relatively weak, indicating that the presence of a membrane at the division plane. In agreement with this observation, labeling $HD5_{ox}$-treated *E. coli* ATCC 25922 with the membrane-binding dye FM4-64 confirmed the presence of this membrane (Figure 3.18). Cell viability, as observed by PI uptake, was inversely correlated to the overall GFP fluorescence intensity of the bacteria (Figure 3.19). When *E. coli* cyto-GFP (1 x 10^8 CFU/mL) were treated with $HD5_{ox}$ (20 μM) and subsequently stained as a result of PI uptake (5 μg/mL), the cells with brighter GFP emission and fewer morphological defects exhibited less PI labeling relative to cells that were affected by $HD5_{ox}$. In agreement with studies using *E. coli* ATCC 25922 (Figure 3.6), negligible changes in morphology and GFP localization were observed for $HD5_{ox}$-treated *E. coli* cyto-GFP in stationary phase.
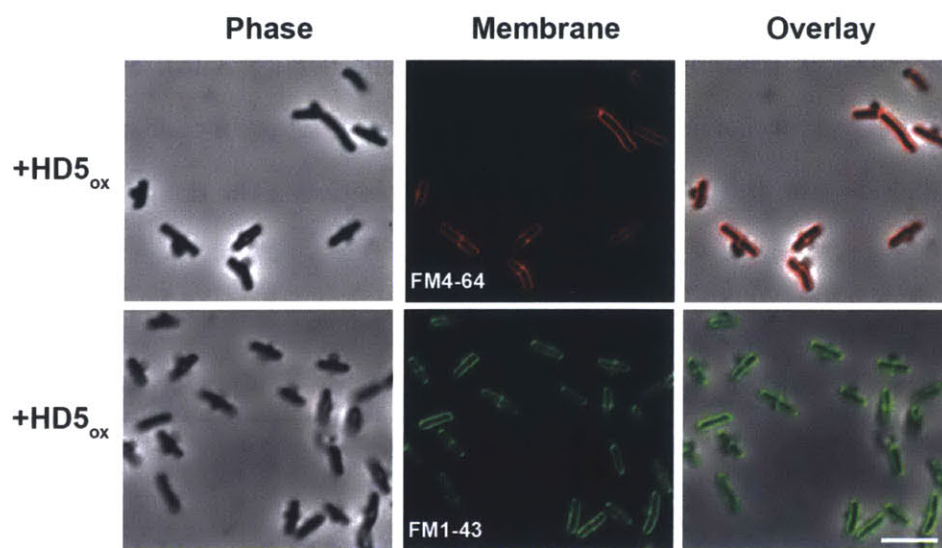
Figure 3.18. Membrane labeling of $HD5_{ox}$-treated bacteria using FM dyes. *E. coli* ATCC 25922 (1 x 10^8 CFU/mL, mid-log phase) treated with 20 μM of $HD5_{ox}$ for 1 h at 37 °C, 130 rpm (10 mM sodium phosphate buffer, 1% v/v TSB without dextrose, pH 7.4) were incubated with 2 μg/mL of FM4-64 (top panels) or FM1-43 (bottom panels) for 15 min prior to imaging (Excitation wavelengths: 561 nm, FM4-64; 488 nm, FM1-43). Scale bar = 5 μm.
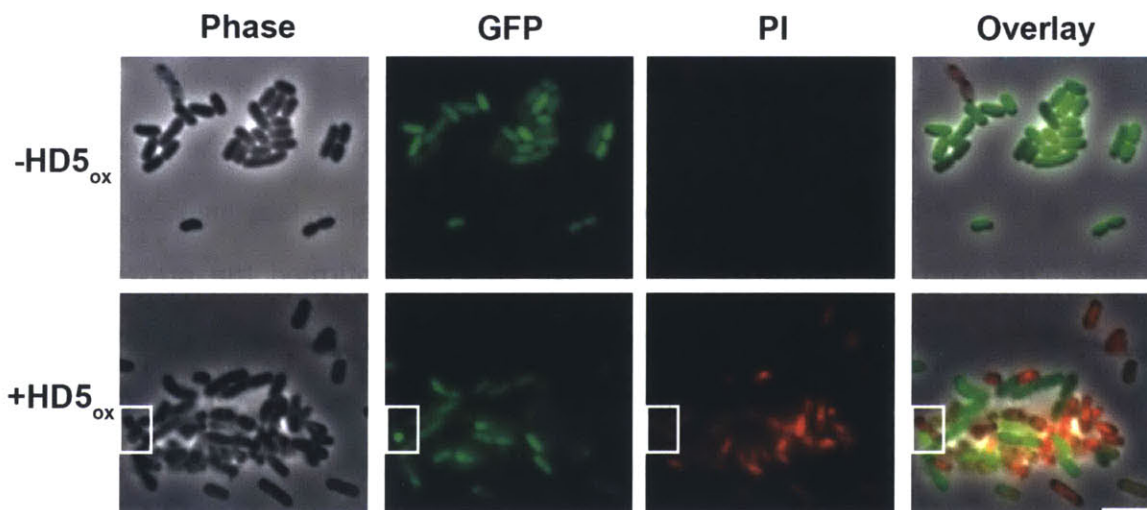
Figure 3.19. Cell viability of *E. coli* cyto-GFP treated with $HD5_{ox}$ by propidium iodide (PI) uptake. *E. coli* cyto-GFP (1 x 10^8 CFU/mL, mid-log phase) treated with 20 μM of $HD5_{ox}$ or for 1 h at 37 °C, 130 rpm (10 mM sodium phosphate buffer, 1% v/v TSB without dextrose, pH 7.4) were incubated with 5 μg/mL of PI for 15 min prior to imaging (Excitation wavelengths: 561 nm, PI; 488 nm, GFP). Scale bar = 5 μm.
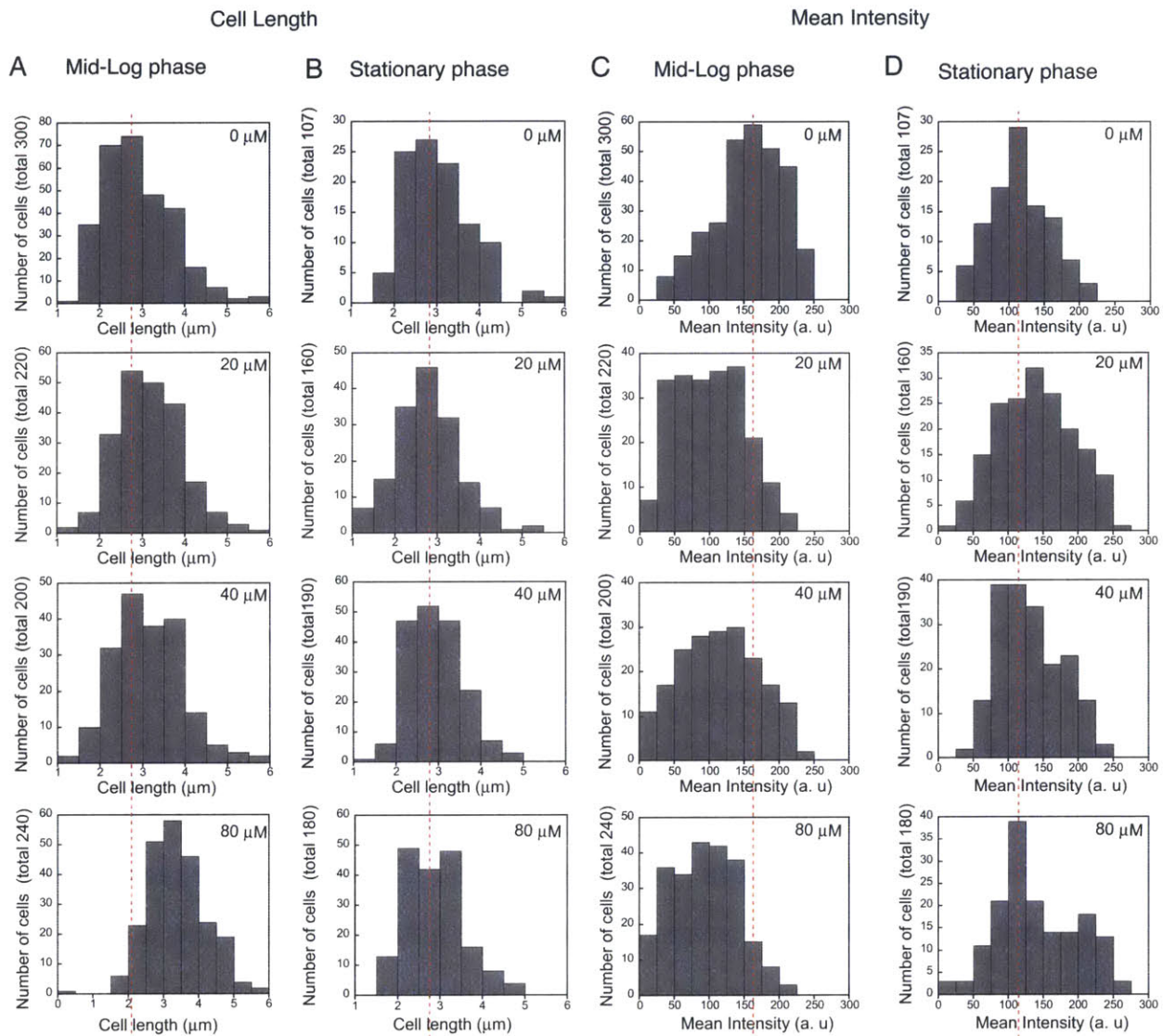
Figure 3.20. The *E. coli* growth phase influences cell length and mean cell intensity following treatment with HD5$_{ox}$. *E. coli* cyto-GFP (1 x 10^8 CFU/mL) were treated with HD5$_{ox}$ (0, 20, 40, and 80 μM) for 1 h at 37 °C, 130 rpm (10 mM sodium phosphate buffer, 1% v/v TSB without dextrose, pH 7.4). The morphology and mean intensity were analyzed using ImageJ. Red dotted lines indicate the mean values for the untreated control.
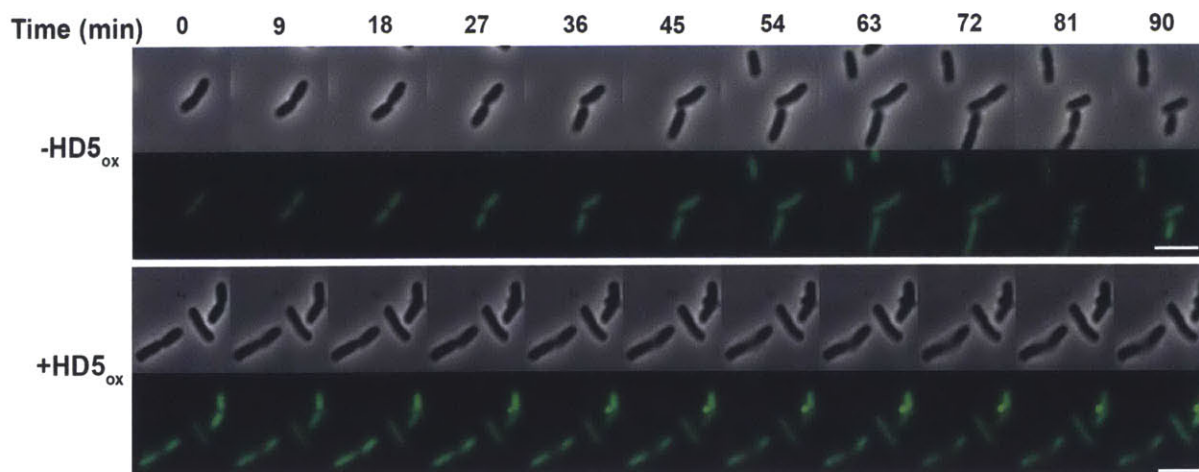
Figure 3.21. Time-lapse imaging of *E. coli* cyto-GFP (1×10^7 CFU/mL, mid log phase) treated with 20 μM HD5$_{ox}$ at 37 °C [10 mM sodium phosphate buffer (pH 7.4) and 1% (v/v) TSB]. Scale bar = 5 μm.

To obtain quantitative comparisons, the GFP intensity and morphological changes for both mid-log phase and stationary-phase *E. coli* cyto-GFP were analyzed (Figure 3.20). The mean cell length for the mid-log phase cells increased from 2.8 ± 0.8 μm to 3.4 ± 1.0 μm (Student's t-test: t-value = 6.32, t-probability = <0.0001) with increasing HD5$_{ox}$ (0-80 μM), and the mean GFP fluorescence intensity decreased accordingly (155 ± 48 units to 93 ± 47 units). Only minor changes in both cell lengths (3.0 ± 0.8 μm to 2.9 ± 0.7 μm) (Student's t-test: t-value = 1.97, t-probability = 0.049) and mean intensities (112 ± 38 units to 139 ± 53 units) were found when stationary phase cells were treated with HD5$_{ox}$. To obtain temporal information on bleb formation and GFP redistribution, we performed time-course experiments where *E. coli* cyto-GFP were treated with HD5$_{ox}$ on the microscope stage and collected images over a 2 h period (Figure 3.21). The replication time for *E. coli* in the standard AMA buffer (10 mM sodium phosphate buffer, pH 7.4, 1% v/v TSB without dextrose) on a MatTek plate ranged from 90-120 min at 37 °C. These cultures were unsynchronized, and bleb formation occurred at different time points depending on the cell. Blebs were observed immediately for some cells whereas others formed blebs after ≈30 min exposure to HD5$_{ox}$. After the appearance of one or more

blebs, GFP intensity in the cell body diminished in all cases observed. Although dividing *E. coli* were observed for untreated cells (Figure 3.21, top panels), cells that were affected by HD5$_{ox}$ no longer divided (Figure 3.21, bottom panels).

vii.   Membrane Composition of the Blebs and Observation of Outer Membrane Vesicles.
The composition of the membrane surrounding the blebs of HD5$_{ox}$-treated *E. coli* was investigated by fluorescence imaging of an *E. coli* strain harboring a plasmid encoding periplasmic GFP (*E. coli* peri-GFP) as well as transmission electron microscopy (TEM) of *E. coli* ATCC 25922. These studies afforded several phenotypes and suggested that two different types of blebs form (Figure 3.22). Some cells exhibited a ring of GFP emission around the blebs, which indicated that both the outer and inner membranes surrounded the bleb and were in tact. Other cells presented uniform GFP emission throughout the bleb. Possible explanations for this phenotype include (i) only the outer membrane surrounded the blebs or (ii) the inner membrane surrounded the bleb, but was damaged and leaked the periplasmic contents into the bleb.
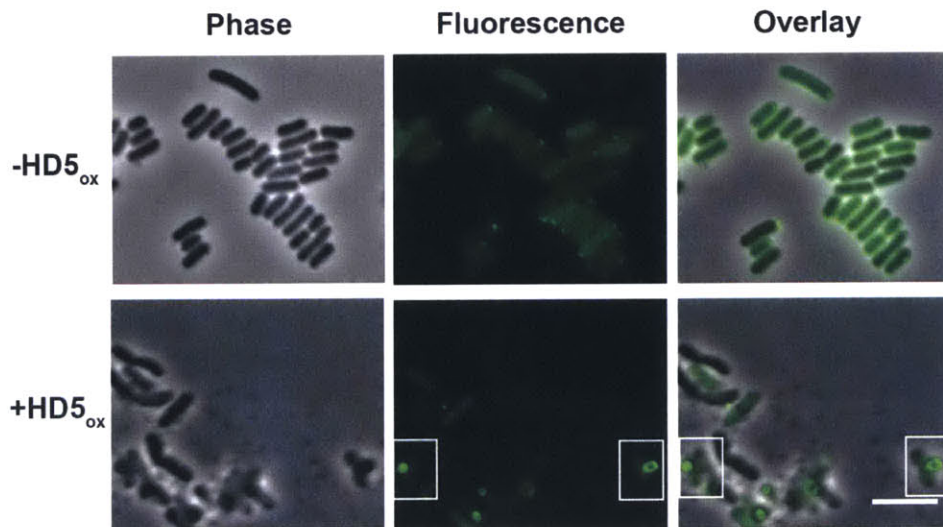
Figure 3.22. Treatment of *E. coli* peri-GFP with HD5$_{ox}$ reveals two types of GFP distribution in the blebs. *E. coli* peri-GFP (1 x 10^8 CFU/mL, mid-log phase) were exposed to 20 µM HD5$_{ox}$ for 1 h at 37 °C (10 mM sodium phosphate buffer, pH 7.4, 1% v/v TSB without dextrose) prior to imaging. Excitation wavelength: 488 nm. Scale bar= 5 µm. The cells highlighted in boxes are representative of the two types of distributions.
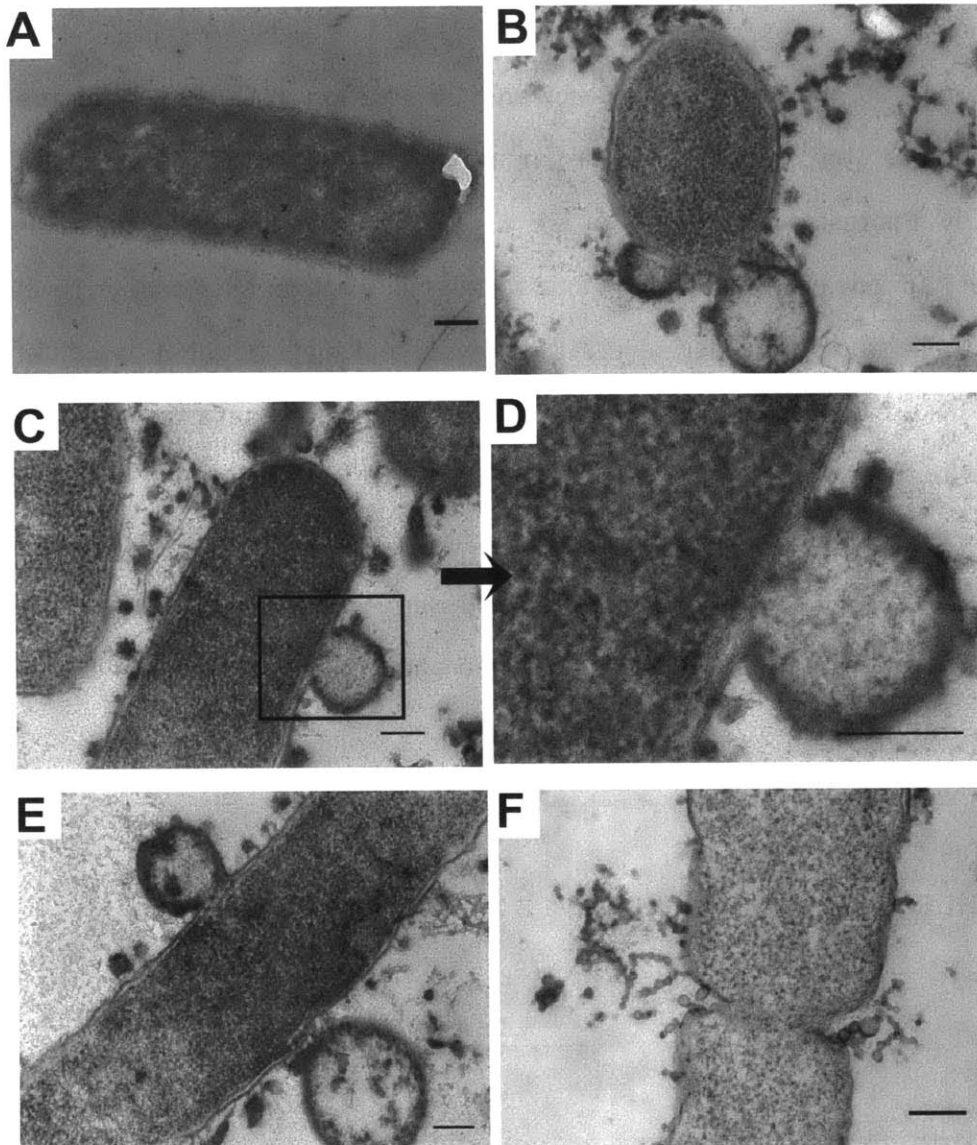
Figure 3.23. TEM images of *E. coli* ATCC 25922 (1×10^8 CFU/mL) treated with HD5$_{ox}$. (A) Untreated cells and (B-F) cells treated with 20 μM HD5$_{ox}$ were incubated for 1 h at 37 °C, 130 rpm (10 mM sodium phosphate buffer, 1% v/v TSB without dextrose, pH 7.4) prior to fixation. Scale bar = 200 nm.

TEM imaging revealed that the blebs are membrane bound; however, it was difficult to confirm whether one or both membranes surround each bleb (Figure 3.23). TEM also revealed profound changes to the *E. coli* cell surface upon HD5$_{ox}$ treatment, including vesicles surrounded by a membrane that often clustered in chain-like arrangements (Figure 3.23F). During phase-contrast imaging of HD5$_{ox}$-treated bacteria, we frequently observed surface-appended structures resembling debris. We attribute these structures, at least in part, to outer membrane vesicle (OMVs) on the basis of TEM and SEM studies (Figure 3.5). Formation of OMVs ($\approx$20-200 nm wide) is an important bacterial stress response pathway, and OMVs contribute to pathogenesis.[59] Thus, we speculate that *E. coli* may attempt to evade HD5$_{ox}$ by generating and shedding OMVs, along with HD5$_{ox,}$ into the extracellular space.

viii. **HD5$_{ox}$ Enters the *E. coli* Cytoplasm and Localizes to the Cell Poles and Division Site.** On the basis of the AMA assay results described in Chapter 2, we first investigated the cellular localization of R-HD5$_{ox}$. This peptide exhibited slightly attenuated antimicrobial activity relative to native HD5$_{ox}$ (Chapter 2, Figures 2.6 and 2.7). We observed HD5$_{ox}$-like morphological changes, including bleb formation, for *E. coli* ATCC 25922 (Figure 3.24) and *E. coli* CFT073 (Figure 3.26). Intracellular fluorescence was also observed. Co-labeling studies with the membrane-binding dye FM1-43 revealed that the FM1-43 emission profile enclosed a significant portion of the R-HD5$_{ox}$ fluorescence intensity profile (Figures 3.24 and 3.25), which indicates that the peptide penetrated the outer and inner membranes and entered the cytoplasm. In most of the cells examined by fluorescence microscopy, the rhodamine emission was most intense at the poles and division plane. This type of labeling pattern was not observed for R-HD5-TE or rhodamine-modified LL-37 (Figure 3.27), both of which provided uniform cytoplasmic fluorescence.
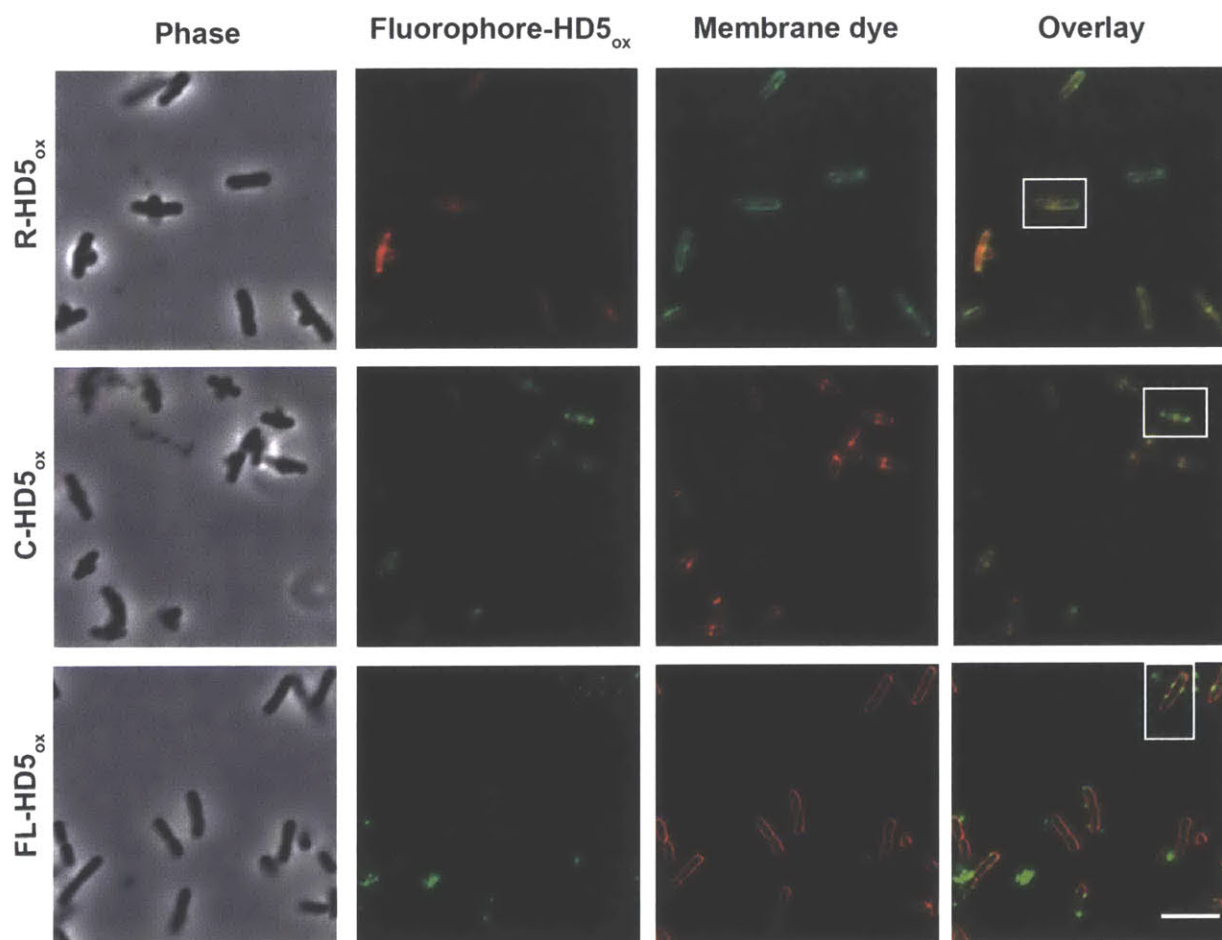
Figure 3.24. Fluorescence imaging of *E. coli* treated with fluorophore-HD5$_{ox}$ conjugates and membrane dyes. *E. coli* ATCC 25922 (1×10^8 CFU/mL, mid log phase) treated with R-HD5$_{ox}$ (20 μM), C-HD5$_{ox}$ (20 μM), and FL-HD5$_{ox}$ (8 μM) at 37 °C [10 mM sodium phosphate buffer (pH 7.4) and 1% (v/v) TSB] and incubated with 2 μg/mL FM1-43 for the R-HD5$_{ox}$ sample and 2 μg/mL FM4-64 for both C-HD5$_{ox}$ and FL-HD5$_{ox}$ samples prior to imaging. The boxed cells are depicted in Figure 3.25. Scale bar = 5 μm.
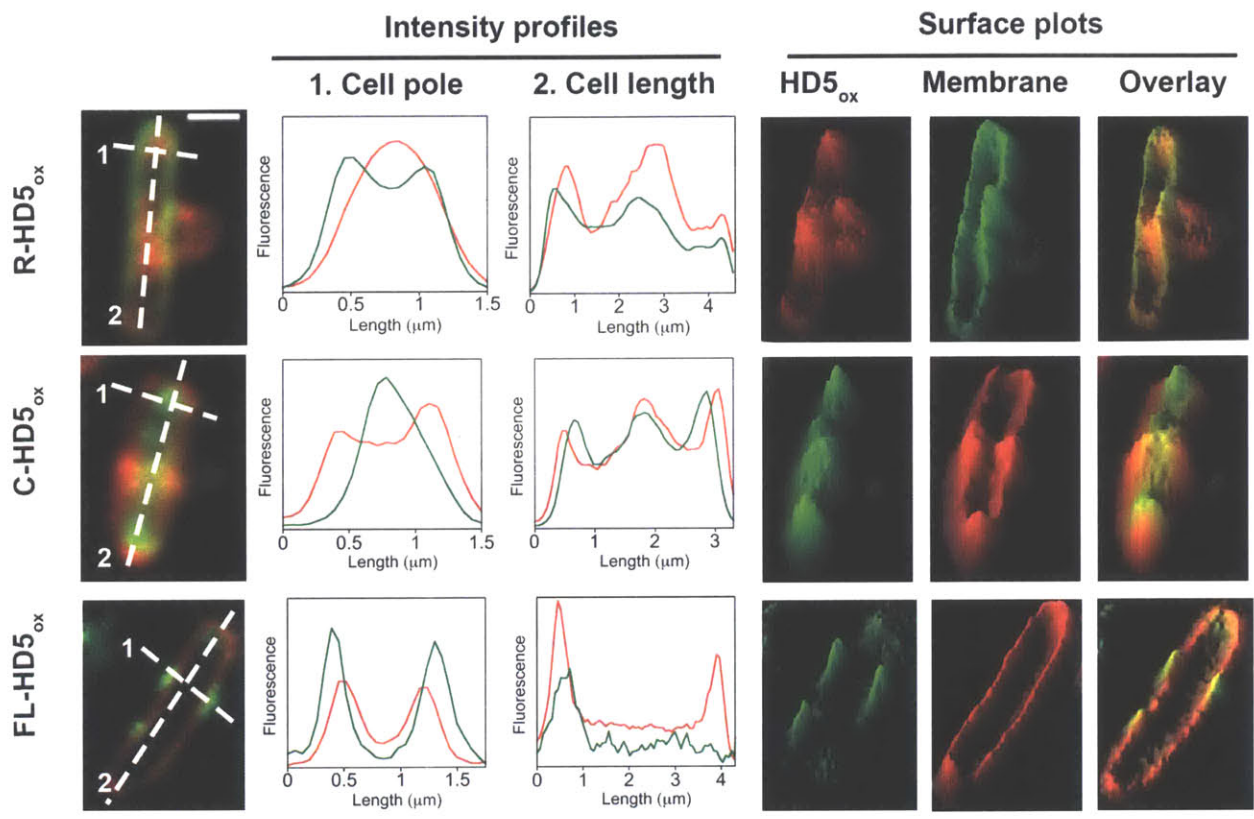
Figure 3.25. Intensity profiles and surface plots of the boxed cells depicted in Figure 3.24. Fluorescence intensities along the cell poles (dashed line 1) and across cell (dashed line 2) are plotted. Surface plots were generated using ImageJ software. Scale bar = 1 μm.

E. coli CFT073

Phase	Fluorescence	Overlay
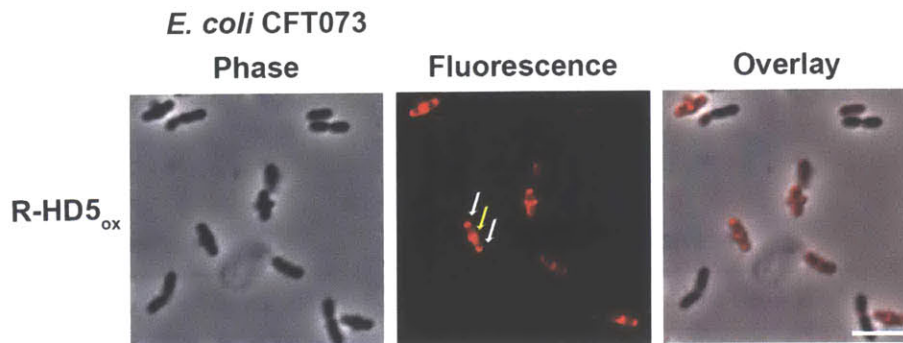
R-HD5$_{ox}$

Figure 3.26. *E. coli* CFT073 treated with R-HD5$_{ox}$ also display preferential labeling at cell poles (white arrows) and division septa (yellow arrow). *E. coli* CFT073 (1 x 10^8 CFU/mL, mid-log phase) was exposed to 20 µM of R-HD5$_{ox}$ for 1 h at 37 °C (10 mM sodium phosphate buffer, pH 7.4, 1% v/v TSB without dextrose) prior to imaging. Excitation laser: 561 nm. Scale bar = 5 µm.

E. coli 25922

Phase	Fluorescence	Overlay

R-HD5[K13R]$_{ox}$

R-HD5-TE

R-LL 37
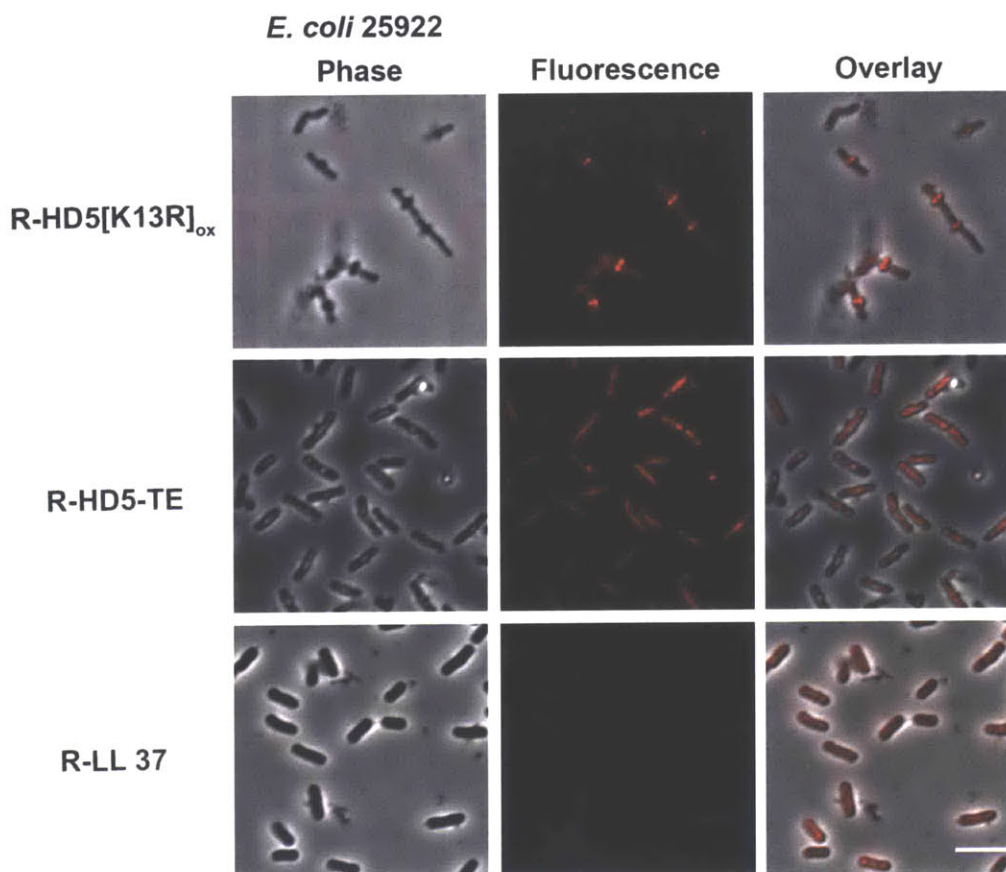
Figure 3.27. Labeling pattern of other rhodamine B-labeled peptides. *E. coli* ATCC 25922 (1 x 10^8 CFU/mL, mid-log phase) was exposed to 20 µM of each peptide for 1 h at 37 °C (10 mM sodium phosphate buffer, pH 7.4, 1% v/v TSB without dextrose) prior to imaging. Excitation wavelength: 561 nm. Scale bar = 5 µm.

When *E. coli* were treated with R-HD5$_{ox}$ under conditions that result in attenuated HD5$_{ox}$ activity (Chapter 2), different labeling patterns were observed. For instance, the presence of NaCl (200 mM) resulted in rhodamine emission only at the cell surface, indicating that R-HD5$_{ox}$ did not enter *E. coli* (Figure 3.28). Stationary-phase *E. coli* treated with R-HD5$_{ox}$ exhibited diminished intracellular fluorescence relative to mid-log phase cells (Figure 3.28). Taken together, these observations support a model whereby HD5$_{ox}$ must overcome the outer membrane permeability barrier and enter the cytosol to exert its full capacity to kill bacteria.
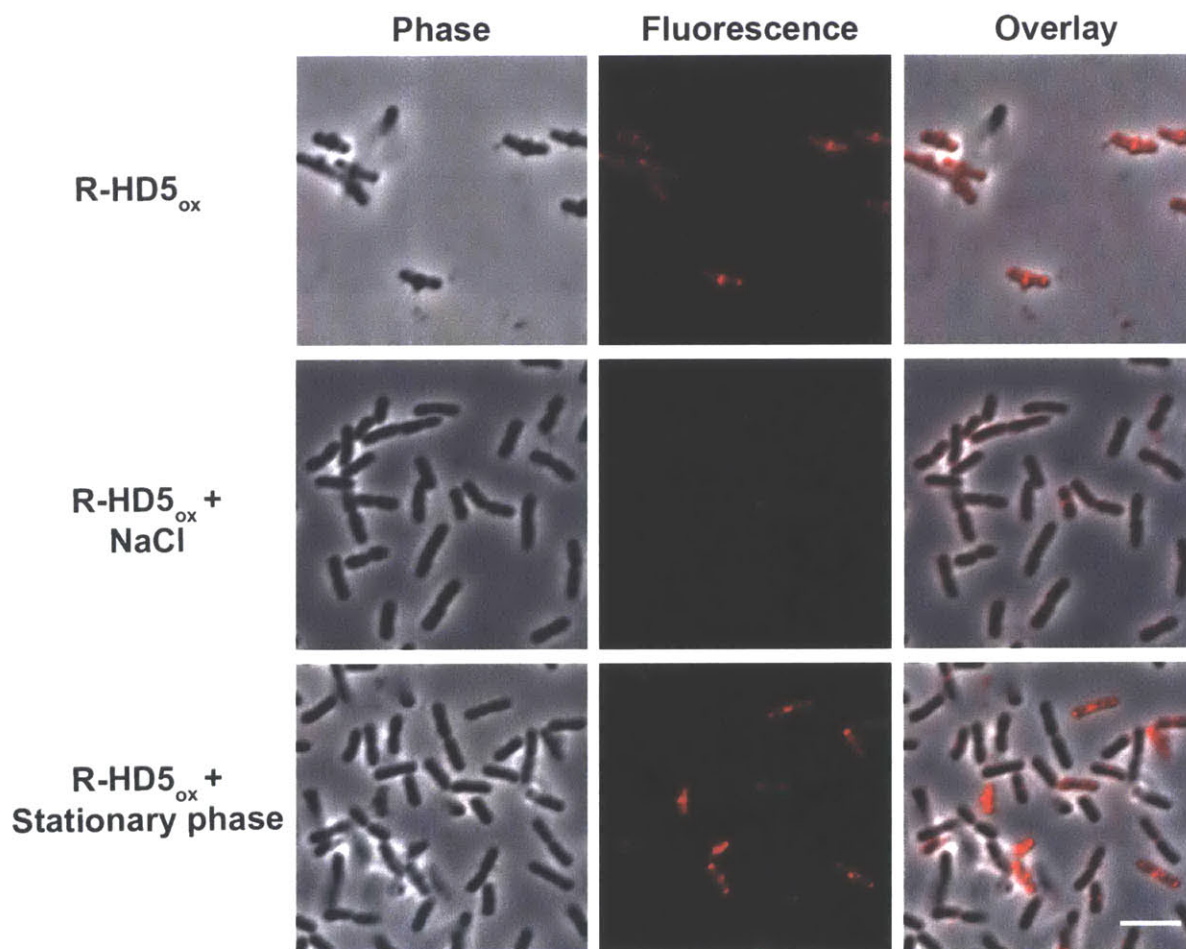
Figure 3.28. Effect of growth phase and salt on the labeling pattern of R-HD5$_{ox}$. *E. coli* ATCC 25922 (1×10^8 CFU/mL) in mid-log phase or stationary phase were exposed to 20 μM of R-HD5$_{ox}$ for 1 h at 37 °C (10 mM sodium phosphate buffer, pH 7.4, 1% v/v TSB without dextrose) in the absence or presence of 200 mM NaCl prior to imaging. Excitation wavelength: 561 nm. Scale bar = 5 μm.
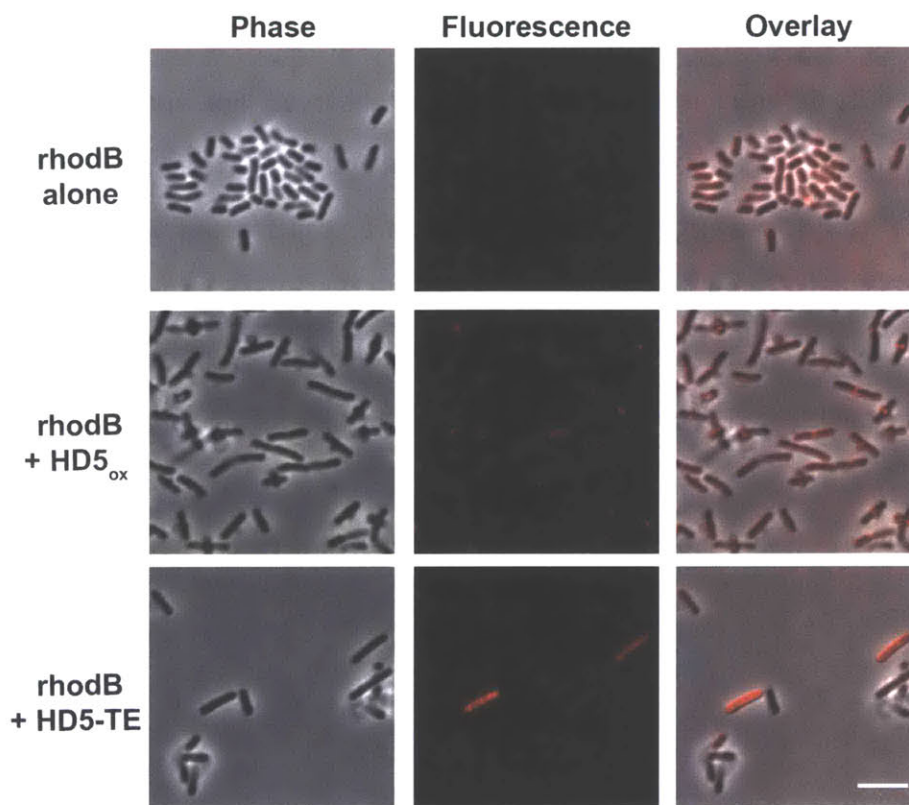
Figure 3.29. Cellular uptake of parent fluorophore rhodamine B. *E. coli* ATCC 25922 (1×10^8 CFU/mL, mid-log phase) was exposed to 20 µM of rhodamine B or rhodamine B and peptide (20 µM) for 1 h at 37 °C (10 mM sodium phosphate buffer, pH 7.4, 1% (v/v) TSB without dextrose) prior to imaging. Excitation wavelength: 561 nm. Scale bar = 5 µm.

Co-incubation of *E. coli* with a 1:1 molar ratio of rhodamine B and $HD5_{ox}$ resulted in uniform cytoplasmic staining whereas treatment of *E. coli* with rhodamine B alone resulted in negligible cellular fluorescence (Figure 3.29). This result suggested that $HD5_{ox}$ treatment allowed for rhodamine B entry as a result of membrane permeabilization, and confirmed that covalent attachment of rhodamine to $HD5_{ox}$ is essential for observing fluorescence localized to the cell poles and division site. The R-HD5[R13K]$_{ox}$ conjugate provided a similar labeling pattern as R-HD5$_{ox}$ and thereby indicated that localization of the rhodamine-HD5$_{ox}$ conjugate is not an artifact resulting from a particular site of rhodamine attachment (Figure 3.27). Moreover, C-HD5$_{ox}$ preferentially labeled the cell poles and cell division sites, and co-labeling with the membrane-binding dye FM 4-64 confirmed its cytoplasmic localization (Figures 3.24 and 3.25).

The fact that the same labeling pattern was observed for HD5$_{ox}$ modified with either rhodamine or coumarin, taken with these modified peptides causing the same morphological changes as observed for unmodified HD5$_{ox}$, provides a strong indication that the localization is a result of HD5$_{ox}$, and not the fluorophore. It should be noted that FL-HD5$_{ox}$, which provided no *in vitro* antibacterial activity against *E. coli* at the highest concentration evaluated (128 μM), did not enter *E. coli*. Rather, the peptide afforded a punctate labeling pattern on and around the bacterial surface (Figures 3.24 and 3.25). We attribute this phenomenon to the overall negative charge of the fluorescein moiety.

The fluorescence imaging studies of HD5$_{ox}$ may be considered in the context of other AMPs that have been examined by similar approaches to probe uptake and mechanism of action. For instance, fluorescence microscopy revealed that buforin II entered the bacterial cytoplasm without permeabilizing the inner membrane.[60] A rhodamine derivative of the only human cathelicidin, LL-37, attacked septating *E. coli* more readily than non-septating cells and permeabilized the bacteria via a carpet-model of membrane destabilization.[61,62] A fluorophore-labeled lantibiotic was shown to interact with lipid II of *B. subtilis* 168.[63] Recent imaging studies of Cy3-derivaitzed HBD2 indicated that HBD2 preferentially localizes to the nascent poles and cell division site of *Enterococcus faecalis*.[20] This focal labeling pattern was attributed to the binding of the HBD2 to anionic lipids in these regions. The cell poles and division site of *E. coli* are also enriched in negatively charged phospholipids that include cardiolipin and phosphatidylglycerol.[64] Whether HD5$_{ox}$ also binds to anionic lipids at the cell poles of *E. coli* and/or another target in these locales is currently unknown. In this regard, as discussed in Chapter 5, we investigated the effect of anionic lipid composition on the antimicrobial activity of HD5$_{ox}$.

3D.   Summary and Outlook

In this Chapter, we defined how the antimicrobial peptide HD5$_{ox}$ affects the morphology of *E. coli* and other Gram-negative bacteria. We established that HD5$_{ox}$ causes distinct

morphological changes to *E. coli* as well as *K. pneumoniae, A. baumannii,* and *P. aeruginosa* that include bleb formation, cellular clumping, and elongation. We also demonstrated that other AMPs, including human LL-37 and murine α-defensin cryptdin-4, do not cause such morphologies. Taken together, these observations indicate that $HD5_{ox}$ kills *E. coli* by a different mechanism than the other peptides examined in this work. Our results highlight the importance of treating host-defense peptides individually, and not generalizing cell-killing mechanisms.

Defensins are often described as membrane-disrupting peptides. Our prior investigations indicate that $HD5_{ox}$ traverses the outer membrane and subsequently damages the inner membrane of *E. coli*.[34,40] In this work, the insights gained from utilizing fluorophore-$HD5_{ox}$ conjugates modified with rhodamine or coumarin support a model that $HD5_{ox}$ enters the *E. coli* cytoplasm. Because the cytoplasm is a reducing environment, intracellular reduction of the $HD5_{ox}$ disulfide array to liberate free cysteine residues may occur. Deciphering whether such redox chemistry contributes to altered cellular morphologies and cell killing warrants exploration. The cytoplasmic localization also supports the possibility that $HD5_{ox}$ (or the reduced form) has an as-yet undiscovered intracellular target. Indeed, the intracellular staining pattern at the cell poles and cell division site routinely observed for *E. coli* treated with R/C-$HD5_{ox}$ suggests the locale of a possible target. On the basis of this localization, coupled with the elongation phenotype observed for *E. coli* and other Gram-negative microbes, we reason that $HD5_{ox}$ may exert antimicrobial activity by affecting cell division. Further investigation is required to address this notion.

3E.   Acknowledgements

3F.   References

(1) Selsted, M. E., and Ouellette, A. J. (2005) Mammalian defensins in the antimicrobial immune response. *Nat. Immunol. 6*, 551–557.

(2) Brogden, K. A. (2005) Antimicrobial peptides: pore formers or metabolic inhibitors in bacteria? *Nat. Rev. Microbiol. 3*, 238–250.

(3) Hilchie, A. L., Wuerth, K., and Hancock, R. E. W. (2013) Immune modulation by multifaceted cationic host defense (antimicrobial) peptides. *Nat. Chem. Biol. 9*, 761–768.

(4) Wehkamp, J., Salzman, N. H., Porter, E., Nuding, S., Weichenthal, M., Petras, R. E., Shen, B., Schaeffeler, E., Schwab, M., Linzmeier, R., Feathers, R. W., Chu, H., Lima, H., Fellermann, K., Ganz, T., Stange, E. F., and Bevins, C. L. (2005) Reduced Paneth cell alpha-defensins in ileal Crohn's disease. *Proc. Natl. Acad. Sci. U. S. A. 102*, 18129–18134.

(5) Ericksen, B., Wu, Z., Lu, W., and Lehrer, R. I. (2005) Antibacterial activity and specificity of the six human alpha-defensins. *Antimicrob. Agents Chemother. 49*, 269–275.

(6) Porter, E. M., van Dam, E., Valore, E. V, and Ganz, T. (1997) Broad-spectrum antimicrobial activity of human intestinal defensin 5. *Infect. Immun. 65*, 2396–2401.

(7) Nuding, S., Zabel, L. T., Enders, C., Porter, E., Fellermann, K., Wehkamp, J., Mueller, H. A. G., and Stange, E. F. (2009) Antibacterial activity of human defensins on anaerobic intestinal bacterial species: a major role of HBD-3. *Microbes Infect. 11*, 384–393.

(8) Wommack, A. J., Ziarek, J. J., Tomaras, J., Chileveru, H. R., Zhang, Y., Wagner, G., and Nolan, E. M. (2014) Discovery and characterization of a disulfide-locked C_2-symmetric defensin peptide. *J. Am. Chem. Soc. 136*, 13494–13497.

(9) Szyk, A., Wu, Z., Tucker, K., Yang, D., Lu, W., and Lubkowski, J. (2006) Crystal structures of human alpha-defensins HNP4, HD5, and HD6. *Protein Sci. 15*, 2749–2760.

(10) Lehrer, R. I., Barton, A., Daher, K. A., Harwig, S. S. L., Ganz, T., and Selsted, M. E. (1989) Interaction of human defensins with *Escherichia coli*. Mechanism of bactericidal activity. *J. Clin. Invest. 84*, 553–561.

(11) Zasloff, M. (2002) Antimicrobial peptides of multicellular organisms. *Nature 415*, 389–95.

(12) Figueredo, S. M., Weeks, C. S., Young, S. K., and Ouellette, A. J. (2009) Anionic amino acids near the pro-alpha-defensin N-terminus mediate inhibition of bactericidal activity in

mouse pro-cryptdin-4. *J. Biol. Chem. 284*, 6826–6831.

(13) Hill, C. P., Yee, J., Selsted, M. E., and Eisenberg, D. (1991) Crystal structure of defensin HNP-3, an amphiphilic dimer: mechanisms of membrane permeabilization. *Science 251*, 1481–1485.

(14) Schneider, T., Kruse, T., Wimmer, R., Wiedemann, I., Sass, V., Pag, U., Jansen, A., Nielsen, A. K., Mygind, P. H., Raventós, D. S., Neve, S., Ravn, B., Bonvin, A. M. J. J., De Maria, L., Andersen, A. S., Gammelgaard, L. K., Sahl, H.-G., and Kristensen, H.-H. (2010) Plectasin, a fungal defensin, targets the bacterial cell wall precursor Lipid II. *Science 328*, 1168–1172.

(15) Schmitt, P., Wilmes, M., Pugnière, M., Aumelas, A., Bachère, E., Sahl, H.-G., Schneider, T., and Destoumieux-Garzón, D. (2010) Insight into invertebrate defensin mechanism of action: oyster defensins inhibit peptidoglycan biosynthesis by binding to lipid II. *J. Biol. Chem. 285*, 29208–29216.

(16) Essig, A., Hofmann, D., Münch, D., Gayathri, S., Künzler, M., Kallio, P. T., Sahl, H.-G., Wider, G., Schneider, T., and Aebi, M. (2014) Copsin, a novel peptide-based fungal antibiotic interfering with the peptidoglycan synthesis. *J. Biol. Chem. 289*, 34953–34964.

(17) de Leeuw, E., Li, C., Zeng, P., Li, C., Diepeveen-de Buin, M., Lu, W.-Y., Breukink, E., and Lu, W. (2010) Functional interaction of human neutrophil peptide-1 with the cell wall precursor lipid II. *FEBS Lett. 584*, 1543–1548.

(18) Sass, V., Schneider, T., Wilmes, M., Körner, C., Tossi, A., Novikova, N., Shamova, O., and Sahl, H.-G. (2010) Human beta-defensin 3 inhibits cell wall biosynthesis in *Staphylococci. Infect. Immun. 78*, 2793–2800.

(19) Wilmes, M., and Sahl, H.-G. (2014) Defensin-based anti-infective strategies. *Int. J. Med. Microbiol. 304*, 93–99.

(20) Kandaswamy, K., Liew, T. H., Wang, C. Y., Huston-Warren, E., Meyer-Hoffert, U., Hultenby, K., Schröder, J. M., Caparon, M. G., Normark, S., Henriques-Normark, B., Hultgren, S. J., and Kline, K. A. (2013) Focal targeting by human β-defensin 2 disrupts localized virulence factor assembly sites in *Enterococcus faecalis. Proc. Natl. Acad. Sci. U. S. A. 110*, 20230–20235.

(21) Chu, H., Pazgier, M., Jung, G., Nuccio, S.-P., Castillo, P. A., de Jong, M. F., Winter, M. G., Winter, S. E., Wehkamp, J., Shen, B., Salzman, N. H., Underwood, M. A., Tsolis, R. M., Young, G. M., Lu, W., Lehrer, R. I., Bäumler, A. J., and Bevins, C. L. (2012) Human α-defensin 6 promotes mucosal innate immunity through self-assembled peptide nanonets. *Science 337*, 477–481.

(22) Chairatana, P., and Nolan, E. M. (2014) Molecular basis for self-assembly of a human host-defense peptide that entraps bacterial pathogens. *J. Am. Chem. Soc. 136*, 13267–13276.

(23) Schroeder, B. O., Ehmann, D., Precht, J. C., Castillo, P. A., Küchler, R., Berger, J., Schaller, M., Stange, E. F., and Wehkamp, J. (2014) Paneth cell α-defensin 6 (HD-6) is an antimicrobial peptide. *Mucosal Immunol. 8*, 661–671.

(24) Clevers, H. C., and Bevins, C. L. (2013) Paneth cells: maestros of the small intestinal crypts. *Annu. Rev. Physiol. 75*, 289–311.

(25) Giblin, L. J., Chang, C. J., Bentley, A. F., Frederickson, C., Lippard, S. J., and Frederickson, C. J. (2006) Zinc-secreting Paneth cells studied by ZP fluorescence. *J. Histochem. Cytochem. 54*, 311–316.

(26) Dinsdale, D. (1984) Ultrastructural localization of zinc and calcium within the granules of rat Paneth cells. *J. Histochem. Cytochem. 32*, 139–145.

(27) Jones, D. E., and Bevins, C. L. (1992) Paneth cells of the human small intestine express an antimicrobial peptide gene. *J. Biol. Chem. 267*, 23216–23225.

(28) Porter, E. M., Liu, L., Oren, A., Anton, P. A., and Ganz, T. (1997) Localization of human intestinal defensin 5 in Paneth cell granules. *Infect. Immun. 65*, 2389–2395.

(29) Ayabe, T., Ashida, T., Kohgo, Y., and Kono, T. (2004) The role of Paneth cells and their antimicrobial peptides in innate host defense. *Trends Microbiol. 12*, 394–398.

(30) Ghosh, D., Porter, E., Shen, B., Lee, S. K., Wilk, D., Drazba, J., Yadav, S. P., Crabb, J. W., Ganz, T., and Bevins, C. L. (2002) Paneth cell trypsin is the processing enzyme for human defensin-5. *Nat. Immunol. 3*, 583–590.

(31) Salzman, N. H., Ghosh, D., Huttner, K. M., Paterson, Y., and Bevins, C. L. (2003) Protection against enteric salmonellosis in transgenic mice expressing a human intestinal defensin. *Nature 422*, 522–526.

(32) Salzman, N. H., Hung, K., Haribhai, D., Chu, H., Karlsson-Sjöberg, J., Amir, E., Teggatz, P., Barman, M., Hayward, M., Eastwood, D., Stoel, M., Zhou, Y., Sodergren, E., Weinstock, G. M., Bevins, C. L., Williams, C. B., and Bos, N. A. (2010) Enteric defensins are essential regulators of intestinal microbial ecology. *Nat. Immunol. 11*, 76–83.

(33) Rajabi, M., Ericksen, B., Wu, X., de Leeuw, E., Zhao, L., Pazgier, M., and Lu, W. (2012) Functional determinants of human enteric α-defensin HD5: crucial role for hydrophobicity at dimer interface. *J. Biol. Chem. 287*, 21615–21627.

(34) Wanniarachchi, Y. A., Kaczmarek, P., Wan, A., and Nolan, E. M. (2011) Human defensin 5 disulfide array mutants: disulfide bond deletion attenuates antibacterial activity against *Staphylococcus aureus*. *Biochemistry 50*, 8005–8017.

(35) de Leeuw, E., Burks, S. R., Li, X., Kao, J. P. Y., and Lu, W. (2007) Structure-dependent functional properties of human defensin 5. *FEBS Lett. 581*, 515–520.

(36) de Leeuw, E., Rajabi, M., Zou, G., Pazgier, M., and Lu, W. (2009) Selective arginines are important for the antibacterial activity and host cell interaction of human alpha-defensin 5. *FEBS Lett. 583*, 2507–2512.

(37) Rajabi, M., de Leeuw, E., Pazgier, M., Li, J., Lubkowski, J., and Lu, W. (2008) The conserved salt bridge in human alpha-defensin 5 is required for its precursor processing and proteolytic stability. *J. Biol. Chem. 283*, 21509–21518.

(38) Wei, G., de Leeuw, E., Pazgier, M., Yuan, W., Zou, G., Wang, J., Ericksen, B., Lu, W.-Y., Lehrer, R. I., and Lu, W. (2009) Through the looking glass, mechanistic insights from enantiomeric human defensins. *J. Biol. Chem. 284*, 29180–29192.

(39) Thomassin, J.-L., Lee, M. J., Brannon, J. R., Sheppard, D. C., Gruenheid, S., and Le Moual, H. (2013) Both group 4 capsule and lipopolysaccharide O-antigen contribute to enteropathogenic *Escherichia coli* resistance to human α-defensin 5. *PLoS One 8*, e82475.

(40) Moser, S., Chileveru, H. R., Tomaras, J., and Nolan, E. M. (2014) A bacterial mutant library as a tool to study the attack of a defensin peptide. *Chembiochem 15*, 2684–2688.

(41) Chileveru, H. R., Lim, S. A., Chairatana, P., Wommack, A. J., Chiang, I.-L., and Nolan, E. M. (2015) Visualizing attack of *Escherichia coli* by the antimicrobial peptide human defensin 5. *Biochemistry 54*, 1767–1777.

(42) Baba, T., Ara, T., Hasegawa, M., Takai, Y., Okumura, Y., Baba, M., Datsenko, K. A., Tomita, M., Wanner, B. L., and Mori, H. (2006) Construction of *Escherichia coli* K-12 in-frame, single-gene knockout mutants: the Keio collection. *Mol. Syst. Biol. 2*, 2006.0008.

(43) Ranjit, D. K., and Young, K. D. (2013) The Rcs stress response and accessory envelope proteins are required for de novo generation of cell shape in *Escherichia coli*. *J. Bacteriol. 195*, 2452–2462.

(44) Billings, N., Millan, M., Caldara, M., Rusconi, R., Tarasova, Y., Stocker, R., and Ribbeck, K. (2013) The extracellular matrix Component Psl provides fast-acting antibiotic defense in *Pseudomonas aeruginosa* biofilms. *PLoS Pathog. 9*, e1003526.

(45) Schmidt, N. W., Mishra, A., Lai, G. H., Davis, M., Sanders, L. K., Tran, D., Garcia, A., Tai, K. P., McCray, P. B., Ouellette, A. J., Selsted, M. E., and Wong, G. C. L. (2011) Criterion for amino acid composition of defensins and antimicrobial peptides based on geometry of membrane destabilization. *J. Am. Chem. Soc. 133*, 6720–6727.

(46) van den Bogaart, G., Guzmán, J. V., Mika, J. T., and Poolman, B. (2008) On the mechanism of pore formation by melittin. *J. Biol. Chem. 283*, 33854–33857.

(47) Falagas, M. E., and Kasiakou, S. K. (2005) Colistin: the revival of polymyxins for the management of multidrug-resistant Gram-negative bacterial infections. *Clin. Infect. Dis. 40*, 1333–1341.

(48) Sochacki, K. A., Barns, K. J., Bucki, R., and Weisshaar, J. C. (2011) Real-time attack on single *Escherichia coli* cells by the human antimicrobial peptide LL-37. *Proc. Natl. Acad. Sci. U. S. A. 108*, E77–E81.

(49) Matsuzaki, K., Sugishita, K., Harada, M., Fujii, N., and Miyajima, K. (1997) Interactions of an antimicrobial peptide, magainin 2, with outer and inner membranes of Gram-negative bacteria. *Biochim. Biophys. Acta 1327*, 119–130.

(50) Spindler, E. C., Hale, J. D. F., Giddings, T. H., Hancock, R. E. W., and Gill, R. T. (2011) Deciphering the mode of action of the synthetic antimicrobial peptide Bac8c.

Antimicrob. Agents Chemother. 55, 1706–1716.

(51) Lee, H., Andalibi, A., Webster, P., Moon, S., Teufert, K., Kang, S., Li, J., Nagura, M., Ganz, T., and Lim, D. J. (2004) Antimicrobial activity of innate immune molecules against *Streptococcus pneumoniae, Moraxella catarrhalis* and *nontypeable Haemophilus influenzae. BMC Infect. Dis. 4*, 12.

(52) Yao, Z., Kahne, D., and Kishony, R. (2012) Distinct single-cell morphological dynamics under beta-lactam antibiotics. *Mol. Cell 48*, 705–712.

(53) Paradis-Bleau, C., Kritikos, G., Orlova, K., Typas, A., and Bernhardt, T. G. (2014) A genome-wide screen for bacterial envelope biogenesis mutants identifies a novel factor involved in cell wall precursor metabolism. *PLoS Genet. 10*, e1004056.

(54) Yeh, Y.-C., Comolli, L. R., Downing, K. H., Shapiro, L., and McAdams, H. H. (2010) The caulobacter Tol-Pal complex is essential for outer membrane integrity and the positioning of a polar localization factor. *J. Bacteriol. 192*, 4847–4858.

(55) Goldman, M. J., Anderson, G. M., Stolzenberg, E. D., Kari, U. P., Zasloff, M., and Wilson, J. M. (1997) Human beta-defensin-1 is a salt-sensitive antibiotic in lung that is inactivated in cystic fibrosis. *Cell 88*, 553–560.

(56) Wommack, A. J., Robson, S. A., Wanniarachchi, Y. A., Wan, A., Turner, C. J., Wagner, G., and Nolan, E. M. (2012) NMR solution structure and condition-dependent oligomerization of the antimicrobial peptide human defensin 5. *Biochemistry 51*, 9624–9637.

(57) Zhang, Y., Cougnon, F. B. L., Wanniarachchi, Y. A., Hayden, J. A., and Nolan, E. M. (2013) Reduction of human defensin 5 affords a high-affinity zinc-chelating peptide. *ACS Chem. Biol. 8*, 1907–1911.

(58) Chung, H. S., Yao, Z., Goehring, N. W., Kishony, R., Beckwith, J., and Kahne, D. (2009) Rapid beta-lactam-induced lysis requires successful assembly of the cell division machinery. *Proc. Natl. Acad. Sci. U. S. A. 106*, 21872–21877.

(59) Kulp, A., and Kuehn, M. J. (2010) Biological functions and biogenesis of secreted bacterial outer membrane vesicles. *Annu. Rev. Microbiol. 64*, 163–184.

(60) Park, C. B., Yi, K.-S., Matsuzaki, K., Kim, M. S., and Kim, S. C. (2000) Structure-activity analysis of buforin II, a histone H2A-derived antimicrobial peptide: the proline hinge is responsible for the cell-penetrating ability of buforin II. *Proc. Natl. Acad. Sci. U. S. A. 97*, 8245–8250.

(61) Barns, K. J., and Weisshaar, J. C. (2013) Real-time attack of LL-37 on single *Bacillus subtilis* cells. *Biochim. Biophys. Acta 1828*, 1511–1520.

(62) Ding, B., Soblosky, L., Nguyen, K., Geng, J., Yu, X., Ramamoorthy, A., and Chen, Z. (2013) Physiologically-relevant modes of membrane interactions by the human antimicrobial peptide, LL-37, revealed by SFG experiments. *Sci. Rep. 3*, 1854.

(63) Bindman, N. A., and van der Donk, W. A. (2013) A general method for fluorescent labeling of the N-termini of lanthipeptides and its application to visualize their cellular

localization. *J. Am. Chem. Soc. 135*, 10362–10371.

(64) Mileykovskaya, E., and Dowhan, W. (2000) Visualization of phospholipid domains in *Escherichia coli* by using the cardiolipin-specific fluorescent dye 10-N-nonyl acridine orange. *J. Bacteriol. 182*, 1172–1175.

Chapter 4

Antimicrobial Activity and HD5$_{ox}$-mediated Phenotypic Effects in Gram-positive Bacteria

4A. Introduction

$HD5_{ox}$ displays broad-spectrum antimicrobial activity against bacteria, and fungi.[1,2] The antimicrobial activity of cationic peptides, including defensins is often attributed to bacterial membrane permeabilization by either pore formation or bacterial membrane destatbilization.[3] However, recent studies have supported other alternative mechanism of actions for defensins. For instance, Plectasin and oyster defensin bind to lipid II and interfere with the peptidoglycan biosynthesis. Even human defensins such as HNP1 and HBD3 bind to lipid II, albeit to a lesser extent.[4] HBD2 induces dislocation of bacterial virulence factor assembly machinery from the septa.[5] $HD5_{ox}$ and HNP1 can cause unfolding of bacterial toxins.[6] Considering such diverse pathways of bacterial killing, further investigation of the mechanism of bacterial killing by HD5 is needed. In Chapter 3, we examined the effect of HD5 treatment on Gram-negative strains and studied the localization of $HD5_{ox}$ during bacterial killing.[7,8] We observed distinct morphological changes induced by $HD5_{ox}$-treated Gram-negative bacteria (bleb formation, clumping and elongation of cells). These morphological changes were not observed in bacteria treated with other antimicrobial peptides such as LL37, colistin, melittin. Certain Gram-negative bacteria including "no ESKAPE" pathogens *Acinetobacter baumannii and Pseudomonas aeruginosa* also displayed the distinct morphological changes upon treatment with $HD5_{ox}$.[7] Therefore, we questioned the antimicrobial activity of HD5 on other organisms, and set out to explore the effects of $HD5_{ox}$ on the Gram-positive bacteria.

Several questions need to be addressed regarding the antimicrobial activity of HD5. How does HD5 kill Gram-positive bacteria? Are there similar modes of killing at play for Gram-positive and Gram-negative bacteria? Are membrane permeabilization and lysis the primary modes of killing of HD5? Does HD5 cause similar phenotypes as pore-forming LL37 and melittin? Several prior studies have addressed the antibacterial activity of HD5 against Gram-positive bacteria. Some of the results suggested different modes of antimicrobial action of $HD5_{ox}$ against Gram-positive and Gram-negative bacteria.[9-11] For instance, the antibacterial activity of L-HD5 and D-HD5 varied against Gram-positive bacteria, specifically *S. aureus*,

although similar activities were observed against Gram-negative bacteria.[12] In another study, the antimicrobial activity of mutants of HD5 lacking one or more disulfide linkages was completely abrogated against Gram-positive bacteria (*S. aureus*); whereas, the mutants retained antimicrobial activity against Gram-negative bacteria (*E. coli*) compared to the native peptide.[9] Consequently, we set out to probe the mechanism of action of HD5 against a set of Gram-positive strains.

In this Chapter, we examined the phenotypic effects observed in selected Gram-positive bacteria treated with HD5 and other AMPs. We probed the effect of $HD5_{ox}$ on Gram-positive bacteria *Staphylococcus aureus*, *Enterococcus faecalis*, and *Bacillus subtilis*. *S. aureus* is a "no ESKAPE" pathogen, causes nosocomial infections and exhibits antibiotic resistance.[13] *E. faecalis* is an opportunistic pathogen responsible for majority of the urogenital infections (UTI) acquired in the hospitals.[13-15] In contrast, *B. subtilis* is a non-pathogenic spore-forming bacteria commonly found in soil and even consumed in large quantities in the Japanese food natto.[16] The genome of *B. subtilis*, a model Gram-positive organism, is one of the most studied only after *E. coli*; Therefore, we employed this strain to study antimicrobial action of $HD5_{ox}$.[17]

4B.   Experimental Section

i.   Media and Buffers. $S7_{50}$ media was prepared as described previously except that concentration of MOPS was 50 mM and $ZnCl_2$ was excluded. We decided to exclude the zinc salts in the $S7_{50}$ media preparation because the antimicrobial action of $HD5_{ox}$ against *E. coli* was attenuated by mere two equivalents of added zinc in the AMA buffer (Chapter 2).CHILE The final composition of the MODIFIED $S7_{50}$ media is 5 mM potassium phosphate (pH 7.0), 10 mM $(NH_4)_2SO_4$, 50 mM MOPS (adjusted to pH 7.0 with KOH), 20 mM potassium glutamate (pH 7.0), 2 mM $MgCl_2$, 0.7 mM $CaCl_2$, 50 μM $MnCl_2$, 5 μM $FeCl_3$, 2 μM thiamine, and 100 mM glucose.[18] Sodium phosphate was obtained from BDH Chemicals.

Peptides. $HD5_{ox}$ and $HD5[Ser^{hexa}]$ were synthesized by Fmoc solid-phase synthesis as reported in Chapter 2.[1,9] LL-37 was purchased from Bachem Americas, Inc. Melittin and colistin

sulfate were obtained from Enzo Life Sciences Inc. All peptide stock solutions were prepared in Milli-Q water, aliquoted, and stored at -20 °C. The peptide solutions and buffers for antimicrobial activity assays were sterile-filtered (0.2-μm filter) prior to the assays. Known masses of LL37, melittin and colistin were dissolved to prepare stock solutions of these peptides. Peptide concentrations of $HD5_{ox}$ and $HD5[Ser^{hexa}]$ were determined using calculated extinction coefficients as described in Chapter 2.

ii. Antimicrobial Activity Assays. Antimicrobial activity (AMA) assays were performed using a micro-drop colony forming units (CFU) method described previously in Chapter 2.[1]

Table 4.1. Strains and Growth Conditions

Strain	Source	Growth medium	Agar plate conditions
S. aureus ATCC 25923	ATCC	TSB w/o dex	TSB (w/o dex)-agar
E. faecalis 1375	Prof. Richard Kolter, Harvard University	BHI media	BHI-agar
B. subtilis PY79	Prof. Alan Grossman, MIT	$S7_{50}$ minimal media	LB-agar

S. aureus and *E. faecalis* were grown overnight in TSB (without dextrose) and BHI media respectively (Table 4.1). The overnight cultures were diluted 1:100 in respective media and grown in to an $OD_{600} \approx 0.6$. The bacterial cultures were centrifuged (3500 rpm x 6 min, 4 °C) and resuspended in AMA buffer (10 mM sodium phosphate buffer, pH 7.4, supplemented with 1% v/v TSB (without dextrose)). The process was repeated once to remove residual medium. The OD_{600} was measured again and adjusted to 0.5 (2.5 x 10^8 CFU/mL), and the cultures were diluted further to a cell count of 1 x 10^8 CFU/mL or 1 x 10^6 CFU/mL for the assays performed at higher and lower CFU/mL, respectively.

For culturing *B. subtilis*, a single colony from freshly streaked LB-plate was grown in $S7_{50}$ media to an $OD_{600} \approx 1.0$ (1x 10^8 CFU/mL). This culture was further diluted to $OD_{600} \approx 0.05$ in fresh 10 mL of S750 media in 250 mL flask and grown to $OD_{600} \approx 0.4 - 0.6$. Depending on the

starting CFU/mL needed for the assay, and the assay conditions, the culture of *B. subtilis* was filtered (cellulose nitrate filter units, 0.2-μm) and resuspended to the desired CFU/mL in either S7$_{50}$ media or AMA buffer. For *B. subtilis*, bacteria were filtered and resuspended when possible as centrifugation causes drop in CFU/mL and loss of viability.

iii.   General Methods and Image Analysis for Microscopy

Phase-contrast microscopy, scanning electron microscopy (SEM) and transmission electron microscopy (TEM) were performed as described in Chapter 3. The image analysis was performed using ImageJ.

4C.   Results and Discussion

i.   HD5 Displays Antimicrobial Activity Against Various Gram-positive Strains. The effects

of HD5$_{ox}$ treatment on three Gram-positive strains, including the opportunistic pathogens *Staphylococcus aureus* and *Enterococcus faecalis*, and non-pathogenic *Bacillus subtilis*, were studied. These bacteria allowed us to examine the morphological changes induced by HD5$_{ox}$ in strains displaying different shapes. The strains represent a sperical *S. aureus*, oval-shaped *E. faecalis* and rod-shaped *B. subtilis*. The antimicrobial activity was measured against bacteria (10^6 CFU/mL) treated with HD5$_{ox}$ (0 - 8 μM), and the data were compared with antimicrobial activity data for HD5[Ser^{hexa}], LL37, melittin, and colistin (Figures 4.1 and 4.2). α-Helical peptide LL37 is the only human cathelicidin peptide, and its antimicrobial activity is attributed to pore-formation and carpet models of bacterial membrane destabilization.[19–21] Melittin, another α-helical pore-forming peptide (from bees) was employed as another control.[22,23] We also selected colistin (polymixin E), a peptide that causes LPS-mediated membrane disruption and thereby bacterial cell death in Gram-negative bacteria. Consequently, colistin is less active against Gram-positive strains.[24,25]

S. aureus. In agreement with previous studies, HD5$_{ox}$ displayed antimicrobial activity against *S. aureus* (MIC = 4 µM) (Figures 4.1).[9] Melittin (MIC = 4 µM) and LL37 (MIC = 8 µM) displayed potent activity against *S. aureus*. Based on the previous study employing HD5[Ser^{hexa}], a linear HD5 mutant peptide with Cys –> Ser mutations, it was demonstrated that the disulfide linkages of HD5 are essential for the antimicrobial activity of HD5 against *S. aureus*.[9] In agreement, HD5[Ser^{hexa}] did not display antimicrobial activity (no reduction in CFU/mL) in the concentration ranges tested (0 - 8 µM). Moreover, as expected, when treated with colistin, no antimicrobial activity against *S. aureus* was observed in the concentration tested.

Figure 4.1. Antimicrobial activity of the peptides against *S. aureus* ATCC 25923 and *E. faecalis* 1375 strains. The bacteria (10^6 CFU/mL) **A)** *S. aureus* and **B)** *E. faecalis* were treated with peptides (0 - 8 µM) at 37 °C (10 mM sodium phosphate buffer, pH 7.4 supplemented with 1% TSB w/o dextrose) for 1 h, (n = 3, standard deviation).

E. faecalis. When *E. faecalis* was treated with the peptides, a similar trend was observed in antimicrobial activities compared to *S. aureus* treated bacteria (Figures 4.1). Lower activity of HD5$_{ox}$ and LL37 was observed against *E. faecalis* 1375 (8 µM, < 3-log reduction in CFU/mL) compared to *S. aureus* (MIC = 8 µM). Similar to *S. aureus*, melittin was potent against *E. faecalis*

(MIC = 4 μM), whereas no AMA was observed for colistin and HD5[Ser^{hexa}] (no reduction in CFU/mL) against *E. faecalis*.

B. subtilis. For determining the antimicrobial activity of the peptides against *B. subtilis*, the AMA assays were performed in both the standard AMA buffer (10mM sodium phosphate buffer supplemented with 1% TSB without dextrose, pH 7.4) and S7$_{50}$ medium (Figures 4.2). When the AMA assay was performed in either the standard AMA buffer or S7$_{50}$ media, similar trends were observed. When treated with HD5$_{ox}$ (4 μM), melittin (4 μM), and LL37 (2 μM)), 4 - log reduction in CFU/mL of *B. subtilis* was observed. However, no antimicrobial activity was observed for colistin and HD5[Ser^{hexa}] (no reduction in CFU/mL) against *B. subtilis*. The antimicrobial activity of HD5$_{ox}$ against *B. subtilis* in a defined growth medium (S7$_{50}$ media) allows us to study the cellular processes such as macromolecule biosynthesis processes and cell division in the presence of HD5$_{ox}$. Considering the activity of HD5$_{ox}$ against *B. subtilis* in S7$_{50}$ media containing milli-molar concentrations of divalent cations, we further investigated the effect of NaCl on the AMA of HD5$_{ox}$.
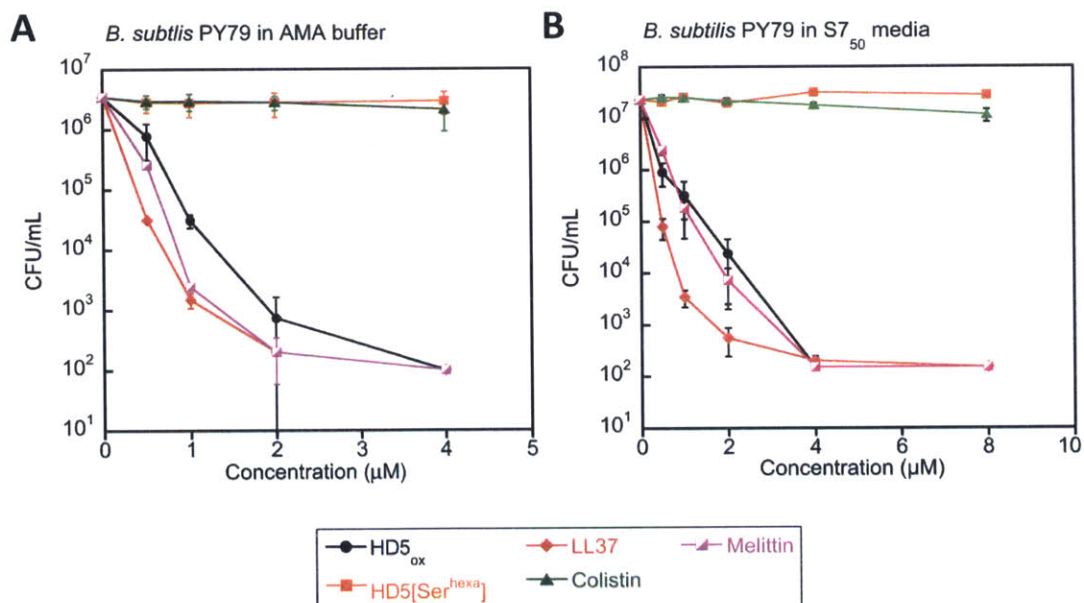
Figure 4.2. Antimicrobial activity of the peptides against *B. subtilis* PY79. The bacteria (10^6 CFU/mL) were treated with peptides (0 - 8 μM) at 37 °C for 1 h, in **A)** 10 mM sodium phosphate buffer, pH 7.4 supplemented with 1% TSB w/o dextrose and **B)** S7$_{50}$ media. Three independent antimicrobial assays are reported (n = 3, standard deviation).
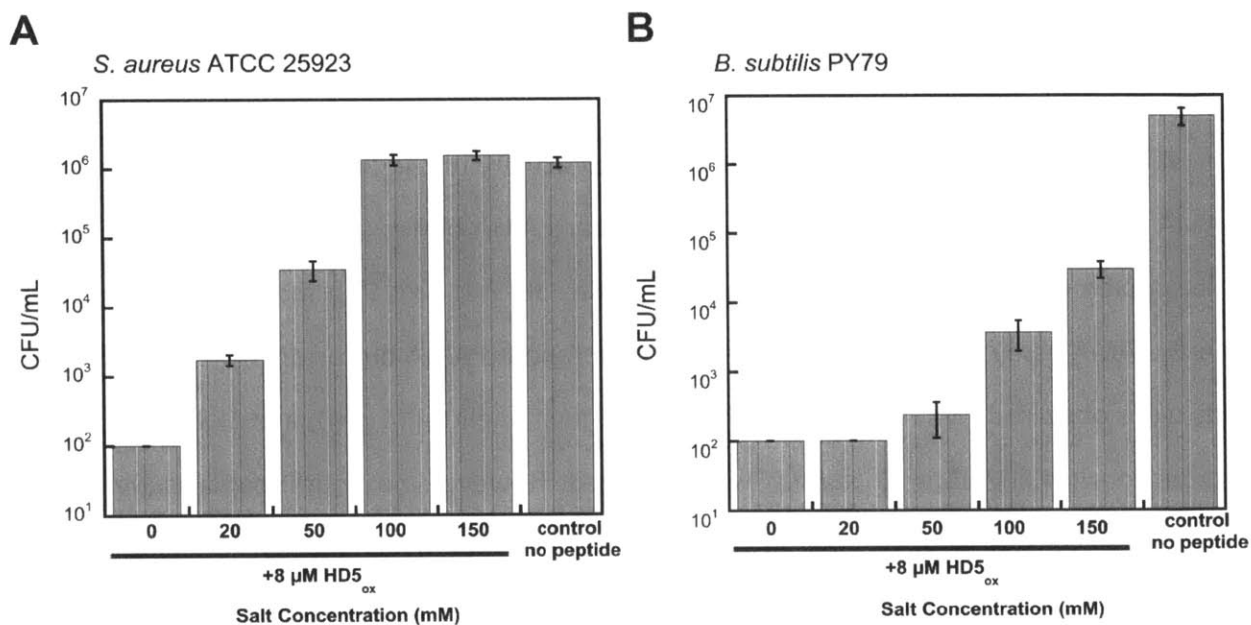
Figure 4.3. Antimicrobial activity of $HD5_{ox}$ in the presence of NaCl. The bacteria (10^8 CFU/mL) **A)** *S. aureus* ATCC 25922, and **B)** *B. subtilis* PY79 were treated with $HD5_{ox}$ (0 and 8 μM) in 10 mM sodium phosphate buffer, pH 7.4 supplemented with 1% TSB containing 0, 20, 50, 100 and 150 mM NaCl for 1 h at 37 °C at 130 rpm (n = 3, standard deviation).

ii. $HD5_{ox}$ is Less Sensitive to NaCl Against Gram-positive Strains. The antimicrobial activities of various human defensins against Gram-negative bacteria are more susceptible to salt concentration in the assay buffer. In contrast, their antimicrobial activity against Gram-positive bacteria is less affected by salt.[2,4,26,27] Several invertebrate defensins are more active against Gram-positive bacteria or fungi.[4] The effect of NaCl and divalent cations on the antimicrobial activity of $HD5_{ox}$ against *E. coli*, a Gram-negative bacteria was examined in Chapter 3.[7] Notably, the antimicrobial activity of $HD5_{ox}$ against *E. coli*, and the induced morphological changes were attenuated in the presence of salt and divalent cations.[7] In order to further examine the effect of salt on the antimicrobial activity of $HD5_{ox}$, the Gram-positive bacteria *B. subtilis* and *S. aureus* (10^6 CFU/mL) were treated with $HD5_{ox}$ (8 μM) in AMA buffer containing NaCl (0 - 150 mM) (Figures 4.3). Against *S. aureus*, the activity of $HD5_{ox}$ (8 uM) was retained (>1-log reduction of CFU/mL) even in the presence of high salt (50 mM NaCl).

Specifically, the antimicrobial activity of $HD5_{ox}$ (8 µM, > 2-log reduction in CFU/mL) was retained against *B. subtilis* even at physiologically relevant salt concentrations (150 mM NaCl).

iii.   **Antimicrobial Activity at Higher CFU/mL for Microscopy.** In order to examine the morphological changes induced in bacteria upon treatment with $HD5_{ox}$, antimicrobial activity of $HD5_{ox}$ and other peptides at 20 µM was determined against a higher CFU/mL (10^8 CFU/mL) of bacteria (Figure 4.4). At these peptide concentrations, a similar trend in the activity against *S. aureus* and *E. faecalis* at both higher (Figure 4.4) and lower CFU/mL (Figure 4.1) was observed. $HD5_{ox}$ (20 µM) was active against *S. aureus* (~ 6-log reduction in CFU/mL) and *E. faecalis* (> 3-log reduction in CFU/mL). The pore-forming α-helical peptides melittin and LL37 were highly potent against both strains. In order to study the killing kinetics, the antimicrobial action was monitored over 2 h (Figure 4.5). The peptides exert their antibacterial activity by the initial 1 h, and most of the killing is complete by 1 h of treatment with the peptides. For the purposes of the microscopy experiments, 1 h treatment with the peptides is sufficient to observe the
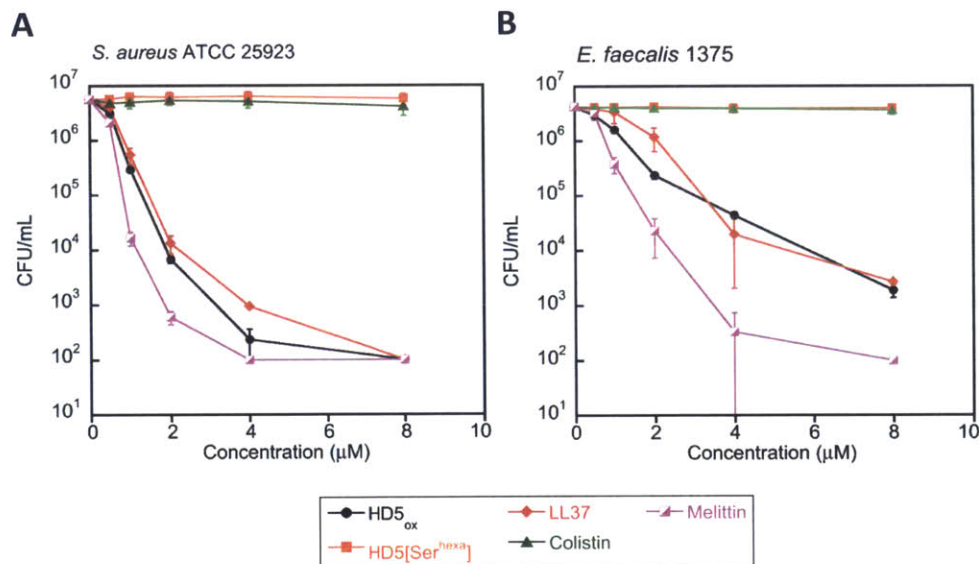
A

B
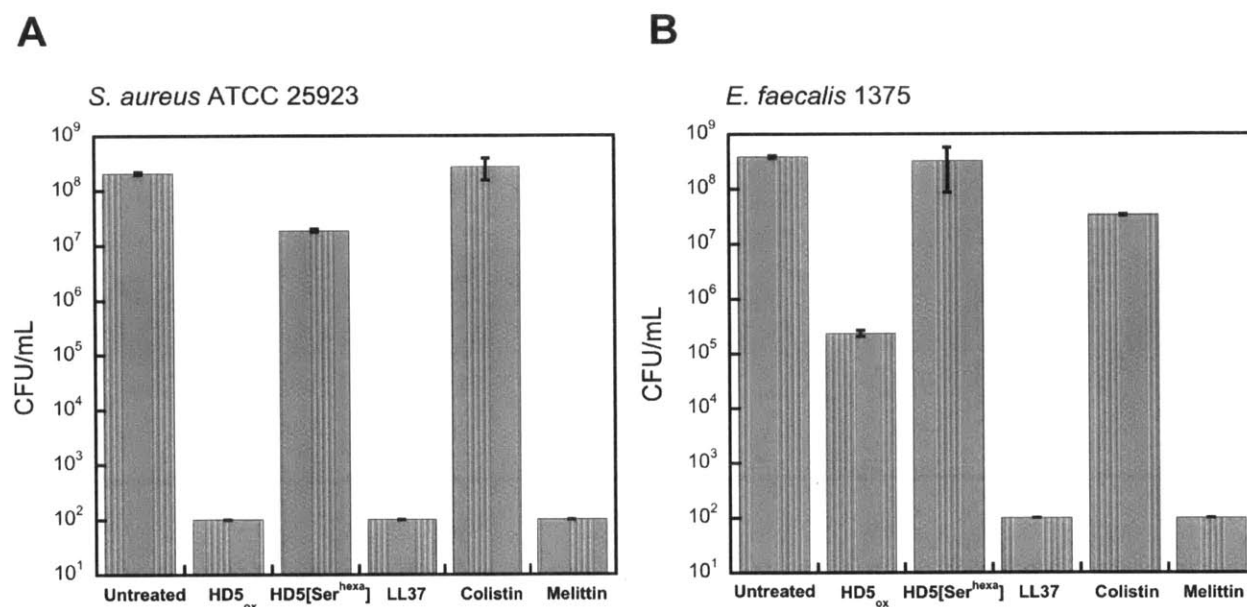
Figure 4.4. Antimicrobial activity of the peptides against **A)** *S. aureus* ATCC 25922 and **B)** *E. faecalis* 1375. The bacteria (10^8 CFU/mL) were treated with peptides (20 µM) in 10 mM sodium phosphate buffer, pH 7.4 supplemented with 1% TSB for 1 h at 37 °C at 130 rpm (n = 3, standard deviation).

morphological changes induced by these peptides.

iv. **HD5$_{ox}$-induced Morphological Changes in** *S. aureus* **ATCC 25923.** To probe the morphological changes displayed by *S. aureus* upon treatment with HD5$_{ox}$ and other AMPs, we

A

S. aureus ATCC 25923
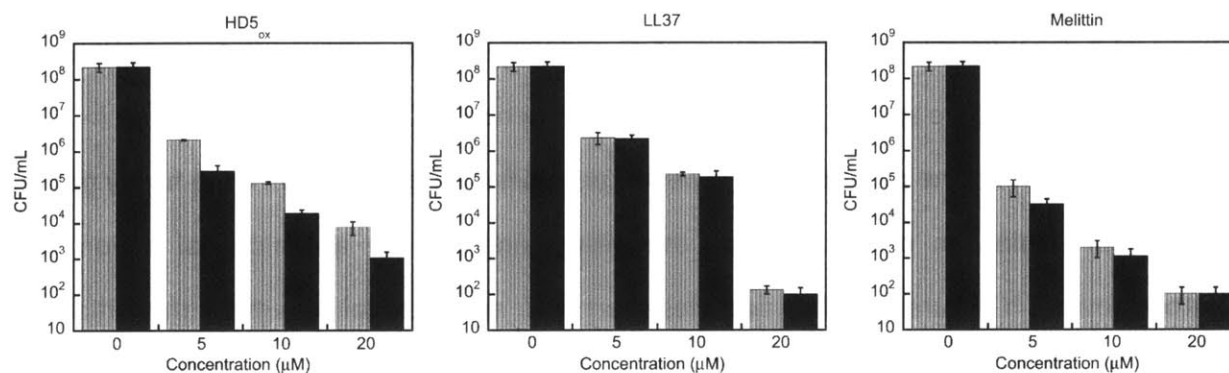
B

E. faecalis 1375
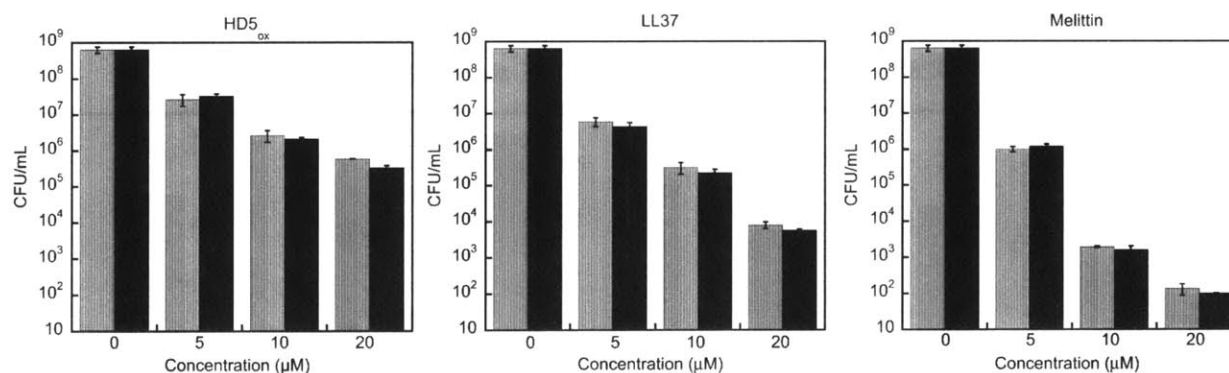
Figure 4.5. Antimicrobial activity of the peptides against **A)** *S. aureus* ATCC 25922 and **B)** *E. faecalis* 1375 determined over 2 h. The bacteria (10^8 CFU/mL) were treated with peptides (0, 5, 10 and 20 µM) in 10 mM sodium phosphate buffer, pH 7.4 supplemented with 1% TSB at 37 °C at 130 rpm and surviving colonies were measured at 1 h and 2 h (n = 3, standard deviation).

incubated *S. aureus* (10^8 CFU/mL) with either HD5$_{ox}$ (20 and 40 μM), or LL37 (20 μM). These

peptide concentrations afforded >4-log reduction of CFU/mL (Figure 4.4).

Untreated *S. aureus* displayed smooth morphology as evident in phase-contrast, SEM

and TEM images. In the phase-contrast images of *S. aureus* treated with HD5$_{ox}$, clumping of

bacteria was observed (Figure 4.6). Further morphological changes were not clearly

distinguishable by phase-contrast microscopy for *S. aureus*. Therefore, SEM (Figure 4.7) and

TEM (Figure 4.8) were employed in subsequent studies. The SEM images revealed that *S. aureus*

treated with HD5$_{ox}$ displayed a rugged surface with protrusions. The pronounced clumping of

bacteria was also observed in the presence of HD5$_{ox}$. When the ultrastructure of bacteria

treated with HD5$_{ox}$ was examined using TEM, abnormal bacterial membranes resembling

mesosomes were highly prominent, notably at the cell septa, along with an increase in cell wall

thickness (Figure 4.8). Mesosomes are distinctive structures primarily comprised of the plasma

membrane and these mesosomes were thought to assist in the oxidative phosphorylation.[28] As

a result, the mesosomes were considered to be the "bacterial mitochondrion".[28] However, the

exact functions of these mesosomes are not yet determined. The formation of mesosomes in *S.*

aureus upon treatment with antimicrobial peptides[29–31] including defensins such as HNP1[32] has

been reported. Furthermore, The cell wall thickening was also observed in bacteria treated with

a mixture of HNP1 and HNP2.[33] As expected, the bacteria treated with inactive peptide

HD5[Ser^{hexa}] resembled the untreated bacteria.

LL37 induced bacterial lysis and cellular debris was observed in both SEM and phase-

contrast images (data not shown). Of the bacteria that were not yet lysed and remained still

intact, it was difficult to distinguish any morphological changes induced by LL37 from the SEM

images alone (Figure 4.7). When the ultrastructure was examined in more detail in the TEM

images, *S. aureus* treated with LL37 display surface disintegration, lysis and separation at the

septa, along with thinning of cell wall also reported previously (Figure 4.7)..[34] All of these

morphological and ultra-structural changes are in agreement with the current models of pore-

formation and subsequent lysis of bacteria as the mode of action of LL37.[21,35] Recently, such cell

wall degradation (particularly at the septa), observed upon treatment with treated with peptides such as Pep5 and θ-defensins (RTD1 and RTD2) was attributed to membrane disruptions and activated autloysins.[36,37] HBD1, HBD2 and HBD3 treated *S. aureus* also displayed cell wall disintegration and prominent lysis.[34]

Untreated   **20 μM HD5[Ser^{hexa}]**

20 μM Melittin   **20 μM HD5$_{ox}$**
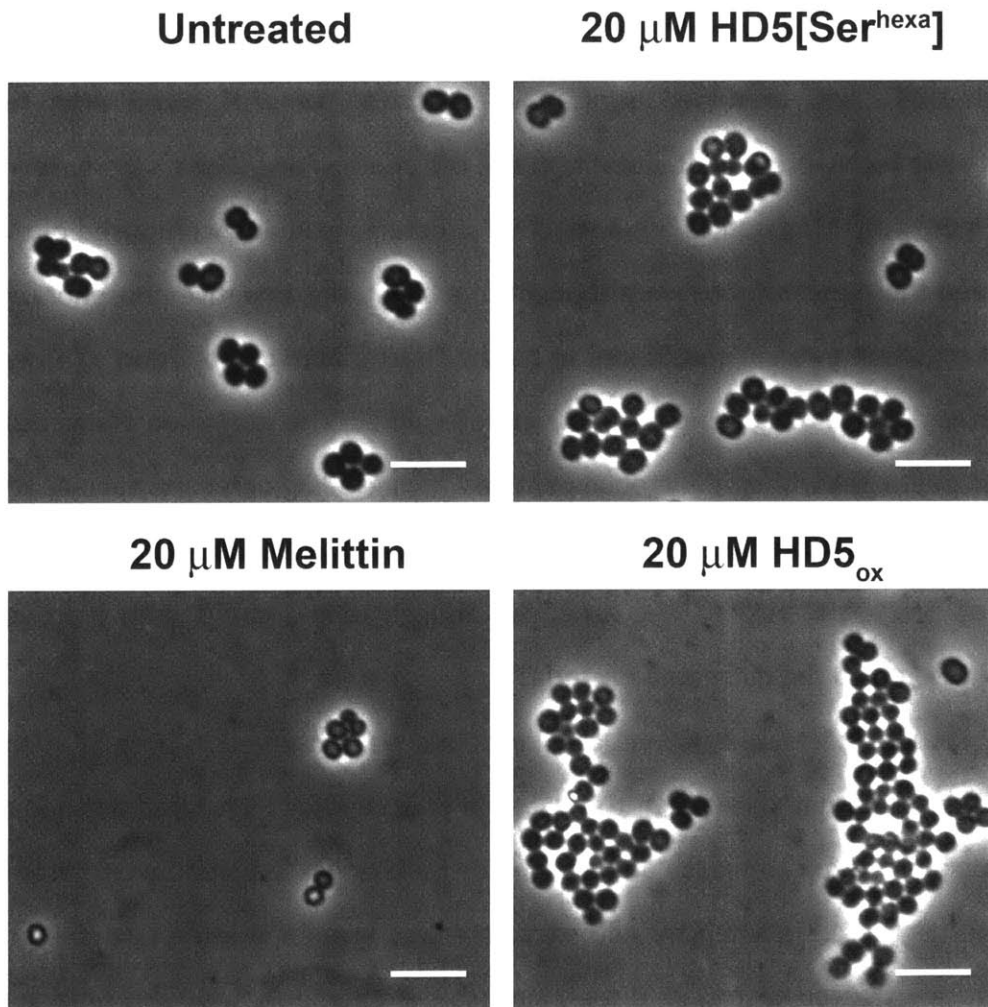
Figure 4.6. Phase-contrast images of *S. aureus* ATCC 25923 treated with various peptides. The morphology of *S. aureus* (1×10^8 CFU/mL) incubated in the absence (untreated) or in the presence of peptides (20 μM) at 37 °C (10 mM sodium phosphate buffer, pH 7.4, 1% v/v TSB w/o dextrose) for 1 h. Scale bar = 5 μm.
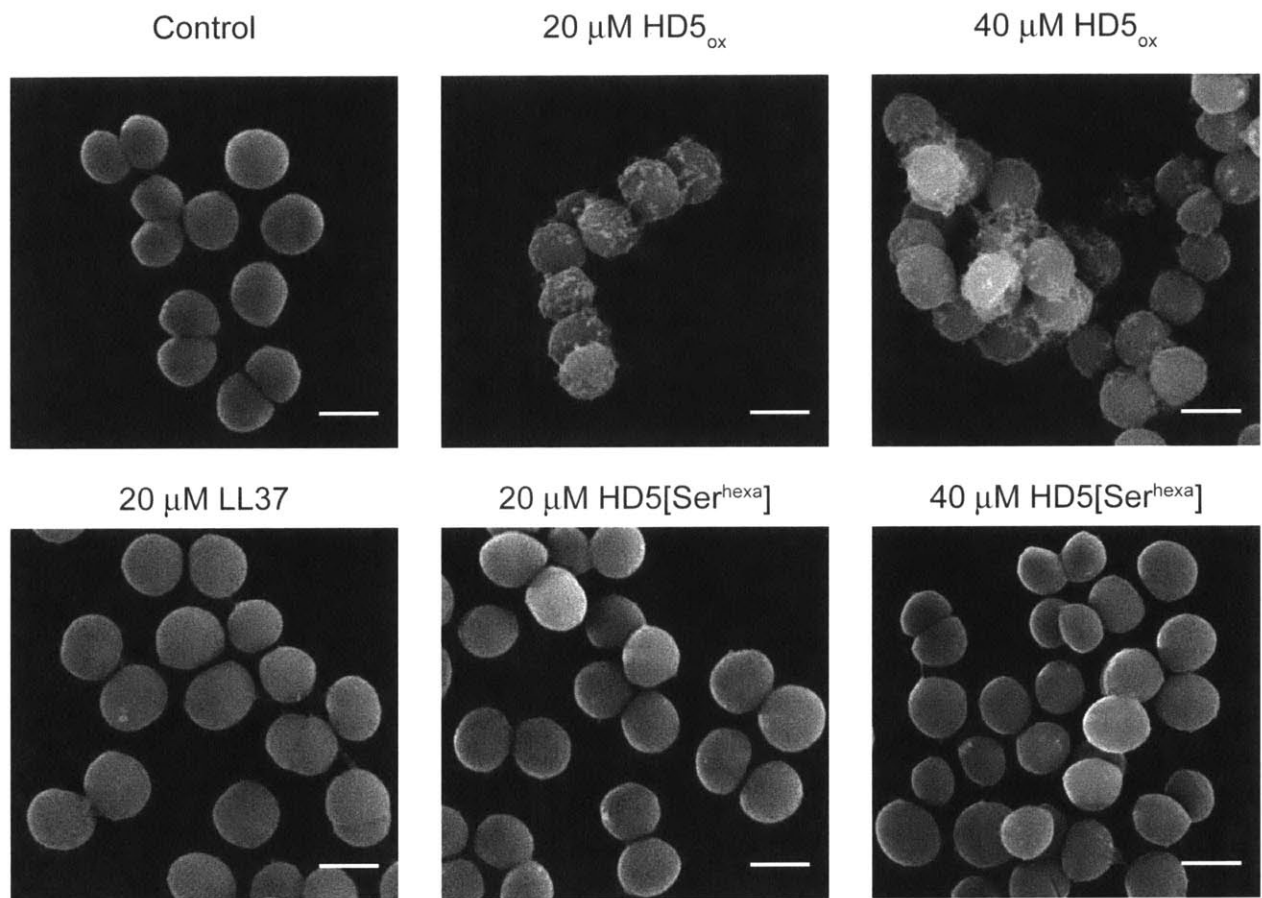
Figure 4.7. SEM images of *S. aureus* ATCC 25923 treated with various peptides. The morphology of *S. aureus* (1×10^8 CFU/mL) incubated in the absence (control) or in the presence of HD5$_{ox}$ (20 μM and 40 μM), HD5[Ser^{hexa}] (20 μM and 40 μM) and LL37 (20 μM) at 37 °C (10 mM sodium phosphate buffer, pH 7.4, 1% v/v TSB w/o dextrose) for 1 h. Scale bar = 1 μm.

Figure 4.8. TEM images of *S. aureus* ATCC 25923 treated with various peptides. The ultrastructure of *S. aureus* (1×10^8 CFU/mL) incubated in the absence (untreated) or in the presence of $HD5_{ox}$ (40 μM) and LL37 (20 μM) at 37 °C (10 mM sodium phosphate buffer, pH 7.4, 1% v/v TSB w/o dextrose) for 1 h. Scale bar = 200 nm.

v. **HD5$_{ox}$-induced Morphological Changes in _E. faecalis_ 1375.** _E. faecalis_ is one of the leading causes of hospital aquired urinary-tract infections (UTIs);[13] _E. faecalis_ can survive in nutrient limited conditions, making it a major problem for root canal infections.[36,37] The bacteria (1 x 10^8 CFU/mL) were treated with HD5$_{ox}$ (0, 10 and 20 μM), LL37 (10 and 20 μM) and HD5[Ser^{hexa}] (20 and 40 μM). _E. faecalis_ treated with HD5$_{ox}$ displayed clumping along with chain-like phenotype when monitored using phase-contrast microscopy (Figure 4.9). In order to further investigate the morphological changes, SEM (Figure 4.10) and TEM microscopy (Figure 4.11) were employed. Upon treatment with HD5$_{ox}$, clumping of the bacteria was observed in the SEM images (Figure 4.10). The clumped cells displayed what appears to be a chain-like morphology, along with surface protrusions resembling blebs. As expected, HD5[Ser^{hexa}]-treated bacteria displayed smooth morphology similar to untreated bacteria.

Untreated	**20 μM HD5$_{ox}$**	**20 μM LL37**
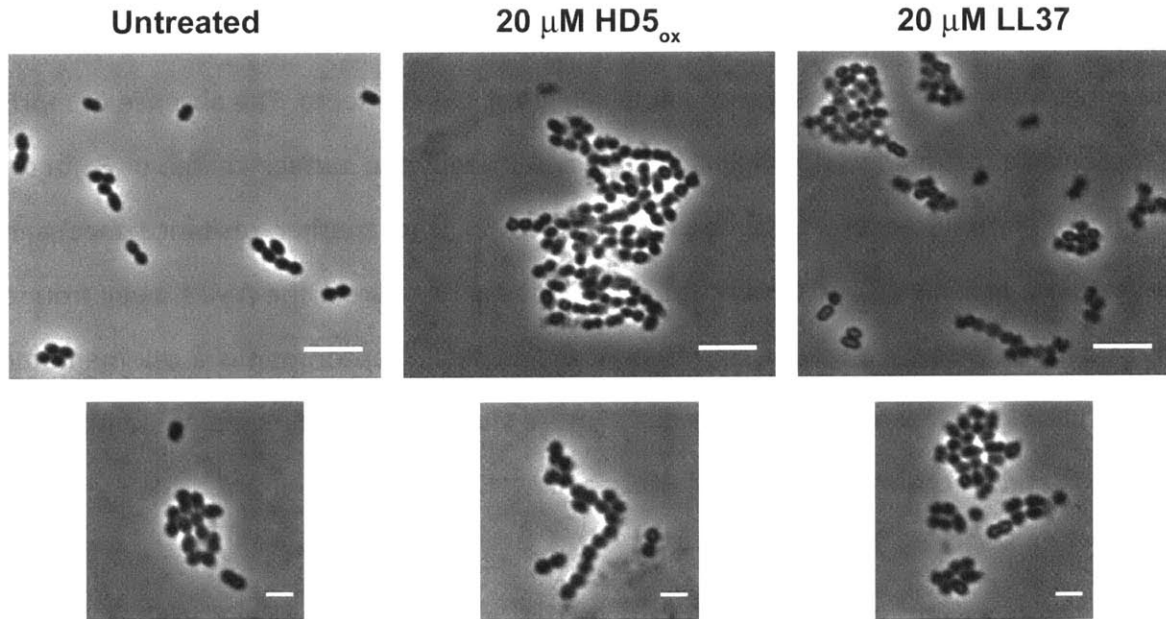
Figure 4.9. Phase-contrast images of _E. faecalis_ 1375 treated with HD5$_{ox}$ and LL37. The morphology of _E. faecalis_ (1 x 10^8 CFU/mL) incubated in the absence (untreated) or in the presence of peptides (20 μM) at 37 °C (10 mM sodium phosphate buffer, pH 7.4, 1% v/v TSB w/o dextrose) for 1 h. Scale bar for top panels = 5 μm and bottom panels = 2 μm.

When the ultra-structure was examined by employing TEM, the surface of the untreated *E. faecalis* was smooth with occasional surface extensions at potential cell septa (Figure 4.11A). The cell septa at division site was fully formed in diploid cells that had started second round of division (Figure 4.11D). In contrast, more significant surface protrusions were observed in bacterial samples treated with $HD5_{ox}$. The membrane in certain cells was disrupted to form an extended structure resembling a bleb (Figure 4.11C). When the ultrastructure of untreated bacteria was examined, initiation of new cell septa was observed only when the old septa was completely formed (Figure 4.11D). However, upon treatment with $HD5_{ox}$, many cells displayed abnormal division septa, including 1) incompleted division septa formation with extra membranous structures at the septa (Figure 4.11F, arrow head), 2) initiation of new division septa where old septa are incomplete (Figure 4.11F, white arrows). The bacteria treated with LL37 lyzed and cell membrane disruption was clearly observed (Figure 4.11B).

Recently, upon treatment with HBD2, disruption of focal targeting of protein synthesis machinery in *E. faecalis* was demonstrated.[5] HBD2 causes disruption of virulence factor assembly potentially by interacting with anionic lipids at the cell septa. The absence of *mprF*, a gene responsible for modification anionic lipids, and thereby the surface charge of *E. faecalis*, was shown to attenuate the focal targeting by HBD2. One another resitance mechanism employed by *E. faecalis* against antimcirobial peptides is to redirect the AMPs away from the septa, as demonstarted in daptomycin-resistant *E. faecalis*.[40] Daptomycin is a cell membrane-targeting cationic antimicrobial lipo-peptide.[41] Future studies will be directed at identifying the site of action and mechanism of action of $HD5_{ox}$ against *E. faecalis*.
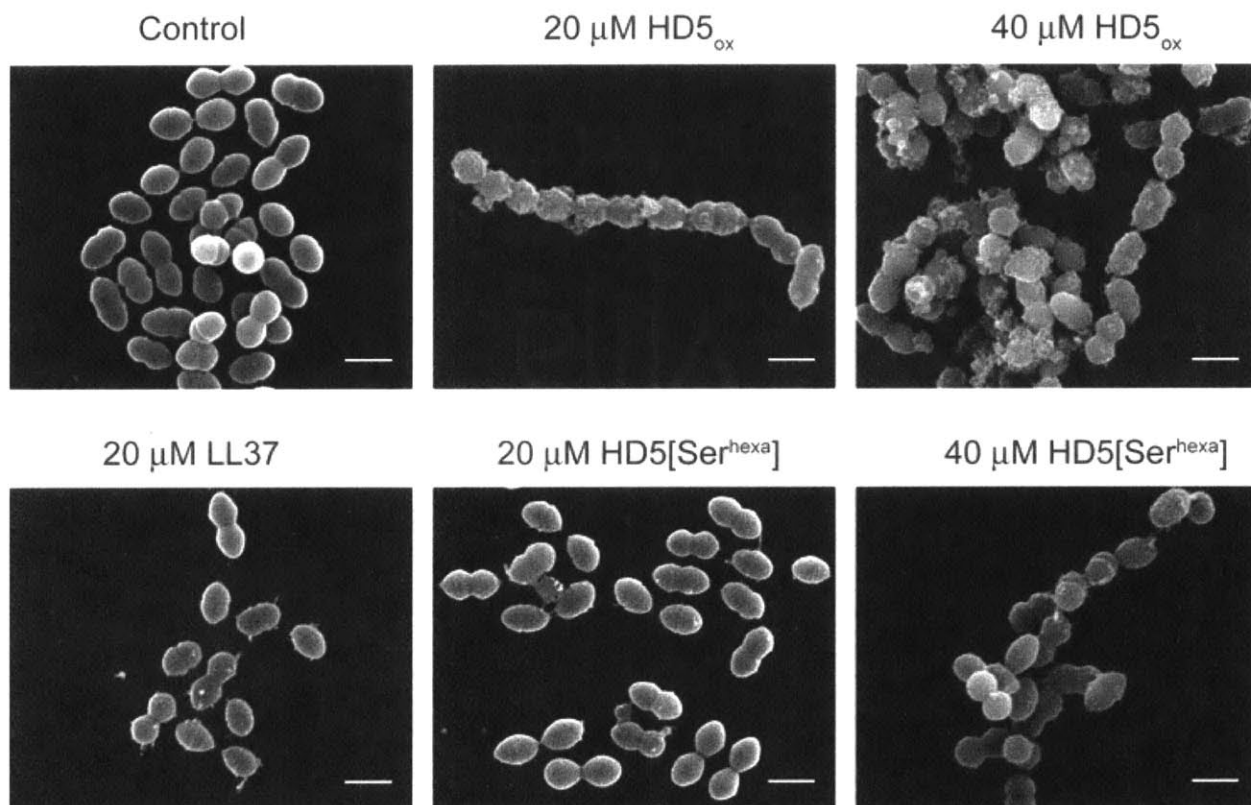
Figure 4.10. SEM images of *E. faecalis* 1375 treated with various peptides. The morphology of *E. faecalis* (1×10^8 CFU/mL) incubated in the absence (control) or in the presence of $HD5_{ox}$ (20 μM and 40 μM), HD5[Ser^hexa] (20 μM and 40 μM) and LL37 (20 μM) at 37 °C (10 mM sodium phosphate buffer, pH 7.4, 1% v/v TSB without dextrose) for 1 h. Scale bar = 1 μm.
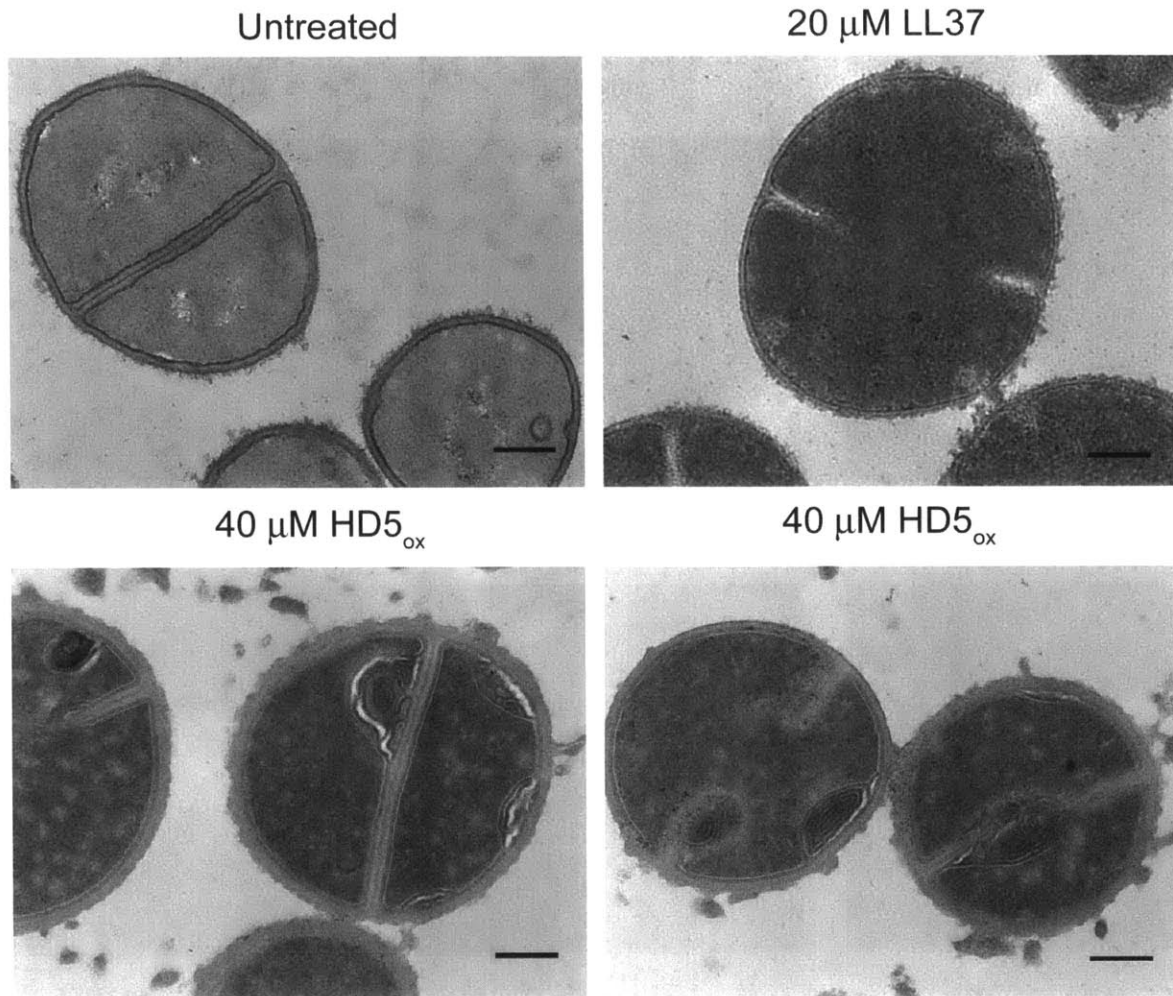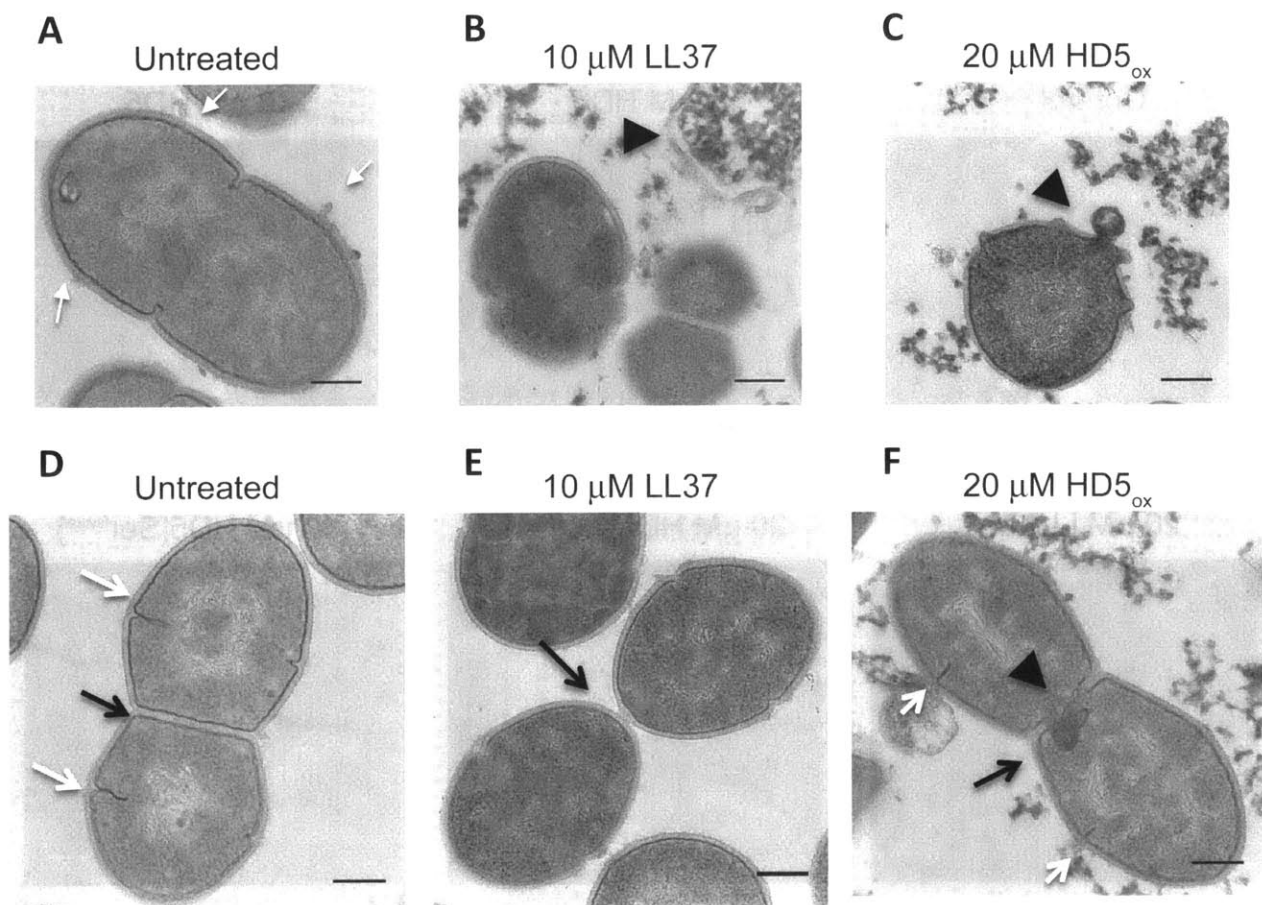
Figure 4.11. TEM images of *E. faecalis* 1375 treated with various peptides. The ultrastructure of *E. faecalis* (1×10^8 CFU/mL) incubated in the absence (untreated) or in the presence of HD5$_{ox}$ (20 µM) and LL37 (10 µM) at 37 °C (10 mM sodium phosphate buffer, pH 7.4, 1% v/v TSB w/o dextrose) for 1 h. Scale bar = 200 nm. Black arrows indicate old septal planes, white arrows indicate new septal planes, and black arrowheads indicate morphological changes induced by peptides.

vi. **HD5$_{ox}$-induced Morphological Changes in *B. subtilis* PY79.** Considering that HD5$_{ox}$ retained the antimicrobial activity against *B. subtilis,* even at high salt concentrations, we performed the subsequent AMA assays and microscopy studies using S7$_{50}$ media. When treated with HD5$_{ox}$, *B. subtilis* did not display loss of phase (Figure 4.12). In contrast, LL37-treated cells displayed clear lysis, as illustrated by the loss of phase and formation of ghost cells. In the phase-contrast microscopy the empty cell envelopes of Gram-negative bacteria are termed bacterial ghost cells. The ultra-structural changes induced upon treatment with HD5$_{ox}$ and LL37 were also examined (Figure 4.13). Strikingly, the LL37-treated bacteria displayed lysis and cell wall and membrane breaks. In contrast, the cells seemed to be intact upon treatment with HD5$_{ox}$ and the cell wall thickness appears to be increased. The cell septa appear to accumulate extra-membranous structures similar to other Gram-positive strains treated with HD5$_{ox}$. From the morphological and phenotypic studies, it appears that the mechanism of action of HD5$_{ox}$ differs from the pore-forming peptide LL37. Further studies are required to understand the exact mechanism of action of HD5$_{ox}$ against *B. subtilis.*

| **Untreated** | **20 μM HD5$_{ox}$** | **20 μM LL37** |
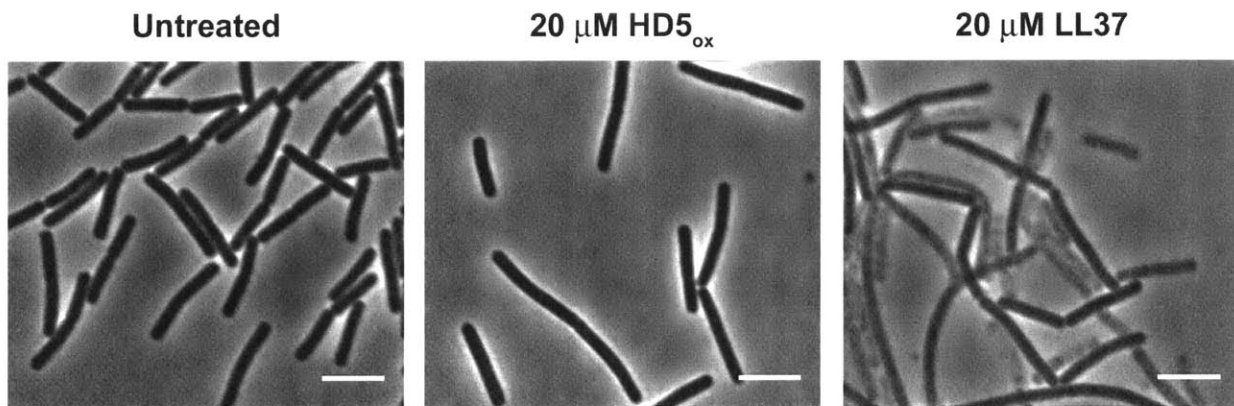
Figure 4.12. Phase-contrast images of *B. subtilis* PY79 treated with HD5$_{ox}$ and LL37. The morphology of *B. subtilis* (1×10^8 CFU/mL) incubated in the absence (untreated) or in the presence of peptides (20 μM) at 37 °C (S7$_{50}$ media) for 1 h. Scale bar = 5 μm.
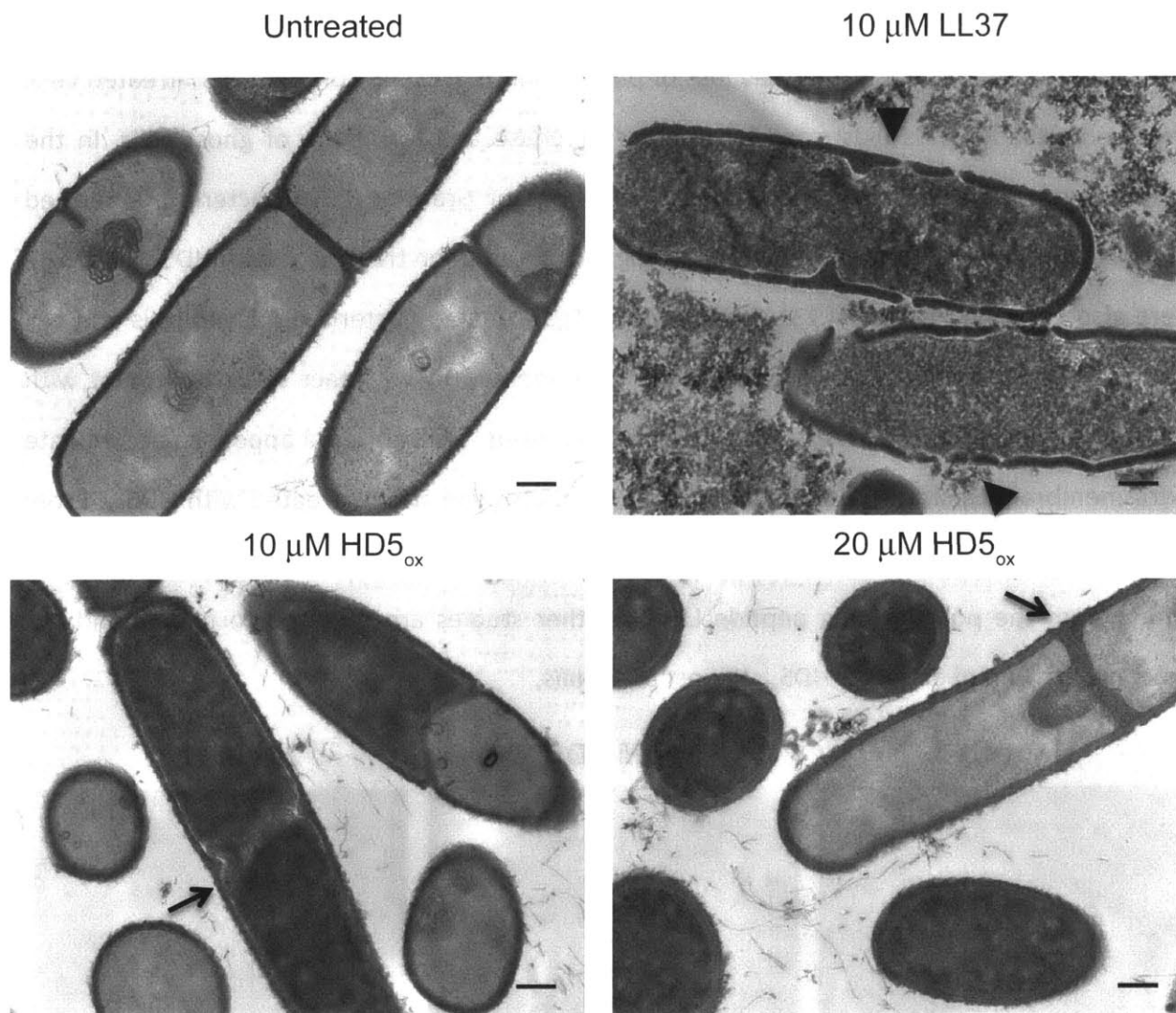
Figure 4.13. TEM images of *B. subtilis* PY79 treated with $HD5_{ox}$ and LL37. The ultrastructure of *B. subtilis* (1×10^8 CFU/mL) incubated in the absence (untreated) or in the presence of $HD5_{ox}$ (10 μM and 20 μM) and LL37 (10 μM) at 37 °C (10 mM sodium phosphate buffer, pH 7.4, 1% v/v TSB w/o dextrose) for 1 h. Scale bar = 200 nm. Arrows indicate mesosomes at septal planes and arrowheads indicate lysis and membrane disruption.

4D.   Summary and Future Directions

In this study, the antimicrobial activity of HD5$_{ox}$ was studied against selected Gram-positive strains and compared with other well-studied antimicrobial peptides that either form pores or disrupt bacterial cell membranes. We determined the HD5$_{ox}$-induced phenotypic effects in bacteria by examining their morphology using various microscopy techniques. These morphological changes indicated that HD5$_{ox}$ kills bacteria via a mechanism different from the pore-forming peptides LL37 and melittin.

Previous studies have indicated that the antimicrobial activity of HD5$_{ox}$ against Gram-positive bacteria is dependent on the disulfide linkages and is attenuated upon changing the chirality (D-HD5$_{ox}$). Notably, the antimicrobial activities of various human defensins against Gram-positive bacteria are less susceptible to salt concentration in the assay buffer compared to activity against Gram-negative bacteria.[2,4,26,27] We have also shown that the AMA activity of HD5$_{ox}$ is less sensitive to salt concentration in buffer. These results suggest a specific bacterial target for HD5$_{ox}$. Further efforts to identify the site of action of HD5 and the mechanism of action of HD5 are needed.

We established the activity of HD5 against *B. subtilis* in S7$_{50}$ medium. This result provides a condition where the antimicrobial activity of HD5$_{ox}$ can be studied in a growth media that allows active cell growth. Previous studies have employed 10 mM sodium phosphate buffer, pH 7.4 supplemented with 1% TSB. This buffered condition can only be used to determine the killing of bacteria that are maintained in metabolically active state. However, we could not actively measure the effect of HD5$_{ox}$ on actively replicating cells. In future, we aim to study the effect of HD5 on cell division and other cellular processes using *B. subtilis* grown in S7$_{50}$ medium.

4E.   Acknowlegements

165

4F.   References

(1) Wommack, A. J., Ziarek, J. J., Tomaras, J., Chileveru, H. R., Zhang, Y., Wagner, G., and Nolan, E. M. (2014) Discovery and characterization of a disulfide-locked C_2-symmetric defensin peptide. *J. Am. Chem. Soc. 136*, 13494–13497.

(2) Porter, E. M., van Dam, E., Valore, E. V, and Ganz, T. (1997) Broad-spectrum antimicrobial activity of human intestinal defensin 5. *Infect. Immun. 65*, 2396–2401.

(3) Brogden, K. A. (2005) Antimicrobial peptides: pore formers or metabolic inhibitors in bacteria? *Nat. Rev. Microbiol. 3*, 238–250.

(4) Wilmes, M., and Sahl, H.-G. (2014) Defensin-based anti-infective strategies. *Int. J. Med. Microbiol. 304*, 93–99.

(5) Kandaswamy, K., Liew, T. H., Wang, C. Y., Huston-Warren, E., Meyer-Hoffert, U., Hultenby, K., Schröder, J. M., Caparon, M. G., Normark, S., Henriques-Normark, B., Hultgren, S. J., and Kline, K. A. (2013) Focal targeting by human β-defensin 2 disrupts localized virulence factor assembly sites in *Enterococcus faecalis*. *Proc. Natl. Acad. Sci. U. S. A. 110*, 20230–20235.

(6) Kudryashova, E., Quintyn, R., Seveau, S., Lu, W., Wysocki, V. H., and Kudryashov, D. S. (2014) Human defensins facilitate local unfolding of thermodynamically unstable regions of bacterial protein toxins. *Immunity 41*, 709–721.

(7) Chileveru, H. R., Lim, S. A., Chairatana, P., Wommack, A. J., Chiang, I.-L., and Nolan, E. M. (2015) Visualizing attack of *Escherichia coli* by the antimicrobial peptide human defensin 5. *Biochemistry 54*, 1767–1777.

(8) Moser, S., Chileveru, H. R., Tomaras, J., and Nolan, E. M. (2014) A bacterial mutant library as a tool to study the attack of a defensin peptide. *Chembiochem 15*, 2684–2688.

(9) Wanniarachchi, Y. A., Kaczmarek, P., Wan, A., and Nolan, E. M. (2011) Human defensin 5 disulfide array mutants: disulfide bond deletion attenuates antibacterial activity against *Staphylococcus aureus*. *Biochemistry 50*, 8005–8017.

(10) de Leeuw, E., Burks, S. R., Li, X., Kao, J. P. Y., and Lu, W. (2007) Structure-dependent

functional properties of human defensin 5. *FEBS Lett. 581*, 515–520.

(11) Lehrer, R. I., Jung, G., Ruchala, P., Andre, S., Gabius, H. J., and Lu, W. (2009) Multivalent binding of carbohydrates by the human alpha-defensin, HD5. *J. Immunol. 183*, 480–490.

(12) Wei, G., de Leeuw, E., Pazgier, M., Yuan, W., Zou, G., Wang, J., Ericksen, B., Lu, W.-Y., Lehrer, R. I., and Lu, W. (2009) Through the looking glass, mechanistic insights from enantiomeric human defensins. *J. Biol. Chem. 284*, 29180–29192.

(13) Rice, L. B. (2008) Federal funding for the study of antimicrobial resistance in nosocomial pathogens: no ESKAPE. *J. Infect. Dis. 197*, 1079–1081.

(14) Miller, W. R., Munita, J. M., and Arias, C. A. (2014) Mechanisms of antibiotic resistance in enterococci. *Expert Rev. Anti. Infect. Ther. 12*, 1221–1236.

(15) Zimlichman, E., Henderson, D., Tamir, O., Franz, C., Song, P., Yamin, C. K., Keohane, C., Denham, C. R., and Bates, D. W. (2013) Health care–associated Infections. *JAMA Intern. Med. 173*, 2039–2046.

(16) de Boer, A. S., and Diderichsen, B. (1991) On the safety of *Bacillus subtilis* and *B. amyloliquefaciens*: a review. *Appl. Microbiol. Biotechnol. 36*, 1–4.

(17) Barbe, V., Cruveiller, S., Kunst, F., Lenoble, P., Meurice, G., Sekowska, A., Vallenet, D., Wang, T., Moszer, I., Médigue, C., and Danchin, A. (2009) From a consortium sequence to a unified sequence: the *Bacillus subtilis* 168 reference genome a decade later. *Microbiology 155*, 1758–1775.

(18) Vasantha, N., and Freese, E. (1980) Enzyme changes during *Bacillus subtilis* sporulation caused by deprivation of guanine nucleotides. *J. Bacteriol. 144*, 1119–1125.

(19) Barns, K. J., and Weisshaar, J. C. (2013) Real-time attack of LL-37 on single *Bacillus subtilis* cells. *Biochim. Biophys. Acta - Biomembr. 1828*, 1511–1520.

(20) Sochacki, K. A., Barns, K. J., Bucki, R., and Weisshaar, J. C. (2011) Real-time attack on single *Escherichia coli* cells by the human antimicrobial peptide LL-37. *Proc. Natl. Acad. Sci. U. S. A. 108*, E77–E81.

(21) Ding, B., Soblosky, L., Nguyen, K., Geng, J., Yu, X., Ramamoorthy, A., and Chen, Z. (2013) Physiologically-relevant modes of membrane interactions by the human antimicrobial peptide, LL-37, revealed by SFG experiments. *Sci. Rep. 3*, 1854.

(22) van den Bogaart, G., Guzmán, J. V., Mika, J. T., and Poolman, B. (2008) On the mechanism of pore formation by melittin. *J. Biol. Chem. 283*, 33854–33857.

(23) Raghuraman, H., and Chattopadhyay, A. (2007) Melittin: a membrane-active peptide with diverse functions. *Biosci. Rep. 27*, 189–223.

(24) Falagas, M. E., and Kasiakou, S. K. (2005) Colistin: the revival of polymyxins for the management of multidrug-resistant Gram-negative bacterial infections. *Clin. Infect. Dis. 40*, 1333–1341.

(25) Catchpole, C. R., Andrews, J. M., Brenwald, N., and Wise, R. (1997) A reassessment of the

in-vitro activity of colistin sulphomethate sodium. *J. Antimicrob. Chemother. 39*, 255–260.

(26) Sass, V., Schneider, T., Wilmes, M., Körner, C., Tossi, A., Novikova, N., Shamova, O., and Sahl, H.-G. (2010) Human beta-defensin 3 inhibits cell wall biosynthesis in *Staphylococci. Infect. Immun. 78*, 2793–2800.

(27) Valore, E. V, Park, C. H., Quayle, A. J., Wiles, K. R., McCray, P. B., and Ganz, T. (1998) Human beta-defensin-1: an antimicrobial peptide of urogenital tissues. *J. Clin. Invest. 101*, 1633–1642.

(28) Greenawalt, J. W., and Whiteside, T. L. (1975) Mesosomes: membranous bacterial organelles. *Bacteriol. Rev. 39*, 405–463.

(29) Friedrich, C. L., Moyles, D., Beveridge, T. J., and Hancock, R. E. (2000) Antibacterial action of structurally diverse cationic peptides on gram-positive bacteria. *Antimicrob. Agents Chemother. 44*, 2086–2092.

(30) Furci, L., Baldan, R., Bianchini, V., Trovato, A., Ossi, C., Cichero, P., and Cirillo, D. M. (2015) New role for human α-defensin 5 in the fight against hypervirulent *Clostridium difficile* strains. *Infect. Immun. 83*, 986–995.

(31) Hartmann, M., Berditsch, M., Hawecker, J., Ardakani, M. F., Gerthsen, D., and Ulrich, A. S. (2010) Damage of the bacterial cell envelope by antimicrobial peptides gramicidin S and PGLa as revealed by transmission and scanning electron microscopy. *Antimicrob. Agents Chemother. 54*, 3132–3142.

(32) Shimoda, M., Ohki, K., Shimamoto, Y., and Kohashi, O. (1995) Morphology of defensin-treated *Staphylococcus aureus. Infect. Immun. 63*, 2886–2891.

(33) Steffen, H., Rieg, S., Wiedemann, I., Kalbacher, H., Deeg, M., Sahl, H.-G., Peschel, A., Götz, F., Garbe, C., and Schittek, B. (2006) Naturally processed dermcidin-derived peptides do not permeabilize bacterial membranes and kill microorganisms irrespective of their charge. *Antimicrob. Agents Chemother. 50*, 2608–2620.

(34) Midorikawa, K., Ouhara, K., Komatsuzawa, H., Kawai, T., Yamada, S., Fujiwara, T., Yamazaki, K., Sayama, K., Taubman, M. A., Kurihara, H., Hashimoto, K., and Sugai, M. (2003) *Staphylococcus aureus* susceptibility to innate antimicrobial peptides, beta-defensins and CAP18, expressed by human keratinocytes. *Infect. Immun. 71*, 3730–3739.

(35) Barns, K. J., and Weisshaar, J. C. (2013) Real-time attack of LL-37 on single *Bacillus subtilis* cells. *Biochim. Biophys. Acta 1828*, 1511–1520.

(36) Wilmes, M., Stockem, M., Bierbaum, G., Schlag, M., Götz, F., Tran, D. Q., Schaal, J. B., Ouellette, A. J., Selsted, M. E., and Sahl, H.-G. (2014) Killing of *staphylococci* by θ-defensins involves membrane impairment and activation of autolytic enzymes. *Antibiot. (Basel, Switzerland) 3*, 617–631.

(37) Bierbaum, G., and Sahl, H. G. (1987) Autolytic system of *Staphylococcus simulans* 22: Influence of cationic peptides on activity of N-acetylmuramoyl-L-alanine amidase. *J.*

Bacteriol. 169, 5452–5458.

(38) Kim, H.-S., Chang, S. W., Baek, S.-H., Han, S. H., Lee, Y., Zhu, Q., and Kum, K.-Y. (2013) Antimicrobial effect of alexidine and chlorhexidine against *Enterococcus faecalis* infection. *Int. J. Oral Sci. 5*, 26–31.

(39) Chivatxaranukul, P., Dashper, S. G., and Messer, H. H. (2008) Dentinal tubule invasion and adherence by *Enterococcus faecalis*. *Int. Endod. J. 41*, 873–882.

(40) Tran, T. T., Panesso, D., Mishra, N. N., Mileykovskaya, E., Guan, Z., Munita, J. M., Reyes, J., Diaz, L., Weinstock, G. M., Murray, B. E., Shamoo, Y., Dowhan, W., Bayer, A. S., and Arias, C. A. (2013) Daptomycin-resistant *Enterococcus faecalis* diverts the antibiotic molecule from the division septum and remodels cell membrane phospholipids. *MBio 4*, e00281–13.

(41) Straus, S. K., and Hancock, R. E. W. (2006) Mode of action of the new antibiotic for Gram-positive pathogens daptomycin: comparison with cationic antimicrobial peptides and lipopeptides. *Biochim. Biophys. Acta 1758*, 1215–1223.

Chapter 5

Investigation of HD5$_{ox}$ Interaction with the Bacterial Cellular Components

5A.   Introduction

The mechanism of action of cationic antimicrobial peptides is often generalized and attributed to their interaction with negatively charged bacterial membranes.[1,2] In accordance, certain antimicrobial peptides such as melittin and colistin belong to this category, and cause pore-formation and bacterial membrane destabilization, respectively.[3,4] However, such broad generalization of the cell killing mechanisms for all AMPs is unwarranted, and each peptide needs to be investigated individually.[2] Indeed, several recent studies have indicated other potential targets for defensins that include lipid II and bacterial toxins.[5–7] Therefore, studying the mechanism of action of $HD5_{ox}$ requires understanding its effect on various bacterial cellular processes, and identifying the affected cellular components. From our work using fluorophore-HD5 conjugates described in Chapter 3, we visualized the localization of $HD5_{ox}$ near the cell poles and cell septa of *Escherichia coli*.[8] This localization pattern prompted us to further study the influence of $HD5_{ox}$ on processes such as cell division. With the help of the extensive family of $HD5_{ox}$ derivatives, we decided to probe the effect of inner- and outer membrane composition on the antimicrobial action of $HD5_{ox}$. Herein, we describe the results of these efforts.

The outer membrane (OM) of Gram-negative bacteria is an asymmetric lipid bilayer.[9–11] The outer leaflet is composed mainly of lipopolysaccharides (LPS) and the inner leaflet is primarily composed of phospholipids.[10] Other constituents of the OM include lipoproteins and membrane-associated proteins such as porins.[9,11] LPS is comprised of membrane-associated Lipid A, a core composed of specific sugar units and enterobacterial common antigen (ECA).[10] LPS provides a permeability barrier and prevents entry of hydrophilic compounds.[11] Moreover, certain AMPs such as colistin, permeabilize the bacteria mediated by binding to the Lipid A portion of LPS and inserting into the OM.[4,12] Colistin (polymixin E) is a cationic cyclic docapeptide with a fatty-acid chain appended at the N-terminus.[13] Colistin binds to anionic lipopolysaccharide (LPS) molecules and disrupts the OM of Gram-negative bacteria, leading to cell death.[14] Certain AMPs play an important role in mitigating endotoxin (LPS)-mediated cell

shock.[15] For instance, LL37 binds to LPS and suppresses inflammatory responses.[16] Comparatively, the effect of OM composition on the activity of $HD5_{ox}$ is not clearly understood. Recently, as a result of a bacterial library screening, Dr. Simone Moser was able to show that the bacteria with compromised OMs are more susceptible to $HD5_{ox}$ treatment.[12] Therefore, we examined the effect of OM composition on the morphological changes induced by $HD5_{ox}$.

Several defensins such as HNP1-3 and cryptdin-4, also permeabilize the inner membrane (IM) and cell death is often attributed to disruption of this membrane.[17,18] Dr. Yoshitha Wanniarachchi, performed the first studies on inner membrane permeabilization cause by $HD5_{ox}$ using *E. coli* ML35, a lactose impermeable strain expressing a cytoplasmic β-galactosidase enzyme (also discussed in Appendix 2).[19,20] The enzymatic cleavage of its substrate *o*-nitrophenyl-β-galactopyranoside (ONPG), results in the release of *o*-nitrophenol, a chromophore having absorption maximum at 405 nm. The substrate added to the assay is available for the enzyme only after the bacterial inner-membrane is compromised. Thus, the integrity of the inner membrane can be evaluated by the measurement of absorbance at 405 nm of the cleavage product (Scheme 5.1).[20]

Scheme 5.1. Determination of Inner Membrane Permeabilization Employing *E. coli* ML35

173
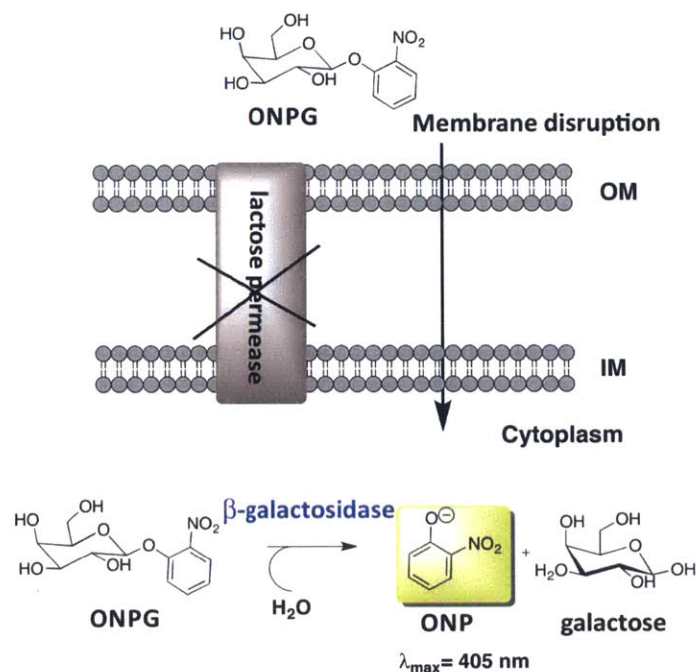
The IM is composed of a phospholipid bilayer, and the anionic phospholipids cardiolipin (CL) and phosphatidylglycerol (PG) are predominantly localized at the cell poles and cell septa. These phospholopids provide necessary stabilization of characteristic curvature of the cell poles and cell septa.[21,22] Considering the localization of HD5 at the cell poles and septa, we examined the role of anionic lipid composition on the AMA and localization of $HD5_{ox}$ by employing mutants lacking these anionic lipids that were kindly provided by Prof. Douglas Weibel at the University of Wisconsin, Madison.[21]

We also examined the effect of $HD5_{ox}$ on cell division. The localization of fluorophore-labeled $HD5_{ox}$ along with the formation of blebs at cell division sites suggested a potential target at these sites. Cell division in *E. coli* requires formation of the FtsZ ring (Z-ring).[23] FtsZ, a tubulin homologue, forms the Z-ring and recruits various other Fts proteins to initiate the cell division and form the cell divisome (the protein assembly driving the cell division).[23,24] In order to probe the effect of $HD5_{ox}$ on the cell division process, we examined the effect of $HD5_{ox}$ on the Z-ring. Lastly, preliminary growth and assay conditions were established for *Caulobacter crescentus*, another well-studied model organism for studying the effect of $HD5_{ox}$ on the cell division process.[25]

5B.   Experimental Section

i.   Peptides and Other Materials. Sodium phosphate was obtained from BDH Chemicals. $HD5_{ox}$ and its analogues including fluorophore-modified HD5 derivatives were synthesized as reported in Chapter 2.[26,20] The peptide solutions and buffers for antimicrobial activity assays were sterile-filtered (0.2-μm filter) prior to the assays. Peptide stock solutions were prepared in Milli-Q water, aliquoted, and stored at -20 °C until use. The concentrations of peptides including fluorophore-labeled peptide stock solutions were determined as described in Chapter 2.

Table 5.1. Sources and Genotype of Various Strains Employed in this Study.

Strain	Genotype	Source	Growth conditions
MG1655	Wild-type parent strain laboratory stock	Prof. Douglas Weibel, University of WIsconsin[21]	TSB (w/o) dextrose
MG1655(BKT12)	MG1655 ΔclsABC::FRT-kan-FRT	Prof. Douglas Weibel, University of WIsconsin[21]	TSB (w/o) dextrose (50 μg/mL of kan)
UE53	MG1655 lpp-2 Δara714 rcsF::mini-Tn10 cam	Prof. Douglas Weibel, University of WIsconsin[21]	TSB (w/o) dextrose
UE54	UE53 ΔpgsA::kan	Prof. Douglas Weibel, University of WIsconsin[21]	TSB (w/o) dextrose (50 μg/mL of kan)
FtsZ-GFP	*E. coli* K12 (CR34; thr-1 leuB6 thyA) attb::[pBADftsZ::GFP]	Prof. Susan Lovett, Brandeis University[28]	TSB (w/o) dextrose
C. crescentus	*C. cresentus* CB15 (ATCC 19089)	Prof. JoAnne Stubbe, MIT[29]	PYE-media

ii.   **General Methods and Image Analysis for Phase Contrast and Fluorescence Microscopy Antimicrobial Activity Assays.** Antimicrobial activity (AMA) assays were performed described previously in Chapter 2.[26] The hypersensitive strains from the Keio Collection and *imp4213* were grown overnight in TSB (without dextrose) medium with 25 μg/mL of kanamycin.[27] MG1655 (BKT12) and UE54 strains were grown overnight in TSB (without dextrose) medium with 50 μg/mL of kanamycin; whereas, the wild type strains MC4100, *E. coli* K-12, MG1655 and UE53 were grown in TSB (without dextrose) in the absence of antibiotics (Table 5.1). *Caulobacter crescentus* CB15 was grown in peptone yeast extract (PYE) media. The overnight cultures were diluted 1:100 and grown in TSB (without dextrose) and appropriate antibiotics when necessary, to an OD_{600} ~0.6. The bacterial cultures were centrifuged (3500 rpm x 6 min, 4 °C) and resuspended in AMA buffer (10 mM sodium phosphate buffer, pH 7.4, supplemented with 1% v/v TSB (without dextrose)). The process was repeated once to remove any residual medium. The OD_{600} was measured again and adjusted to 0.6 (2.5 x 10^8 CFU/mL), the culture was diluted 2.5-fold to afford 1 x 10^8 CFU/mL. AMA assays were performed in 96-well plates. Each well contained 10 μL of stock peptide solution (10x concentration in Milli-Q

water) and 90 μL of bacterial culture (1×10^8 CFU/mL). For the control wells containing no peptide, 10 μL of Milli-Q water was combined with 90 μL of the bacterial culture. The assay plates were incubated for 1 h (130 rpm, 37 °C). For assays with fluorophore-labeled peptides, the plates were incubated in the dark (covered with aluminum foil).

Growth Conditions for *Caulobacter crescentus* CB15 (ATCC 19089). *C. crescentus* CB15 (ATCC 19089) was obtained from Prof. JoAnne Stubbe at MIT. The bacteria were streaked on peptone-yeast extract (PYE) media-agar plate (~ 3 days, 30 °C), and a single colony was picked and grown to saturation in PYE media (~ 60 h, 30 °C). The culture was diluted 1: 500 and grown to an OD_{600}~0.2 (~ 16 h, 30 °C) (1×10^8 CFU/mL). The culture was centrifuged and resuspended (2 x 3500 rpm x 5 min at 4 °C) in 10 mM sodium phosphate buffer supplemented with 1% TSB (without dextrose), pH 7.4. The AMA assay was set up in 96-well plates for both the phase-contrast and SEM imaging as described in Chapter 3.

Synchronization of *C. crescentus* CB15.[29] A 6-mL culture of *C. crescentus* were grown to OD_{600} ~0.4, centrifuged (2 x 3500 rpm x 5 min at 4 °C) and resuspended in 600 μL of 10 mM sodium phosphate buffer supplemented with 1% TSB (without dextrose), pH 7.4. The bacterial culture (600 μL) was mixed with 600 μL of Percoll (Sigma Aldrich) and gently mixed. The mixture was centrifuged at 10,000 x g for 20 min at 20 °C. The supernatant was gently removed and lower fraction afforded synchronized swarmer cells. A 5-μL aliquot from the lower fraction of cells was plated on 1% agarose pads for phase contrast microscopy. The remaining synchronized cells from the 6-mL culture were resuspended in 500 μL of fixative and subjected to SEM imaging as described in Chapter 3.

Phase Contrast Microscopy. Following each 1-h incubation in the AMA assay, a 5-μL sample from each condition was placed on 1% agarose pads and each sample was covered with a coverslip. A Zeiss Axioplan2 upright microscope was employed for imaging and the data was acquired at W.M. Keck Biological Imaging Facility of the Whitehead Institute (Cambridge, MA).

Assay Conditions for Fluorescence Microscopy Experiments. Fluorescence microscopy experiments were performed by using either agar pads or poly-D-lysine coated MatTek plates. For images acquired using agar pads, the standard AMA assays were performed in 96-well plates as described above except that the plates were covered in aluminum foil, and 5-μL of each final sample was plated on the 1% agarose pad as described above. All experiments were performed with 1 x 10^8 CFU/mL *E. coli*. For images acquired using MatTex plates, the bacteria (180 μL of a 1 x 10^8 CFU/mL culture suspended in 10 mM sodium phosphate buffer, 1% TSB without dextrose, pH 7.4) were placed on a poly-D-lysine coated MatTek plate, and 20 μL of a 10x peptide stock solution was added. The AMA assay was performed following the standard method except that the plates were incubated in the dark for 1 h (130 rpm, 37 °C). Then, the bacteria on the MatTex plate were thoroughly yet gently washed with AMA buffer (3 x 3 mL), which removed detached bacteria and excess fluorophore. Then, 3 mL of AMA buffer was added and the plate was covered and sealed with parafilm.

Fluorescence Microscopy and Image Analysis. Confocal microscopy was performed with an Andor Spinning Disk Confocal microscope. The confocal microscopy data were collected using Andor IQ acquisition software and Andor iXion+ EMCCD cameras. Excitation lasers set at 488 and 561 nm were used for the green and red channels, respectively. All images were collected, irrespective of microscope, using 100x oil-immersion objective lenses. Image analysis was performed with the ImageJ software. Fluorescence background subtraction was performed using rolling ball method with a radius of 150 pixels.

iii.   Scanning Electron Microscopy (SEM). For SEM imaging of the synchronized cells, *Caulobacter Crescentus* cells were either synchronized or treated with HD5$_{ox}$. The samples were fixed and SEM imaging was performed following the protocol described in Chapter 3.

5C. Results and Discussion

i. **Effect of HD5$_{ox}$ on *E. coli* Mutants with Defective Outer Membrane.** To identify the cellular pathways and components affected by HD5$_{ox}$ treatment, Dr. Simone Moser designed an unbiased genetic screen using the Keio Collection,[27] a library of mutants of *E. coli* K-12, where each of the non-essential genes are replaced by a kanamycin resistance cassette.[12] The AMA was performed in the presence and absence of HD5$_{ox}$, and a normalized fitness ratio (termed ϕ) was determined to characterize the susceptibility of the strains to HD5$_{ox}$. Strains that are as susceptible to HD5$_{ox}$ as the WT are characterized by $\phi = 1$, and hypersensitive strains by $\phi < 1$. Employing such a classification, from this bacterial library screening, strains corresponding to thirty-one genes were identified as hypersensitive to HD5$_{ox}$ treatment.[12] In order to examine the effect of HD5$_{ox}$ on the morphology of hypersensitive mutants from the screening, eight strains that are most sensitive to HD5$_{ox}$ treatment were selected. These selected strains correspond to knockouts in genes *lpcA, gmhB, rfaE, rfaD, rfaF, surA, secB* and *tolB* (Table 5.2) involved in LPS biosynthesis and overall membrane biosynthesis. We observed distinct morphological changes including bleb formation, elongation and clumping of *E. coli* ATCC 25922 when treated with HD5$_{ox}$ as described in Chapter 3. Untreated strains Keio WT (BW25113) and hypersensitive mutants display smooth morphology. Correspondingly, when treated with HD5$_{ox}$ (40 µM), selected hypersensitive strains displayed similar morphological changes as the WT (BW25113) including blebs formation (Figure 5.1 and 5.2).

Table 5.2. Corresponding genes and affected pathways in selected hypersensitive strains.

Gene knockouts	Pathway/process affected
lpcA, rfaE, gmhB, rfaD, and *rfaF*	Lipid A biosynthesis
surA, and *secB*	Membrane assembly and Unfolded protein binding
surA, *secB*, and *tolB*	Protein transport and establishment of protein localization
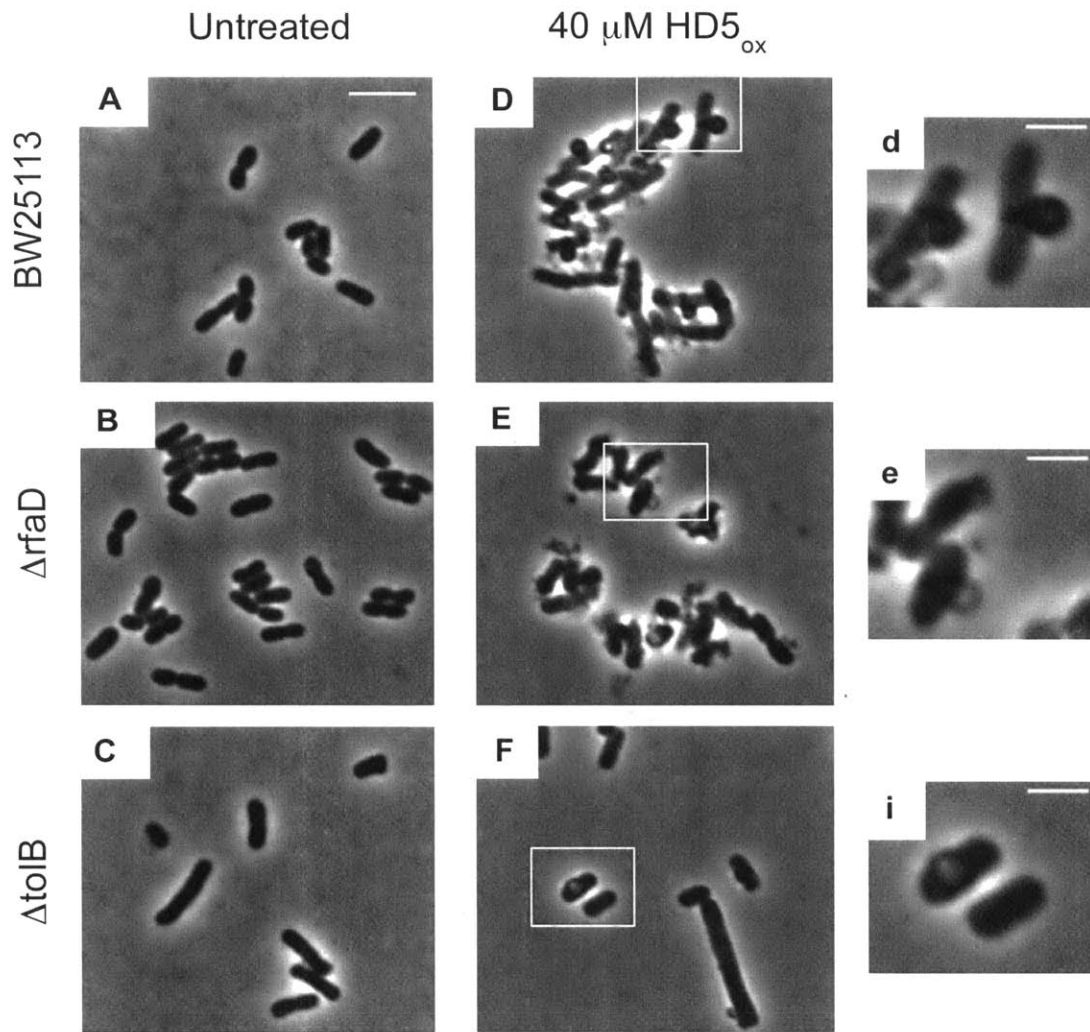
Figure 5.1. Morphology of the hypersensitive mutants treated with $HD5_{ox}$. (**A-C**) Phase-contrast images of untreated bacteria (1×10^{8} CFU/mL) indicate smooth morphology, and (**D-F**) in the presence of 40 µM $HD5_{ox}$ display blebs. Scale bar= 5 µm. (**d-f**) Phase-contrast images of single cells further illustrate the bleb formation caused by $HD5_{ox}$. Scale bar = 2 µm. Bacteria were treated with $HD5_{ox}$ in standard AMA buffer (10 mM NaPB, 1% TSB w/o dextrose, pH 7.4) at 37 °C for 1 h with shaking at 130 rpm.
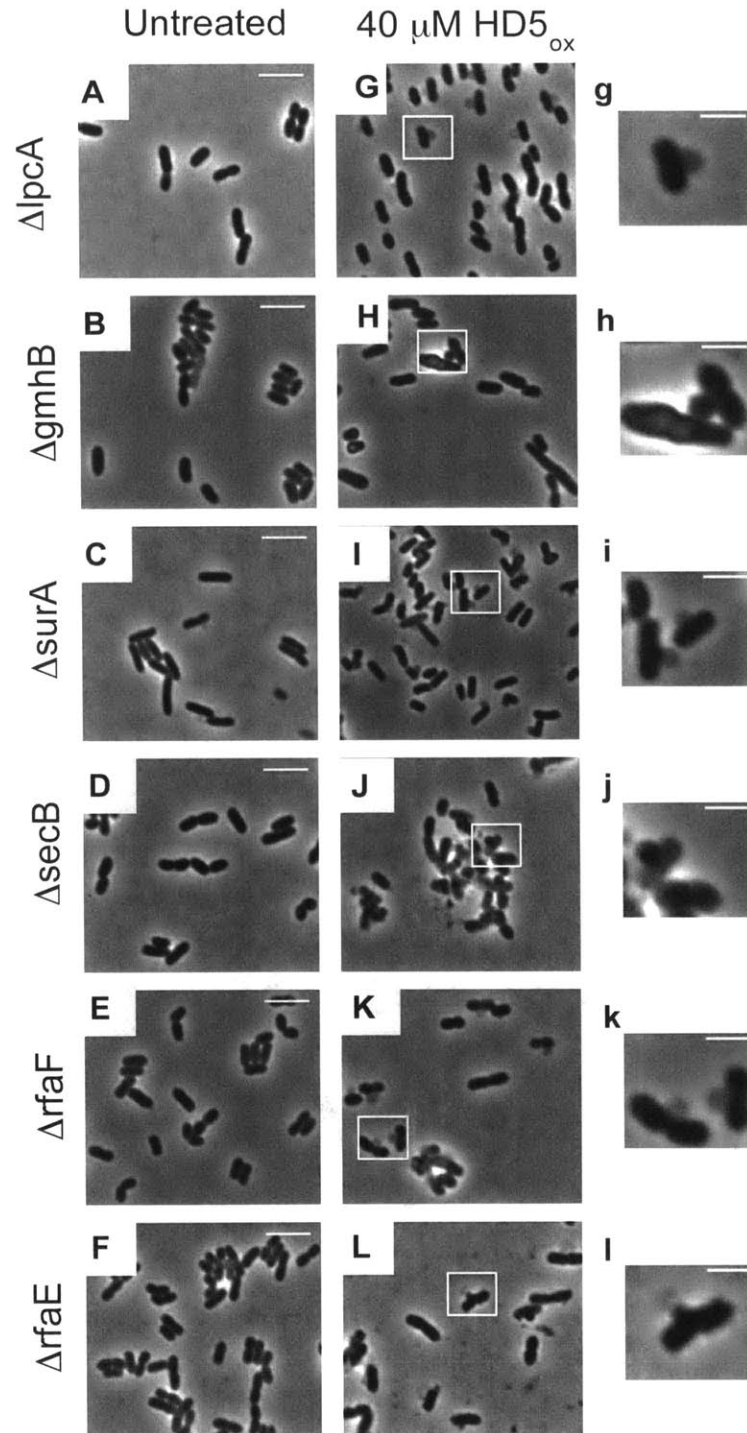
Figure 5.2. HD5$_{ox}$ causes similar morphological changes in hypersensitive mutants ($\Delta lpcA$, $\Delta gmhB$, $\Delta surA$, $\Delta secB$, $\Delta rfaF$ and $\Delta rfaE$). (**A-F**) Phase-contrast images of untreated bacteria (1 x 10^8 CFU/mL) indicate smooth morphology. Scale bar= 5 μm. (**G-L**) Upon treatment of bacteria with 40 μM HD5$_{ox}$, all the strains show similar morphological changes as WT (bleb formation). (**g-l**) Phase-contrast images of single cells illustrate the bleb formation caused by HD5$_{ox}$. Scale bar = 2 μm. Bacteria were treated with HD5$_{ox}$ in standard AMA buffer (10 mM NaPB, 1% TSB w/o dextrose, pH 7.4) at 37 °C for 1 h with shaking at 130 rpm.

Notably, of these hypersensitive mutants, the top five strains most sensitive to $HD5_{ox}$ treatment (with lowest normalized fitness ratio φ) were a set of mutants corresponded to LPS biosynthesis and outer membrane biosynthesis. Moreover, $HD5_{ox}$ was able to bind to the LPS, albeit to a lower extent than colistin.[4,12] On the basis of these results, we postulated that the LPS layer on the OM weakly binds to and prevents the uptake of $HD5_{ox}$. Thereby, the OM acts as a permeability barrier for $HD5_{ox}$ uptake and antimicrobial action.

A mutant strain *E. coli imp4213*,[30] which is characterized by a leaky outer membrane, was selected in order to test our hypothesis that strains with compromised OM are more susceptible to $HD5_{ox}$ treatment. Dr. Simone Moser examined the antimicrobial activity of $HD5_{ox}$ against the parent strain (MC4100) and *imp4213*. As expected, the leaky strain (3-log reduction in CFU/mL for *imp4213*) was more susceptible to $HD5_{ox}$ (8 μM), compared to parent strain (1-log reduction in CFU/mL for MC4100).[12] The treatment of *E. coli* ATCC 25922 with rhodamine- and coumarine-derivatives of $HD5_{ox}$ resulted localization at the cell poles and cell division sites (Chapter 3).[8] However, FL-$HD5_{ox}$ was both completely inactive (>128 μM) and only labeled the surface of bacteria. One hypothesis is that FL-$HD5_{ox}$ cannot overcome the permeability barrier of OM. Alternatively, it may have lost its binding affinity to an as-yet unidentified target on the membrane. In order to probe the effect of the permeability barrier on the uptake of FL-$HD5_{ox}$, *imp4213* was employed (Figure 5.3). The uptake and labeling pattern of both FL-$HD5_{ox}$ (20 μM) and R-$HD5_{ox}$ (20 μM) was examined in *imp4213* (10^8 CFU/mL) and compared with the uptake in WT (MC4100) strain. A distinct localization pattern at cell poles and cell divisions sites was observed for R-$HD5_{ox}$ treated *imp4213* and the WT (MC4100) strains, similar to the labeling pattern in *E. coli* 25922. As expected, FL-$HD5_{ox}$ (20 μM) labeled the WT bacteria only on the surface. Moreover, leaky *E. coli imp4213* were significantly labeled by FL-$HD5_{ox}$ compared to the WT strain (Figure 5.3), and the labeling was uniform inside of the cell. Previously, a diffuse labeling pattern was also observed when *E. coli* were co-treated with $HD5_{ox}$ and the parent fluorophore (rhodamine derivative (**3**)) as described in Chapter 3. Therefore, the diffuse labeling pattern suggested that the loss of permeability barrier facilitated the uptake of FL-

HD5$_{ox}$. Compared to the specific labeling pattern of R-HD5$_{ox}$, the diffuse labeling pattern of FL-HD5$_{ox}$ also suggests a loss of binding interaction between FL-HD5$_{ox}$ and potential bacterial target. It needs to be verified if FL-HD5$_{ox}$ retained any antimicrobial activity against *imp4213*.
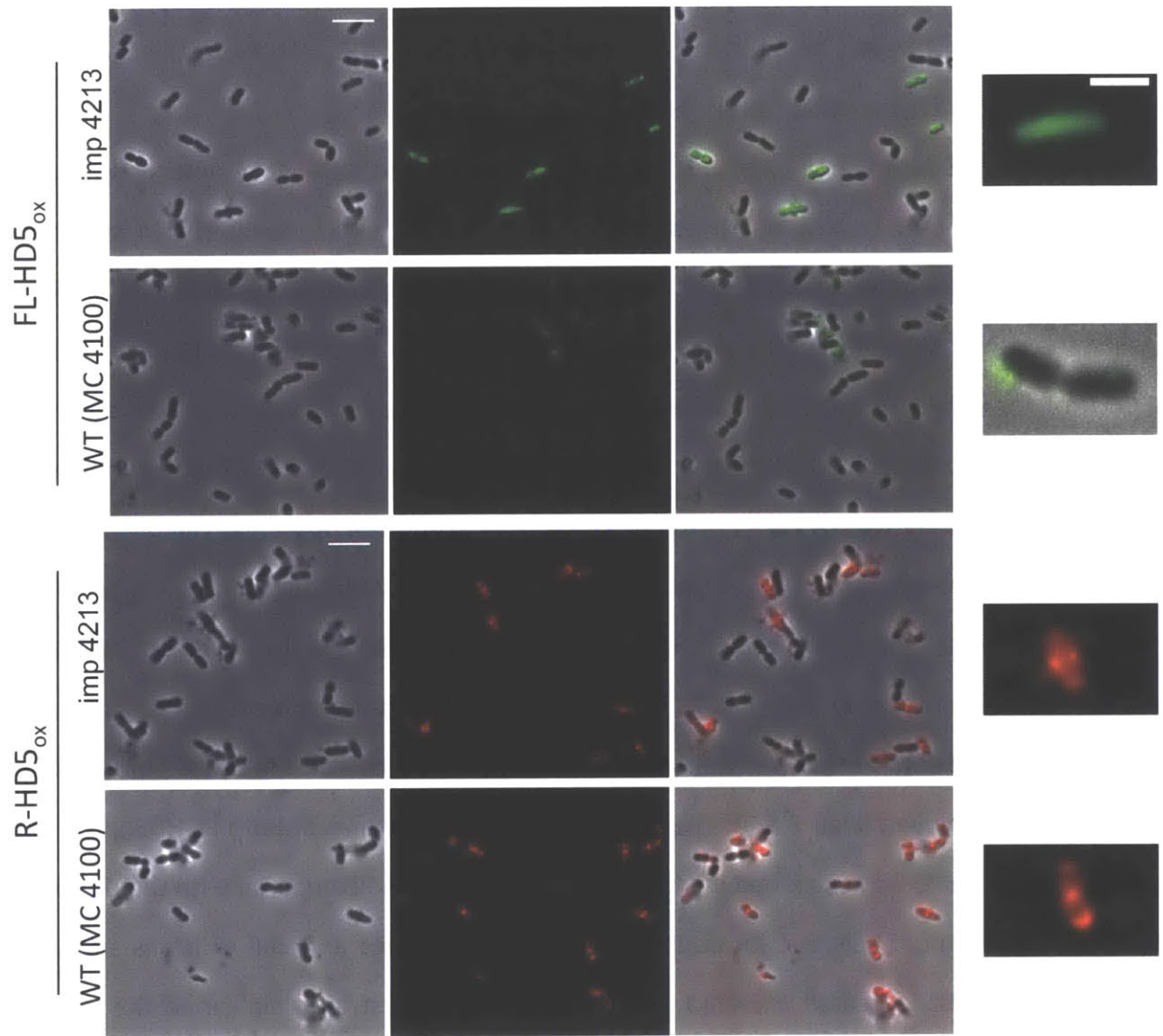
Figure 5.3. Effect of OM permeability barrier on FL- and R-HD5$_{ox}$ uptake and localization. *E. coli imp4213* and WT (MC4100) (10^8 CFU/mL) were treated with HD5 analogues (20 μM) in standard AMA buffer (10 mM NaPB, 1% TSB w/o dextrose, pH 7.4) at 37 °C for 1 h with shaking at 130 rpm. A 5-μL suspension from each sample was plated on 1% agarose pads and imaged at (Ex: 488 nm and Ex: 561 nm for GFP and RFP channels, respectively). Scale bar = 5 μm.

ii.   Effect of Membrane Lipid Composition on the Uptake and Labeling of R-HD5$_{ox}$. The

bacterial membranes are composed of distinct negatively charged phospholipids such as

cardiolipin (CL) and phosphatidylglycerol (PG). These lipids are asymmetrically distributed and

are concentrated at curved surfaces such as the cell poles and cell division sites.[21] Considering

our observation of R-HD5$_{ox}$ labeling at near cell poles and cell septa (Chapter 3), it is possible

that the interaction of HD5$_{ox}$ with these anionic lipids causes the observed labeling patterns of

R-HD5$_{ox}$. In order to probe how the lipid composition affects the localization of HD5$_{ox}$, we

examined (i) *E. coli* BKT12, a strain that is deficient in CL production, and (ii) *E. coli* UE54, a

strain with mutation in *pgsA*, a gene essential in the synthesis of both CL and PG (Table 5.1).

The mutation of *pgsA* is lethal for *E. coli*. However, another mutation in *lpp*, an outer

membrane lipoprotein, results in the survival of the ΔpgsA strain.[31] The effect of HD5$_{ox}$ on the

morphology of (iii) *E. coli* UE53, the parent strain with mutation in *lpp* alone was also tested.

These strains were kindly provided by Prof. Douglas Weibel at University of Wisconsin,

Madison. The localization of anionic lipids in these mutants was confirmed with anionic lipid

specific dye 10-*N*-nonyl acridine orange (NAO).[21]

Similar to the WT (MC4100), HD5$_{ox}$-treated (20 μM) *E. coli* BKT12 displayed blebs (Figure

5.4), indicating that loss of CL does not affect the morphological changes induced by HD5.

When the localization of HD5$_{ox}$ was probed in BKT12, the bacteria were highly labeled at the

cell poles and cell division sites by R-HD5$_{ox}$ (20 μM) (Figure 5.5); Thus, loss of CL did not perturb

the labeling of R-HD5$_{ox}$. When treated with R-HD5$_{ox}$, *E. coli* UE53 (Δlpp2), a strain used for

constructing UE54 (Table 5.1), displayed punctate labeling on the bacteria (Figure 5.5). In

contrast, *E. coli* UE54 (ΔpgsA) treated with HD5$_{ox}$ did not display blebs. Furthermore, R-HD5$_{ox}$

entered the bacteria and was uniformly distributed. Therefore, loss of both CL and PG results in

loss of the specific labeling pattern. One possible explanation for these results could be that

HD5$_{ox}$ binding to the anionic lipids regulates the uptake and labeling of HD5$_{ox}$ at the cell poles

and cell division site. However, one caveat to this interpretation is that the anionic lipids

themselves govern the specific localization of various proteins,[32,33] one or more of which could

bind HD5$_{ox}$. Recently, the dislocation of certain polar membrane proteins, including the chemoreceptor assemblies, was observed in mutants without the anionic lipids (CL) and (PG).[33] When these lipid localizations were disrupted, the localization of membrane-associated chemoreceptor proteins was also disrupted. Intriguingly, the observed labeling pattern of R-HD5$_{ox}$ is similar to the localization pattern of chemoreceptor YFP-CheR in respective anionic lipid knockout mutants, including more diffuse labeling in UE54.[33]
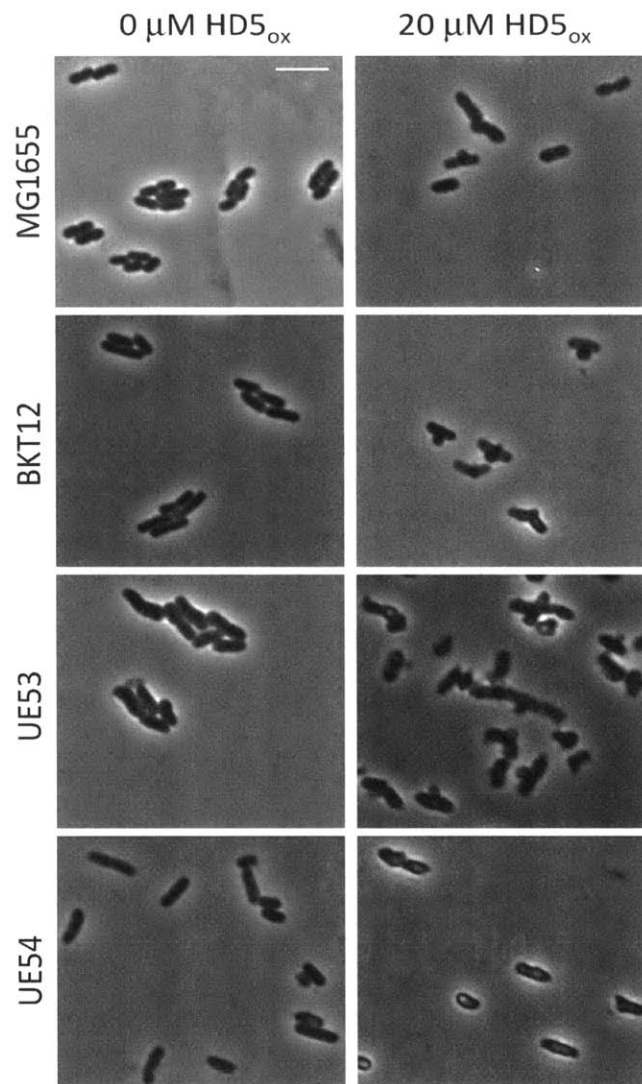
Figure 5.4. Effect of anionic lipid composition of *E. coli* on the HD5$_{ox}$ induced morphological changes. The anionic lipid knockout mutants (BKT12 and UE54) and their parent strains (MG1655 and UE53) (10^8 CFU/mL) were treated with HD5$_{ox}$ (20 µM) in standard AMA buffer (10 mM NaPB, 1% TSB w/o dextrose, pH 7.4) at 37 °C for 1 h with shaking at 130 rpm. A 5-µL suspension from each sample is plated on 1% agarose pads and imaged. Scale bar = 5 µm.
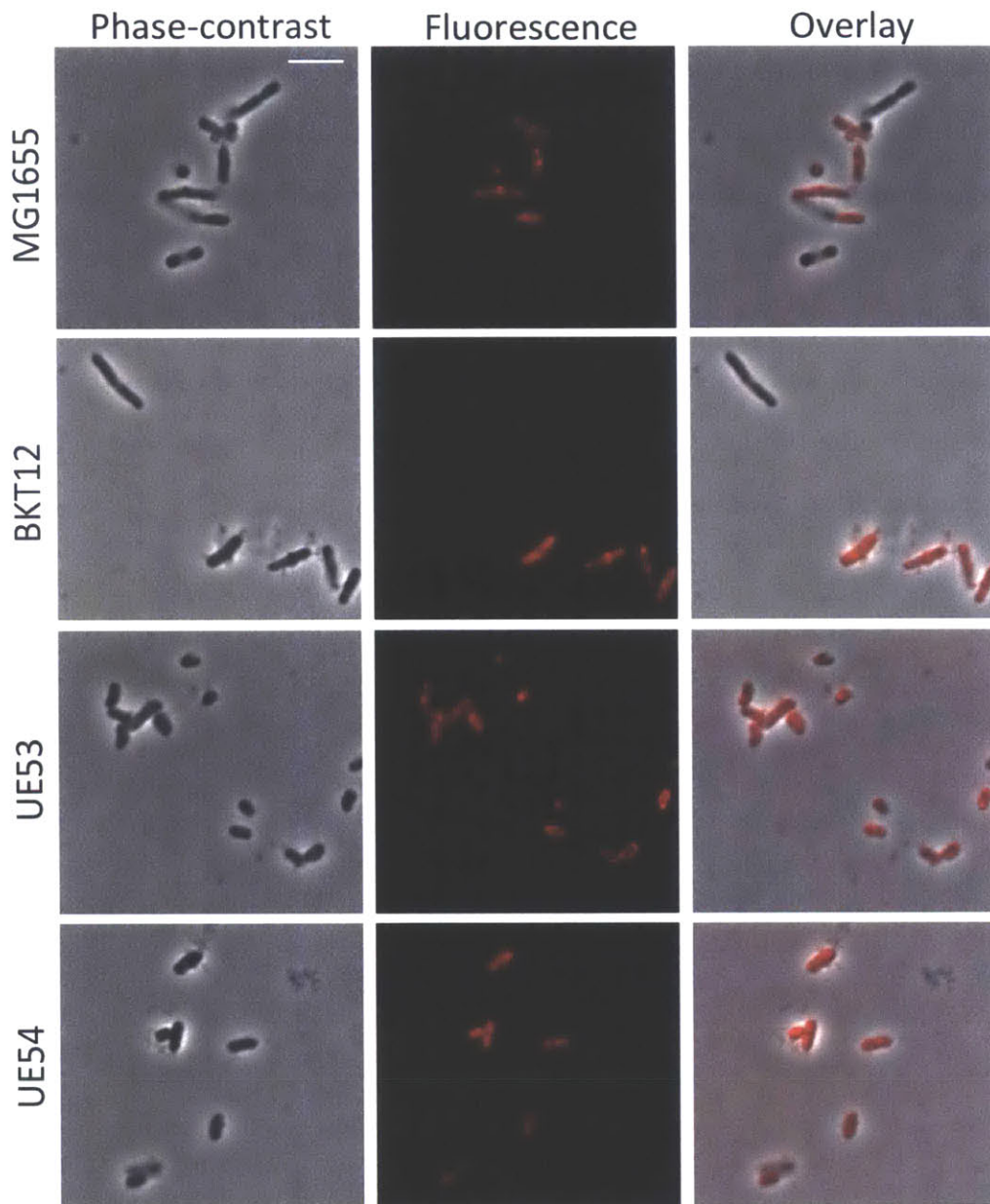
Figure 5.5. Effect of anionic lipid composition of *E. coli* on the localization of R-HD5$_{ox}$. The anionic lipid knockout mutants (BKT12 and UE54) and their parent strains (MG1655 and UE53) (10^8 CFU/mL) were treated with R-HD5$_{ox}$ (20 μM) in standard AMA buffer (10 mM NaPB, 1% TSB w/o dextrose, pH 7.4) at 37 °C for 1 h with shaking at 130 rpm. A 5-μL suspension from each sample is plated on 1% agarose pads and imaged (Ex: 561 nm for RFP channel). Scale bar = 5 μm.

iii. **Effect of HD5$_{ox}$ on the Cell Division Process.** FtsZ is a tubulin homologue that forms a ring structure at the mid-cell and recruits many other cell division proteins. This process results in the formation of a protein complex called the divisiome.[23] *E. coli* expressing FtsZ-GFP was kindly provided by Prof. Susan Lovett, at Brandeis University, Waltham. The protein overexpression was induced with 0.2% arabinose. In untreated bacteria, the formation of the FtsZ ring was clearly observed at the mid-cell (Figure 5.6). In contrast, when the bacteria were treated with HD5$_{ox}$, the FtsZ-GFP rings were not observed in the cells displaying blebs. Rather, overall diffuse labeling was observed (Figure 5.6). Also, the number of cells with FtsZ rings was lower compared to the untreated cells. These results further strengthen our hypothesis that HD5$_{ox}$ treatment interferes with the cell division process.
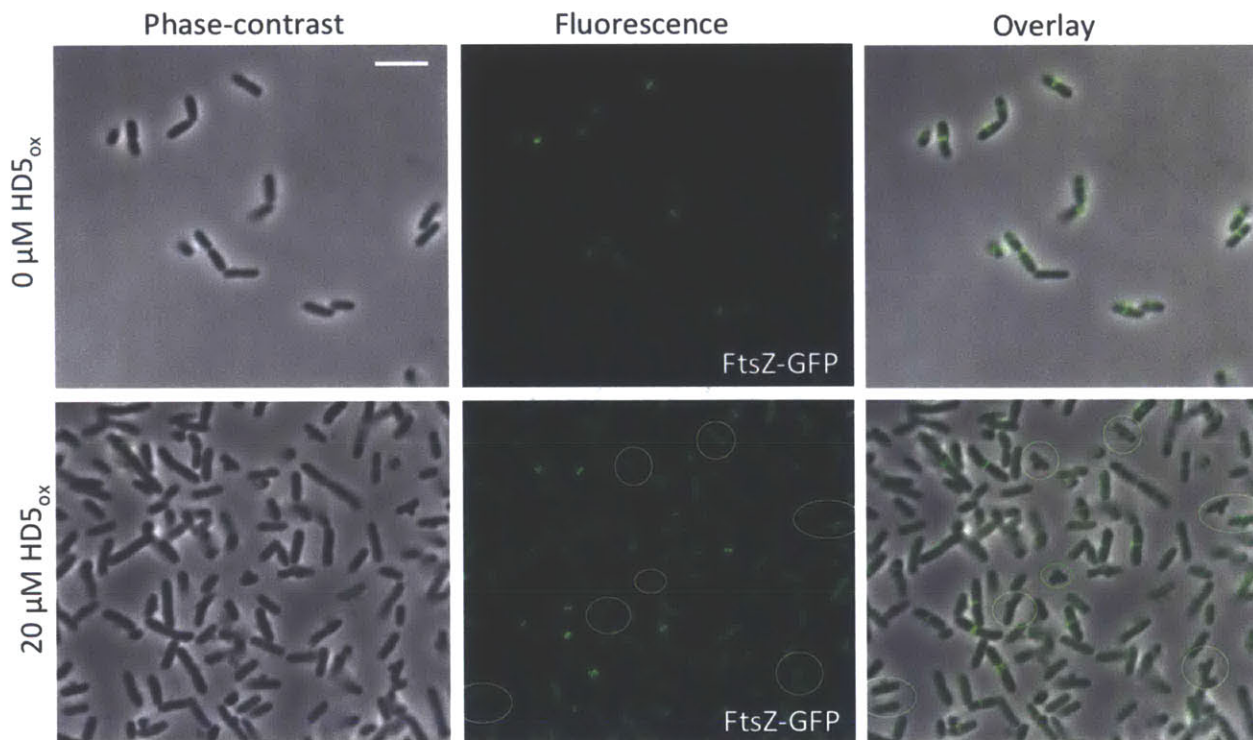
Figure 5.6. Effect of HD5$_{ox}$ on the FtsZ ring formation. *E. coli* expressing FtsZ-GFP (10^8 CFU/mL) were treated with 0 mM and 20 mM of HD5$_{ox}$ in standard AMA buffer (10 mM NaPB, 1% TSB w/o dextrose, pH 7.4) at 37 °C for 1 h, 130 rpm. A 5-μL of each sample is plated on 1% agarose pads and imaged. (Ex: 488 nm for GFP channel). Scale bar = 5 μm.

iv.   Development of Methods to Study the Effect of HD5$_{ox}$ on the Cell Division using *Caulobacter crescentus*. In order to further study the effect of HD5$_{ox}$ on the cell division process, we chose a model organism, *Caulobacter crescentus*. *C. cresentus*, a Gram-negative bacteria, undergoes asymmetric cell division resulting in a stalked cell and a swarmer cell.[25] Cell division is thoroughly studied in *C. cresentus*,[34,35] making it a model organism for examining the effect of HD5$_{ox}$ on the cell division process. First, we probed the morphological changes in *C. crescentus* induced upon treatment with HD5$_{ox}$. Like other Gram-negative bacteria, *C. crescentus* displayed morphological changes such as bleb formation, clumping and elongation upon treatment with HD5$_{ox}$ (Figure 5.7). *C. crescentus* can be synchronized by using a Percoll® (Sigma) gradient procedure as shown in Figure 5.8.[36] Thus, in future work, we aim to employ synchronized cells in studying the effect of HD5$_{ox}$ on the cell division through time-lapse
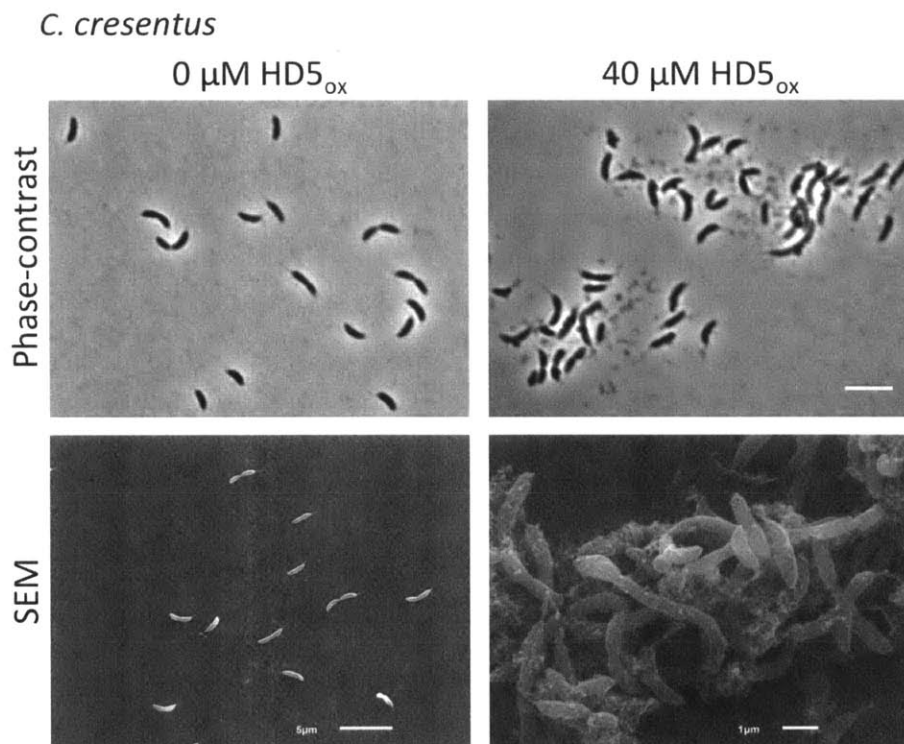
Figure 5.7. Morphology of HD5$_{ox}$ treated *C. crescentus* CB15. *C. crescentus* (10^8 CFU/mL) were treated with 0 μM and 40 μM of HD5$_{ox}$ in standard AMA buffer (10 mM NaPB, 1% TSB w/o dextrose, pH 7.4) at 30 °C for 1 h, 130 rpm. A 5-μL of each sample is plated on 1% agarose pads and imaged (top panels-phase contrast, Scale bar = 5 μm) and (5 x 100 μL) samples were fixed overnight and processed for SEM (Scale bar: bottom left panel= 5 μM and right panel = 1 μM).

microscopy experiments. These experiments may indicate that a particular step in the cell division process is affected the most when treated with $HD5_{ox}$.

| Unsynchronized | Synchronized with Percoll® gradient |
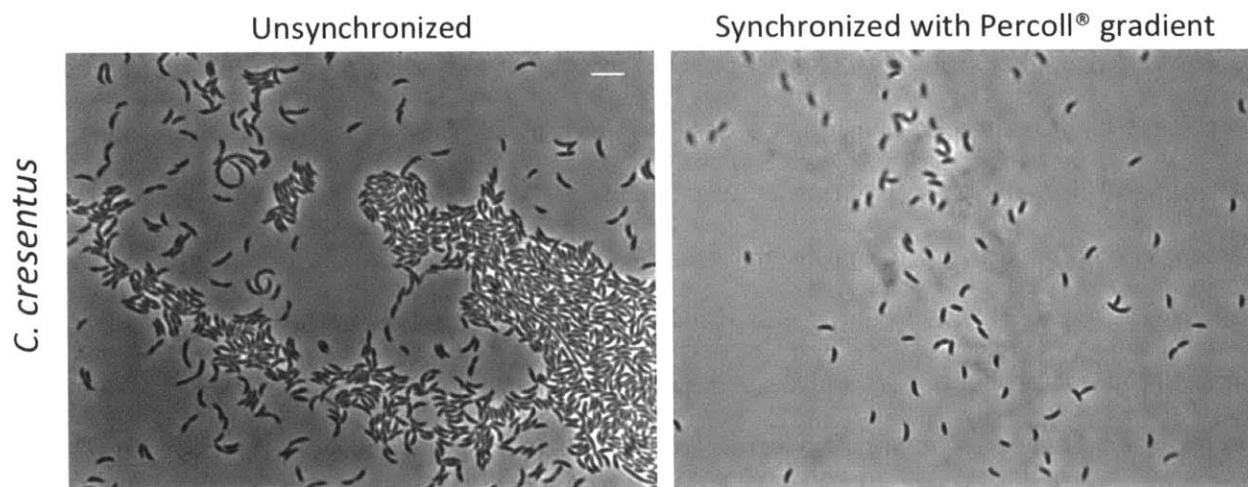
Figure 5.8. Synchronization of *C. crescentus* CB15. A 6-mL culture of *C. crescentus* (OD_{600} = 0.4) was centrifuged and resuspended in 600 μL of standard AMA buffer (10 mM NaPB, 1% TSB w/o dextrose, pH 7.4). To this suspension, 600 μL of Percoll was added and mixture was centrifuged at 10000 x g for 20 min, at 20 °C. The lower fraction afforded synchronized swarmer cells. A 5-μL of before and after synchronization samples were plated on 1% agarose pads and imaged. Scale bar = 5 μm.

5D.   Summary and Outlook

In summary, we examined how the composition of the *E. coli* inner- and outer membranes affects the localization of $HD5_{ox}$, and various morphological changes induced by $HD5_{ox}$. We also examined the effect of $HD5_{ox}$ on cell division process. From these studies, our current hypothesis is that $HD5_{ox}$ needs to cross the outer membrane barrier and permeablize the inner membrane for the peptide to exert its antimicrobial activity. The peptide could either interact with a potential target near the cell poles and septa that is either on or close to the cytoplasmic membrane of bacteria. Alternate possibility is that the peptide might cause slow membrane damage and disruption, and thereby result in cell death.

Upon treatment with HD5, blebs were observed predominantly at cell poles and cell septa, FtsZ ring formation is affected, along with elongation of bacteria. All these results indicate that HD5 affects cell division. With the establishment of assay conditions where the antimicrobial activity of $HD5_{ox}$ in actively growing cells (*Bacillus subtilis* and *C. crescentus*) can be examined, in future we aim to further study the effect of $HD5_{ox}$ on cell division.

5E.   Acknowledgements

5F.   References

(1) Schmidt, N. W., Mishra, A., Lai, G. H., Davis, M., Sanders, L. K., Tran, D., Garcia, A., Tai, K. P., McCray, P. B., Ouellette, A. J., Selsted, M. E., and Wong, G. C. L. (2011) Criterion for amino acid composition of defensins and antimicrobial peptides based on geometry of membrane destabilization. *J. Am. Chem. Soc. 133*, 6720–6727.

(2) Brogden, K. A. (2005) Antimicrobial peptides: pore formers or metabolic inhibitors in bacteria? *Nat. Rev. Microbiol. 3*, 238–250.

(3) van den Bogaart, G., Guzmán, J. V., Mika, J. T., and Poolman, B. (2008) On the mechanism of pore formation by melittin. *J. Biol. Chem. 283*, 33854–33857.

(4) Storm, D. R., Rosenthal, K. S., and Swanson, P. E. (1977) Polymyxin and related peptide antibiotics. *Annu. Rev. Biochem. 46*, 723–763.

(5) Wilmes, M., and Sahl, H.-G. (2014) Defensin-based anti-infective strategies. *Int. J. Med. Microbiol. 304*, 93–99.

(6) Kandaswamy, K., Liew, T. H., Wang, C. Y., Huston-Warren, E., Meyer-Hoffert, U., Hultenby, K., Schröder, J. M., Caparon, M. G., Normark, S., Henriques-Normark, B., Hultgren, S. J., and Kline, K. A. (2013) Focal targeting by human β-defensin 2 disrupts localized virulence factor assembly sites in *Enterococcus faecalis*. *Proc. Natl. Acad. Sci. U. S. A. 110*, 20230–20235.

(7) Wilmes, M., Stockem, M., Bierbaum, G., Schlag, M., Götz, F., Tran, D. Q., Schaal, J. B., Ouellette, A. J., Selsted, M. E., and Sahl, H.-G. (2014) Killing of *staphylococci* by θ-defensins involves membrane impairment and activation of autolytic enzymes. *Antibiot. (Basel, Switzerland) 3*, 617–631.

(8) Chileveru, H. R., Lim, S. A., Chairatana, P., Wommack, A. J., Chiang, I.-L., and Nolan, E. M. (2015) Visualizing attack of *Escherichia coli* by the antimicrobial peptide human defensin 5. *Biochemistry 54*, 1767–1777.

(9) Duong, F., Eichler, J., Price, A., Leonard, M. R., and Wickner, W. (1997) Biogenesis of the Gram-negative bacterial envelope. *Cell 91*, 567–573.

(10) Raetz, C. R. H., and Whitfield, C. (2002) Lipopolysaccharide endotoxins. *Annu. Rev. Biochem. 71*, 635–700.

(11) Nikaido, H. (2003) Molecular basis of bacterial outer membrane permeability revisited. *Microbiol. Mol. Biol. Rev. 67*, 593–656.

(12) Moser, S., Chileveru, H. R., Tomaras, J., and Nolan, E. M. (2014) A bacterial mutant library as a tool to study the attack of a defensin peptide. *Chembiochem 15*, 2684–2688.

(13) Falagas, M. E., and Kasiakou, S. K. (2005) Colistin: the revival of polymyxins for the management of multidrug-resistant Gram-negative bacterial infections. *Clin. Infect. Dis. 40*, 1333–1341.

(14) Schindler, M., and Osborn, M. J. (1979) Interaction of divalent cations and polymyxin B with lipopolysaccharide. *Biochemistry 18*, 4425–4430.

(15) Scott, M. G., Yan, H., and Hancock, R. E. (1999) Biological properties of structurally related alpha-helical cationic antimicrobial peptides. *Infect. Immun. 67*, 2005–2009.

(16) Rosenfeld, Y., Papo, N., and Shai, Y. (2006) Endotoxin (lipopolysaccharide) neutralization by innate immunity host-defense peptides: peptide properties and plausible modes of action. *J. Biol. Chem. 281*, 1636–1643.

(17) Lehrer, R. I., Barton, A., Daher, K. A., Harwig, S. S. L., Ganz, T., and Selsted, M. E. (1989) Interaction of human defensins with *Escherichia coli*. Mechanism of bactericidal activity. *J. Clin. Invest. 84*, 553–561.

(18) Hadjicharalambous, C., Sheynis, T., Jelinek, R., Shanahan, M. T., Ouellette, A. J., and Gizeli, E. (2008) Mechanisms of alpha-defensin bactericidal action: comparative membrane disruption by Cryptdin-4 and its disulfide-null analogue. *Biochemistry 47*, 12626–12634.

(19) Wong, P. T. S., Kashket, E. R., and Wilson, T. H. (1970) Energy coupling in the lactose transport system of *Escherichia coli*. *Proc. Natl. Acad. Sci. 65*, 63–69.

(20) Wanniarachchi, Y. A., Kaczmarek, P., Wan, A., and Nolan, E. M. (2011) Human defensin 5 disulfide array mutants: disulfide bond deletion attenuates antibacterial activity against *Staphylococcus aureus*. *Biochemistry 50*, 8005–8017.

(21) Oliver, P. M., Crooks, J. A., Leidl, M., Yoon, E. J., Saghatelian, A., and Weibel, D. B. (2014)

Localization of anionic phospholipids in *Escherichia coli* cells. *J. Bacteriol. 196*, 3386–3398.

(22) Mileykovskaya, E., and Dowhan, W. (2000) Visualization of phospholipid domains in *Escherichia coli* by using the cardiolipin-specific fluorescent dye 10-N-nonyl acridine orange. *J. Bacteriol. 182*, 1172–1175.

(23) Goehring, N. W., and Beckwith, J. (2005) Diverse paths to midcell: assembly of the bacterial cell division machinery. *Curr. Biol. 15*, R514–R526.

(24) Aarsman, M. E. G., Piette, A., Fraipont, C., Vinkenvleugel, T. M. F., Nguyen-Distèche, M., and den Blaauwen, T. (2005) Maturation of the *Escherichia coli* divisome occurs in two steps. *Mol. Microbiol. 55*, 1631–1645.

(25) Skerker, J. M., and Laub, M. T. (2004) Cell-cycle progression and the generation of asymmetry in *Caulobacter crescentus*. *Nat. Rev. Microbiol. 2*, 325–337.

(26) Wommack, A. J., Ziarek, J. J., Tomaras, J., Chileveru, H. R., Zhang, Y., Wagner, G., and Nolan, E. M. (2014) Discovery and characterization of a disulfide-locked C_2-symmetric defensin peptide. *J. Am. Chem. Soc. 136*, 13494–13497.

(27) Baba, T., Ara, T., Hasegawa, M., Takai, Y., Okumura, Y., Baba, M., Datsenko, K. A., Tomita, M., Wanner, B. L., and Mori, H. (2006) Construction of *Escherichia coli* K-12 in-frame, single-gene knockout mutants: the Keio collection. *Mol. Syst. Biol. 2*, 2006.0008.

(28) Zaritsky, A., and Woldringh, C. L. (2003) Localizing cell division in spherical *Escherichia coli* by nucleoid occlusion. *FEMS Microbiol. Lett. 226*, 209–214.

(29) Nierman, W. C., Feldblyum, T. V, Laub, M. T., Paulsen, I. T., Nelson, K. E., Eisen, J., Heidelberg, J. F., Alley, M. R. K., Ohta, N., Maddock, J. R., Potocka, I., Nelson, W. C., Newton, A., Stephens, C., Phadke, N. D., Ely, B., DeBoy, R. T., Dodson, R. J., Durkin, A. S., Gwinn, M. L., Haft, D. H., Kolonay, J. F., Smit, J., Craven, M. B., Khouri, H., Shetty, J., Berry, K., Utterback, T., Tran, K., Wolf, A., Vamathevan, J., Ermolaeva, M., White, O., Salzberg, S. L., Venter, J. C., Shapiro, L., and Fraser, C. M. (2001) Complete genome sequence of *Caulobacter crescentus*. *Proc. Natl. Acad. Sci. U. S. A. 98*, 4136–4141.

(30) Ruiz, N., Kahne, D., and Silhavy, T. J. (2006) Advances in understanding bacterial outer-membrane biogenesis. *Nat. Rev. Microbiol. 4*, 57–66.

(31) Raetz, C. R. H., and Dowhan, W. (1990) Biosynthesis and function of phospholipids in *Escherichia coli*. *J. Biol. Chem. 265*, 1235–1238.

(32) Romantsov, T., Battle, A. R., Hendel, J. L., Martinac, B., and Wood, J. M. (2010) Protein localization in *Escherichia coli* cells: Comparison of the cytoplasmic membrane proteins ProP, LacY, ProW, AqpZ, MscS, and MscL. *J. Bacteriol. 192*, 912–924.

(33) Santos, T. M. A., Lin, T.-Y., Rajendran, M., Anderson, S. M., and Weibel, D. B. (2014) Polar localization of *Escherichia coli* chemoreceptors requires an intact Tol-Pal complex. *Mol. Microbiol. 92*, 985–1004.

(34) Grünenfelder, B., Rummel, G., Vohradsky, J., Röder, D., Langen, H., and Jenal, U. (2001)

Proteomic analysis of the bacterial cell cycle. *Proc. Natl. Acad. Sci. U. S. A. 98*, 4681–4686.

(35) Laub, M. T., Chen, S. L., Shapiro, L., and McAdams, H. H. (2002) Genes directly controlled by CtrA, a master regulator of the *Caulobacter* cell cycle. *Proc. Natl. Acad. Sci. U. S. A. 99*, 4632–4637.

(36) Aakre, C. D., Phung, T. N., Huang, D., and Laub, M. T. (2013) A bacterial toxin inhibits DNA replication elongation through a direct interaction with the β sliding clamp. *Mol. Cell 52*, 617–628.

Appendix I

Tryptophan Mutants of HD5

A1.A. Introduction

In an initial study, we appended tryptophan, a natural fluorophore, at various positions including C-terminus, N-terminus or at both termini. Site-directed mutagenesis of the plasmid containing native HD5 sequence was performed to obtain the tryptophan mutants. In this regard, a C-terminal tryptophan mutant, (HD5-W), a N-terminal tryptophan mutant, (W-HD5), a double tryptophan mutant (W-HD5-W), and a ENLYFQW-HD5-W mutant, were obtained. The mutants were overexpressed, purified, and characterized. The N-terminal modification retained antimicrobial activity the most, suggesting that further modification of HD5 (including fluorophores) can be appended at the N-terminus.

A1.B. Experimental Section

i. Chemicals, Solvents, and Buffers. All solvents, reagents, and chemicals were purchased from commercial suppliers in the highest available purity and used as received. Oligonucleotide primers were synthesized by Integrated DNA Technologies (Coralville, IA), and subjected to standard desalting protocol and used as received. A Biorad MyCyclerthermocycler was employed for all polymerase chain reactions (PCR). Chemically competent *E. coli* TOP10 and BL21(DE3)cells were prepared in-house via standard protocols. A Qiagen miniprep kit was employed for plasmid isolations. PfuTurbo DNA polymerase was purchased from Stratagene; T4 DNA ligase from New England Biolabs; and all restriction enzymes were purchased from New England Biolabs. Staff of the Biopolymers Facility, MIT (Cambridge, MA), performed DNA sequencing. HPLC-grade acetonitrile (MeCN) and HPLC-grade trifluoroacetic acid (TFA) were purchased from either EMD Chemicals or Alfa Aesar. ULTROL-grade HEPES was purchased from Calbiochem; guanidine hydrochloride from AMRESCO, Inc; and sodium phosphate was obtained from BDH Chemicals.

Peptides. HD5 was overexpressed from *E. coli* BL21(DE3) cells containing a plasmid encoding pET-28b-Met-HD5, and $HD5_{ox}$ was purified following His_6-tag cleavage and oxidative

folding as described previously.[1] The tryptophan mutants of HD5 were obtained as described below. All peptides were stored in powdered form at -20 °C.

The peptide solutions and buffers for antimicrobial activity assays were sterile-filtered (0.2-μm filter) prior to the assays. Peptide stock solutions were prepared in Milli-Q water, aliquoted, and stored at -20 °C until use. Peptide concentrations were routinely determined using calculated extinction coefficients (Table A1.3) and a BioTek Synergy HT plate-reader outfitted with a BioTek Take 3 Micro-Volume Plate.

ii.   General Methods

HPLC. Preparative-scale HPLC was performed on an Agilent PrepStar 218 instrument outfitted with an Agilent ProStar 325 dual-wavelength UV-Vis detector, and a Luna 100 Å C-18 column (10-μm pore, 21.2 x 250 mm, Phenomenex) at a flow rate of 10 mL/min. An Agilent 1200 series instrument equipped with an autosampler set at 4 °C and column compartment set at 20 °C was employed for analytical and semi-preparative HPLC. Analytical HPLC was performed using a Clipeus C-18 column (5-μm pore, 4.6 x 250 mm, Higgins Analytical, Inc.) operated at a flow rate of 1 mL/min. For semi-preparative HPLC, a Zorbax C-18 column (5-μm pore, 9.4 x 250 mm, Agilent Technologies, Inc.) at a flow rate of 5 mL/min was employed. For each HPLC system, solvent A was Milli-Q water containing 0.2% TFA that was passed through a 0.2-μm filter before use and solvent B was HPLC-grade MeCN containing 0.2% TFA.

ESI-MS. ESI-MS was performed on a LC/MS system comprised of an Agilent 1260 LC outfitted with a Poroshell 120 EC, C-18 column (2.7-μm pore, 3.0 x 50 mm, Agilent Technologies, Inc.) and connected to an Agilent 6230 TOF system housing an Agilent Jetstream ESI source. LC/MS-grade water and MeCN containing 0.1% formic acid (Fluka Chemicals) were used as solvent A and solvent B, respectively. The samples were run at a flow rate of 0.4 mL/min using a gradient of 5-95% of solvent B over 5 min.

iii. **Cloning, Overexpression and Purification of Tryptophan mutants of HD5.** A plasmid containing the desired gene of interest corresponding to native HD5, in pET28b as previously reported, was obtained from Dr. Yoshitha Wanniariachi in the Nolan Lab.[1] In this plasmid pET-28b-Met-HD5, the TEV protease site at the N-terminus of HD5 corresponding to ENLYFQ**G** was mutated to His$_6$-ENLYFQ**M**-HD5 in order to incorporate a methionine residue.

The nucleotide sequence of pET-28b-Met-HD5.

Nde1 –*ENLYFQ-Met*-HD5 – stop – Xhol (*E. coli*) optimized sequence:

CATATG*GAGAACTTGTATTTCCAA*ATGGCGACTTGCTATTGTCGTACCG
GTCGTTGTGCAACCCGTGAGAGCCTGAGCGGTGTGTGTGAAATCAGCGGCCGTCTGTATC
GCCTGTGCTGCCGTTAACTCGAG

Site-directed Mutagenesis of HD5. A modified Quick-change site-directed mutagenesis protocol (Stratagene) was employed to generate the HD5 mutants (Table A1.1). For the first round of mutagenesis, pET-28b-Met-HD5 was used as the template.[1] The primers and primer pairings used for HD5 tryptophan mutants W-HD5, HD5-W, W-HD5-W and ENLYFQ-W-HD5-W are listed in Tables A1.1 and A1.2. The amino acid sequence of these peptides are given in Table A1.3. The PCR amplification was performed with PfuTurbo DNA polymerase and the residual plasmid was digested with *DpnI* as reported previously.[1] For a 50-µL PCR reaction, 2 µL of *DpnI* was added in two-step additions of 1 µL each at t = 0 and 1.5 h and the reaction was continued for 3 h at 37 °C. The *DpnI* digests were transformed into chemically competent *E. coli* TOP10 cells. Overnight cultures (5 mL, 50 µg/mL kanamycin) were grown from single colonies, and the plasmids were extracted and purified by using a Qiagen miniprep kit. To an aliquot of 10 µL of the plasmid from the mini-prep, 2 µL of 1 µM T7 terminator primer was added and the samples were analyzed by DNA sequencing (MIT Biopolymers Laboratory, Cambridge, MA). The DNA sequences and presence of the desired mutation(s) were verified by DNA sequencing. We

discovered that we obtained a plasmid encoding ENLYFQ-W-HD5-W by accident, as confirmed by the DNA sequencing.

Table A1.1. Primers Employed for Site-Directed Mutagenesis.[a]

Primer	Sequence
P1	5'-GAACTTGTATTTCCAAATGGCGACTTGCTATTGTCG-3'
P2	5'-CGACAATAGCAAGTCGCCATTTGGAAATACAAGTTC-3'
TTHSP1	5'-CATATGGAGAACTTGTATTTCCAATGGGCGACTTGCTATTGTCGTA- 3'
TTHSP2	5'-TACGACAATAGCAAGTCGCCCATTGGAAATACAAGTTCTCCATATG- 3'
MTHSP1	5'-CATATGGAGAACTTGTATTTCATGTGGGCGACTTGCTATTGTCGTA- 3'
MTHSP2	5'-TACGACAATAGCAAGTCGCCCACATGAAATACAAGTTCTCCATATG- 3'
MHTSP1	5'-GTATCGCCTGTGCTGCCGTTGGTAAGAGCACCACCACCACCAC- 3'
MHTSP2	5'-GTGGTGGTGGTGGTGCTCTTACCAACGGCAGCACAGGCGATAC- 3'
MHSSP1	5'-GTATCGCCTGTGCTGCCGTTAATAAGAGCACCACCACCAC- 3'
MHSSP2	5'-GTGGTGGTGGTGCTCTTATTAACGGCAGCACAGGCGATAC- 3'

[a] The codons containing the mutations are underlined and highlighted in red.

Table A1.2. Templates and Primer Pairings Employed in Site-Directed Mutagenesis.

Template	Product	Primer Pairing
pET28b-ENLYFQ-G-HD5 [1]	pET28b-ENLYFQ-M-HD5-Stop	P1, P2 [1]
pET28b-ENLYFQ-M-HD5	pET28b-ENLYFQ-W-HD5-Stop	TTHSP1, TTHSP2
pET28b-ENLYFQ-M-HD5-Stop	pET28b-ENLYFQ-M-HD5-W-Stop	MHTSP1, MHTSP2
pET28b-ENLYFQ-M-HD5-W-Stop	pET28b-ENLYFQ-W-HD5-W-Stop	TTHSP1, TTHSP2
pET28b-ENLYFQ-W-HD5-W-Stop	pET28b-ENLYFM-W-HD5-W-Stop	MTHSP1, MTHSP2
pET28b-ENLYFM-W-HD5-W-Stop	pET28b-ENLYFM-W-HD5-Stop-Stop	MHSSP1, MHSSP2

Overexpression and Purification of HD5 and Tryptophan-HD5 Mutants. The plasmids with the desired mutations were transformed in to chemically competent *E. coli* BL21(DE3) cells. Single colonies of the transformed cells were selected and grown to saturation in LB media with 50 µg/mL of kanamycin. For the cell freezer stock, 500 µL of cell culture mixed with 500 µL of 50% glycerol was stored at -80 °C. Overexpression and purification of the His_6-tagged and corresponding reduced mutant peptides were conducted as described previously for His_6-Met-HD5.[1] Following the established protocol,[1] the starter culture from these cells was grown to saturation overnight in LB media supplemented with 50 µg/mL of kanamycin at 37 °C, 150 rpm for 16 h. The starter culture was diluted 1:100 into LB media with 50 µg/mL of kanamycin. The secondary culture was grown to OD_{600} ~ 0.5 at 37 °C, 150 rpm before induction with 500 µM IPTG, and incubated for 3-4 h until OD_{600} reached 1.0-1.5. The cells were then centrifuged at 4200 rpm, 4 °C for 30 min. The cell pellets from cultures (3 x 2-L, 6-L cell cultures) (~10 g) were combined in 50-mL pre-weighed falcon tubes and stored at -80 °C until further use. The 6-L cell pellets were thawed on ice and re-suspended in 30 mL of cold lysis buffer (10 mM Tris, 100 mM NaH_2PO_4, 6 M GuHCl, pH 8.0). To this mixture, the protease inhibitor phenylmethyl sulfonyl fluoride PMSF (~3 mM) was added before sonicating for 1 min (at 10% amplitude with pulse on for 1 s and pulse off for 4 s). The sonication was repeated twice, each with the addition of PMSF (~3 mM). The crude lysate was centrifuged at 13000 rpm at 4 °C for 30 min. The clear supernatant was then added to prewashed Ni-NTA resin (6 mL of slurry washed thrice with 10 mL of Milli-Q water) from Qiagen. This mixture was incubated with gentle shaking for 1.5 h at 4 °C. The resin was then loaded on to a column and washed with 30 mL of cold wash buffer (20 mM Tris, 300 mM NaCl, 6 M GuHCl, pH 8.0). His_6-tagged-peptide was subsequently eluted with 30-40 mL of the cold elution buffer (10 mM Tris, 100 mM NaH_2PO_4, 200 mM NaCl, 1 M imidazole, 6 M GuHCl, pH 6.5). The eluent was placed in a membrane (3500 MWCO) and dialyzed against 5% acetic acid (4 L) for 24 h and 0.1% acetic acid (4 L) for another 24 h before lyophylization. The His_6-tagged HD5 mutants (170-230 mg) were stored as powder at -20 °C until further use. In order to check the purity of the peptides, each sample was dissolved in 100

μL of buffer (75 mM HEPES, pH 8.2) and reduced using TCEP (5 μL of 100 mM stock), and analyzed using analytical RP-HPLC C18 column.

CNBr Cleavage of His$_6$-tagged HD5 and Trp-HD5 Mutants and Isolation of Reduced Peptides.
His$_6$-tagged peptides (170-230 mg) were dissolved in 80% formic acid at 2 mg/mL in a 500 mL round bottom flask. A solution of CNBr (20 mg/mL dissolved in 80% formic acid) was added slowly to dilute the solution to a final peptide concentration of 1 mg/mL, and the reaction mixture was stirred at room temperature for 5 h. The reaction was quenched with 340-460 mL of Milli-Q water to dilute peptide. The solution was transferred to an acid-resistant membrane (3500 MWCO) and dialyzed against 20 L of Milli-Q water for (2 x 24 h). The sample was then lyophilized to dryness. The crude product (~ 80-90 mg) was dissolved in 20 mL of buffer (75 mM HEPES, pH 8.2) with gentle mixing for 3 h at room temperature. A 1-mL aliquot of 100 mM TCEP was added and the solution was further incubated for 15 min, and quenched with 6 mL of 6% TFA. The product was then purified by semi-preparative RP-HPLC using a gradient of 10-40% B over 15 min (A: 0.2% TFA/water and B: 0.2% TFA/acetonitrile), which afforded pure reduced forms of tryptophan-HD5 mutants (10-12 mg).

Oxidative Folding and Purification of HD5$_{red}$ and Tryptophan Mutants. Following the reported procedure,[1] isolated reduced forms of tryptophan-HD5 mutants (2 mg/mL) were dissolved in of 8 M GuHCl containing 3 mM reduced and 0.3 mM oxidized glutathione. The peptide solution was adjusted to pH 8.3 by the drop wise addition of 0.25 M NaHCO$_3$ to a final concentration of 0.5 mg/mL of peptide, and the mixture was incubated at room temperature for 4 h. HD5$_{ox}$ and the oxidized tryptophan mutants were purified by semi-preparative RP-HPLC using a gradient of 10-60%B over 30 min (A: 0.2% TFA/water and B: 0.2% TFA/acetonitrile) to yield pure HD5$_{ox}$ (~1 mg).

iv. **Inner-membrane Permeability Assay using *E. coli* ML35.** Inner-membrane permeability assays were performed using *E. coli* ML35.[2,3] An overnight culture of bacteria (*E. coli* ML35) was grown in trypticase soy broth (TSB) without dextrose for 17 h at 37 °C. The culture was diluted 1:100 times into a culture tube containing 6 mL of fresh TSB without dextrose. The culture was grown for 2 h at 37 °C until an OD_{600} ~ 0.6 (2.5 x 10^8 CFU/mL) was attained. The cells were centrifuged at 3500 rpm, 4 °C for 10 min and the supernatant was removed. The cells were washed with 10 mM sodium phosphate buffer supplemented with 1% TSB without dextrose at pH 7.4, described in previous Chapters as "AMA buffer". All solutions including the AMA buffer that are required for the assays were sterile filtered through 0.2-μm filters before the assay. Upon centrifugation of the cells at 3500 rpm, 4 °C for 10 min, the cells were resuspended twice in AMA buffer to obtain an OD_{600}=0.44 (1.25 x 10^8 CFU/mL). The bacterial culture was further diluted 1:100 into 5 mL of AMA buffer. The assay was set up in a 96-well plate with each well containing 80 μL of bacterial culture, 10 μL of 10x stock peptide solution and 10 μL of 25 mM *o*-nitrophenyl-β-galactopyranoside (ONPG), added in the above order. The 96-well plate was incubated at 37 °C for 2 h with gentle shaking and the absorbance at 405 nm was recorded every 5 min using a plate reader.

v. **Circular Dichroism Spectroscopy.** Peptides were dissolved in buffer (5 mM sodium phosphate, pH 7.0) to a final concentration of 20 μM (300 μL) and transferred to a quartz CD cell (Hellma) with a path length of 1 mm. The CD spectra were collected over a wavelength range from 260-190 nm at 1 nm intervals (10 s averaging time, three independent scans). The spectral data were averaged using Excel (Microsoft Office 2011). The CD spectrum for each peptide was also obtained in the presence of 10 mM sodium dodecylsulfate (SDS) to analyze the change in the secondary structure in the presence of a membrane mimic. To 300 μL of each peptide solution, 3 μL of 1 mM SDS was added and the sample was incubated for ~2.5 h at room temperature before the CD spectrum obtained.

A1.C.   Results and Discussion

i.   Design of Tryptophan Mutants and Site-directed Mutagenesis of HD5. The tryptophan mutants were designed to contain tryptophan residues at either one or both termini: N-terminal mutant, W-HD5; C-terminal mutant, HD5-W; and both termini, W-HD5-W (Table A1.3). The pET28b-Met-HD5 plasmid was used as template for site-directed mutagenesis (Table A1.1). Mutations in two codons at the C-terminus of pET28b-ENLYFQM-HD5-**Stop** afforded pET28b-ENLYFQ-M-HD5-**W**-**Stop** (HD5-W). Similarly, when mutagenesis of two codons at the N-terminus of pET28b-ENLYF**Q**-**M**-HD5 was performed to obtain W-HD5 (pET28b-ENLYF**M**-**W**-HD5-Stop), the PCR product did not possess the desired mutation. Even with desired mutation, the transformation into *E. coli* BL21(DE3) gave abnormal colonies, which were killed upon induction with IPTG. As a result, first the pET28b-ENLYFQ-**M**-HD5-**W**-Stop (M-HD5-W) was used as template to obtain pET28b-ENLYFQ-**W**-HD5-**W**-Stop (ENLYFQ-W-HD5-W) that was further mutated to get the pET28b-ENLYF**M**-**W**-HD5-W-Stop (W-HD5-W). This pET28b-ENLYF**M**-**W**-HD5-**W**-Stop was then used as template to get pET28b-ENLYF**M**-**W**-HD5-**Stop**-Stop (W-HD5) (Table A1.2).

ii.   Overexpression and Purification of Tryptophan-HD5 Mutants. The plasmids were transformed into *E. coli* BL21(DE3) cells and the peptides were overexpressed by following the reported procedure as described for His$_6$-M-HD5.[1] The overexpression from 12 L of *E. coli* BL21(DE3) cultures afforded: W-HD5 (270 mg, 90 mg), HD5-W (190 mg, 80 mg), W-HD5-W (270 mg, 130mg) and ENLYFQW-HD5-W (170 mg, 70 mg) corresponding to yield after Ni-NTA column purification and yield after CNBr cleavage, respectively. After CNBr cleavage of the His$_6$-tag, the peptides were treated with excess TCEP (100 mM) in 75 mM HEPES, pH 8.2 buffer and the reduced form of the peptides were collected by RP-HPLC (Figure A1.1). The peptides were folded following the standard folding procedure as for HD5. The tryptophan mutants folded to single peaks. The peptides were purified and later confirmed by the mass spectrometry analysis shown in Table A1.4.

Table A1.3. Molecular Weights (MW) and Extinction Coefficients for HD5 and Tryptophan Mutant Peptides.

Peptide	Sequence	MW (Da) [a]	ε_{278} $(M^{-1}cm^{-1})$ [b]
HD5$_{ox}$	ATCYCRTGRCATRESLSGVCEISGRLYRLCCR	3582.1	3181
HD5$_{red}$	ATCYCRTGRCATRESLSGVCEISGRLYRLCCR	3588.2	2800
W-HD5$_{ox}$	**W**ATCYCRTGRCATRESLSGVCEISGRLYRLCCR	3768.4	8781
W-HD5$_{red}$	**W**ATCYCRTGRCATRESLSGVCEISGRLYRLCCR	3774.4	8400
HD5-W$_{ox}$	ATCYCRTGRCATRESLSGVCEISGRLYRLCCR**W**	3768.4	8781
HD5-W$_{red}$	ATCYCRTGRCATRESLSGVCEISGRLYRLCCR**W**	3774.4	8400
W-HD5-W$_{ox}$	**W**ATCYCRTGRCATRESLSGVCEISGRLYRLCCR**W**	3954.61	14381
W-HD5-W$_{red}$	**W**ATCYCRTGRCATRESLSGVCEISGRLYRLCCR**W**	3960.61	14000
ENLYFQW-HD5-W$_{ox}$	**ENLYFQW**ATCYCRTGRCATRESLSGVCEISGRLYRLCCR**W**	4748.2	15781
ENLYFQW-HD5-W$_{red}$	**ENLYFQW**ATCYCRTGRCATRESLSGVCEISGRLYRLCCR**W**	4752.2	15400

[a] Molecular weights were calculated by using PROTEIN CALCULATOR v3.3 available at http://www.scripps.edu/~cdputnam/protcalc.html. [b] Extinction coefficients (278 nm) were calculated by using PROTEIN CALCULATOR v3.3.

During initial preparations, the yields of reduced forms of tryptophan mutants (5-10 mg) were low compared to native HD5 (10-12 mg of HD5$_{red}$). The lower yield was attributed to solubility problems of the tryptophan mutants potentially because of hydrophobic tryptophan residues. The problem of incomplete reduction and precipitation of tryptophan mutants was solved by the addition of 6 M GuHCl to the 75 mM HEPES, pH 8.2 buffer solution prior to purification of the reduced peptides. This GuHCl addition not only increased the solubility, but also pushed the reaction towards the complete reduction of the peptide. After optimization of solubility, His$_6$-tagged W-HD5-W peptide was cleaved and purification of the peptide afforded 50 mg of W-HD5-W$_{red}$ (Table A1.4 and Figure A1.1).

Table A1.4. HPLC Retention Time, Calculated and Observed *m/z* Values for HD5 and Tryptophan Mutant Peptides.

Peptide	HPLC retention time (min)[a]	Calculated *m/z* (Monoisotopic)[b]	Observed m/z (Monoisotopic)[b]
HD5$_{ox}$	16.1	3579.62	3579.62
HD5$_{red}$	21.5	3585.67	3585.76
W-HD5$_{ox}$	16.5	3765.70	3765.71
W-HD5$_{red}$	21.0	3771.75	3771.76
HD5-W$_{ox}$	17.4	3765.70	3765.71
HD5-W$_{red}$	22.1	3771.75	3771.74
W-HD5-W$_{ox}$	18.5	3954.61	3954.60
W-HD5-W$_{red}$	22.6	3960.61	3960.59
ENLYFQW-HD5-W$_{ox}$	20.3	4746.14	4746.14
ENLYFQW-HD5-W$_{red}$	26.1	4752.18	4752.18

[a] Retention times determined by using analytical RP-HPLC on a C18 column and a gradient of 10–60% B in 30 min. [b] *m/z* values for peptides calculated using MolE-Molecular Mass Calculator v2.02 available at http://library.med.utah.edu/masspec/mole.htm.

The folding assay of the reduced mutants with GSH/GSSH gave single peaks in the HPLC traces indicating the formation of single isomers. The oxidized products were purified by RP-HPLC and analyzed by ESI-MS. The retention time of ENLYFQW-HD5-W (hydrophobic Trp residues) was greater than the retention times of other mutants as expected (Table A1.4 and Figure A1.1).
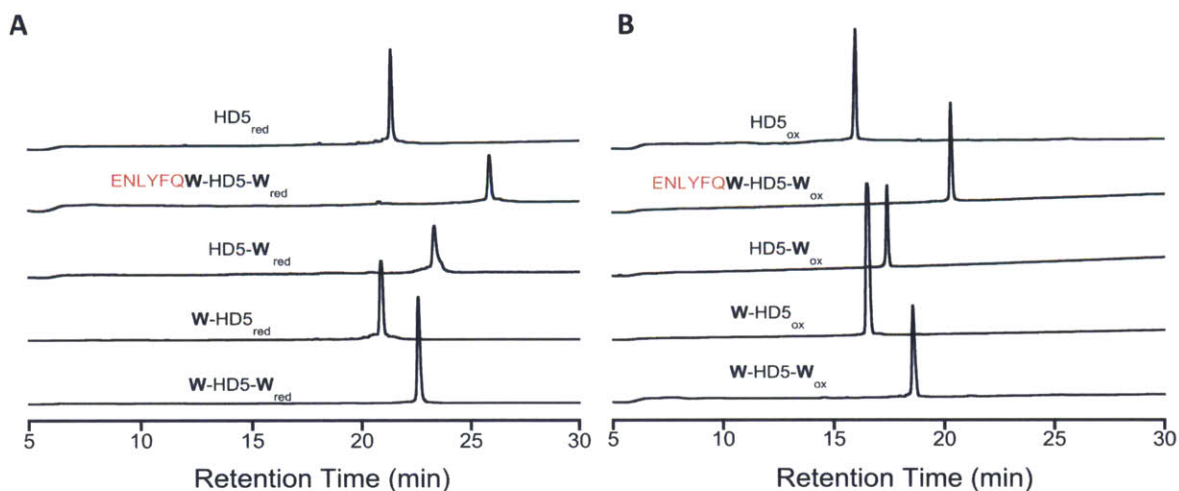
Figure A1.1. The analytical HPLC traces of the purified tryptophan-HD5 mutants in their **A)** reduced forms and **B)** oxidized forms. The samples were subjected to a gradient of 10-60 % solvent B at a flowrate of 1 mL/min for 30 min and absorbance was measured at 220 nm.

iii. **CD Spectroscopy of HD5 and Tryptophan Mutants.** Circular dichroism (CD) spectra of $HD5_{ox}$ and the folded HD5 tryptophan mutants were obtained to characterize the secondary structure and ascertain whether these peptides adopt the characteristic β-sheet conformation in the presence of a membrane mimic (SDS). In the absence of SDS, the peptides adopt random coil structures with peak around 200 nm. In the presence of SDS, the CD spectra of native $HD5_{ox}$ and N- and C-terminal tryptophan mutants exhibited a new peak ~209 nm, which is indicative of more β-sheet structure. In contrast, the peak shifted to only ~203 nm in case of N-terminal short peptide tagged-HD5 (ENLYFQW-HD5-W) compared to other mutants, indicating the structure of tagged- mutant did not alter much or could not be easily detected upon addition of SDS (Figure A1.2).
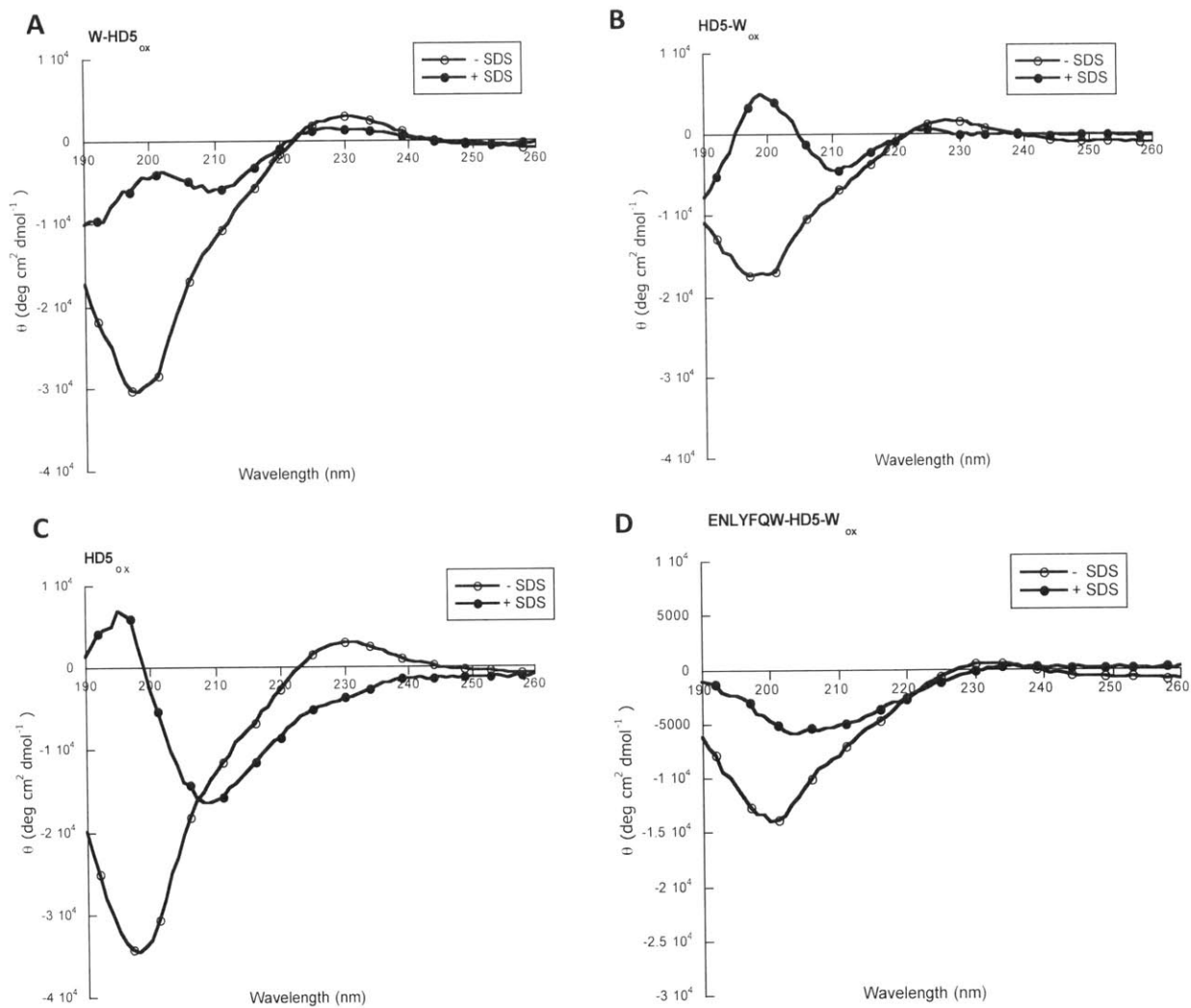
Figure A1.2. CD spectra of **A**) W-HD5$_{ox}$, **B**) HD5-W$_{ox}$, **C**) HD5$_{ox}$ and **D**) ENLYFQW-HD5-W$_{ox}$ in the absence and presence of 10 mM SDS (5 mM sodium phosphate buffer, pH 7.0).
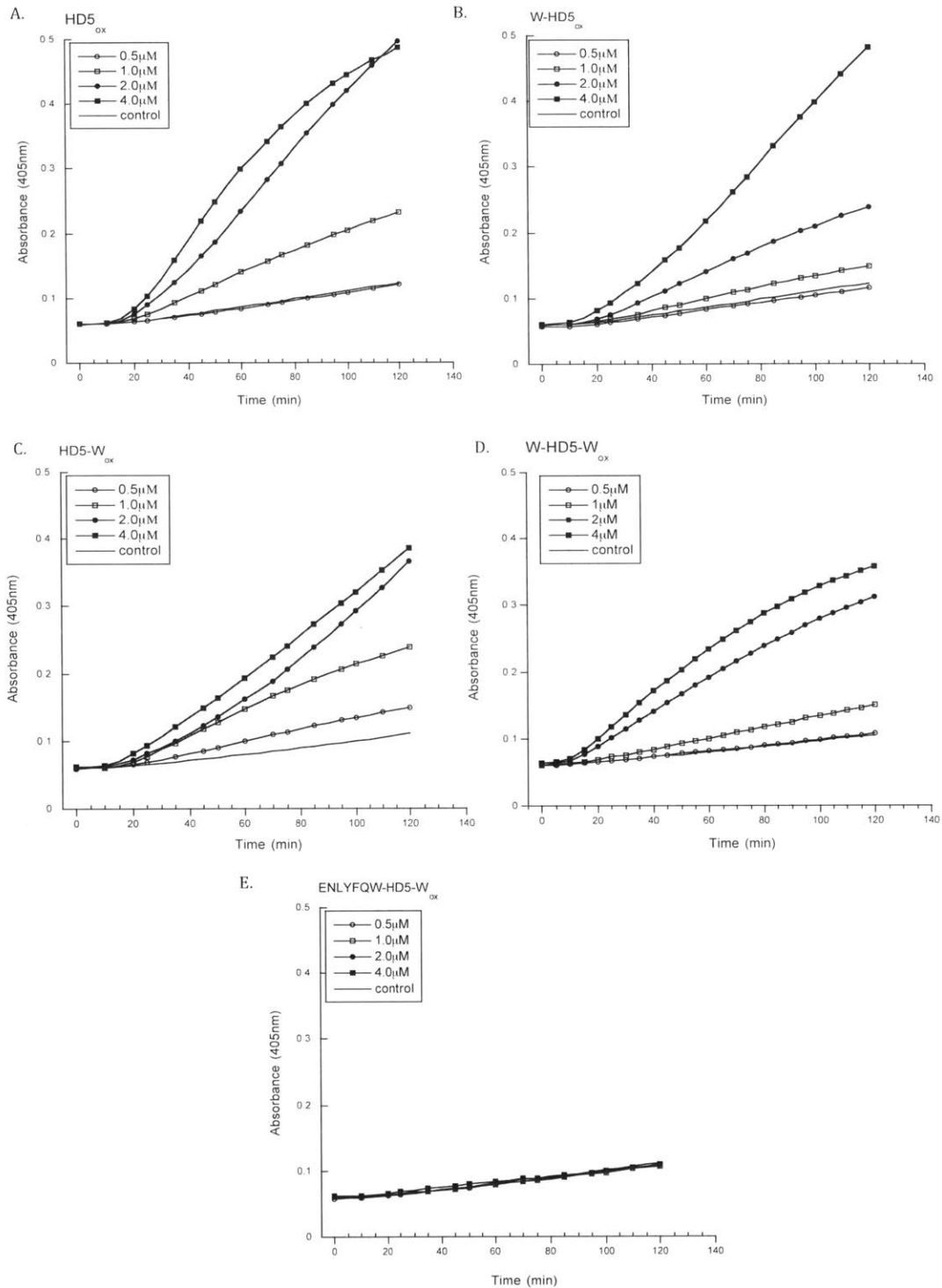
Figure A1.3. Representative inner-membrane permeabilization assays employing *E. coli* ML-35 (1×10^6 CFU/mL) in AMA buffer (10 mM sodium phosphate buffer containing 1% TSB (w/o dextrose), pH 7.4, 37 °C) containing 2.5 mM ONPG and 0, 0.5, 1, 2, 4 μM of **A)** $HD5_{ox}$ and **B)** $W\text{-}HD5_{ox}$ **C)** $HD5\text{-}W_{ox}$ **D)** $W\text{-}HD5\text{-}W_{ox}$ and **E)** $ENLYFQW\text{-}HD5\text{-}W_{ox}$. As a control, water was added to a well containing bacteria in AMA buffer. Absorbance at 405 nm was monitored at 5 min intervals.

iv.   Inner-membrane Permeability Assay. The assay was performed using *E. coli* ML35, which possesses a β-galactosidase enzyme in the cytoplasm (Chapter 5, Scheme 5.1). The assay was performed with the tryptophan mutants obtained along with native HD5 (Figure A1.3). The antimicrobial activity of the mutants containing single tryptophan at termini was retained compared to ENLYFQ-W-HD5-W (a six-amino acid tag containing mutant) having no activity in the concentration ranges tested. The results indicated that inner membrane damage occurs when treated with mutants with tryptophan on the termini of HD5. Although, appending a larger molecules such as a peptide tag-might completely attenuate the activity.

A1.D.   Summary and Outlook

HD5 displays potent antimicrobial activity against broad-range of pathogens.[4-6] To probe the structural and functional properties of the HD5 fluorescence-based techniques were considered as described in Chapters 3 and 5. In order to study the effect of a fluorophore on the proper folding of the peptide, initial studies were performed with tryptophan appended to the termini to obtain W-HD5, HD5-W, W-HD5-W and ENLYFQW-HD5-W. The folding assays revealed that all the mutants including those with the N- and C- terminal tryptophan, folded into single isomers. The *E. coli* ML35 assay performed with mutants and HD5 suggested that W-HD5, HD5-W and W-HD5-W retained some of the antibacterial activity. In contrast, appending a short peptide-tag on N-terminus (ENLYFQW-HD5-W) completely attenuated activity in the concentration range tested. In summary, the antimicrobial activity was retained the most in N- and C-terminal tryptophan mutants, making the termini as ideal positions for further modification of HD5.

A1.E.   Acknowledgements

A1.F. References

(1) Wanniarachchi, Y. A., Kaczmarek, P., Wan, A., and Nolan, E. M. (2011) Human defensin 5 disulfide array mutants: disulfide bond deletion attenuates antibacterial activity against *Staphylococcus aureus*. *Biochemistry 50*, 8005–8017.

(2) Lehrer, R. I., Barton, A., Daher, K. A., Harwig, S. S. L., Ganz, T., and Selsted, M. E. (1989) Interaction of human defensins with *Escherichia coli*. Mechanism of bactericidal activity. *J. Clin. Invest. 84*, 553–561.

(3) Figueredo, S. M., Weeks, C. S., Young, S. K., and Ouellette, A. J. (2009) Anionic amino acids near the pro-alpha-defensin N terminus mediate inhibition of bactericidal activity in mouse pro-cryptdin-4. *J. Biol. Chem. 284*, 6826–6831.

(4) Porter, E. M., van Dam, E., Valore, E. V, and Ganz, T. (1997) Broad-spectrum antimicrobial activity of human intestinal defensin 5. *Infect. Immun. 65*, 2396–2401.

(5) Wommack, A. J., Ziarek, J. J., Tomaras, J., Chileveru, H. R., Zhang, Y., Wagner, G., and Nolan, E. M. (2014) Discovery and characterization of a disulfide-locked C_2-symmetric defensin peptide. *J. Am. Chem. Soc. 136*, 13494–13497.

(6) Gounder, A. P., Wiens, M. E., Wilson, S. S., Lu, W., and Smith, J. G. (2012) Critical determinants of human α-defensin 5 activity against non-enveloped viruses. *J. Biol. Chem. 287*, 24554–24562.

Appendix 2

Tools to Study HD5

A2.A.   Introduction

The mechanism of antimicrobial action of defensins, as with other cationic antimicrobial peptides (AMPs), was initially proposed to be mediated by pore-formation or bacterial membrane destabilization leading to cell death.[1] Recently, several other modes of antibacterial activity of these AMPs involving inhibition of cell wall biosynthesis,[2] activation of autolysins,[3] binding to intracellular components such as DNA,[4] and inhibition of processes such as transcription, translation and replication[5] were identified. One major concern in delineating the mode of action is identification of primary mode of killing and differentiating the secondary effects that result from AMP action. As a result, direct target identification might assist in identification of mechanism of action of AMPs.

In order to study the mechanism of action of HD5, we successfully designed, synthesized and analyzed fluorophore-modified HD5 analogues (Chapter 2). Employing these analogues, we visualized the attack of HD5 on Gram-negative bacteria (Chapter 3) and demonstrated that $HD5_{ox}$ entered bacterial cytoplasm and accumulated near cell poles and cell septa. In order to examine the bacterial cellular targets of $HD5_{ox}$, we initiated preliminary studies on the effect of $HD5_{ox}$ on certain bacterial cellular processes (Chapter 5). However, we needed more reagents and tools to detect the specific bacterial target interacting with HD5. For this purpose, we appended 1) affinity tags such as biotin on HD5 for affinity-based enrichment of the target; and 2) an orthogonal functional group such as azide-moiety that can be used to append desired functional moieties using click chemistry. In future, employing these diverse tools, we aim to identify the bacterial targets of HD5.

A2.B.   Experimental Section

i.   Chemicals, Solvents, and Buffers. All solvents, reagents, and chemicals were purchased from commercial suppliers in the highest available purity and used as received. 5-azidopentanoic acid was purchased from Bachem Americas, Inc. D-Biotin, Fmoc-γ-amino butyric acid (Fmoc-ABU-OH), EDT, and TIS were purchased from Sigma Aldrich. Piperidine was obtained

from Alfa Aesar. Fmoc-Arg(pbf)-Novasyn@TGA resin was purchased from EMD Chemicals. Fmoc-protected amino acids were purchased from AAPPTec, LLC. All peptide-coupling reagents were obtained from AK Scientific, Inc. HPLC-grade acetonitrile (MeCN) and HPLC-grade trifluoroacetic acid (TFA) were purchased from either EMD Chemicals or Alfa Aesar. Guanidine hydrochloride was purchased from AMRESCO, Inc; and sodium phosphate was obtained from BDH Chemicals. All reagents and buffers used for antimicrobial assays were sterile-filtered through 0.2-μm filters. A calibrated BioTek Take3 multi-well plate was used for determination of peptide concentration.

ii. General Methods

HPLC. Preparative-scale HPLC was performed on an Agilent PrepStar 218 instrument outfitted with an Agilent ProStar 325 dual-wavelength UV-Vis detector, and a Luna 100 Å C-18 column (10-μm pore, 21.2 x 250 mm, Phenomenex) at a flow rate of 10 mL/min. An Agilent 1200 series instrument equipped with an autosampler set at 4 °C and column compartment set at 20 °C was employed for analytical and semi-preparative HPLC. Analytical HPLC was performed using a Clipeus C-18 column (5-μm pore, 4.6 x 250 mm, Higgins Analytical, Inc.) operated at a flow rate of 1 mL/min. For semi-preparative HPLC, a Zorbax C-18 column (5-μm pore, 9.4 x 250 mm, Agilent Technologies, Inc.) at a flow rate of 5 mL/min was employed. For each HPLC system, solvent A was Milli-Q water containing 0.1% TFA that was passed through a 0.2-μm filter before use and solvent B was HPLC-grade MeCN containing 0.1% TFA.

ESI-MS. ESI-MS was performed on LC/MS system using Agilent 1260 LC fitted with Agilent Poroshell 120 EC, C-18 column (2.7-μm pore, 3.0 x 50 mm, Agilent Technologies, Inc.) and connected to an Agilent 6230 TOF system housing an Agilent Jetstream ESI source. LC/MS-grade water containing 0.1 % formic acid as solvent A and LC/MS grade acetonitrile containing 0.1 % formic acid as solvent B were used as the solvent systems for all of the LC/MS analysis. All samples were run at a 0.4 mL/min flow rate with a gradient of 5%-95% B for 15 min.

iii.   Antimicrobial Activity Assays. Antimicrobial activity (AMA) assays were performed using a micro-drop colony forming units (CFU) method described previously in Chapter 2.[6] For the microscopy experiments, 5-μL aliquot from each sample was plated on 1% agarose pads and topped with a coverslip prior to imaging.

Data Collection for Microscopy Experiments. The data collection was performed in the W. M Keck facility in the Whitehead Institute using Zeiss Axioplan2 microscope fitted with 100x objective. Images were obtained with the Hamamatsu ORCA CCD camera. Image analysis was performed with ImageJ software.

iv.   Fmoc-based Solid-phase Peptide Synthesis. HD5 was synthesized using the Fmoc-based solid phase peptide synthesis following the optimized procedure reported in the Chapter 2. The synthesis was performed on a 0.2-mmol scale of arginine-preloaded Fmoc-Arg(pbf)-Novasyn@TGA resin. The psuedoprolines were retained in the sequence (HD5: ATCYCRTGRC$^\Psi$ATRES$^\Psi$LSGVCE$^\Psi$ISGRLYRLCCR) as previously reported (Chapter 2). Following the addition of final amino acid residue, the resin was divided and portions of Fmoc-protected HD5 on the resin were used for N-terminal Biotin coupling and azido-functionalized HD5.

A2.C.   Results and Discussion

i.   Fmoc-based Solid-phase Peptide Synthesis of Fmoc-HD5. The flow-based solid-phase peptide synthesis of HD5 was performed and the Fmoc-HD5 on the resin (0.2 mmol scale, 3 g wet weight) was divided into three portions of 1 g each. A test-scale cleavage was performed on the Fmoc-protected HD5 to confirm the complete synthesis (Figure A2.1). A 500 mg portion (0.0345 mmol) of the resin was Fmoc-deprotected and cleaved off resin to obtain 80 mg of crude peptide (64 % overall yield). The crude peptide was reduced in the presence of reducing agent TCEP and purified using preparative HPLC column to achieve 19 mg (15% overall yield) of HD5$_{red}$ (ESI-MS m/z calcd [M+H]$^+$: 3579.7, Obs [M+H]$^+$: 3579.6). The folding of 19 mg of HD5$_{red}$ afforded 7 mg (6 % overall yield) of HD5$_{ox}$ (ESI-MS m/z calcd [M+H]$^+$: 3585.7, Obs [M+H]$^+$:

3585.7). The other portions of Fmoc-protected HD5 on the resin was used for N-terminal biotin coupling and azido-functionalized HD5.
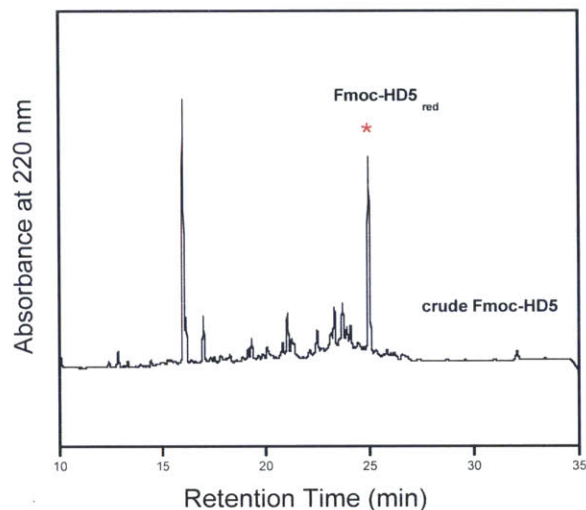

Figure A2.1. Analytical HPLC trace of crude Fmoc-HD5 in the presence of TCEP. Sample was run at a gradient of 10-60% B for 30 min at a flow rate of 1 mL/min.

ii.   Azido-functionalized HD5 (N₃-HD5)

Synthesis of N-terminal Azido-functionalized HD5 (N₃-HD5). The synthesis of Azido-HD5 was performed on a 0.064-mmol scale of Fmoc-HD5 on resin. The Fmoc-deprotection was performed using 20% piperidine in DMF. The N-terminal free amine was coupled to the 5-azidopentanoicacid (90 µL, 10 eq, 0.645 mmol) dissolved in DMF containing the HATU (10 eq), HOAt (10 eq) and DIPEA (20 eq). The reaction was performed twice with HATU for 30 min each before leaving another overnight coupling reaction with PyAOP to ensure complete coupling. The peptide was cleaved from the resin with global deprotection using the standard cleavage mixture. The peptide was precipitated from the cleavage mixture and redissolved in a water/acetonitrile (1: 1) mixture containing 0.1 N HCl. This solution was lyophilized. Cleavage resulted in 130 mg, 54% overall yield of crude peptide from 0.0645-mmol scale of synthesis. When the crude peptide was subjected to analytical HPLC column, the desired peptide was

identified (Figure A2.2A) along with a few other peaks. The crude mixture was subjected to purification using preparative HPLC column, resulting in 17 mg, 7% overall yield of N_3-HD5$_{red}$ (Figure A2.2B). Oxidative folding of 17 mg N_3-HD5$_{red}$ afforded 8 mg, 4% overall yield of N_3-HD5$_{ox}$ (Figure A2.2B).

Antimicrobial Activity and the Morphological Changes Induced by N_3-HD5. The antimicrobial activity of N_3-HD5 was determined against *E. coli* ATCC 25922. Surprisingly, the AMA activity of N_3-HD5$_{ox}$ was completely abrogated even at 40 μM (no loss of CFU/mL), compared to native HD5$_{ox}$ (at 8 μM, 4-log reduction of CFU/mL). When the morphology of *E. coli* treated with N_3-HD5$_{ox}$ was examined, the characteristic morphological changes induced by HD5$_{ox}$ such as bleb formation was not observed (Figure A2.4).
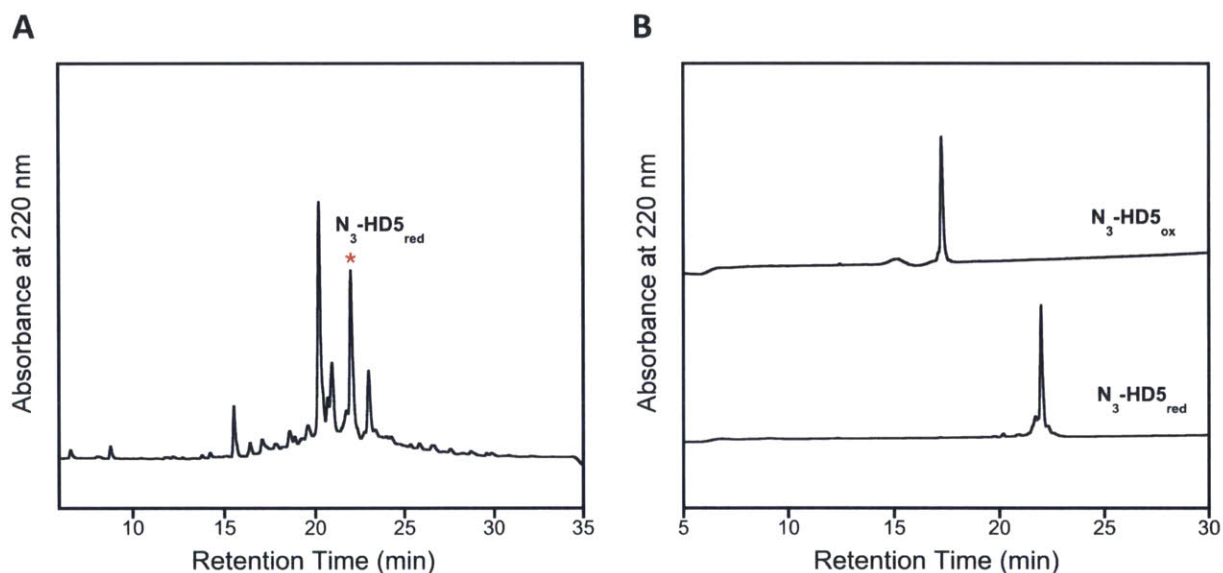

Figure A2.2. Analytical HPLC traces of **A)** crude N_3-HD5 peptide and the desired peptide N_3-HD5$_{red}$ is highlighted with an asterix (*); and **B)** N_3-HD5$_{red}$ peptide and N_3-HD5$_{ox}$ peptide. Absorbance at 220 nm is reported. Samples were subjected to a gradient of 10-60% B for 30 min at flow rate of 1 mL/min.
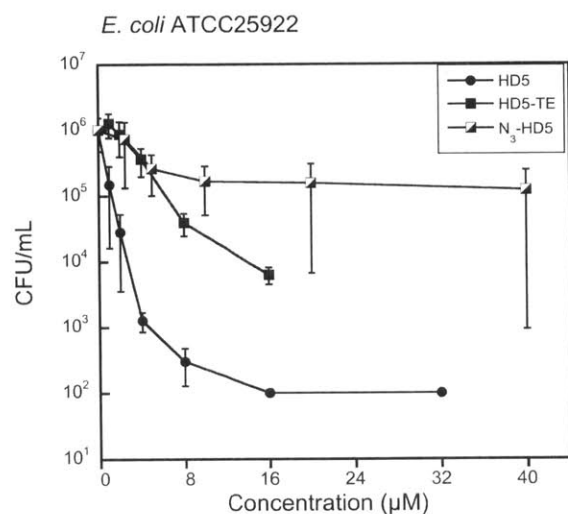
Figure A2.3. Antimicrobial activity of N_3-HD5$_{ox}$, HD5$_{ox}$ and HD5-TE against *E. coli* ATCC 25922. The bacteria (1×10^6 CFU/mL) were treated with peptides for 1 h at 37 °C, 150 rpm (10 mM sodium phosphate buffer, 1% v/v TSB w/o dextrose, pH 7.4) (mean ± SD, n = 3).
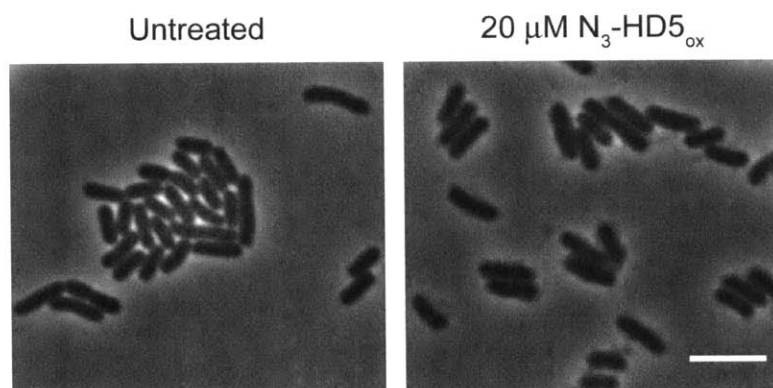
Figure A2.4. N_3-HD5$_{ox}$-induced morphological changes in *E. coli* ATCC 25922. The bacteria (1 $\times 10^8$ CFU/mL) were either untreated or treated with N_3-HD5$_{ox}$ (20 μM) for 1 h at 37 °C, 150 rpm (10 mM sodium phosphate buffer, 1% v/v TSB w/o dextrose, pH 7.4) prior to imaging. Scale bar = 5 μM.

iii. **Synthesis of Biotin-Abu-HD5 (B-HD5).** The synthesis of Biotin-Abu-HD5 was performed on a 0.0274-mmol scale of Fmoc-HD5 resin. After Fmoc deprotection, the N-terminus of HD5 was coupled twice with Fmoc-ABU-OH (95 mg, 10 eq, 0.28 mmol) dissolved in 5 mL of DMF containing HATU (10 eq), HOAt (10 eq) and DIPEA (20 eq). The Fmoc-group was removed before

addition of D-biotin (70 mg, 10 eq, 0.28 mmol) activated with HATU (10 eq), HOAt (10 eq) and DIPEA (20 eq). The coupling reaction was performed thrice before cleaving the Biotin-Abu-HD5 from the resin. The crude peptide was precipitated off the cleavage mixture using precooled ether. The peptide pellet was redissolved in 0.1 N HCl containing water and acetonitrile (1: 1) mixture. The solution was lyophilized to obtain 70 mg of crude peptide (65 % overall yield) as a white powder. The crude peptide dissolved in 75 mM HEPES, 6 M GuHCl, pH 8.2 was reduced using TCEP before quenching reaction with 6% TFA solution (Figure A2.5A). The reduced peptide was purified on preparative HPLC column to obtain 14 mg (13 % overall yield) of B-HD5$_{red}$. The purified peptide was characterized by both analytical HPLC (Figure A2.5B) and ESI-MS (m/z calcd $[M+H]^+$: 3898.9, Obs $[M+H]^+$: 3598.9). A 4-mg portion of B-HD5$_{red}$ was folded using GSH and GSSG oxidative folding mixture, a single major peak of desired product was observed. The reaction mixture was purified on preparative RP-HPLC column to afford 2.5 mg (62% folding yield) of BHD5$_{ox}$. The final product was subjected to analytical HPLC column (Figure A2.5B) and ESI-MS (m/z calcd $[M+H]^+$: 3892.7, Obs $[M+H]^+$: 3892.8) to verify purity.
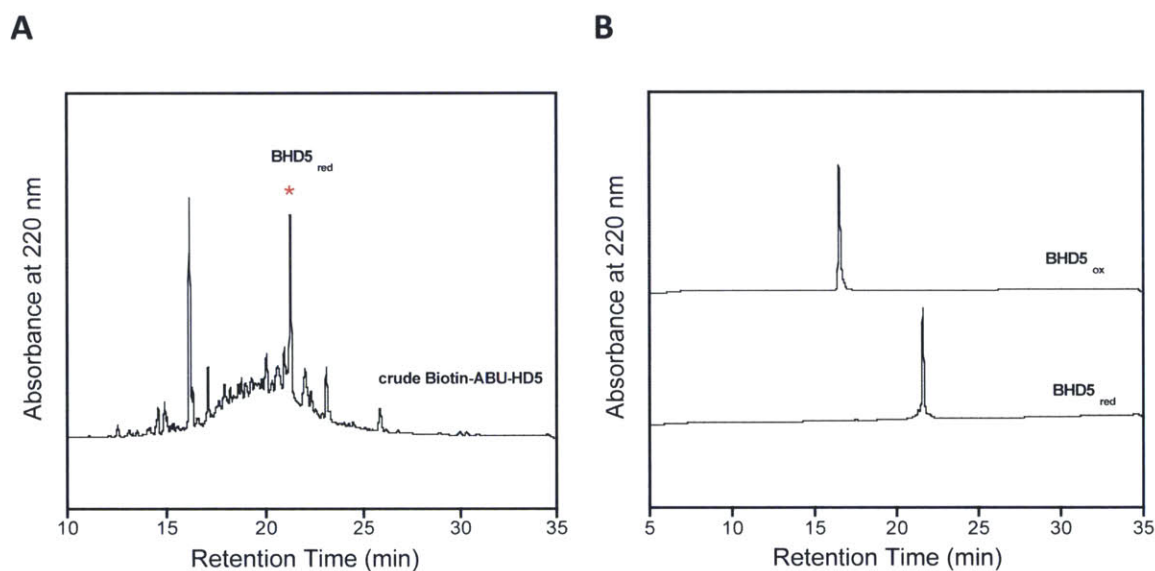

Figure A2.5. Analytical HPLC traces of A) crude Biotin-ABU-HD5 (BHD5) from the synthesis (the desired BHD5$_{red}$ is highlighted with an asterix (*) and B) purified BHD5$_{red}$ and BHD5$_{ox}$. Samples were subjected to a gradient of 10-60% B for 30 min at a flow rate of 1 mL/min.

iv. Synthesis of Linear Peptide BHD5-TE with Carboxymethylation using 2-Iodoacetamide

Capping. $BHD5_{red}$ was dissolved at a 0.5-mg/mL concentration in 470 μL of 0.6 M Tris. HCl, 6M

GduHCl, pH 8.6 containing 30-μL aliquot of freshly prepared (75 μM) TCEP. To this mixture, a 75

μL of a 400-μM stock solution of 2-iodoacetamide was added in dark and incubated for 2 h. The

reaction was monitored using analytical HPLC and the reaction mixture was purified on a semi-

preparative RP-HPLC column to obtain the desired BHD5-TE. The synthesis was performed on a

2-mg scale of $B-HD5_{red}$ to obtain 2 mg of BHD5-TE (Figure A2.6A) and formation of BHD5-TE

(Figure A2.6A) was confirmed by ESI-MS (m/z $[M+H]^+$ calcd 4241.16, Obs $[M+H]^+$: 4241.12).

Table A2.1. HPLC Retention Time, Calculated and Observed Mass of HD5 and its Derivatives

Peptide	Retention time (min) [a]	Calculated mass $[M+H]^+$ m/z	Observed mass [b] $[M+H]^+$ m/z	Overall/folding Yield [c] (%)
$HD5_{red}$	20.4	3585.67	3585.76	6 %
$HD5_{ox}$	15.3	3579.62	3579.62	4 %/70 %
HD5-TE	16.6	3928.92	3928.91	72%
$BHD5_{red}$	21.6	3898.81	3898.92	13 %
$BHD5_{ox}$	16.4	3892.73	3892.75	8 %/62 %
BHD5-TE	17.4	4241.16	4241.12	90%
N_3-HD5_{red}	21.1	3712.81	3712.81	7%
N_3-HD5_{ox}	17.3	3706.42	3706.42	4%/ 57%

[a] Retention times were determined on analytical C18 RP-HPLC column with a gradient of 10–60% B run for 30 min at a flow rate of 1 mL/min [A: water (0.1% TFA), B: acetonitrile (0.1% TFA)]. [b] MolE-Molecular Mass Calculator v2.02 available at http://library.med.utah.edu/masspec/mole.html was used for calculating m/z values for peptides. [c] The yields are calculated based on the resin loading as the theoretical 100% yield.
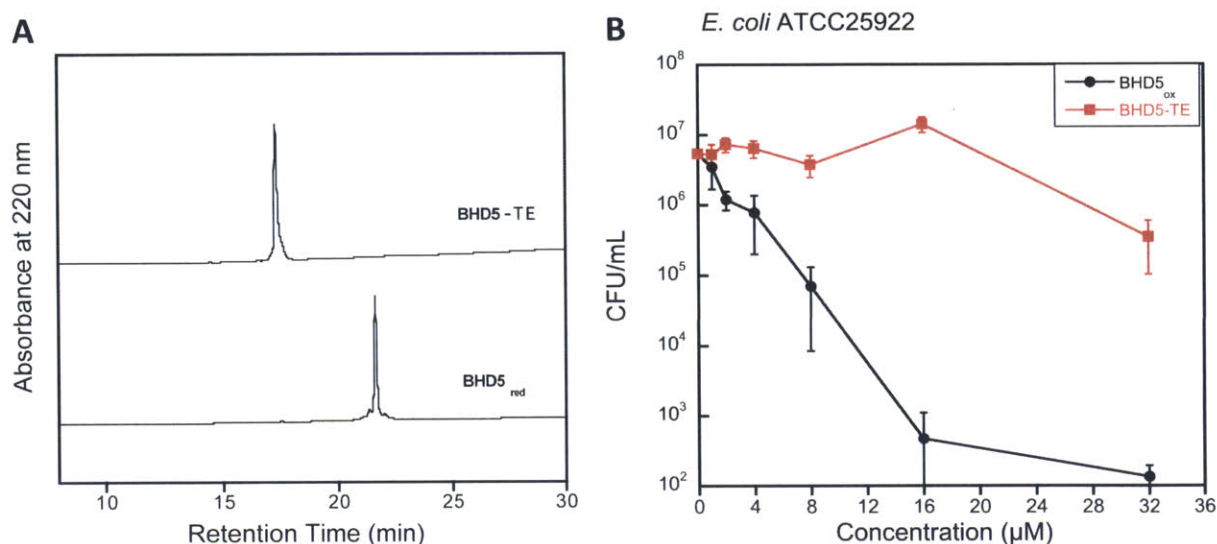
Figure A2.6. A) Analytical HPLC traces (absorbance at 220 nm) of $BHD5_{red}$ and BHD5-TE. Samples were subjected to a gradient of 10-60% B for 30 min at flow rate of 1 mL/min. **B)** Antimicrobial activity of the Biotin-HD5 analogues against *E. coli* ATCC 25922). The bacteria (1×10^6 CFU/mL) were treated with peptides for 1 h at 37 °C, 150 rpm (10 mM sodium phosphate buffer, 1% v/v TSB without dextrose, pH 7.4) (mean ± SD, n = 3).

v.   Determination of Localization of $HD5_{ox}$ using Biotin-HD5 Derivatives

Morphological Changes Induced in Bacteria Treated with Biotin-HD5 Analogues. For the identification of a bacterial target interacting with HD5, we synthesized and characterized biotin-HD5 analogues, $BHD5_{ox}$ and BHD5-TE. B-$HD5_{ox}$ (at 16 µM, > 4-log reduction in CFU/mL) was active against *E. coli* ATCC 25922 and retained its antimicrobial activity. As expected, the linear BHD5-TE (at 32 µM, 1-log reduction in CFU/mL) was less active against *E. coli* ATCC 25922 (Figure A2.6B). In accordance with the AMA results, the morphology of *E. coli* treated with B-$HD5_{ox}$ displayed blebs and other morphological changes specific to native $HD5_{ox}$ (Figure A2.7). Linear BHD5-TE analogue did not induce the bleb formation; moreover, the morphology was very similar to the HD5-TE treated bacteria (Figure A2.7). These results indicate that the biotin analogues can be used as promising surrogates for studying the localization of $HD5_{ox}$ and HD5-TE. Commercial streptavidin-probes for both TEM imaging and fluorescence microscopy are available. One limitation of this method is the presence of active uptake mechanisms of

218

biotinylated-peptides.[7] To overcome this limitation, knockout mutants of these transport pathways were studied for the localization of biotinyated-HD5 analogues.
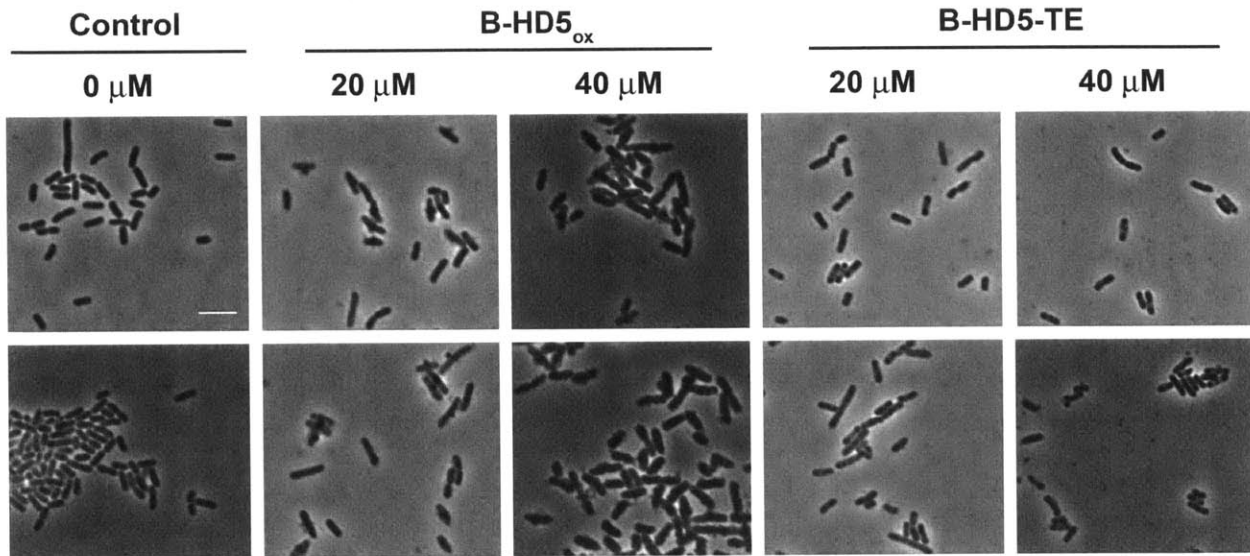

Figure A2.7. Morphology of *E. coli* treated with biotin-HD5 analogues. *E. coli* ATCC 25922 (10^8 CFU/mL) were treated with control (0 µM), B-HD5$_{ox}$ (20 µM and 40 µM), and B-HD5-TE (20 µM and 40 µM), [both top and bottom panels] in standard AMA buffer (10 mM sodium phosphate buffer, 1% TSB w/o dextrose, pH 7.4) at 37 °C for 1 h with shaking at 130 rpm. A 5-µL suspension from each sample is plated on 1% agarose pads and imaged.

A high-affinity biotin transporter in *E. coli* K-12 is identified as YigM,[8,9] a membrane protein. By employing a knockout mutant of this protein (available in Keio Collection),[10] the uptake and labeling of HD5 was further probed using biotinylated analogues (Figure A2.8). Upon treatment with the biotin analogues, the ΔyigM mutant displayed similar morphological changes as the parent strain. Therefore, these biotin-HD5 analogues can be employed for further localization studies.
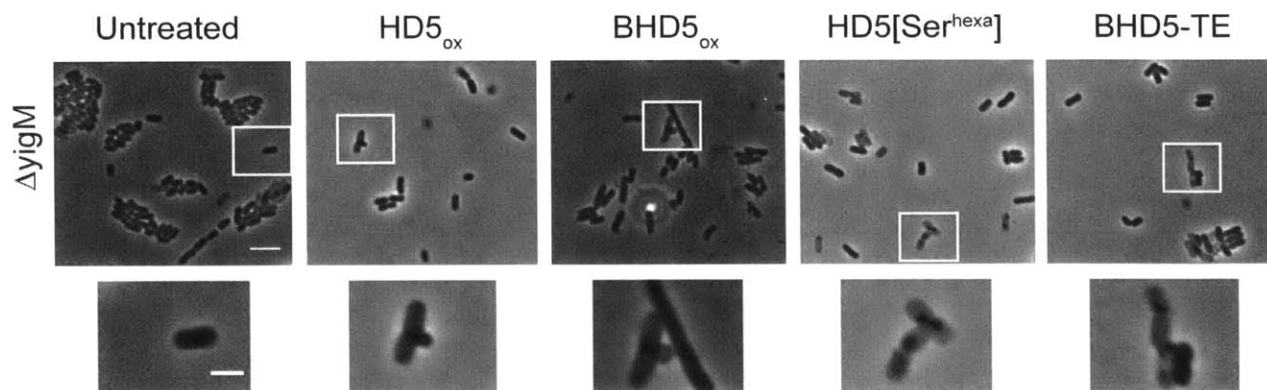
Figure A2.8. Morphology of ΔyigM treated with biotin-HD5 analogues. ΔyigM (10^8 CFU/mL) untreated and bacteria treated with 20 μM of peptides in standard AMA buffer (10 mM sodium phosphate buffer, 1% TSB w/o dextrose, pH 7.4) at 37 °C for 1 h with shaking at 130 rpm, and plated on 1% agarose pads and imaged. Scale bar = 5 μm and 2 μm: top and bottom panels respectively.

A2.D. Summary and Outlook

In summary, we were able to generate HD5 derivatives by appending many desired functionalities such as biotin and azido-functional groups at the N-terminus of HD5. Biotin modifications provide a handle on HD5 for applications involving target identification, localization of HD5 and affinity-based assays. The biotin modification did not abrogate the antimicrobial activity of HD5$_{ox}$. *E. coli* treated with BHD5$_{ox}$ and BHD5-TE displayed similar morphological changes as HD5ox and HD5[Ser^{hexa}].

In this study, we also generated azido-functionalized HD5 (N$_3$-HD5). The antimicrobial activity of N$_3$-HD5$_{ox}$ was however completely abrogated. Similar loss of activity was observed when the N-terminus of HD5 was modified with fatty acid moieties (Chapter 5). Further studies are needed to understand the effect of N-terminal alkyl-chain modifications.

A2.E. Acknowledgments

A2.F. References

(1) Brogden, K. A. (2005) Antimicrobial peptides: pore formers or metabolic inhibitors in bacteria? *Nat. Rev. Microbiol. 3*, 238–250.

(2) Wilmes, M., and Sahl, H.-G. (2014) Defensin-based anti-infective strategies. *Int. J. Med. Microbiol. 304*, 93–99.

(3) Wilmes, M., Stockem, M., Bierbaum, G., Schlag, M., Götz, F., Tran, D. Q., Schaal, J. B., Ouellette, A. J., Selsted, M. E., and Sahl, H.-G. (2014) Killing of *staphylococci* by θ-defensins involves membrane impairment and activation of autolytic enzymes. *Antibiot. (Basel, Switzerland) 3*, 617–631.

(4) Park, C. B., Yi, K.-S., Matsuzaki, K., Kim, M. S., and Kim, S. C. (2000) Structure-activity analysis of buforin II, a histone H2A-derived antimicrobial peptide: the proline hinge is responsible for the cell-penetrating ability of buforin II. *Proc. Natl. Acad. Sci. U. S. A. 97*, 8245–8250.

(5) Lehrer, R. I., Barton, A., Daher, K. A., Harwig, S. S. L., Ganz, T., and Selsted, M. E. (1989) Interaction of human defensins with *Escherichia coli*. Mechanism of bactericidal activity. *J. Clin. Invest. 84*, 553–561.

(6) Wommack, A. J., Ziarek, J. J., Tomaras, J., Chileveru, H. R., Zhang, Y., Wagner, G., and Nolan, E. M. (2014) Discovery and characterization of a disulfide-locked C_2-symmetric defensin peptide. *J. Am. Chem. Soc. 136*, 13494–13497.

(7) Walker, J. R., and Altman, E. (2005) Biotinylation facilitates the uptake of large peptides by *Escherichia coli* and other gram-negative bacteria. *Appl. Environ. Microbiol. 71*, 1850–1855.

(8) Finkenwirth, F., Kirsch, F., and Eitinger, T. (2013) Solitary BioY proteins mediate biotin transport into recombinant *Escherichia coli*. *J. Bacteriol. 195*, 4105–4111.

(9) Hebbeln, P., Rodionov, D. A., Alfandega, A., and Eitinger, T. (2007) Biotin uptake in prokaryotes by solute transporters with an optional ATP-binding cassette-containing module. *Proc. Natl. Acad. Sci. U. S. A. 104*, 2909–2914.

(10) Baba, T., Ara, T., Hasegawa, M., Takai, Y., Okumura, Y., Baba, M., Datsenko, K. A., Tomita, M., Wanner, B. L., and Mori, H. (2006) Construction of *Escherichia coli* K-12 in-frame, single-gene knockout mutants: the Keio collection. *Mol. Syst. Biol. 2*, 2006.0008.

Appendix 3

Perspective on Human Defensin 5

Previously, the focus on HD5 as detailed in **Chapter 1**, was directed at identifying the structural elements that influence the antimicrobial action of HD5. In this direction, the effect of disulfide linkages, salt-bridge forming residues, arginine residues, and the hydrophobic residues on the AMA assays were studied. Moreover, the lectin-like behavior in binding to the glycoproteins and self-aggregation/oligomerization properties of HD5 was demonstrated. The ability of HD5 to permeabilize the inner membrane of *E. coli* was also indicated. However, the exact mechanism of antibacterial action of HD5 was not clearly understood. We therefore focused on identifying the site(s) of antimicrobial action of HD5 and studying the corresponding bacterial response(s) in order to gain new insights into the antimicrobial mechanism of HD5.

One of the main difficulties in studying HD5 has been obtaining significant amounts of HD5 with native disulfide linkages (**Chapter 2**). Further, modification of HD5 to obtain analogues, including HD5 derivatives harboring fluorophores or other functional moieties, required a robust solid-phase peptide synthesis procedure, and optimizing this synthesis was a focus of this thesis. HD5 and fluorophore-modified derivatives were synthesized using a manual Fmoc-based solid-phase peptide synthesis protocol. Considering that HD5 is a 32-residue peptide, modifying the peptide with any fluorophore might alter its properties, including its antimicrobial activity. In the literature, we noticed that when fluorophore-labeled AMPs were employed in studies of uptake or mechanism, the effects of fluorophore modification on the structure and function of the peptides were not considered in detail. Therefore, we prepared a family of fluorophore-modified HD5 analogues and evaluated the antimicrobial activity and photophysical properties of these peptides. These studies revealed fluoroprhore modifications that disrupted the antimicrobial activity (e.g. $FL\text{-}HD5_{ox}$) and those that minimally altered the properties of HD5 (e.g. $R\text{-}HD5_{ox}$). With this family of HD5 analogues in hand, the effect of HD5 on the morphology of various bacteria and their responses to HD5 treatment were investigated.

When studying defensins, certain limitations needed to be considered when developing assays. For example, nutrient-rich growth media regularly used for standard AMA assays of antibiotics is not typically not useful for studies of defensins. HD5, and many characterized

defensins, are not active under these conditions. Rather, the *in vitro* antimicrobial activity of defensins is typically studied using bacterial cultured in a buffer (e.g., sodium phosphate buffer, MOPS buffer) containing a nutrient supplement (e.g., 1% TSB). These conditions maintain the bacteria in metabolically active state over the course of the assay (typically 1 h).[1] Although the data is not included in this thesis, we observed that antimicrobial activity of HD5 against *E. coli* was attenuated when the assay buffer was not supplemented with 1% TSB. This observation is in agreement with prior literature[1,2] and suggests the importance of the metabolic state of *E. coli* for the activity of HD5. Moreover, the antimicrobial activity of many defensins, including HD5, against *E. coli* is highly affected by the presence of salt in the AMA buffer.[2-5] However, it appears that the antimicrobial activity of defensins against Gram-positive strains is less affected by the presence of salt (**Chapter 4**). This differential susceptibility of HD5 towards the salt concentration in assay buffer was not explored previously in detail. Furthermore, the importance of disulfide linkages for the AMA activity of HD5 differs against Gram-positive versus Gram-negative strains. These observations along with other results, suggest different modes of action of HD5 against Gram-positive and Gram-negative bacteria. For this reason, we decided to investigate the effect of HD5 on both Gram-negative and Gram-positive bacteria.

We studied the effect of HD5 on *E. coli,* a model Gram-negative organism (**Chapter 3**). HD5 induced distinct morphological changes such as bleb formation (0.5-1 μm diameter), clumping and elongation of bacteria. The blebs were observed mainly at the cell poles and cell division sites. Moreover, the distinct morphological changes were also observed in other Gram-negative bacteria. These morphological changes suggest that the HD5 kills Gram-negative bacteria via a common mechanism of action and the bacteria might be responding to HD5 treatment by displaying the blebs and surface protrusions. The outer membrane vesicle (OMV) formation (20-200 nm diameter) is a general bacterial resistance mechanism by which the bacteria excrete the antimicrobial agents and prevent them from entering the bacteria. The bleb formation resembles the outer membrane vesicle formation, albeit in much larger size. The bacteria also display clumping and more extracellular structures resembling biofilm like

structures. These phenotypes could indicate a coping mechanism employed by bacteria in order to evade HD5 action by clumping and preventing the AMP entry.

Phenotypes such as bleb formation in bacteria were difficult to compare to the literature reports, as there are few studies detailing various bacterial phenotypes caused by AMPs and, in particular, defensins. In the literature, terms such as blebs, protrusions, or bulges have been used to describe morphologies caused by AMPs without clear definitions. The studies employing defensins often indicate blebs when referring to the outer membrane vesicle like structures of 20 - 200 nm protruding from the surface of bacteria. These structures, along with bulges comprised of the outer membrane alone with diameters as big as 1 μm, were also reported following treatment of nontypeable Haemophilus influenzae (NTHi) and *E. coli* with certain defensins. An observation that puzzled us was the ultrastructure of the blebs formed in *E. coli* upon treatment with HD5. In the studies employing cytoplasmic-GFP expressing *E. coli* strains (**Chapter 3**), bacteria upon treatment with HD5 displayed blebs containing GFP emission. Inner membrane permeabilization causes the redistribution of cytoplasmic contents observed in the blebs. Similarly, periplasmic-GFP expressing *E. coli* strains displayed blebs of both phenotypes of ring-like GFP emission and uniform overall distribution. A ring-like distribution of fluorescence could result from blebs composed of both inner and outer membranes, whereas uniform distribution from outer membrane alone or both membranes albeit with permeabilization of inner membrane. Thus, the blebs seemed to be comprised of sometimes one membrane alone, and more often seemingly both inner and outer membranes. These structures of blebs raise the questions such as 1) is the integrity of peptidoglycan layer maintained upon treatment with HD5? 2) Are the phospholipid, LPS and protein composition of these blebs altered? 3) The composition of the outer membrane governs the uptake of $HD5_{ox}$, and the LPS-deficient strains are more susceptible to $HD5_{ox}$ treatment than the parent strain; thus, is HD5 interacting with the lipid or protein components of the blebs or both? 4) Is HD5 entry in to the bacteria prevented by exclusion of the blebs from cytoplasmic contents? 5) What are the structural elements of HD5 that are required for the bleb formation?

The localization of HD5 with fluorophore-modified HD5 derivatives at the cell poles and division sites indicates a potential target at these sites. The potential target could be the anionic phospholipids such as CL and PG present at these sites. In order to address this hypothesis, *E. coli* deficient in the anionic lipids were subjected to HD5 treatment and we studied the phenotypes of these bacterial along with localization of labeled-HD5 derivatives (**Chapter 5**). Although we initially considered CL anionic lipids to be potential interacting moieties at cell poles and cell septa, we found that the *E. coli* mutant lacking CL displayed WT-like phenotypes upon treatment with HD5, and R-HD5$_{ox}$ was localized at cell poles and cell septa similar to WT. However, when the mutant lacking both anionic lipids was subjected to HD5 treatment, bleb formation was not observed and a uniform labeling pattern inside the bacteria was observed. This result suggests the following possibilities: 1) both the anionic lipids CL and PG are required at cell poles and cell septa, and interact with HD5$_{ox}$, resulting in bleb formation and localization patterns at these sites; or 2) these anionic lipids themselves regulate the localization of a potential protein target of HD5 thereby regulating the localization of HD5 and bleb formation. Currently, both hypotheses are equally possible and further studies are required to identify the exact target and mechanism of action of HD5.

In the studies employing *S. aureus*, *E. faecalis* and *B. subtilis* as three representative Gram-positive strains, we observed other phonotypes caused by HD5 treatment (**Chapter 4**). These phenotypes observed in all three bacterial strains include clumping of bacteria, membrane perturbations (commonly referred to as mesosome formation), and clear differences in the ultrastructures of HD5-treated and pore-forming LL37-treated bacteria. Although characterization of the phenotypes of defensin-treated *S. aureus* is reported, this work has not been extended to additional different Gram-positive strains. Evaluating the phenotypes of different strains treated with AMPs might provide insights into the mechanism of action of these peptides against various bacteria. In this respect, we observed another general trend: the thickness of the PG layer as evidenced from the TEM studies is markedly greater for HD5-treated bacteria compared to the LL37-treated bacteria or even the untreated

bacteria. However, more quantitative analyses are needed to firmly indicate any statistical significance of such differences in the PG thickness. We can at least conclude that morphological changes induced by HD5 are quite different from a pore-forming peptide LL37. How these morphological differences correlate to the mechanism of action of HD5 needs to be studied further.

When exploring the different susceptibility of Gram-negative and Gram-positive bacteria to the salt concentration in the AMA buffer, we observed that in general, HD5 retains AMA activity against Gram-positive bacteria even in the presence of higher NaCl concentrations. It is to be tested whether this difference in AMA activity is due to the membrane compositions alone (absence of LPS) or another cause. Currently, our hypothesis is that the HD5 antimicrobial action is due to the effect of HD5 on the cytoplasmic membrane and/or components near this cytoplasmic membrane including cell division machinery. For HD5 to encounter its targets in Gram-negative bacteria, HD5 needs to overcome the outer membrane (LPS) barrier, and in the presence of higher NaCl and divalent cations that strengthen integrity of LPS layer, this barrier is difficult to overcome. However, in case of LPS-deficient or defective strains of Gram-negative bacteria, HD5 can enter bacteria more readily. Similarly, in case of Gram-positive strains with no outer membrane, we can hypothesize that even at higher NaCl concentrations, HD5 can penetrate/damage the cytoplasmic membrane. Further studies are required in this direction to confirm our hypothesis.

In the field of defensins, and in case of HD5 in particular, the following questions are yet unanswered. 1) Is the membrane damage a primary requirement for bacterial cell death? 2) Are other processes such as transcription, translation or replication/division affected? 3) In the human gut, how are the physiological conditions such as presence of mucin, redox environment, other AMPs influencing the antimicrobial activity of HD5? How do these morphological changes such as bleb formation, clumping and surface protrusions in bacteria influence the other factors of human innate immune responses? Are there other AMPs that induce similar phenotypes in bacteria as HD5? In conclusion, we need more fundamental

studies on understanding the attack of these antimicrobial peptides on bacteria and determine the bacterial responses to such peptides in order to widen our knowledge on the host-pathogen interactions.

A3.A. References

(1) Lehrer, R. I., Barton, A., Daher, K. A., Harwig, S. S. L., Ganz, T., and Selsted, M. E. (1989) Interaction of human defensins with *Escherichia coli*. Mechanism of bactericidal activity. *J. Clin. Invest. 84*, 553–561.

(2) Porter, E. M., van Dam, E., Valore, E. V, and Ganz, T. (1997) Broad-spectrum antimicrobial activity of human intestinal defensin 5. *Infect. Immun. 65*, 2396–2401.

(3) Goldman, M. J., Anderson, G. M., Stolzenberg, E. D., Kari, U. P., Zasloff, M., and Wilson, J. M. (1997) Human beta-defensin-1 is a salt-sensitive antibiotic in lung that is inactivated in cystic fibrosis. *Cell 88*, 553–560.

(4) García, J. R., Krause, a, Schulz, S., Rodríguez-Jiménez, F. J., Klüver, E., Adermann, K., Forssmann, U., Frimpong-Boateng, a, Bals, R., and Forssmann, W. G. (2001) Human beta-defensin 4: a novel inducible peptide with a specific salt-sensitive spectrum of antimicrobial activity. *FASEB J. 15*, 1819–1821.

(5) Chileveru, H. R., Lim, S. A., Chairatana, P., Wommack, A. J., Chiang, I.-L., and Nolan, E. M. (2015) Visualizing attack of *Escherichia coli* by the antimicrobial peptide human defensin 5. *Biochemistry 54*, 1767–1777.